# "THE KINEMATICS OF INTERFERENCE MECHANISMS IN CERTAIN MACHINING OPERATIONS"

A Thesis submitted to

The University of Aston in Birmingham

as partial requirement

for the degree of

Doctor of Philosophy

by

Richard A Etheridge, BSc(Hons), C Eng, M I Prod E, M I Mech E.

JULY 1976

SUMMARY

The mechanism of "Helical Interference" in milled slots is examined and a coherent theory for the geometry of such surfaces is presented.

An examination of the relevant literature shows a fragmented approach to the problem owing to its normally destructive nature, so a complete analysis is developed for slots of constant lead, thus giving a united and exact theory for many different setting parameters and a range of cutter shapes. For the first time, a theory is developed to explain the "Interference Surface" generated in variable lead slots for cylindrical work and attention is drawn to other practical surfaces, such as cones, where variable leads are encountered. Although generally outside the scope of this work, an introductory analysis of these cases is considered in order to develop the cylindrical theory.

Special emphasis is laid upon practical areas where the interference mechanism can be used constructively and its application as the rake face of a cutting tool is discussed. A theory of rake angle for such cutting tools is given for commonly used planes, and relative variations in calculated rake angle between planes is examined. Practical tests are conducted to validate both constant lead and variable lead theories and some design improvements to the conventional dividing head are suggested in order to manufacture variable lead workpieces, by use of a "superposed" rotation. A prototype machine is manufactured and its kinematic principle given for both linear and non-linearly varying superposed rotations. Practical workpieces of the former type are manufactured and compared with analytical predictions,

while theoretical curves are generated for non-linear workpieces and then compared with those of linear geometry.

Finally suggestions are made for the application of these principles to the manufacture of spiral bevel gears, using the "Interference Surface" along a cone as the tooth form.

CONTENTS

## LIST OF ILLUSTRATIONS

Figure

## NOMENCLATURE

| | | |
|---|---|---|
| $T_{min}$ | = | Minimum number of teeth on a pinion |
| $K_w$ | = | Fraction of a module |
| R | = | Gear ratio or cutter radius |
| $k_{/n}$ | = | Lead of milling machine screw |
| $D_o$ | = | Base cylinder diameter |
| $\sigma$ | = | Helix angle or torsion of helix |
| $\rho$ | = | Principal radius of curvature of helix |
| L | = | Lead |
| a | = | Base cylinder radius vector |
| b | = | Linear displacement constant |
| $\theta$ | = | Angular displacement of radius vector |
| $\phi$ | = | Angular displacement in cutter framework |
| s | = | Length of curvature |
| $\bar{T},\bar{t},\bar{t}'$ | = | Unit tangent vectors |
| $\bar{B},\bar{b},\bar{b}'$ | = | Unit Bi - normal vectors |
| $\bar{N},\bar{n},\bar{n}'$ | = | Unit normal vectors |
| d | = | Cutter's depth of projection below base cylinder radius |
| w | = | Half cutter width |
| x,y,z | = | Cartesian axes |
| x',y',z' | = | Rotated axes |
| $\beta$ | = | Angle subtended by a cutter due to offset from centre |
| $\delta$ | = | Parameter of cutter shape or angular displacement in rotated system |
| u,v, | = | Network curves for a surface |
| $\bar{r}$ | = | Position vector |
| $\alpha$ | = | Angular displacement of rotated axes |
| $\psi$ | = | Rake angle |
| $\tau$ | = | Semi-cone angle |
| m | = | Slope of cone |
| $r_o a_o$ | = | Base radius of cone |
| k | = | Exponential coefficient of constant magnitude or superposed rotation |
| $r_c$ | = | Radius of end mill |
| $\lambda$ | = | Scale factor |
| w' | = | Cutter width at arbitrary point on a profile |

DECLARATION

No part of the work described in this thesis has been submitted in support of an application for another degree or qualification of this or any other University or other institute of learning.

No part of the work described in this thesis has been done in collaboration with any other person.

Richard A. Etheridge

ACKNOWLEDGEMENTS

The Author would like to thank Professor R. H. Thornley for both his help and encouragement in supervising the project and at the same time for his permission to carry out the work in the Department of Production Engineering.

I would also like to thank my colleague Dr. D. A. Scrimshire for teaching me "Conversational Fortran" and Mr. R. Clarke of the Mathematics Department for checking the initial solutions.

The Laboratory staff of the Department of Production Engineering are thanked for their assistance and co-operation and I am particularly grateful to Mr. G. Yardley whose skill in constructing the improved dividing head contributed so much to its successful function.

I also wish to acknowledge the source of two of the diagramms, namely those due to A. J. A. Scott and J. A. Waynham, and I would particularly like to thank the Model Engineer for permission to reproduce Plate 1.

Finally, I would like to thank my Wife, Pamela, whose patience and typing skills contributed significantly to this finished form.

LIST OF PLATES

# CHAPTER I

## INTRODUCTION

The use of standardisation procedures within engineering design practice quite often leads to difficulties in service or manufacture owing to the fact that under certain circumstances the component or machine tool is required to operate outside the standardised parameters.

Interference mechanisms arise in manufacture as a consequence of this requirement and in most instances the physical manifestation of the problem is a departure from the component's required design geometry. In certain machining operations it may well be that the interference is a physical phenomena owing to rubbing between a cutting tool and the workpiece because a small change has been made to the workpiece design parameters or the machine settings. A very good example of this is the case of tool flank interference with the work when cutting multi-start threads or worms, in this instance it is necessary to increase the tool flank clearance to avoid serious damage to the thread flank.

It is true to say that in most circumstances "Interference Mechanisms" are totally destructive and for this reason are usually avoided if at all possible by designing engineering components strictly within the appropriate boundary conditions.

It is equally true to say that the same reasons have precluded any wide examination of either the problem, its geometry or kinematics and it is only in the field of gears and gearing that any comprehensive examination of an "Interference Mechanism" has been carried out.

This particular mechanism is usually called undercutting or root thinning of gear teeth and is produced as a direct result of designing gear teeth

which require to work outside the boundary conditions defined by the standardisation parameters. The difficulty encountered by the designer here, is that standard pressure angles and diametral pitches are defined for involute gears primarily for reasons of interchangability but this places a stricture upon the size of gear which can maintain a correct involute form over the entire tooth length for a given pressure angle. If for reasons of space, the designer is forced to use a gear having a number of teeth less than the defined minimum,then root thinning occurs owing to the generating principle involved in gear manufacture and the tooth shape degenerates into a Trochoidal undercut rather than the required Involute in the root area.

Owing to its marked effect upon gear tooth strength and consequently transmission design this particular mechanism is well documeted[3,4,5,6,7,8] and although a thorough analysis exists, by far and away the most attention has been devoted to avoiding its manifestation. As a consequence design standards and a set of ground rules have been developed to minimise the problem, of which the first rule is usually - "redesign to avoid interference".

There are a number of other examples of interference in manufacturing industry mostly associated with cutting tool design or manufacture, of which the most important is that produced by a disc type fluting cutter moving around a helical path. This mechanism is always evident to some extent in the manufacture of small tools such as drills, reamers, slab mills and end mills. It also has some implications in gear manufacture because a hob producing a helical gear is susceptable to this mechanism as also is the disc cutter when used for producing one off helical gears or milled worms.

In this particular area of work no comprehensive analysis of the mechanism is available and this thesis is concerned with producing a coherent theory of "Helical Interference" for both constant lead and variable lead work-pieces.

The limitations relating to this problem, of existing machine tool systems are analysed and some practical design improvements to the conventional dividing head are demonstrated whereby the "Helical Interference" mechanism can be used constructively and with some advantage in cutting tool manufacture.

## CHAPTER II

## THE GENERAL PROBLEM OF INTERFERENCE

Owing to its generally destructive nature the mechanism of interference has received scant attention in the literature, in spite of the many examples arising in engineering practice.

The best documented example of such a mechanism is that associated with gear design and gear manufacture. In this case the physical limitations imposed by standardisation of the design parameters, produce an "Interference Mechanism" which leads not only to root thinning in conventional gearing but also to tip rubbing in internal gears. Such problems are well reported and the solutions posed were derived by the pioneer workers Buckingham[3] in America and Tuplin[4] and Meritt[5] in England.

Their theoretical treatments show that there are minimum numbers of teeth permissible in pinions of a given pressure angle to avoid interference and further that the minimum requirement varies with the meshing condition, namely

Rack and pinion $$T_{min} = \frac{2k_w}{\sin^2\phi}$$

Gears in ratio "R" $$T_{min} = \frac{2k_w R}{\sqrt{1 + R(R+2)\sin^2\phi} - 1}$$

Equal pinions in mesh $$T_{min} = \frac{2k_w}{\sqrt{1 + 3\sin^2\phi} - 1}$$

where $k_w$ is some defined fraction of addendum and $\phi$ is the pressure angle.

Normally interference will be avoided by the designer but if this proves impossible then the implications within manufacture are obvious, because they lead automatically to modification of machine tool settings in order to avoid the mechanism. The following are the most commonly recommended methods to minimise interference in small pinions,

a) Radius the tip of the largest gear (or annulus in internal gears)

b) Reduce the outside diameter of mating gear (stub tooth system)

c) Make pinion oversize and reduce gear diameter

d) Increase the pressure angle

e) Increase pinion diameter and centre distance

f) Redesign.

Bevan[8] gives a geometric analysis of the tooth space when undercutting takes place and further shows that it is Trochoidal in nature as distinct to the required Involute surface. A particularly graphic example of the mechanisms destructive nature is shown in Figure (1)

Other examples of destructive interference occur in machining systems where form tools are used and although the mechanism is not totally destructive the workpiece shape departs significantly from that required and so a method of form tool correction is desirable. Dent[9] describes the difficulties encountered with circular form tools and gives a corrective proceedure based on simple geometric considerations to ensure that the correct workpiece form is produced. The same author describes the necessary corrections to form cutters used in the form relief of milling cutters and hobs.

Trochoidal interference is also encountered in the design of hob tooth forms which are required to produce non-gear shapes, eg knuckles,

castellations and splines. Semi-graphical techniques such as the branch angle method are used whereby the hob tooth form is derived from the required profile by simulating the hob-workpiece contact path on a drawing board. Clearly the base generating circle for the system must be carefully chosen to avoid root thinning of the machined form, because the final machining process is identical with gear manufacture. Such methods for the definition of hob tooth form necessary to avoid interference are standard tool design techniques.

Helical interference although mentioned in the literature is very fragmented and largely qualitative in nature since the phenomena is usually considered undesirable. Gear cutting texts refer to the problem of helical interference both in the case of formed helical gears made on the milling machine using disc cutters and of worms milled from the solid. In the former case although helical interference is described[6] its effect is usually neglected owing to the other inaccuracies inherent in the process, i.e. the errors due to the approximate form on the cutter used.

Where milled helicoids are used in the manufacture of worms the prime requisite is to achieve tangential contact between the cutter and the worm such that conjugate action is maintained between the pair. Probably the best account of helicoids used for worms is to be found in Buckingham[3] while special applications of conjugate theory to such workpieces are given by Dudley and Poritsky[10] and Young[11].

Fundamental analysis of the slot geometry produced in the milled helicoid is very limited and in most instances is restricted to approximate solutions. There are a number of qualitative discussions about the mechanism, of which probably the best are Chapman[12] and

Parkinson and Dawney[6]. Of the quantative discussions probably the earliest is that due to Buckingham[3] (1949) who gives a formulae, but no derivation, for the flank profile of a milled worm, whilst Hugo [13] (1962) described a simple geometric approach to calculating the width of a helical slot from point to point.

Several approximate theories have been proposed for calculating the plane geometry of the slot produced by a disc cutter moving around a helical path, and of these the simplest is the semi-graphical technique proposed by Etheridge[14]. This method assumes a first approximation of a circular involute whereby the fluting cutter's profile is moved around an involute path in the normal plane of the workpiece. The envelope of the fluting cutter profile as it moves is assumed to be a good approximation to the slot profile. Figure(2) shows the method. Kudinov[15] on the other hand develops a plane geometric approach using the mathematical theory of envelopes but restricts the discussion to simple straight line profiles, while Etheridge's method permits examination of more complex fluting cutter shapes.

An exact solution using computer methods has been proposed by Friedman, Boleslavski, and Meister[16] where an infinitely thin cutter is rolled along a helical path in the workpiece and its coordinates computed. The cutter is then stepped out from the centre-line by successive small amounts and its path recomputed, until the width of the real cutter is reached. This technique permits investigation of profiled cutters since the computer is capable of accommodating diameter changes in the infinitely thin cutter.

All these methods, however, have distinct disadvantages owing to either, their inherent innaccuracy or laborious nature and in most cases they do not represent a coherent theory which is capable of application to

the wide ranging problems involved.

The work developed here recognises this fact and a general theory applicable to all types of helically fluted workpieces using disc type cutters is developed. Vector Differential Geometry is used throughout because it is a very powerful tool in this type of analysis.

# CHAPTER III

## DEFINITION OF HELICAL INTERFERENCE PROBLEM

### INTRODUCTION

Before examining the difficulties arising from the milling of helical surfaces it is worthwhile examining the kinematics of machine tool systems, for their somewhat restrictive nature contributes to the interference mechanism.

### THE GENERATING PRINCIPLE

From kinematics any body in space has six independent degrees of freedom - three rotational and three translational - unless acted upon by an external force system which restricts some or all of these freedoms.

The principle of generation used in machine tools utilises this fact and a machine tool system is defined to be a group of elements partially kinematically restrained such that their combined motions when applied to a cutting tool and workpiece achieve a desired geometry upon the work.

To illustrate the complexity of motion possible when using a large number of elements within a machine tool system it is best to examine the engraving engines of the Eighteenth and early Nineteenth centuries. These machines were used to produce complex engraved patterns on watch cases and similar articles. Plate 1† shows a typical engine and workpieces.

The rapid growth of industrialisation during the Nineteenth century, however, required engineering components of ever increasing accuracy

† Courtesy of "The Model Engineer".

and more restrictive geometry. It is for these reasons that our modern machine tools evolved with small groups of accurate elements arranged to produce a restricted workpiece geometry, eg. surfaces of revolution and ruled surfaces. Typical kinematic chains are shown in Figure(3)

The reliability of such an approach is highlighted by the fact that it is only in the wake of the computer that the pioneering ideas of Maudsley[1] and Whitworth[2] are finally being questionned. Even so, the idea of small groups of elements is retained whilst at the same time improved facility is achieved by using more sophisticated controls, with multi-axial arrangements and independent programmable tool storage.

However, it is true to say that wherever the generating principle is used there are circumstances whereby the motion of the tool relative to the workpiece occasionally produces a departure from the desired workpiece geometry, thus precipitating discussions such as the following.

## THE PRODUCTION OF HELICAL SURFACES

Helical surfaces may be produced in a variety of ways depending upon the final requirement in terms of accuracy or component utility, but the most common methods are as follows:

1. Screw helicoid using the lathe
2. Milled helicoid using the milling machine or thread milling machine.
3. Hobbed helicoid with or without using differential mechanisms.
4. Complex helicoids using bevel gear generators.
5. Dual helicoids using a relieving lathe with differential attachment.

Figures (4), (5), (6), (7) and (8) show the kinematic diagrams for each one.

Interference can be present in all these methods in some form or another whether it be the simple case of flank rubbing in case 1, Trochoidal undercutting in cases 3 and 4, or incorrect rake face geometry in case 5.

In all these circumstances, the interference mechanism can be either eliminated by choice of design parameters or cutting tool modification using existing analysis, whereas in the case of the milled helicoid this is not so. It is for such a reason that this kinematic chain is analysed in detail prior to proposing a mathematical model for the interference produced.

GENERATION OF THE MILLED HELICOID

Figure( 5) shows the functional relationship between the disc milling cutter and the workpiece for helical milling while Figure( 5b) shows an end mill used for the same purpose.

The required motion between the tool-workpiece pair is that the work shall rotate at constant velocity while the table translates at constant velocity with the cutter consequently moving through the work at some predetermined depth. The cutter has a rotation at such speed that it will remove metal from the workpiece in the form of a helical groove.

The table receives its motion via a leadscrew and nut while the work rotation is produced by a dividing head of fixed gear ration 40/1, input rotation to this head being provided by a gear train of ratio "R" between the leadscrew and dividing head. It is readily determined that the required ratio is

$$R = \frac{40k/n}{L} = \frac{\text{lead of machine}}{\text{lead to be cut}}$$

where R is the gear ratio to increase or decrease the lead produced on the workpiece

L is the required lead on the workpiece

$\frac{k}{n}$ is the lead of the machine screw.

Alignment between the cutter axis and the helical path is necessary to minimise interference and is achieved by swinging the milling machine table through some appropriate angle. Even so, some pattern of interference is still evident because the helical path in the workpiece is a warped surface and the disc cutter is a rigid body of finite path contact. The deviation by the cutter flank from the true helical path in the slot is the interference pattern. End mills can be used to further minimise the problem since they have a line contact with the slot sides as distinct to the chordal contact of the disc cutter.

Conical workpieces can be produced by inclining the dividing head to the angle of some base cone around which a helical groove is to be machined. This complicates the pattern of interference produced between the workpiece and cutter since the machine table is set to a fixed angle based upon a cylinder of known diameter passing through the cone.

Further changes in the interference mechanism can be produced by offsetting the fluting cutter from the workpiece axis or by changing the shape of the fluting cutter. Some cutter shapes are less susceptible to helical interference than others and the following analysis identifies and quantifies this.

# PART 1 THEORETICAL STUDY

# CHAPTER IV

## THEORY OF HELICAL INTERFERENCE IN A SLOT OF CONSTANT LEAD

### INTRODUCTION

When using disc type cutters for producing milled helicoids of constant lead some pattern of "interference" is almost always present. The only exceptions being the particular cases where a required slot profile is defined and ultimately maintained by designing the mating cutter for conjugate action with the profiled surface[10]. Such action is expensive and, therefore, usually precluded except for certain instances such as in gear manufacture where a gear's design performance dictates what geometric errors will be tolerated. (e.g. worms milled from solid).

For most other cases where milled helicoids are encountered, e.g. barrel mills, end mills, reamers, drills, etc., some compromise is accepted, such that "interference" is minimised. This is usually achieved by careful choice of an available "standard" cutter and an equally careful choice of machine setting procedure; unfortunately such choices are inevitably based on "custom and practice" for the particular workshop and the experience of the tool setter concerned. The tool designer rarely has any control over the final outcome.

In any analysis of the "interference mechanism" using disc cutters for milled helicoids, deference should, therefore, be made to the techniques currently in use. This initial analysis will consequently be examined under the following headings:

Case (a) Straight Sided Disc Cutter Set Over the Axial Centreline of the Workpiece.

Case (b) Form Type Disc Cutter Set Over the Axial Centreline of the Workpiece.

Case (c) Straight Sided Disc Cutter Offset from the Axial Centreline of the Workpiece.

Case (d) Form Type Disc Cutter Offset from the Axial Centreline of the Workpiece.

These are shown diagrammatically in Figures 9(a), (b), (c) and (d).

## (a) STRAIGHT SIDED DISC CUTTER SET OVER THE AXIAL CENTRELINE OF THE WORKPIECE

A careful physical examination of the process indicates that one flank of the helicoidal slot is generated by the cutter's leading edge and the other by the cutters trailing edge and further that there is a cylindrical surface within the workpiece upon which a base generating helix may be considered to be drawn. Points on the cutter which lie below this base cylinder generate a form of helical undercutting, whilst points on the cutter lying above the base cylinder generate a form of helical epicycloid.

The terms "HELITROCHOID" and "EPIHELICYCLOID" will be used to define these curves for given base cylinders.

If the workpiece is considered stationary and all motions are ascribed to the cutter, then the contact path of the cutter with respect to the surface generated must be the locus of a point on the cutter's periphery as it rolls around the base generating helix. The resulting

surface must, therefore, be formed by a non-orthogonal network of these curves and a family of helices.

Figure(10)shows the interdependence of helix angle ($\sigma$) and base cylinder ($D_o$) for maintaining a given constant lead (L). So clearly any change in helix angle set on the machine will produce a related change in base circle diameter, thus giving rise to changes in the geometry of the work-flank profile. Figure(11)shows three particular geometries related to a base generating cylinder,located with respect to the work, in the outer surface, bisecting the slot depth and tangential with the base of the slot respectively.

Normally, the lead and helix angle are defined by the designer, obviously giving a determinable slot profile which invariably has to be modified at shop floor level to give a practicable rake face if the helicoidal gash is to be one tooth space in a cutting tool.

The following theoretical treatment assumes that a base generating cylinder is defined for a given constant lead.

## Theoretical Treatment

### (i) Geometry of Base Helix

From vector differential geometry and considering Figure(12):

For a right handed system

$$\bar{r} = a\cos\theta\ \bar{i} + a\sin\theta\ \bar{j} + b\theta\ \bar{k} \qquad \ldots\ldots\ldots(1)$$

$$\frac{d\bar{r}}{d\theta} = -a\sin\theta\ \bar{i} + a\cos\theta\ \bar{j} + b\ \bar{k} \qquad \ldots\ldots\ldots(2)$$

$$\frac{ds}{d\theta} = \sqrt{a^2 + b^2} \qquad \ldots\ldots\ldots(3)$$

From (2) and (3) the unit tangent vector to the base helix is

$$\bar{T} = \frac{d\bar{r}}{ds} = \frac{-a\sin\theta}{\sqrt{a^2 + b^2}}\,\bar{i} + \frac{a\cos\theta}{\sqrt{a^2 + b^2}}\,\bar{j} + \frac{b}{\sqrt{a^2 + b^2}}\,\bar{k} \qquad \ldots\ldots\ldots(4)$$

$$\frac{d\bar{T}}{ds} = \frac{-a\cos\theta}{a^2 + b^2}\,\bar{i} - \frac{a\sin\theta}{a^2 + b^2}\,\bar{j} \qquad \ldots\ldots\ldots(5)$$

But $\left|\frac{d\bar{T}}{ds}\right| = \kappa = \frac{a}{a^2 + b^2}$

Hence the principal normal radius of curvature of the base helix is given by

$$\rho = \frac{1}{\kappa} = \frac{a^2 + b^2}{a} \qquad \ldots\ldots\ldots(6)$$

From (5) and (6) the normal unit vector to the base helix is

$$\bar{N} = \rho\,\frac{d\bar{T}}{ds} = -(\cos\theta\,\bar{i} + \sin\theta\,\bar{j}) \qquad \ldots\ldots(7)$$

From (5) and (7) the binormal unit vector to the base helix is

$$\bar{B} = \bar{T} \times \bar{N} = \frac{1}{\sqrt{a^2 + b^2}}\left[b\sin\theta\,\bar{i} - b\cos\theta\,\bar{j} + a\,\bar{k}\right] \qquad \ldots\ldots\ldots(8)$$

Consequently the principal binormal radius of curvature is

$$\left|\frac{d\bar{B}}{ds}\right| = \tau = \frac{b}{a^2 + b^2}$$

Therefore $\sigma = \frac{a^2 + b^2}{b}$ $\qquad \ldots\ldots\ldots(9)$

(ii) Locus of Point on Cutter Flank

Figure(13) shows the orthogonal arrangement of the unit vectors relative to the base helix while Figure( 14) demonstrates that each orthogonal axis in the cutter is colinear with one of these base unit vectors as the cutter rolls through the given slot.

It is seen from Figure (15)

$$qq_1 = S = \int_o^\theta \sqrt{a^2 + b^2}\, d\theta = \theta\sqrt{a^2 + b^2}$$

For the rolling condition

$$(R-d)\phi = \theta \sqrt{a^2 + b^2}$$

Therefore $\phi = c\theta = \dfrac{\sqrt{a^2 + b^2}}{(R-d)}\,\theta$ .....(10)

The locus of a point on the cutter's periphery will be defined by the instantaneous position vector $\overline{OP}$

Hence $\overline{OP} = \bar{r}_p = \bar{r}_q + \overline{qo}_1 + \overline{o_1p_1} + \overline{p_1p}$ .....(11)

$$= \bar{r}_q - (R-d)\bar{N} + R\cos\phi\ \bar{N} - R\sin\phi\ \bar{T} + w\ \bar{B}$$

$$= \bar{r}_q + \left[R(1 - \cos c\theta) - d\right]\bar{N} - \left[R \operatorname{Sin} c\theta\right]\bar{T} + \left[w\right]\bar{B}$$

From which the parametric equations can be written

$$x = A_1 \cos\theta + A_2 \sin\theta$$

$$y = A_1 \sin\theta - A_2 \cos\theta \qquad .....(12)$$

$$z = b\theta + A_3$$

where $A_1 = (a - d) + R(1 - \cos c\theta)$

$$A_2 = \frac{bw + Ra \sin c\theta}{\sqrt{a^2 + b^2}}$$

$$A_3 = \frac{aw - Rb \sin c\theta}{\sqrt{a^2 + b^2}}$$

therefore

$$\overline{OP} = (A_1 \cos\theta + A_2 \sin\theta)\ \bar{i} + (A_1 \sin\theta - A_2 \cos\theta)\ \bar{j}$$

$$+ (b\theta + A_3)\ \bar{k} \qquad .....(13)$$

This may be more succinctly written in the matrix form;

$$\begin{bmatrix} x \\ y \\ z \end{bmatrix} = \begin{bmatrix} -\cos\theta & \frac{b\sin\theta}{\sqrt{a^2+b^2}} & \frac{-a\sin\theta}{\sqrt{a^2+b^2}} \\ -\sin\theta & \frac{-b\cos\theta}{\sqrt{a^2+b^2}} & \frac{a\cos\theta}{\sqrt{a^2+b^2}} \\ 0 & \frac{a}{\sqrt{a^2+b^2}} & \frac{b}{\sqrt{a^2+b^2}} \end{bmatrix} \begin{bmatrix} R\cos c\theta \\ w \\ -R\sin c\theta \end{bmatrix} + \begin{bmatrix} (a+R-d)\cos\theta \\ (a+R-d)\sin\theta \\ b\theta \end{bmatrix} \quad ..(14)$$

which is the affine transformation of the cutter system into that of the workpiece and represents either a Helitrochoid or Epihelicycloid of a helix with base cylinder radius "a" and constant lead $2\pi b$, depending upon the value taken by the parameter "d".

(b) FORM TYPE DISC CUTTER SET OVER THE AXIAL CENTRELINE OF THE WORKPIECE

In the case of a profiled cutter the contact path between the generated flank profile and the cutter is clearly some function of the cutter section. This is shown by considering Figure(16)and Figure(17).

If the profile of the cutter is considered as being formed by a series of infinitely thin discs of varying radius then each disc will generate its own peripheral locus as it rolls along the slot. The envelope of this group of curves must, therefore, determine the shape of the final groove. The red line ab in Figure(16) is the line along which the envelope would be constructed and may be considered as the line along which a point in the cutter surface moves as the disc rolls along the base helix. This is clearly the contact path made between the profiled flank of the disc and the resulting slot.

Referring to Figure(15)it is apparent that the instantaneous vector $\overline{OP}$ will be dependent upon the profile shape for the given disc cutter and is defined by the vector equation

$$\overline{OP} = \overline{r_p} = \overline{r_q} + \overline{qo_1} + \overline{o_1p_1} + (\text{Shape function})\ \bar{B} \qquad \ldots\ldots\ldots(15)$$

The "shape function" necessarily varies with the profile of the disc cutter used, but is usually independent of the angle $\phi$ turned through as the disc rolls along the base helix. Considering the case of the semi-circular profile shown in Figure(18)the instantaneous width of the cutter ($w'$) at the path of contact is

$$w' = r \sin \delta \qquad \ldots\ldots\ldots(16)$$

where r = profile radius

R = cutter radius

$\delta$ = is a parameter of cutter shape

This means that the previous equations (12) and (13) only differ from equation (15) by the "shape function" and consequently the matrix statement would be modified as follows

$$\begin{bmatrix} x \\ y \\ z \end{bmatrix} = \begin{bmatrix} -\cos\theta & \dfrac{b\sin\theta}{\sqrt{a^2+b^2}} & \dfrac{-a\sin\theta}{\sqrt{a^2+b^2}} \\ -\sin\theta & \dfrac{-b\cos\theta}{\sqrt{a^2+b^2}} & \dfrac{a\cos\theta}{\sqrt{a^2+b^2}} \\ 0 & \dfrac{a}{\sqrt{a^2+b^2}} & \dfrac{b}{\sqrt{a^2+b^2}} \end{bmatrix} \begin{bmatrix} X' \\ (\text{cutter}) \\ (\text{Shape} \\ \text{Factor}) \\ Z' \\ (\text{cutter}) \end{bmatrix} + \begin{bmatrix} (a+R-d)\cos\theta \\ (a+R-d)\sin\theta \\ b\theta \end{bmatrix} \qquad \ldots\ldots(17)$$

The 3 by 1 matrix defined by the vector

$$\bar{r}_c = X'(\text{cut})\ \bar{N} - Z'(\text{cut})\ \bar{T} + (\text{Shape factor})\ \bar{B} \qquad \ldots\ldots\ldots(18)$$

is clearly the contact path co-ordinates defined in the framework of the cutter itself and will vary with the shape of the cutter profile as equation (16) shows.

For the particular case of the semi-circular form (Figure(19))

$$\bar{r}_c = (\text{x cutter})\ \bar{N} + (\text{z cutter})\ \bar{T} + (r \sin\delta)\ \bar{B} \qquad \ldots\ldots\ldots(19)$$

and for the other commonly occurring shape, namely, the vee section cutter of semi-angle $\delta$ the vector statement in the cutter framework is

$$\bar{r}_c = (\text{x cutter})\ \bar{N} + (\text{z cutter})\ \bar{T} + (h \tan\delta)\ \bar{B} \qquad \ldots\ldots\ldots(20)$$

where h is an arbitrary constant.

(c) STRAIGHT SIDED DISC CUTTER OFFSET FROM THE AXIAL CENTRELINE OF THE WORKPIECE

For an offset cutter the geometric relationship between the base helix and the cutter axes is as shown in Figure(20) and an equivalent system is described by the rotated axis arrangement of Figure(21)

From the vector algebra, transformation from the cutter system into that of the work is

$$\begin{aligned}
\bar{b}' &= (\bar{b}'\cdot\bar{B})\ \bar{B} + (\bar{b}'\cdot\bar{N})\ \bar{N} + (\bar{b}'\cdot\bar{T})\ \bar{T} \\
\bar{n}' &= (\bar{n}'\cdot\bar{B})\ \bar{B} + (\bar{n}'\cdot\bar{N})\ \bar{N} + (\bar{n}'\cdot\bar{T})\ \bar{T} \qquad \ldots\ldots\ldots(21) \\
\bar{t}' &= (\bar{t}'\cdot\bar{B})\ \bar{B} + (\bar{t}'\cdot\bar{N})\ \bar{N} + (\bar{t}'\cdot\bar{T})\ \bar{T}
\end{aligned}$$

Hence for the system of Figure(21) the required relationships are

$$\begin{aligned}
\bar{b}' &= \cos\beta\ \bar{B} - \sin\beta\ \bar{N} \\
\bar{n}' &= \sin\beta\ \bar{B} + \cos\beta\ \bar{N} \qquad \ldots\ldots\ldots(22) \\
\bar{t}' &= \bar{T}
\end{aligned}$$

Substituting the values of $\bar{N}$ $\bar{B}$ and $\bar{T}$ into equation (22)

$$\begin{aligned}
\bar{b}' &= (p_1 \sin\theta + q_1 \cos\theta)\ \bar{i} + (-p_1 \cos\theta + q_1 \sin\theta)\ \bar{j} + (s_1)\bar{k} \\
\bar{n}' &= (p_2 \sin\theta - q_2 \cos\theta)\ \bar{i} - (p_2 \cos\theta + q_2 \sin\theta)\ \bar{j} + (s_2)\bar{k} \qquad ..(23) \\
\bar{t}' &= (-p_3 \sin\theta)\ \bar{i} + (p_3 \cos\theta)\ \bar{j} + (s_3)\ \bar{k}
\end{aligned}$$

where the values of $p_1$ $p_2$ $q_1$ $q_2$ etc. are

$$p_1 = \frac{b\cos\beta}{\sqrt{a^2 + b^2}} \qquad q_1 = \sin\beta \qquad s_1 = \frac{a\cos\beta}{\sqrt{a^2 + b^2}}$$

$$p_2 = \frac{b\sin\beta}{\sqrt{a^2 + b^2}} \qquad q_2 = \cos\beta \qquad s_2 = \frac{a\sin\beta}{\sqrt{a^2 + b^2}} \qquad \ldots\ldots(24)$$

$$p_3 = \frac{a}{\sqrt{a^2 + b^2}} \qquad s_3 = \frac{b}{\sqrt{a^2 + b^2}}$$

From Figure(22)the locus of a point on the cutter periphery will be given by the locus of the instantaneous vector $\overline{OP}$

Hence $\overline{OP} = \bar{r}_p = \bar{r}_q + \overline{qo}_1 + \overline{o_1p_1} + \overline{p_1p}$

$$= \bar{r}_q + \left[R\ (1 - \cos\theta) - d\right]\bar{n}' - \left[R\sin\theta\right]\bar{t}' + w\,\bar{b}'$$

The required transformation matrix representing this equation is

$$\begin{bmatrix} x \\ y \\ z \end{bmatrix} = \begin{bmatrix} -(p_2\sin\theta - q_2\cos\theta) & (p_1\sin\theta + q_1\cos\theta) & -(p_3\sin\theta) \\ -(p_2\cos\theta + q_2\sin\theta) & (-p_1\cos\theta + q_2\sin\theta) & (p_3\cos\theta) \\ s_2 & s_1 & s_3 \end{bmatrix} \begin{bmatrix} R\cos c\theta \\ w \\ -R\sin c\theta \end{bmatrix} + \begin{bmatrix} (a+R-d)\cos\theta \\ (a+R-d)\sin\theta \\ b\theta \end{bmatrix} \qquad ..(25)$$

N.B. Upon examination, if angle $\beta$ is zero then this matrix statement reduces to the same form as that of the transformation (14)

(d) FORM TYPE DISC CUTTER OFFSET FROM THE AXIAL CENTRELINE OF THE WORKPIECE

The most general case will be that of an offset form cutter and it is readily deduced that the required transformation will be

$$\begin{bmatrix} x \\ y \\ z \end{bmatrix} = \begin{bmatrix} l_{11} & l_{12} & l_{13} \\ l_{21} & l_{22} & l_{23} \\ l_{31} & l_{32} & l_{33} \end{bmatrix} \begin{bmatrix} x' \\ \text{(Shape Function)} \\ z' \end{bmatrix} + \begin{bmatrix} a_1 \\ a_2 \\ a_3 \end{bmatrix} \quad \ldots\ldots(26)$$

where x y z = Workpiece system

$l_{ij}$ = Direction cosines made by $\bar{b}'$ $\bar{n}'$ $\bar{t}'$

x' y' z' = Contact path co-ordinates in cutter system

$a_1$ $a_2$ $a_3$ = Co-ordinates of cutter centre in workpiece system

Obviously the three previous results can be derived from the above generalised case.

# CHAPTER V

## GEOMETRY OF THE INTERFERENCE SURFACE

### THE INTERFERENCE SURFACE FOR DISC CUTTER SET OVER AXIAL CENTRELINE

A knowledge of the surface geometry is important because most engineering components utilising the milled helicoid are either required to transmit motion or to act as a cutting tool. In both cases it is usually necessary to construct normal and tangent planes to the generated surface for the purposes of either motion analysis or rake angle determination.

In general a surface is described by a network of two individual families of curves which do not intersect within the family but intersect with the other family orthogonally, or non-orthogonally depending upon the individual characteristics. The respective families are designated "u" curves and "v" curves having a common base point $(u_o, v_o)$ and intersection co-ordinates (u, v). At any such point (u,v) a tangent plane may be constructed containing the two directional derivatives $\frac{\partial \bar{r}}{\partial v}$ with u = c and $\frac{\partial \bar{r}}{\partial u}$ with v = c. Clearly a normal to the plane at this point will be $\frac{\partial \bar{r}}{\partial u} \times \frac{\partial \bar{r}}{\partial v}$ and is shown in Figure(23), together with the tangent plane.

The surface generated by the disc cutter in a helical slot will be a non-orthogonal network of "u" curves defining circular helices and "v" curves defining helitrochoids or epihelicycloids of a base helix. Figure(24) shows the network while Figure(25) is a projection of the

surface into the xy plane because, provided a starting point "$u_p$" for a given helix is chosen on the "$v_o$" curve, then the helix constructed around a cylinder of radius "a" will contain all the other points "$u_p$" on the respective $u_1$ .... $u_n$ curves, and will project into xy as shown.

If the point "$u_p$" is specified in the cartesian framework of the surface by $x_o$ $y_o$ $z_o$ and a general point along the helix upon this cylindrical surface by x y z, then it is possible to develop the parametric equations of the surface in terms of a radius vector in the xy plane, the angle "$\delta$" swept out in this plane and the lead constant "b". Figure (26) is a rotated axes system equivalent to the surfaces projection into the xy plane where "p" is a general point on the helix wound on a cylinder of radius $|\bar{a}|$; this point is invariant under the rotation. The point $x_o$ $y_o$ is a projection of a point lying on the epihelicycloid "$v_o$" and the rotated axes contain the point $(x_o\ y_o)$ and $(-y_o\ x_o)$.

Vector $\bar{a}$ makes an angle "$\alpha$" with the x' y' axes and these in turn make an angle "$\delta$" with the cartesian frame of the surface xy.

Since "p" is invariant under the rotation the required transformation is

$$x = (\bar{i}'\cdot\bar{i})\ x' + (\bar{j}'\cdot\bar{i})\ y' = x_o \cos\delta - y_o \sin\delta$$

$$y = (\bar{i}'\cdot\bar{j})\ x' + (\bar{j}'\cdot\bar{j})\ y' = y_o \cos\delta + x_o \sin\delta \qquad \text{.....(27)}$$

These equations are clearly of the A sin $(\delta-\alpha)$ form and can be written as

$$x = -A \sin(\delta-\alpha)$$

$$y = A \cos(\delta-\alpha) \qquad \text{.....(28)}$$

where $A = |\bar{a}|$ $\qquad\qquad \alpha = \tan^{-1}\dfrac{y_o}{x_o}$

Obviously the remaining parametric equations will have the form

$$z = A_3 + b(\delta + \alpha) \qquad \ldots\ldots\ldots(29)$$

From the previous geometry the magnitude of the vector $\bar{a}$ will be given by reference to equation (12).

i.e.

$$|\bar{a}| = \sqrt{(A_1 \cos\theta + A_2 \sin\theta)^2 + (A_1 \sin\theta - A_2 \cos\theta)^2}$$

$$= \sqrt{A_1^2 + A_2^2} \qquad \ldots\ldots\ldots(30)$$

The vector equation for the surface becomes, therefore

$$\bar{r}_p = -\left[|\bar{a}| \sin(\delta-\alpha)\right] \bar{i} + \left[|\bar{a}| \cos(\delta-\alpha)\right] \bar{j} + \left[A_3 + b(\delta-\alpha)\right] \bar{k} \quad ..(31)$$

where $\alpha$ $A_1$ and $A_2$ are all functions of the parameter $\theta$.

THE TANGENT PLANE TO THE SURFACE

The tangent plane at any point on the surface will contain the directional derivatives along the two network curves that intersect at the point chosen and for the surface under consideration the two variable parameters concerned are $\theta$ for the "v" curves and $\delta$ for the "u" curves. Obviously the directional derivative along the helix will be

From equations (27) and (29)

$$\bar{r}_p = (x\cos\delta - y\sin\delta)\,\bar{i} + (x\sin\delta + y\cos\delta)\,\bar{j} + (Z + b\delta)\,\bar{k} \quad ..(32)$$

$$\frac{\partial \bar{r}}{\partial \delta} = -(x\sin\delta + y\cos\delta)\,\bar{i} + (x\cos\delta - y\sin\delta)\,\bar{j} + (b)\,\bar{k}$$

$$= -\left[r\cos(\delta-\alpha)\right]\bar{i} - \left[r\sin(\delta-\alpha)\right]\bar{j} + \left[b\right]\bar{k} \qquad \ldots\ldots\ldots(33)$$

The directional derivative along the helitrochoid will be

$$\frac{\partial \bar{r}}{\partial \theta} = \left[\frac{\partial x}{\partial \theta}\cos\delta - \frac{\partial y}{\partial \theta}\sin\delta\right]\bar{i} + \left[\frac{\partial x}{\partial \theta}\sin\delta + \frac{\partial y}{\partial \theta}\cos\delta\right]\bar{j} + \left[\frac{\partial z}{\partial \theta}\right]\bar{k}$$

$$= \left[B_1 \cos\delta - B_2 \sin\delta\right] \bar{i} + \left[B_1 \sin\delta + B_2 \cos\delta\right] \bar{j} + \left[B_3\right] \bar{k}$$

$$= -\left[r_1 \sin(\delta-\beta)\right] \bar{i} + \left[r_1 \cos(\delta-\beta)\right] \bar{j} + \left[B_3\right] \bar{k} \quad \ldots\ldots\ldots(34)$$

where $\alpha = \tan^{-1}\left[y/x\right]$ $\qquad r = \sqrt{x^2 + y^2}$

$\beta = \tan^{-1}\left[B_2/B_1\right]$ $\qquad r_1 = \sqrt{B_1^2 + B_2^2}$

THE UNIT NORMAL TO THE SURFACE

As previously stated a normal to the surface will be given by the vector statement $\frac{\partial \bar{r}}{\partial \delta} \times \frac{\partial \bar{r}}{\partial \theta}$

i.e.

$$\bar{N}_i = \frac{\partial \bar{r}}{\partial \delta} \times \frac{\partial \bar{r}}{\partial \theta} = \begin{vmatrix} \bar{i} & \bar{j} & \bar{k} \\ -r\cos(\delta-\alpha) & -r\sin(\delta-\alpha) & b \\ -r_1 \sin(\delta-\beta) & r_1 \cos(\delta-\beta) & B_3 \end{vmatrix}$$

Therefore

$$\bar{N}_i = \left[-C_1 \sin(\delta-\alpha) + C_2 \cos(\delta-\beta)\right] \bar{i} + \left[C_1 \cos(\delta-\alpha) - C_2 \sin(\delta-\beta)\right] \bar{j} - \left[C_3 \cos(\beta-\alpha)\right] \bar{k} \quad ..(35)$$

where $C_1 = B_3 r \qquad C_2 = b r_1 \qquad C_3 = r r_1$

and a unit normal inwards from the surface will be

$$\frac{\bar{N}_i}{|N_i|} = \frac{Nx\,\bar{i} + Ny\,\bar{j} + Nz\,\bar{k}}{\sqrt{Nx^2 + Ny^2 + Nz^2}}$$

where Nx, Ny and Nz have meanings derived from equation (35).

THE EQUATION OF THE TANGENT PLANE

From Figure(27)

$$\bar{r} = x\bar{i} + y\bar{j} + z\bar{k}$$

$$\bar{r}_o = x_o\bar{i} + y_o\bar{j} + z_o\bar{k}$$

Hence

$$\bar{OA} = \bar{r} - \bar{r}_o = (x - x_o)\,\bar{i} + (y - y_o)\,\bar{j} + (z - z_o)\,\bar{k}$$

and by vector algebra the equation of the plane will be

$$(\bar{r} - \bar{r}_o)\cdot\bar{N} = 0 \qquad \text{.....(36)}$$

from which the required scalar equation is derived

i.e.

$$(x - x_o)\,N_x + (y - y_o)\,N_y + (z - z_o)\,N_z = 0 \qquad \text{.....(37)}$$

THE NORMAL PLANE

The equation of a normal plane will be given by

$$\overline{pq}_2 \cdot (\bar{N} \times \overline{pq}_1) = 0$$

where $\overline{pq}_2$ and $\overline{pq}_1$ take particular values depending upon whether the normal plane is perpendicular to the YZ plane or it contains the normal and binormal vector to the surface. The former is called the BASE NORMAL plane and the latter the TRUE NORMAL plane.

THE TRUE NORMAL PLANE

When it is required to calculate a true normal rake angle at a point, it is necessary to construct the plane which contains the unit normal, the unit binormal, and a radial to the point considered.

From Figure(28)the necessary condition for this plane is

$$\overline{pq}_2 \cdot (\bar{N} \times \bar{B}) = 0 \qquad \text{.....(38)}$$

where

$$\overline{pq}_2 = (x - x_o)\,\bar{i} + (y - y_o)\,\bar{j} + (z - z_o)\,\bar{k}$$

$$\bar{N} = (N_x)\,\bar{i} + (N_y)\,\bar{j} + (N_z)\,\bar{k}$$

$$\bar{B} = (B_x)\,\bar{i} + (B_y)\,\bar{j} + (B_z)\,\bar{k}$$

From which the vector equation of the plane may be stated as

$$\overline{pq_2} \cdot (\bar{N} \times \bar{B}) = \begin{vmatrix} (x-x_o) & (y-y_o) & (z-z_o) \\ N_x & N_y & N_z \\ B_x & B_y & B_z \end{vmatrix} = 0 \qquad \ldots\ldots(39)$$

and the required scalar is

$$(x-x_o)(N_yB_z-N_zB_y) - (y-y_o)(N_xB_z-N_zB_y) + (z-z_o)(N_xB_y-N_yB_x) = 0 \qquad ..(40)$$

RAKE ANGLE DETERMINATION

In order to determine the rake angle at a point it is necessary to determine vector $\overline{pq}_2$ which is the required radial.

From Figure(29), the line of the intersection will be given by

$$\begin{vmatrix} -x_o & (y-y_o) & (z-z_o) \\ N_x & N_y & N_z \\ B_x & B_y & B_z \end{vmatrix} = 0 \qquad \ldots\ldots(41)$$

and the point of intersection with the z axis is

$$\begin{vmatrix} -x_o & -y_o & (z-z_o) \\ N_x & N_y & N_z \\ B_x & B_y & B_z \end{vmatrix} = 0 \qquad \ldots\ldots(42)$$

From which the required scalar intercept is derived.

$$z_i = x_o \left[\frac{N_yB_z - N_zB_y}{N_xB_y - N_yB_x}\right] - y_o \left[\frac{N_xB_z - N_zB_x}{N_xB_y - N_yB_x}\right] + z_o \qquad \ldots\ldots(43)$$

It is evident from Figure(30) that the true radial rake angle is the angle made by $\overline{pq}_2$ with the tangent plane, namely the angle $\Psi$.

where $$\Psi = 90 - \eta \qquad \text{.....(44)}$$

and $$\cos \eta = \frac{\bar{N} \cdot \overline{pq}_2}{|\bar{N} \cdot \overline{pq}_2|} \qquad \text{.....(45)}$$

THE INTERSECTION CURVE OF THE SURFACE IN XY

A further curve of interest which can be derived from the surface is the intersection curve made with a transverse plane of which the simplest is that xy plane which contains all the points z = 0

From equation 31 the required parametric equations of the surface are

$$x = \sqrt{A_1^2 + A_2^2} \sin(\delta - \alpha)$$

$$y = \sqrt{A_1^2 + A_2^2} \cos(\delta - \alpha) \qquad \text{.....(46)}$$

$$z = A_3 + b(\delta + \alpha)$$

For the condition z = 0 the required intersection will be given by translation of a point on a line of constant "α" along a given helix, i.e.

$$0 = A_3 + b(\delta + \alpha)$$

$$\delta = -A_3/b - \alpha = -(A_4 + \alpha)$$

Clearly this is a negative rotation into the xy plane and it is easily deduced that the required intersection equations are

$$x = -A \sin(\delta - \alpha)$$

$$y = A \cos(\delta - \alpha) \qquad \text{.....(47)}$$

where

$$A = \sqrt{A_1^2 + A_2^2} \qquad \text{Tan } \alpha = \frac{y}{x} \qquad \delta = -(A_4 + \alpha)$$

The transverse intersection curve is probably the most widely used plane section in practical cases since it is normally the plane of rotation irrespective of whether the helical groove is part of a transmission system, or the tooth space in a milling cutter. For the latter use it is important to be able to derive the rake angle at any such point in this plane.

From Figure(31), therefore, the rake angle "ψ" is given by

$$\frac{\frac{d\bar{r}}{ds} \cdot \bar{re}_r}{\left|\frac{d\bar{r}}{ds} \cdot \bar{re}_r\right|} = \cos \psi \qquad \ldots\ldots\ldots(48)$$

where $\bar{re}_r$ is the position vector in a radial co-ordinate system and $\frac{d\bar{r}}{ds}$ is the tangent vector to the intersection curve.

From equation 47 the position vector for the intersection curve is given by

$$\bar{r} = -\left[A \sin (-A_4-2\alpha)\right] \bar{i} + \left[A \cos (-A_4-2\alpha)\right] \bar{j}$$

and the unit tangent to the curve is

$$\bar{T} = \frac{d\bar{r}}{ds} = \frac{d\bar{r}}{d\theta} \frac{d\theta}{ds} \qquad \ldots\ldots\ldots(49)$$

which has similar meaning in the transverse plane to the directional derivative $\frac{\partial \bar{r}}{\partial \theta}$ in the normal plane,

while

$$(r)\bar{e}_r = \sqrt{A_1^2 + A_2^2}\, \bar{e}_r$$

$$= -\left[\sqrt{A_1^2 + A_2^2} \sin (-A_4-2\alpha)\right] \bar{i} + \left[\sqrt{A_1^2 + A_2^2} \cos (-A_4-2\alpha)\right] \bar{j} \qquad \ldots\ldots\ldots(50)$$

while the co-efficients $A_1$ and $A_2$ have the previously described meanings.

# CHAPTER VI

## THEORY OF HELICAL INTERFERENCE IN SLOTS OF VARYING LEAD

### INTRODUCTION

There are a group of problems primarily concerned with tool engineering where the interference mechanism becomes complex owing to the fact that the lead of the helicoid changes from point to point. This obviously gives rise to an interference surface whose geometry is some function of a variable lead.

One such case was examined by Etheridge and Waynham[17] where the interference mechanism was shown "qualitatively" for the case of helically fluted conical cutters of constant lead. This particular example more than adequately demonstrated the totally destructive nature of the interference mechanism when variations in lead or geometry are encountered. In this instance the effect of changing radius coupled with constant lead produced a varying interference pattern as the section diameter changed. Plate II and Figure (32) show typical workpieces.

Thornley[18] described Mabbon and Sabberwal's[19] work with helically fluted cylindrical slab mills of varying lead and a test piece reproducing the effect is shown in Plate III. Here once again the use of a disc cutter yields a totally inadequate rake face on a cutting tool when a shortening helix is encountered, whereas a positive radial rake angle is achieved if a disc cutter is used in a slot where the helix is lengthening. The rake angle will vary from point to point in such a cutting tool as

Sabberwal demonstrated[20] during his investigations. This is readily appreciated by comparing the two workpieces in Plate III where the effect of lengthening helix is seen in the right hand frame, and shortening helix in the left hand frame. Mabbon and Sabberwal, however, used end mills to minimise interference and consequently produced a surface which was a non-orthogonal network of straight lines and helices, while the workpiece shown in Plate III for the lengthening helix is a network of helitrochoids and helices of variable lead as a direct consequence of using the disc cutter.

Etheridge and Waynham in their study demonstrated a correcting mechanism which effectively increased the rate of rotation of the conical specimen for a given constant lead, so that the helix angle was maintained constant at any diameter of the cone. This corrective measure gave rise to a pattern of interference similar to that for constant lead cylindrical work.

The superposed rotation was achieved by using an attachment to the conventional dividing head which consisted of a bevel gear differential whose cage was rotated by a cam follower, the work being attached to the output side of the mechanism. This device made by Waynham is shown in Plate IV.

Mabbon and Sabberwal"s device[19] similarly was an attachment to the dividing head and consisted essentially of a connecting rod driving the work on a parallel axis through a variable rise cam mounted on the work table and driven by the dividing head chuck. Although independently proposed both mechanisms are essentially variable lead attachments whose cam profiles are determined by empirical or semi-graphical techniques.

It is possible, however, to define analytical procedures for determining the magnitude of the superposed rotation for particular variations in lead and these are developed as part of this work. Since there are many different lead forms which can be produced, the theoretical treatment will be restricted to an analysis of that superposed rotation required to maintain the helix angle constant along a conical workpiece surface.

Whilst a complete analysis of conical cases lies outside the scope of this text, the lead form derived for this situation will be used to develop a theory of interference for cylindrical workpieces of variable lead.

## ANALYSIS FOR THE SUPERPOSED ROTATION

### (a) THE CONICAL WORKPIECE

The limitations imposed by the design of the conventional milling machine and dividing head are such that only helices of uniform lead can be produced and further the table must be set to a predetermined helix angle of constant magnitude. This setting angle defines the base generating cylinder referred to in Chapter III.

Clearly, if a helical flute is to be machined in a conical workpiece, the physical cutter is aligned relative to some path on the cone, while the framework containing the cutter is moving along a cylindrical helix defined by the setting parameters. Figures (33) and (34) show the system and it is readily deduced that the framework containing the cutter system is colinear with the BINORMAL, NORMAL and TANGENTIAL unit vector directions of the CIRCULAR HELIX. The contact path of the cutter, however, is

defined by the conical helix traced out on the base generating surface and the orthogonal axes of the cutter's centre are colinear with the BINORMAL, NORMAL and TANGENTIAL unit vector directions to the CONICAL HELIX. It will be shown that this curve is an Archimedian Helix of uniform lead.

Theoretical Treatment

(i) Archimedian Helix

Consider the element shown in Figure(35)

$$\frac{dr}{dz} = \tan\gamma = m$$

where m is the slope of the semi-cone

therefore

$$dr = m\, dz$$

where $dz = b\, d\theta$ since the workpiece has a constant lead

therefore

$$dr = m\, b\, d\theta$$

integrating

$$r = m\, b\, \theta = a_o\theta \qquad \text{.....(51)}$$

This is the equation of the plane Archimedian Spiral and the vector equation of the base cone helix is seen to be

$$\bar{r}_1 = r\bar{e}_r + b\theta\bar{e}_z$$

$$= a_o\theta\bar{e}_r + b\theta\bar{e}_z \qquad \text{.....(52)}$$

The axes passing through the cutter centre are colinear with the following unit vector directions i.e. $\bar{b}'$, $\bar{n}'$, $t'$.

$$\bar{b}' = \frac{-B1\,\bar{e}_r - B2\,\bar{e}_\theta + B3\,\bar{e}_z}{\left[a_o^2(1+\theta^2) + b^2\right]\sqrt{a_o^2(2+\theta^2)^2 + b^2(4+\theta^2)}}$$

where

$$B1 = -2a_o b\left[a_o^2(1+\theta^2) + b^2\right]\bar{e}_r$$

$$B2 = ba_o\theta\left[a_o^2(1+\theta^2) + b^2\right]\bar{e}_\theta$$

$$B3 = a_o^2(1+\theta^2)\left[a_o^2(2+\theta^2) + b^2\right]\bar{e}_z$$

$$\bar{n}' = \frac{-N1\,\bar{e}_r + N2\,\bar{e}_\theta - N3\,\bar{e}_z}{\sqrt{a_o^2(1+\theta^2) + b^2}\,\sqrt{a_o^2(2+\theta^2)^2 + b^2(4+\theta^2)}}$$

where

$$N1 = -a_o\theta\left[a_o^2(2+\theta^2) + b^2\right]\bar{e}_r$$

$$N2 = a_o\left[a_o^2(2+\theta^2) + 2b^2\right]\bar{e}_\theta$$

$$N3 = -\left[ba_o^2\,\theta\right]\bar{e}_z$$

$$\bar{t}' = \frac{a_o\bar{e}_r + a_o\theta\bar{e}_\theta + \bar{e}_z}{\sqrt{a_o^2(1+\theta^2) + b^2}}$$

It will now be shown that the necessary correction will be logarithmic in nature in order to maintain a constant helix angle on the surface of the cone; at the same time ensuring colinearity of the moving cutter framework and the cutter axes. (Figure 36).

(ii) Logarithmic Helix

The superposed rotation when used to correct conical cutters must be such that the helix angle on the base cone is constant. Consider the element shown in Figure 37

$$\cos\sigma = \frac{dz'}{oc} \qquad \text{.....(53)}$$

where $\sigma$ is the defined constant helix angle.

$$dz' = \sqrt{m^2 + 1}\, dz \qquad \text{.....(54)}$$

where m is the slope of the semi-cone.

now $oc^2 = ob^2 + bc^2$

therefore

$$oc^2 = dr^2 + dz^2 + r^2 d\theta^2 \qquad \text{.....(55)}$$

Substituting (54) and (55) into (53)

$$\cos\sigma = \frac{\sqrt{m^2 + 1}\, dz}{\sqrt{dr^2 + dz^2 + r^2 d\theta^2}}$$

which becomes upon squaring

$$c^2 = \frac{A^2\, dz}{dr^2 + dz^2 + r^2 d\theta^2}$$

where c and A have obvious meanings.

Therefore

$$c^2 m^2 \left[\frac{dz}{d\theta}\right]^2 + c^2 \left[\frac{dz}{d\theta}\right]^2 + c^2 r^2 = A^2 \left[\frac{dz}{d\theta}\right]^2$$

Collecting terms and taking the square root yields

$$B \frac{dz}{d\theta} = C(r_o + mz) \qquad \text{.....(56)}$$

where

$$B = \sqrt{(m^2 + 1) \sin^2\sigma}$$

therefore

$$\theta = \frac{B}{cm} \log_e \left[r_o + mz\right] + K_1 \qquad \text{.....(57)}$$

But at $z = 0$ $\theta = 0$

therefore

$$K_1 = \frac{B}{cm} \log_e r_o$$

The required superposed rotation is, therefore

$$\theta = D \log_e \left[ 1 + \frac{mz}{r_o} \right] \qquad \ldots\ldots\ldots(58)$$

where

$$D = \frac{B}{cm}$$

and B, c and m have their previously ascribed meanings.

Equation (58) may be rewritten in its exponential form as follows:

$$e^{\frac{\theta}{D}} = 1 + \frac{mz}{r_o} \qquad \ldots\ldots\ldots(59)$$

and it follows that

$$r_o + mz = r_o e^{\frac{\theta}{D}}$$

But $r_o + mz$ is the instantaneous radius (r) of the cone at any point. Therefore

$$r = r_o e^{k\theta} \qquad \ldots\ldots\ldots(60)$$

This is easily recognised as the polar equation of the plane logarithmic spiral.

(b) THE CYLINDRICAL WORKPIECE

When the logarithmic rotation is superposed for a cylindrical workpiece the cutter is aligned relative to a constant lead circular helix. i.e. the cutters principal axes are colinear with the BINORMAL ($\bar{B}$), NORMAL ($\bar{N}$) and TANGENTIAL ($\bar{T}$) unit vectors to this helix. The workpiece, however, owing to the superposed rotation is moving in such a way that a logarithmic helix is traced out on a base generating cylinder of radius $r_o$ and there is clearly a moving unit vector triad of BINORMAL ($\bar{b}'$)

NORMAL ($\bar{n}'$) and TANGENT ($\bar{t}'$) vectors to this logarithmic helix. As this triad moves along the base logarithmic helix the cutter axes make particular direction cosines with the moving frame and a point on the cutter's periphery has to be transformed from $\bar{B}\bar{N}\bar{T}$ directions through $\bar{b}'\bar{n}'\bar{t}'$ and into the cartesian reference frame xyz. The inter-relationship between these is shown in Figure (38).

Whilst these basic relationships remain the same irrespective of whether an end mill or a disc cutter is used the surface geometry will inevitably be different owing to the distinctly individual patterns of motion of each cutter within its own reference frame. This is shown in Figures (39) and (40).

Theoretical Treatment

(i) Geometry of Base Logarithmic Helix.

From equation (59) the vector equations for the required helix in a radial co-ordinate system are

$$\bar{r} = r_o \bar{e}_r + \frac{r_o}{m}\left[e^{k\theta} - 1\right]\bar{e}_z \qquad \ldots\ldots\ldots(61)$$

and

$$\frac{d\bar{r}}{d\theta} = r_o \bar{e}_\theta + Ae^{k\theta}\,\bar{e}_z \qquad \ldots\ldots\ldots(62)$$

therefore

$$\frac{ds}{d\theta} = \sqrt{r_o^{\,2} + A^2 e^{2k\theta}} \qquad \ldots\ldots\ldots(63)$$

and

$$\bar{t}' = \frac{d\bar{r}}{ds} = \frac{r_o \bar{e}_\theta + Ae^{k\theta}\,\bar{e}_z}{\sqrt{r_o^{\,2} + A^2 e^{2k\theta}}} \qquad \ldots\ldots\ldots(64)$$

where $A = \frac{kr_o}{m}$ and $k = \frac{cm}{\sqrt{m^2 + 1}\ \sin\sigma}$

From equations (62) and (63) the normal unit vector will be

$$\bar{n}' = \frac{d\bar{t}'}{ds} \Big/ \left| \frac{d\bar{t}'}{ds} \right|$$

therefore

$$\bar{n}' = \frac{-\left[r_o^2 + A^2e^{2k\theta}\right]\bar{e}_r - \left[kA^2e^{2k\theta}\right]\bar{e}_\theta + \left[r_o kAe^{k\theta}\right]\bar{e}_z}{\sqrt{r_o^2 + A^2e^{2k\theta}}\ \sqrt{r_o^2 + (k^2+1)\,A^2e^{2k\theta}}} \qquad \ldots\ldots\ldots(65)$$

and

$$\bar{b}' = \bar{t}' \times \bar{n}'$$

$$= \frac{\left[kAe^{k\theta}\right]\bar{e}_r - \left[Ae^{k\theta}\right]\bar{e}_\theta + \left[r_o\right]\bar{e}_z}{\sqrt{r_o^2 + (k^2+1)\,A^2e^{2k\theta}}} \qquad \ldots\ldots\ldots(66)$$

Equations (61) to (66) describe the situation for a lengthening logarithmic lead, but it is also possible to determine a group of equations for when a shortening lead is required.

From equation (59)

$$e^{-k\theta} = 1 - \frac{mz}{r_o}$$

therefore

$$z = \frac{r_o}{m}\left[1 - e^{-k\theta}\right]$$

and the required vector equations will be

$$\bar{r} = r_o\bar{e}_r + \frac{r_o}{m}\left[1 - e^{-k\theta}\right]\bar{e}_z$$

and

$$\frac{d\bar{r}}{d\theta} = \sqrt{r_o^2 + A^2e^{-2k\theta}}$$

where A and k have previously defined meanings.

The unit vector triad for this system is

$$\bar{t}_1' = \frac{r_o \bar{e}_\theta + Ae^{-k\theta} \bar{e}_z}{\sqrt{r_o^2 + A^2 e^{-2k\theta}}} \qquad \ldots\ldots(67)$$

$$\bar{n}_1' = \frac{-\left[r_o^2 + A^2 e^{-2k\theta}\right] \bar{e}_r + \left[kA^2 e^{-2k\theta}\right] \bar{e}_\theta - \left[r_o kAe^{-k\theta}\right] \bar{e}_z}{\sqrt{r_o^2 + A^2 e^{-2k\theta}} \sqrt{r_o^2 + (k^2 + 1) A^2 e^{-2k\theta}}} \qquad \ldots(68)$$

$$\bar{b}_1' = \frac{-\left[kAe^{-k\theta}\right] \bar{e}_r - \left[Ae^{-k\theta}\right] \bar{e}_\theta + \left[r_o\right] \bar{e}_z}{\sqrt{r_o^2 + (k^2 + 1) A^2 e^{-2k\theta}}} \qquad \ldots\ldots(69)$$

(ii) Locus of a Point on Cutter Flank.

The geometry produced by the cutter's flank will be examined for both end mills of constant section and disc cutters of uniform thickness.

(ii)a: The End Mill.

From Figure (39) the co-ordinates of a point on the cutter's periphery in its own axial frame, will be given by the vector equation

$$\bar{r}_{pc} = (d - \lambda) \bar{N} + (r_c) \bar{B}$$

where

d = Depth below base cylinder radius

$\lambda$ = Scale factor along cutter's length

$r_c$ = Radius of the end mill

In order to examine the motion of such a point as the cutter moves around the workpiece, it is necessary to transform this point into the $\bar{b}'$, $\bar{n}'$, $\bar{t}'$ framework to determine its position in the moving system. The required transformation is

$$\begin{bmatrix} x'' \\ y'' \\ z'' \end{bmatrix} = \begin{bmatrix} \bar{N}\cdot\bar{n}' & \bar{B}\cdot\bar{n}' & \bar{T}\cdot\bar{n}' \\ \bar{N}\cdot\bar{b}' & \bar{B}\cdot\bar{b}' & \bar{T}\cdot\bar{b}' \\ \bar{N}\cdot\bar{t}' & \bar{B}\cdot\bar{t}' & \bar{T}\cdot\bar{t}' \end{bmatrix} \begin{bmatrix} x' \\ y' \\ z' \end{bmatrix}$$

and for the case of the end mill this becomes

$$\begin{bmatrix} x'' \\ y'' \\ z'' \end{bmatrix} = \begin{bmatrix} \bar{N}\cdot\bar{n}' & \bar{B}\cdot\bar{n}' & \bar{T}\cdot\bar{n}' \\ \bar{N}\cdot\bar{b}' & \bar{B}\cdot\bar{b}' & \bar{T}\cdot\bar{b}' \\ \bar{N}\cdot\bar{t}' & \bar{B}\cdot\bar{t}' & \bar{T}\cdot\bar{t}' \end{bmatrix} \begin{bmatrix} (d-\lambda) \\ r_c \\ 0 \end{bmatrix} \quad ..(70)$$

In order to locate a point on the cutter in the x, y, z cartesian frame it is required to further transform equation (69). i.e. For the added rotation

$$\begin{bmatrix} x \\ y \\ z \end{bmatrix} = \begin{bmatrix} \bar{n}'\cdot\bar{i} & \bar{b}'\cdot\bar{i} & \bar{t}'\cdot\bar{i} \\ \bar{n}'\cdot\bar{j} & \bar{b}'\cdot\bar{j} & \bar{t}'\cdot\bar{j} \\ \bar{n}'\cdot\bar{k} & \bar{b}'\cdot\bar{k} & \bar{t}'\cdot\bar{k} \end{bmatrix} \begin{bmatrix} x'' \\ y'' \\ z'' \end{bmatrix} + \begin{bmatrix} r_o\cos\beta \\ r_o\sin\beta \\ b\theta \end{bmatrix} \quad ..(71)$$

where $\beta = \frac{1}{k}\log_e\left[1 + \frac{mz}{r_o}\right]$ and $r_o$, m and k have the values previously ascribed, whilst $\bar{n}'$, $\bar{b}'$ and $\bar{t}'$ have the meanings given in equations (64), (65) and (66).

For the case of a subtracted rotation the transformation will be

$$\begin{bmatrix} x_1'' \\ y_1'' \\ z_1'' \end{bmatrix} = \begin{bmatrix} \bar{N}\cdot\bar{n}_1' & \bar{B}\cdot\bar{n}_1' & \bar{T}\cdot\bar{n}_1' \\ \bar{N}\cdot\bar{b}_1' & \bar{B}\cdot\bar{b}_1' & \bar{T}\cdot\bar{b}_1' \\ \bar{N}\cdot\bar{t}_1' & \bar{B}\cdot\bar{t}_1' & \bar{T}\cdot\bar{t}_1' \end{bmatrix} \begin{bmatrix} (d-\lambda) \\ r_c \\ 0 \end{bmatrix} \quad ..(72)$$

and

$$\begin{bmatrix} x \\ y \\ z \end{bmatrix} = \begin{bmatrix} \bar{n}_1' \cdot \bar{i} & \bar{b}_1' \cdot \bar{i} & \bar{t}_1' \cdot \bar{i} \\ \bar{n}_1' \cdot \bar{j} & \bar{b}_1' \cdot \bar{j} & \bar{t}_1' \cdot \bar{j} \\ \bar{n}_1' \cdot \bar{k} & \bar{b}_1' \cdot \bar{k} & \bar{t}_1' \cdot \bar{k} \end{bmatrix} \begin{bmatrix} x_1'' \\ y_1'' \\ z_1'' \end{bmatrix} + \begin{bmatrix} r_o \cos\beta \\ r_o \sin\beta \\ b\theta \end{bmatrix} \quad ..(73)$$

where $\beta = -\frac{1}{k} \log_e \left[1 - \frac{mz}{r_o}\right]$

(ii)b: The Disc Cutter.

From Figure (40) the co-ordinates of a point on the periphery of the disc cutter in its own frame are given by the vector equation

$$\bar{r}_{pc} = \left[d - R(1 - \cos\phi)\right] \bar{N} + \left[W\right] \bar{B} - \left[R \sin\phi\right] \bar{T}$$

where

d = Depth below base cylinder radius

R = Cutter radius

$\phi$ = Angle turned through in cutter's frame

W = Half width of the cutter

Transformation of this point into $\bar{b}'$, $\bar{n}'$, $\bar{t}'$ is given by

$$\begin{bmatrix} x'' \\ y'' \\ z'' \end{bmatrix} = \begin{bmatrix} \bar{N} \cdot \bar{n}' & \bar{B} \cdot \bar{n}' & \bar{T} \cdot \bar{n}' \\ \bar{N} \cdot \bar{b}' & \bar{B} \cdot \bar{b}' & \bar{T} \cdot \bar{b}' \\ \bar{N} \cdot \bar{t}' & \bar{B} \cdot \bar{t}' & \bar{T} \cdot \bar{t}' \end{bmatrix} \begin{bmatrix} [d-R(1-\cos\phi)] \\ W \\ -R \sin\phi \end{bmatrix} \quad ..(74)$$

and for the added rotation this transforms into xyz by

$$\begin{bmatrix} x \\ y \\ z \end{bmatrix} = \begin{bmatrix} \bar{n}' \cdot \bar{i} & \bar{b}' \cdot \bar{i} & \bar{t}' \cdot \bar{i} \\ \bar{n}' \cdot \bar{j} & \bar{b}' \cdot \bar{j} & \bar{t}' \cdot \bar{j} \\ \bar{n}' \cdot \bar{k} & \bar{b}' \cdot \bar{k} & \bar{t}' \cdot \bar{k} \end{bmatrix} \begin{bmatrix} x'' \\ y'' \\ z'' \end{bmatrix} + \begin{bmatrix} r_o \cos\beta \\ r_o \sin\beta \\ b\theta \end{bmatrix} \quad ..(75)$$

where $\beta = \frac{1}{k} \log_e \left[1 + \frac{mz}{r_o}\right]$

For the subtracted rotation, equation (75) would be modified in a similar way to equation (73) by using the appropriate subtractive unit vectors and the required statement for $\beta$.

i.e.

$$\beta = -\frac{1}{k} \log_e \left[1 - \frac{mz}{r_o}\right]$$

(ii)c: The Plane Intersection Curve.

Owing to its geometry the disc cutter will generate a different intersection curve in each transverse plane it passes through while moving along the z direction. The geometry of the curve is determined by projecting back along the variable lead helix using equation (22).

i.e.

$$x_p = x \cos \delta - y \sin \delta$$

$$y_p = x \sin \delta + y \cos \delta$$

$$z_p = z + \frac{r_o}{m} \left[e^{k\delta} - 1\right]$$

where

$$\delta = \frac{1}{k} \log_e \left[\frac{m}{r_o} (z_p - z) + 1\right] \qquad \text{.....(76)}$$

If the $z_p = 0$ plane intersection curve is required, equation (76) reduces to

$$\delta = \frac{1}{k} \log_e \left[1 - \frac{mz}{r_o}\right]$$

For the subtracted rotation the required equations will be

$$x_p = x \cos \delta - y \sin \delta$$

$$y_p = x \sin \delta + y \cos \delta$$

$$z_p = z + \frac{r_o}{m} \left[ 1 - e^{-k\theta} \right]$$

where

$$\delta = - \frac{1}{k} \log_e \left[ 1 - \frac{m}{r_o} (z_p - z) \right] \qquad \text{.....(77)}$$

and for the z = 0 plane intersection curve

$$\delta = - \frac{1}{k} \log_e \left[ 1 + \frac{mz}{r_o} \right]$$

# PART 2 PRACTICAL STUDY

# CHAPTER VII

## EXAMINATION OF INTERFERENCE IN SLOTS OF CONSTANT LEAD

### INTRODUCTION

The practical studies will be discussed under three distinct headings

(a) The Production and Physical Examination of Practical Workpiece Profiles

(b) Comparison Between Predicted Geometry and Practical Result

(c) Application of Theory to Rake Angle Determination for a Practical Cutter.

### (a) THE PRODUCTION AND PHYSICAL EXAMINATION OF PRACTICAL WORKPIECE PROFILES

For the purpose of examining the helical interference mechanism a number of workpieces were produced with a small range of fluting cutters commonly used in manufacturing practice by the small tool industry. Figure (41) shows some of these fluting cutter types and their setting arrangements, together with information about the type of small cutting tool which would be produced by the particular method.

The general arrangement between the cutter and test workpiece for producing the specimens is shown in Plate V and the workpiece fixture in Figure (42). A thin disc was chosen as a workpiece because this made physical examination on the "Nikon" projector easier and at the same time eliminated the problems of shadows formed when using thicker workpieces owing to the receding helical surface. The workpiece dimensions are shown in Figure (42).

For the purpose of examining setting parameter effects upon the helical interference mechanism, three basic cutter shapes were used for both axial and offset arrangements in conjunction with a range of base cylinder settings.

Table 1 shows the range of tests devised, and Plate VI shows the various cutters.

Table 1

| Cutter Type | Cutter Dimensions | Cutter Settings | |
|---|---|---|---|
| | | Over work Axial Centre | Offset from Work Centre |
| Side and Face | 5" x $\frac{1}{2}$" x 1" | Yes | Yes |
| Equal "Vee" Notch (90° inc) | 4" x $\frac{3}{4}$" x 1" | Yes | Yes |
| Convex Radius | $2\frac{3}{4}$" x $\frac{5}{8}$" x 1" | Yes | Yes |

Test Procedure

A constant lead of 20 inches was chosen and the milling machine was set for this purpose. The disc workpiece was mounted on the fixture and this in turn was set between the dividing head centres and properly secured.

For the case of flutes milled with the cutter set over the axial centre line of the work, the machine table was not rotated initially until the central plane of the cutter had been located over the work axis. When this had been done, the work table was set to a helix angle calculated with respect to the appropriate base generating cylinder and the fluting cutter set to the required cutting depth. A suitable cutting speed and

table feed were chosen and the cutter was then passed through the workpiece and the machine clutch disengaged prior to resetting.

In order to demonstrate the effect of helix angle choice, the machine table was reset successively to previously calculated angular settings and the workpiece indexed to a new position prior to cutting a slot. For those grooves produced with a Side and Face cutter, nine different settings were used because it was possible to physically observe the position of the base cylinder in the slot geometry, whereas for the other types of cutter this was not the case. For the other examples, only three settings were made since these profiles would be used simply for comparison with those predicted by the theory.

A similar series of tests were conducted where the fluting cutter was offset from the work axis in order to compare the practical result with those predicted by the theory. The cutter offsets were made by firstly aligning the cutter mid-plane with the work axis at a work table angular setting of zero degrees, then winding the cross-slide over to the required displacement from centre. The table was then rotated to the required helix angle and the cut taken.

Each specimen was removed, cleaned and then defrazed prior to being labelled for identification purposes. Physical examination of the A and H specimens was carried out on the Societe Genevoise MU 214B where the generating cylinder radii were measured using a crosswire microscope. Workpiece profiles were traced off from the 10x projected image on the Nikon screen.

The following tables summarise the test series.

Test 1 Cutter Over Axial Centre-line of Work

| Workpiece "A" | | 5" x ½" x 1" S & F Cutter | | |
|---|---|---|---|---|
| Slot Code | Theoretical Base Cylinder Dia. (in) | Table Setting Angle (deg) | Cutting Depth (in) | Measured Base Cylinder Dia. (in) |
| A1 | 4.0 | 32.14 | 0.75 | 3.940 |
| A2 | 4.2 | 33.41 | " | 4.309 |
| A3 | 4.4 | 34.65 | " | 4.477 |
| A4 | 4.6 | 35.85 | " | 4.682 |
| A5 | 4.8 | 37.02 | " | 4.877 |
| A6 | 5.0 | 38.15 | " | 5.067 |
| A7 | 5.2 | 39.24 | " | 5.340 |
| A8 | 5.4 | 40.31 | " | - |
| A9 | 5.5 | 40,83 | " | - |

Test 2 Cutter With Simple Offset 0.5 in

| Workpiece "H" | | 5" x ½" x 1" S & F Cutter | | |
|---|---|---|---|---|
| Slot Code | Theoretical Base Cylinder Dia. (in) | Table Setting Angle (deg) | Cutting Depth (in) | Measured Base Cylinder Dia. (in) |
| H1 | 4.482 | 35.15 | 0.5 | 4.562 |
| H2 | 4.992 | 38.1 | " | 5.076 |
| H3 | 5.5 | 40.82 | " | - |

Test 3 Cutter Over Axial Centre-line of Work

| Workpiece "B" | | 4" x ¾" x 1" "Vee" Cutter (90° inc) | |
|---|---|---|---|
| Slot Code | Theoretical Base Cylinder Dia. (in) | Table Setting Angle (deg) | Cutting Depth (in) |
| B1 | 5.5 | 40.82 | 0.4 |
| B2 | 5.1 | 38.70 | " |
| B3 | 4.7 | 36.43 | " |

Test 4 Cutter with Simple Offset 0.5 in

| Workpiece "C" | | 4" x ¾" x 1" "Vee" Cutter (90° inc) | |
|---|---|---|---|
| Slot Code | Theoretical Base Cylinder Dia. (in) | Table Setting Angle (deg) | Cutting Depth (in) |
| C1 | 5.123 | 38.82 | 0.375 |
| C2 | 5.311 | 39.83 | " |
| C3 | 5.50 | 40.82 | " |

Test 5 Cutter Over Axial Centre-line of Work

| Workpiece "K" | | $2\frac{3}{4}$" x $\frac{5}{8}$" x 1" Convex Radius Cutter | |
|---|---|---|---|
| Slot Code | Theoretical Base Cylinder Dia. (in) | Table Setting Angle (deg) | Cutting Depth (in) |
| K1 | 4.5 | 35.26 | 0.5 |
| K2 | 5.0 | 38.15 | " |
| K3 | 5.5 | 40.83 | " |

Test 6 Cutter With Simple Offset 0.5 in

| Workpiece "L" | | $2\frac{3}{4}$" x $\frac{5}{8}$" x 1" Convex Radius Cutter | |
|---|---|---|---|
| Slot Code | Theoretical Base Cylinder Dia. (in) | Table Setting Angle (deg) | Cutting Depth (in) |
| L1 | 4.514 | 35.34 | 0.5 |
| L2 | 5.007 | 38.19 | " |
| L3 | 5.5 | 40.83 | " |

(b) COMPARISON BETWEEN PREDICTED GEOMETRY AND PRACTICAL RESULT

In order to validate the theory it was considered most practical to generate sets of curves which represented intersection with the transverse xy plane at $z = 0$. This was an obvious choice because it is the intersection curve exposed at the surface of any given workpiece. It also lent itself to examination by optical projection. In order to generate this curve theoretically it was necessary to determine the surface geometry and then project into the desired plane. The surface geometry quite clearly is dependent upon the cutter geometry and its appropriate contact path so, each case, therefore, will be examined separately.

(i) Straight Sided Disc Cutter

As was shown in Chapter IV this cutter type produces two distinctly different surfaces depending upon the setting parameters, i.e. undercutting if the cutter tip lies below the generating cylinder and Backcutting if the cutter tip lies above the generating cylinder. If the base cylinder lies within the workpiece and the cutter is set to a depth which places its tip below this cylinder, then the surface becomes discontinuous along its intersection with this base cylinder surface. See Figure (43). It was shown experimentally that the trailing edge of the cutter produces undercutting in this circumstance and the leading edge backcutting.

To account for this phenomena in the theoretical treatment, it was necessary to use the parameter "$+\theta$" for undercutting and "$-\theta$" for backcutting in the equations for the helitrochoid and the epihelicycloid respectively.

The intersection curve in xy was obtained by using the computer to solve the equations for the given cutter's peripheral locus at particular values of $\theta$, and then projecting back along the required helical path into the z = 0 plane. In the case of an offset cutter the required equations for peripheral locus are

$$x = A_1 \cos\theta + A_2 \sin\theta$$

$$y = A_2 \sin\theta - A_2 \cos\theta$$

$$z = A_3 + b\theta$$

where

$$A_1 = a - d + R(1 - \cos\beta \cos\phi) + w \sin\beta$$

$$A_2 = \left[bw \cos\beta + R(a \sin\phi + b \sin\beta \cos\phi)\right] \Big/ \sqrt{a^2 + b^2}$$

$$A_3 = \left[aw \cos\beta + R(a \sin\beta \cos\phi - b \sin\phi)\right] \Big/ \sqrt{a^2 + b^2}$$

and theta with its incremental steps satisfies the condition $0<\theta$ for the trailing edge, while theta satisfies the condition $0>\theta$ for the leading edge.

In the event of the cutter being set over the axial centreline of the work, the parameter $\beta$ will be zero and the coefficients $A_1$, $A_2$ and $A_3$ reduce to the form given on Page 17. The projection into the $Z_o$ plane from the calculated point x, y, z is obtained by applying equation (27) derived from Figure (26)

i.e.

$$X_1 = x \cos\delta - y \sin\delta$$

$$Y_1 = y \cos\delta + x \sin\delta$$

$$Z_1 = z + b\delta = 0.0$$

and

$$\delta = -z/b \qquad \text{since } \dot{z}1 = 0$$

The flowchart and computer programme for this cutter are given in Appendix 1 under the name REFORMO and can be used to calculate intersection profiles for both offset and axially aligned cutters for any range of cutter workpiece characteristics.

Table II gives the setting parameters and geometry for tests A1, A5 and A9.

Table II

| Interference Type | Test Piece | a (in) | b (in/rad) | R (in) | w (in) | d (in) | Theta$_S$ (rad) | Theta$_F$ (rad) |
|---|---|---|---|---|---|---|---|---|
| Backcutting | A1 | 2.0 | 3.1835 | 2.5 | 0.25 | 0.0 | 0.0 | -0.7 |
| Backcutting | A5 | 2.4 | " | " | " | 0.4 | " | -0.7 |
| Undercutting | A5 | 2.4 | " | " | " | 0.4 | " | +0.7 |
| Undercutting | A9 | 2.75 | " | " | " | 0.75 | " | +0.7 |

Graphical results for this series of tests are shown in Figures (44), (45) and (46), with the theoretical prediction in open circles and the actual workpiece geometry in bold outline. The nature of the discontinuity in test A5 is clearly seen in Figure (45) and observation of the bold outline shows that the portion of the backcutting curve below

the base cylinder radius has been removed by the trailing edge of the cutter, whilst the reverse is true above the base cylinder radius.

It can be seen from the tabular results of test 1 on Page 48 that the theoretical base cylinder diameter and the measured diameters compare relatively favourably although some error is present. This can be attributed to an interaction of two factors, namely, the setting errors for table inclination, because the machine had no vernier scale and rounding of the workpiece at the base cylinder radius. An angular setting error of 0.1 degrees produces 0.010 in error in the base circle radius. The effects of rounding at the intersection are easily seen from Figure (45) and the difficulties in estimating the true intersection point under a measuring microscope are obvious, and must be, therefore, the major contributing factor to error in the measured radius.

Table III gives the data for an offset cutter and it relates to the designated variables and constants in computer programmes for predicting the shape of such test pieces. The theoretical and actual workpiece geometries are given in Figures (47), (48) and (49).

Table III

| Inter-ference Type | Test Piece | a (in) | b (in/rad) | R (in) | w (in) | d (in) | β (rad) | ThetaS (rad) | ThetaF (rad) |
|---|---|---|---|---|---|---|---|---|---|
| Back-cutting | H1 | 2.241 | 3.1835 | 2.5 | 0.25 | 0.0 | 0.1828 | 0.0 | -0.7 |
| Back-cutting | H2 | 2.496 | " | " | " | 0.25 | " | " | -0.7 |
| Under-cutting | H2 | 2.496 | " | " | " | 0.25 | " | " | +0.7 |
| Under-cutting | H3 | 2.75 | " | " | " | 0.5 | " | " | +0.7 |

(ii) Vee Form Cutter

The contact path for form cutters is quite different from that for a straight sided disc cutter and in most circumstances the path is independent of the angle turned through by the cutter. For a Vee form cutter its contact path is always a straight line which lies in the work surface and at the same time is in a plane which contains the binormal and normal vectors to the base helix, i.e. the NORMAL PLANE. Figure (50) demonstrates this fact.

The equations of the contact path for an offset Vee form cutter are

$$x = A_1 \cos\theta + A_2 \sin\theta$$

$$y = A_1 \sin\theta - A_2 \cos\theta$$

$$z = A_3 + b\theta$$

where

$$A_1 = a - d + R(1 - \cos\beta) + h(\cos\beta - \sin\beta \tan\gamma)$$

$$A_2 = \frac{b}{\sqrt{a^2 + b^2}} \left[ h(\cos\beta \tan\gamma - \sin\beta) + R \sin\beta \right]$$

$$A_3 = \frac{a}{\sqrt{a^2 + b^2}} \left[ h(\cos\beta \tan\gamma - \sin\beta) + R \sin\beta \right]$$

and h is a parameter.

For the condition $\theta = 0$ the equations for x, y and z reduce to the constants $A_1$, $A_2$ and $A_3$, thus defining a straight line in space which is the $v_o$ curve for the surface. All other v curves are straight lines but displaced along the base helix depending upon the value chosen for theta. The intersection curve in the $z_o$ plane is obtained in the same manner as previously.

i.e.

$$X_1 = x \cos\delta - y \sin\delta$$

$$Y_1 = y \cos\delta + x \sin\delta$$

$$Z_1 = z + b\delta = 0.0$$

where $\delta = -z/b$ since $Z1 = 0$

The flowchart and computer programme for this cutter are given in Appendix 1 under the name of VEEFORMΩ. This programme is applicable to all types of Vee form cutter. Setting values for the axially aligned tests are given in Table IV while offset cutter characteristics are given in Table V.

Table IV

| Test Piece | a (in) | b (in/rad) | GA (rad) | R (in) | d (in) | β (rad) | hS (in) | hF (in) |
|---|---|---|---|---|---|---|---|---|
| B1 | 2.75 | 3.1835 | 0.7854 | 2.0 | 0.4 | 0.0 | 0.0 | 0.4 |
| B2 | 2.55 | " | " | " | 0.2 | " | " | " |
| B3 | 2.35 | " | " | " | 0.0 | " | " | " |

Table V

| Test Piece | a (in) | b (in/rad) | GA (rad) | R (in) | d (in) | β (rad) | hS (in) | hF (in) |
|---|---|---|---|---|---|---|---|---|
| C3 | 2.750 | 3.1835 | 0.7854 | 2.0 | 0.375 | 0.1828 | 0.0 | 0.4 |
| C2 | 2.655 | " | " | " | 0.1875 | " | " | " |
| C1 | 2.562 | " | " | " | 0.0 | " | " | " |

The results for this series of tests are summarised in Figures (51) to (56) where the experimental curve is in bold outline. A curved profile in the $Z_o$ plane would be expected from the geometry of the system.

(iii) Convex Form Cutter.

The contact path for this cutter is a circular arc with a radius and centre of curvature equivalent to that of the cutter. This profile lies in the normal plane.

The equations for this system are

$$x = A_1 \cos\theta + A_2 \sin\theta$$

$$y = A_1 \sin\theta - A_2 \cos\theta$$

$$z = A_3 + b\theta$$

where

$$A_1 = a - d + R(1 - \cos\beta) + r\left[\cos\beta(1 - \cos\delta) + \sin\beta \sin\delta\right]$$

$$A_2 = \frac{b}{\sqrt{a^2 + b^2}}\left[\sin\beta(R - r(1 - \cos\delta)) + r \cos\beta \sin\delta\right]$$

$$A_3 \quad \frac{a}{\sqrt{a^2 + b^2}}\left[\sin\beta(R - r(1 - \cos\delta)) + r \cos\beta \sin\delta\right]$$

and $\delta$ is a parameter.

For the condition $\theta = 0$ once again the equations for x, y and z reduce to the constants $A_1$, $A_2$ and $A_3$, thus defining a circular arc in space which is the $v_o$ curve for the surface. Increasing the value of theta simply displaces the v curve along the base helix. The intersection curve is derived as before by using the same group of equations.

i.e.

$$X_1 = x \cos\delta' - y \sin\delta'$$

$$Y_1 = y \cos\delta' + x \sin\delta'$$

$$Z_1 = z + b\delta' = 0.0$$

where $\delta'$ is the angle turned through to find the Z plane.

and

$$\delta' = - z/b \qquad \text{since } Z1 = 0$$

The flowchart and computer programme appear under the name of CIRFORMO and it is applicable to all circular convex form cutters. Table VI and Table VII give the cutter characteristics for axially aligned and offset cutters respectively.

Table VI

| Test Piece | a (in) | b (in/rad) | r (in) | R (in) | d (in) | β (rad) | DeltaS (rad) | DeltaF (rad) |
|---|---|---|---|---|---|---|---|---|
| K1 | 2.25 | 3.1835 | 0.3125 | 1.375 | 0.0 | 0.0 | 0.0 | 0.5 |
| K2 | 2.50 | " | " | " | 0.25 | " | " | " |
| K3 | 2.75 | " | " | " | 0.5 | " | " | " |

Table VII

| Test Piece | a (in) | b (in/rad) | r (in) | R (in) | d (in) | β (rad) | DeltaS (rad) | DeltaF (rad) |
|---|---|---|---|---|---|---|---|---|
| L1 | 2.257 | 3.1835 | 0.3125 | 1.375 | 0.0 | 0.1828 | 0.0 | 0.5 |
| L2 | 2.504 | " | " | " | 0.25 | " | " | " |
| L3 | 2.750 | " | " | " | 0.5 | " | " | " |

Figures (57) to (62) summarise this test series and once again the experimental curves are in bold outline.

It is clearly evident that the nature of the work surface geometry for a given cutter is dependent upon the characteristics of the coefficients $A_1$, $A_2$ and $A_3$ which necessarily change from cutter to cutter, owing to the format of matrix (26).

Of the three cases examined here, only the cutter path for the straight sided disc is dependent upon the angle turned through by the cutter, so therefore, care must be taken to determine the specific characteristics of any individual cutter's contact path in order to assign correct values to the coefficients. Once this path is determined the procedures for establishing the intersection curves are identical because all the work surfaces comprise "u" curves which are circular helices and "$_v$" curves representing the appropriate contact path.

(c) APPLICATION OF THE THEORY TO RAKE ANGLE DETERMINATION FOR A PRACTICAL CUTTER

When a helical surface is used as the rake face of a cutting tool it is normally a tedious exercise to determine the true normal rake angle. Owing to such difficulties, therefore, it is usual practice to calculate the normal rake angle in a given base plane; an expedient used by Etheridge and Scott[21] when they experienced such problems when examining the uneven flank wear on a large, helically gashed form cutter. This cutter was used to form mill the steam face of turbine blades fitted to the low pressure side of power generating plant, made at the English Electric Company Limited, Rugby, England.

Whilst it is perfectly possible to apply the theory to rake angles for an experimental workpiece it seemed of more practical advantage to extend the theory to the more complex cutter used in the machinability tests conducted by Scott[22]. The cutter dimensions and geometry are shown in Figure (63). The rake angles of this cutter, measured in a base normal plane are presented solely for the purpose of comparison and validation of the theory now developed.

(i) The Surface Geometry of the English Electric Cutter

The fluting cutter used to manufacture this heavy duty form cutter was an unequal "Vee" of $20^{\circ}/10^{\circ}$ flanks, with an outside diameter of 7.5 in and a tip radius of 0.130 in. The $20^{\circ}$ flank was used to generate the rake face, prior to final grinding with a "saucer" wheel of similar geometry. For the purpose of theoretical treatment the tip radius will be ignored since it is only specified to produce the root fillet radius of the tooth space.

From Figure (23) and the equations on page 25 the position vector of a general point $x_p$, $y_p$, $z_p$ on this surface is

$$\bar{r}_p = (A_1 \cos\theta + A_2 \sin\theta)\,\bar{i} + (A_1 \sin\theta - A_2 \cos\theta)\,\bar{j} + (A_3 + b\theta)\,\bar{k} \qquad \ldots\ldots(78)$$

and the directional derivative along the "u" curve is

$$\frac{\partial \bar{r}_p}{d\theta} = (-A_1 \sin\theta + A_2 \cos\theta)\,\bar{i} + (A_1 \cos\theta + A_2 \sin\theta)\,\bar{j} + (b)\,\bar{k} \qquad \ldots.(79)$$

which may be rewritten in the form

$$\frac{\partial \bar{r}_p}{\partial\theta} = \left[r_2 \sin(\delta - \theta)\right]\bar{i} + \left[r_2 \cos(\delta - \theta)\right]\bar{j} + \left[b\right]\bar{k} \qquad \ldots\ldots(80)$$

where

$$\delta = \tan^{-1}\left[A_2/A_1\right] \quad \text{and} \quad r_2 = \sqrt{A_1^2 + A_2^2}$$

The coefficients $A_1$, $A_2$ and $A_3$ have the same form as those for the vee cutter described on page 55

The directional derivative along the "v" curve is

$$\frac{\partial \bar{r}_p}{\partial h} = (B_1 \cos\theta + B_2 \sin\theta)\,\bar{i} + (B_1 \sin\theta - B_2 \cos\theta)\,\bar{j} + (B_3)\,\bar{k} \quad \ldots.(81)$$

where

$$B_1 = \frac{\partial A_1}{\partial h} = \cos\beta - \sin\beta \tan\gamma$$

$$B_2 = \frac{\partial A}{\partial h} = \frac{b}{\sqrt{a^2 + b^2}}\left[\cos\beta \tan\gamma - \sin\beta\right]$$

$$B_3 = \frac{\partial A_3}{\partial h} = \frac{a}{\sqrt{a^2 + b^2}}\left[\cos\beta \tan\gamma - \sin\beta\right]$$

which may be rewritten in the form

$$\frac{\partial \bar{r}_p}{\partial h} = \left[r_1 \cos(\alpha - \theta)\right]\bar{i} - \left[r_1 \sin(\alpha - \theta)\right]\bar{j} + \left[B_3\right]\bar{k} \quad \ldots\ldots.(82)$$

where

$$\alpha = \tan^{-1}\left[B_2/B_1\right] \quad \text{and} \quad r_1 = \sqrt{B_1^2 + B_2^2}$$

An inward normal to this surface is

$$\bar{N} = \frac{\partial \bar{r}_p}{\partial h} \times \frac{\partial \bar{r}_p}{\partial \theta}$$

$$= -\left[C_1 \cos(\delta - \theta) + C_2 \sin(\alpha - \theta)\right]\bar{i} + \left[C_1 \sin(\delta - \theta) - C_2 \cos(\alpha - \theta)\right]\bar{j} + \left[C_3 \cos(\delta - \alpha)\right]\bar{k} \quad \ldots\ldots.(83)$$

where $C_1 = A_3 r_2 \qquad C_2 = b r_1 \qquad C_3 = r_2 r_1$

A unit normal to this surface is

$$\bar{n} = \frac{\bar{N}}{|\bar{N}|} = \frac{-Nx\,\bar{i} + Ny\,\bar{j} + Nz\,\bar{k}}{\sqrt{Nx^2 + Ny^2 + Nz^2}}$$

where Nx, Ny and Nz are readily derived from equation (83) above, and

$$|\bar{N}| = \sqrt{C_1^2 + C_2^2 - 2\,C_1\,C_2 \sin(\delta - \alpha) + C_3^2 \cos^2(\delta - \alpha)}$$

(ii) True Normal Rake Angle

The true normal rake angle was calculated using equation (40), (41), (43), (44) and (45) of Chapter V by means of the computer programme named VESCO. The flowchart and programme designed for this purpose are included in Appendix 1.

The practical cutter varied in radius around the form and it was necessary to specify both the radius and the plane containing the point on the profile, at which the rake angle was required. These were specified as ABAR and Z1 in the computer programme and Figure (64) shows the cutter sections used in the calculations.

Table VIII gives the detailed dimensions used in the calculations for this cutter and the theoretical values for true normal rake angle are given in Table IX.

Table VIII

| | a (in) | b (in/rad) | GA (rad) | R (in) | d (in) | β (rad) | Step (rad) | Offset (in) |
|---|---|---|---|---|---|---|---|---|
| | 3.75 | 12.732 | 0.1745 | 3.75 | 1.8591 | 0.1845 | 0.1 | 0.6875 |
| Abar (in) | 2.375 | 3.050 | 3.520 | 3.550 | 3.300 | 2.990 | 2.700 | 2.578 |
| Z1 (in) | 0.0000 | 0.3125 | 0.8125 | 1.3125 | 1.8125 | 2.3125 | 2.8125 | 3.1250 |

Table IX

| Zi(in) | 0.0000 | 0.3125 | 0.8125 | 1.3125 | 1.8125 | 2.3125 | 2.8125 | 3.1250 |
|---|---|---|---|---|---|---|---|---|
| Theoret-ical Rake Angle | 15.70 | 11.19 | 9.02 | 8.90 | 9.96 | 11.51 | 13.24 | 14.09 |
| Measur-ed Rake Angle | - | - | 12.75 | 12 | 14 | 18.2 | 18.75 | - |

(iii) Rake Angle In A Base Normal Plane

The base normal plane contains the x axis and the binormal vector to the surface at the base cylinder radius. For the particular surface considered, the binormal vector is also one of the network curves and all points where the rake angle is required, lie along it. The rake angle at any point is obtained by the dot product of the two unit vectors $\bar{b}$ and $\bar{r}$ which lie in this plane. i.e. the unit binormal and the unit vector in the direction of the radial to the point.

where

$$\bar{B} = \frac{(B_1 \cos\theta + B_2 \sin\theta)\ \bar{i} + (B_1 \sin\theta - B_2 \cos\theta)\ \bar{j} + (B_3)\ \bar{k}}{\sqrt{B_1^2 + B_2^2 + B_3^2}}$$

and

$$\bar{r} = \frac{x_p\ \bar{i} + y_p\ \bar{j} + (z_p - z_i)\ \bar{k}}{\sqrt{x_p^2 + y_p^2 + (z_p - z_i)^2}}$$

Here $B_1$, $B_2$ and $B_3$ have their previous meaning; $x_p$, $y_p$ and $z_p$ are the co-ordinates of the required point and $z_i$ is the intercept which the radial makes at the z axis. The most convenient point will clearly be

$z = 0$, with $\theta$ set to zero for this to be valid.

The computer programme and flowchart for this purpose is called VENSCO and the results are summarised in Table X. The setting parameters were the same as those given in Table VIII.

Table X

| Z1(in) | 0.0000 | 0.3125 | 0.8125 | 1.3125 | 1.8125 | 2.3125 | 2.8125 | 3.1250 |
|---|---|---|---|---|---|---|---|---|
| Theo: Rake Angle (deg) | 17.31 | 13.41 | 11.60 | 11.50 | 12.38 | 13.68 | 15.18 | 15.90 |
| Meas: Rake Angle (deg) | - | - | 12.75 | 12 | 14 | 18.2 | 18.75 | - |

(iv) Rake Angle In A Transverse Plane

In order to determine the rake angle in a transverse plane it is necessary to project each point on the surface into the required plane. An obviously convenient plane is that where $Z = 0$. The slope of the intersection curve is then determined at each point under consideration and the unit tangent to a point in the plane will be given by

$$\frac{d\bar{r}_p}{dS} = \frac{-(x \sin\delta + y \cos\delta)\ \bar{i} + (x \cos\delta - y \sin\delta)\ \bar{j} + (b)\ \bar{k}}{\sqrt{x^2 + y^2 + Z^2}}$$

and from equation (27) the radial is

$$\bar{r}_p = (x \cos\delta - y \sin\delta)\ \bar{i} + (x \sin\delta + y \cos\delta)\ \bar{j} + (z + b\delta)\ \bar{k}$$

The rake angle once again is calculated by the dot product of the unit tangent with a unit vector in the direction of the radial. VETSCO is

the computer programme developed for this purpose and the setting parameters have the previously stated values. Table XI gives the results for this plane together with those previously discussed, so that variations can easily be seen.

Table XI

| | Z1(in) | 0.0000 | 0.3125 | 0.8125 | 1.3125 | 1.8125 | 2.3125 | 2.8125 | 3.1250 |
|---|---|---|---|---|---|---|---|---|---|
| Theoretical | True Normal Rake (deg) | 15.70 | 11.19 | 9.02 | 8.90 | 9.96 | 11.51 | 13.24 | 14.09 |
| | Base Normal Rake (deg) | 17.31 | 13.41 | 11.60 | 11.50 | 12.38 | 13.68 | 15.18 | 15.90 |
| | Trans verse Rake (deg) | 26.05 | 30.7 | 32.77 | 32.88 | 31.88 | 30.38 | 28.62 | 27.75 |
| | Meas: Rake (deg) | - | - | 12.75 | 12 | 14 | 18.2 | 18.75 | - |

It is readily recognised that significant variations occur by using different reference planes and, therefore, care should be exercised in practical application when discussing the effects of rake angle in machining operations.

# CHAPTER VIII

## EXAMINATION OF INTERFERENCE IN SLOTS OF VARIABLE LEAD

### INTRODUCTION

In order to examine the interference mechanism in slots of variable lead it was necessary to develop a reliable mechanism for superposing the additional rotation previously described in Chapter VI. The device made by Waynham was too cumbersome for practical application owing to its inherent setting problems, so a new approach was made by considering a redesign of the conventional dividing head to incorporate the principle demonstrated by Etheridge and Waynham.

The practical studies involved in this area of work will be examined under the following three headings.

(a) Some Design Improvements to the Conventional Dividing Head.

(b) Superposition of a Uniform Rotation.

(c) Superposition of a Variable Rotation.

### (a) SOME DESIGN IMPROVEMENTS TO THE CONVENTIONAL DIVIDING HEAD

Before discussing modifications to the conventional dividing head, it's design principle will be examined.

#### (i) The Universal Dividing Head

The dividing head used on the universal milling machine has a wide ranging facility, but, nevertheless has changed little in design principle since the late 19th Century.

Figure (65) shows a typical design and it is readily seen from Figure (5) there is a fixed relationship between the workspindle and the indexing spindle owing to the worm and wheel geared arrangement. The ratio of this gear pair is always 40/1 by convention.

Accurate division of a workpiece is achieved by applying an appropriate step input to the worm, thus giving a fixed rotation to the workspindle via the worm wheel. An indexing plate which may either rotate freely on the worm shaft or remain fixed relative to the dividing head body is used for providing circular division of a workpiece where directly factorisable ratios of 40 are not possible. This facility is provided by holes arranged around concentric pitch circles on the plate. If prime number division is required the workspindle is geared independently to the index plate so that motion of the worm spindle causes a differential motion of the plate.

The dividing head may also be used for the production of helices of constant lead or cam surfaces of constant lead by fixing the index plate and worm relative to one another and driving them from the table screw via a gear train (Figure 5). Clearly the lead produced is dependent upon the lead of the machine screw and the gear ratio chosen.

The range of work capable of being produced using this standard piece of equipment is indeed large but even so, non-uniform rise cams, non-cylindrical helicoids and variable lead helices are precluded owing to the fixed ratios in the machine system. Development of the dividing head is, therefore, feasible if the principle of the superposed rotation can be incorporated without loss of benefit in other ways.

(ii) The Design Modification

In order to incorporate an additional rotation within the head itself and at the same time retain a compact size, it was decided to use a differential mechanism in place of the normal worm and wheel arrangement. A uniform superposed rotation was to be achieved by gearing the input worm to the differential arm so that the output rotation was either increased or decreased for a given travel of the work table. If a non-linear superposed rotation is required then the gear train connecting the input to the cage would be replaced by a cam, with a rack and pinion follower.

The advantages to be gained by this design modification are as follows:

(a) Short leads may be produced directly within the head.

(b) Prime number division is automatically incorporated.

(c) Helical surfaces of constant lead coupled with prime number division is accommodated.

(d) Variable leads and non-uniform rise cams may be produced.

The particular differential mechanism chosen was a simple three element epicyclic which is shown diagrammatically in Figure (66) and a detailed sectional elevation with leading dimensions of the complete head is given in Figure (67). Three views of the partially assembled prototype are shown in Plates VII, VIII and IX, from which the mode of operation is readily deduced.

This design was chosen because of its compact nature and greater rigidity when compared with the bevel gear differential, tapes and plate

cams used in the original attachment produced by Waynham. Clearly the use of a geared system for superposing the rotation has the distinct benefit of greater accuracy. Plate X shows the gear train for superposing a uniform rotation.

The complete design specification and a Kinematic analysis of the mechanism is given in Appendix 2.

(b) SUPERPOSITION OF A UNIFORM ROTATION

The superposition of a uniform rotation was achieved by means of a gear train interconnecting the primary and secondary worms in the differential. This is shown clearly in Plate X and it is readily deduced that the device is effectively a short lead mechanism automatically incorporated within the head.

However, it is possible with suitable setting techniques, to produce variable lead helices by aligning the machine table to a helix angle for one set lead and superposing a uniform rotation so that the workpiece moves relative to a shorter or longer helix. This means, effectively, that the cutter is rolling along the real helix but its axes are aligned relative to that helix dictated by the machine table setting. Figure (68) shows the relative angular displacements. The variable lead is produced as a consequence of the fixed angular displacement of the cutter within the triad of unit vectors, $b'$, $\bar{n}'$, $t'$ as they move along the real helix generated by the head.

(i) Geometry of The Uniform Superposed Lead

From Appendix 2 and Figure (68) the displacement z along the work is

$$z = b\theta = b'\phi$$

where

$b$ = lead per radian of the machine

$b'$ = lead per radian of the system

$\theta$ = angle turned through in machine reference frame

$\phi$ = angle turned through in real helix reference frame

But from the Kinematics of the system

$$\phi = \left[1 \pm 2k\right] \theta$$

therefore

$$b' = \frac{b}{1 \pm 2k} = Ab$$

A position vector on the real helix will be

$$\bar{r}_p = r_o \bar{e}_r + Ab\theta \bar{e}_z \qquad \text{.....(84)}$$

and

$$\frac{d\bar{r}_p}{d\theta} = r_o \bar{e}_\theta + Ab\bar{e}_z$$

while

$$\left| \frac{d\bar{r}_p}{d\theta} \right| = \frac{ds}{d\theta} = \sqrt{r_o^2 + A^2 b^2}$$

therefore

$$\bar{t}' = \frac{d\bar{r}_p}{d\theta} \cdot \frac{d\theta}{ds} = \frac{r_o \bar{e}_\theta + Ab\,\bar{e}_z}{\sqrt{r_o^2 + A^2 b^2}} \qquad \text{.....(85)}$$

and

$$\bar{n}' = \frac{d\bar{t}'}{ds} \Bigg/ \left| \frac{d\bar{t}'}{ds} \right| = -\bar{e}_r \qquad \text{.....(86)}$$

while

$$\bar{b}' = \bar{t}' \times \bar{n}' = \frac{-Ab\bar{e}_\theta + r_o \bar{e}_z}{\sqrt{r_o^2 + A^2 b^2}} \qquad \text{.....(87)}$$

(ii) Application of Theory To An End Mill

Plate XI shows an end mill being used in conjunction with the modified dividing head and the test parameters are given in Table XII

Table XII

| Test Piece | $r_o$ (in) | $r_c$ (in) | d (in) | b (in/r) | k | Slambda | Flambda | Step |
|---|---|---|---|---|---|---|---|---|
| VL1E | 1.125 | 0.5 | 0.1563 | 1.5916 | +0.41485 | 0.0 | 1.0 | 0.1 |
| VL2E | " | " | " | " | -0.41485 | " | " | " |

The theory developed for the logarithmic superposed rotation given in Chapter VI is directly applicable in this case except that equations (85), (86) and (87) must be used for the various dot products instead of equations (64), (65) and (66).

The required direction cosines are, therefore

$$\bar{T}\cdot\bar{t}' = \frac{ar_o + Ab^2}{\sqrt{a^2 + b^2}\sqrt{r_o^2 + A^2b^2}} \qquad \bar{N}\cdot\bar{t}' = 0.0$$

$$\bar{T}\cdot\bar{b}' = \frac{-aAb + br_o}{\sqrt{a^2 + b^2}\sqrt{r_o^2 + A^2b^2}} \qquad \bar{N}\cdot\bar{b}' = 0.0$$

$$\bar{T}\cdot\bar{n}' = 0.0 \qquad \bar{N}\cdot\bar{n}' = 1.0$$

$$\bar{B}\cdot\bar{t}' = \frac{-br_o + aAb}{\sqrt{a^2 + b^2}\sqrt{r_o^2 + A^2b^2}} \qquad \bar{n}'\cdot\bar{i} = -\cos\theta$$

$$\bar{B}\cdot\bar{b}' = \frac{Ab^2 + ar_o}{\sqrt{a^2 + b^2}\sqrt{r_o^2 + A^2b^2}} \qquad \bar{n}'\cdot\bar{j} = -\sin\theta$$

$$\bar{B}\cdot\bar{n}' = 0.0 \qquad \bar{n}'\cdot\bar{k} = 0.0$$

$$\bar{b}' \cdot \bar{i} = \frac{Ab \sin\theta}{\sqrt{r_o^2 + A^2b^2}} \qquad \bar{t}' \cdot \bar{i} = \frac{-r_o \sin\theta}{\sqrt{r_o^2 + A^2b^2}}$$

$$\bar{b}' \cdot \bar{j} = \frac{-Ab \cos\theta}{\sqrt{r_o^2 + A^2b^2}} \qquad \bar{t}' \cdot \bar{j} = \frac{r_o \cos\theta}{\sqrt{r_o^2 + A^2b^2}}$$

$$\bar{b}' \cdot \bar{k} = \frac{r_o}{\sqrt{r_o^2 + A^2b^2}} \qquad \bar{t}' \cdot \bar{k} = \frac{Ab}{\sqrt{r_o^2 + A^2b^2}}$$

The computer programme developed for this surface is called VALREFORMOE and it is given in Appendix I in a form suitable for the solution of a logarithmic superposed rotation. This programme only needs modification for the direction cosines in order to be directly applicable to this case, because in every other way both solutions are identical.

Figures (69) and (70) show the surface produced by projecting a series of straight lines representing the cutter flank into the xy plane. These represent shortening and lengthening helices respectively.

(iii) Application of The Theory To a Disc Cutter

In the case of a disc cutter distinctly different intersection curves are produced depending upon which transverse plane is encountered. This is readily seen from Plate III. The reason for this is, that as the cutter rolls along the real helix, its leading or trailing edge (depending upon the setting parameters) is interfering at some point ahead or behind its axial reference frame. Since the relative position of the cutter framework is changing from point to point owing to the differential variation in lead, the "Interference Surface", and hence the plane intersection curve will also vary from point to point.

Table XIII gives the parameters for the tests carried out with disc cutters and they relate to the computer programme VALREFORMOD given in Appendix 1. Once again this programme is defined in terms of the direction cosines for a logarithmic lead and so for the uniform superposed rotation solution, therefore, dot products given on page 71 should be used for this case.

Table XIII

| Test Piece | $r_o$ (in) | b (in/rad) | w (in) | R (in) | d (in) | k | B1S (rad) | B1F (rad) | Step (rad) |
|---|---|---|---|---|---|---|---|---|---|
| VL1D | 1.125 | 1.5916 | 0.1875 | 2.5 | 0.1563 | 0.41485 | 0.0 | -1.0 | 0.05 |
| VL2D | 1.125 | " | " | " | 0.1563 | -0.41485 | " | 1.0 | " |
| VL3D | 0.643 | " | " | " | -0.3258 | 0.41485 | " | -1.0 | " |
| VL4D | 0.643 | " | " | " | -0.3258 | -0.41485 | " | 1.0 | " |

Figures (71) to (75) summarise the results for this test series and demonstrate the geometries of the plane intersection curves in several planes common for all four specimens. These curves were originally plotted on a 10x magnification for comparison with the practical results on the optical projector, but are now scaled down in presentation owing to their large size.

(c) SUPERPOSITION OF A VARIABLE ROTATION

The time available in the development programme for the prototype head precluded a practical examination of a variable superposed rotation, but the necessary design modifications and principles are given in Appendix 2. However, it was thought desirable to apply the analysis

to a theoretical workpiece similar in characteristics to those given in section (b) of this chapter and to compare the theoretical predictions with the results for a uniformly applied superposed rotation.

The computer programmes VALREFORMOE and VALREFORMOD in Appendix 1 were devised for this purpose using the equations derived in Chapter VI and the setting parameters of Tables XII and XIII. The results are shown by Figures (76) to (79).

# CHAPTER IX

## DISCUSSION

### INTRODUCTION

It has been clearly demonstrated that an exact and unified theory to explain the phenomena of helical interference is possible and further, as a consequence of the knowledge gained, that practical advantage can accrue from a mechanism which is generally regarded as destructive. It is to this end that the practical results will be discussed.

### (a) INTERFERENCE IN SLOTS OF CONSTANT LEAD

An examination of Figures (44),(45) and (46) shows that the leading edge of a straight sided disc cutter produces a back-cutting effect, while the trailing edge produces under-cutting and further that either or both these effects may be present depending upon the base generating cylinder chosen. To be of practical use as the rake face of a cutting tool, therefore, the most effective surface must be that where the base generating cylinder lies at the outside diameter of the workpiece, thus always ensuring a positive radial rake angle. Further modification to the rake face can be achieved by offsetting the fluting cutter, by setting the base generating cylinder diameter to be larger than the work, or by a combination of both. The current practices to some extent recognise this, but the problem has really been resolved by the design of special fluting cutters and setting techniques (Figure (41)) to minimise interference, largely from lack of knowledge about the mechanics of the process.

Obviously, for this current work to be of practical value at shop floor level it will be necessary to draw up data charts giving setting conditions for producing particular rake face geometries, together with the required tool characteristics.

(b) CALCULATION OF RAKE ANGLE

From the work described in their joint paper, Etheridge and Scott[21] showed that current cutting tool manufacturing methods leave a great deal to be desired owing to the rather uncertain geometry of the rake face produced. The particular cutter examined (Figure (63)) was designed to have a constant radial rake angle of + $10^{o}$ over the entire face and yet, at the same time, be helically gashed. The theoretical treatment developed here, in fact, shows that these two basic requirements are incompatible and further that the rake face in the transverse plane defined, will never be flat. The radial rake angle will always increase with changing radius in such a plane, as Table XI more than adequately demonstrates.

Apart from providing, for the first time, a method of accurate rake angle determination for such tools, the equations given in Chapter VII permit the designer to choose in which plane it is most important to specify the radial rake angle for cutter performance; then to design a rake face accordingly. Once again the practical importance of the work lies in providing the tool designer with the data charts and computer programmes for such design work.

The most important criticism arising from current practice is that cutting tools appear to be designed by "Custom and Practice" without recourse to any theoretical considerations, so that tool performance is never predictable. For the cutter used in the Scott[22] experiments

this was disasterous and expensive, because examination of Table XI shows that only at the tip radius in the true normal plane does the theoretical rake angle approach the design recommendation. In the transverse plane specified, the minimum radial rake angle predicted for the design parameters is 26.05°. Clearly the 20°/10° fluting cutter should never have been specified for this form cutter design. This cutter was examined theoretically because it graphically illustrated a particularly difficult practical problem arising from emperical tool design methods.

(c) INTERFERENCE IN SLOTS OF VARYING LEAD

Although "qualitative" assessments of this mechanism have been carried out by Mabbon and Sabberwal[19] and Etheridge and Waynham[17], in both instances the basic requirement was to produce a variable lead and yet minimise interference. The former workers achieved this by the use of End Mills, while the latter used setting technique to give a suitable rake face on their conical cutters.

The most important aspect of the analysis developed here is that it demonstrates a method by which variable leads can be produced, simply by setting techniques. Although exhaustive tests of the method were precluded owing to time, those which were carried out proved the principle and also the marked change in interference pattern from one plane section to another. The plane intersection curves of Figure (71) for specimens VL1D and VL3D were produced with the same cutter and settings, except that the base cylinder for VL1D was 1.125 in, giving a table setting angle of 35.25°, while the base cylinder for VL2D was

0.643 in, giving a table setting angle of $22^{\circ}$. Obvious differences exist between the intersection curves and the variable leads produced as a consequence of these setting procedures.

It is once again possible to use the interference surface produced by disc cutters as the rake face of a cutting tool provided that the variable lead is achieved by a subtractive rotation, because this ensures positive radial rake. The reason for this type of interference being produced is that subtracting a rotation means that the effective base cylinder lies outside the work diameter.

The theoretical curves generated for the logarithmic incremental superposed rotation are similar to those for the above cases, but exhibit more curvature in the initial stages for reasons which can be deduced from the table of logarithmic increments in Appendix 2.. While some advantage can be gained by using a logarithmic superposed rotation for cylindrical work, its main benefit will be found in applications such as that proposed by Etheridge and Waynham in their conical investigations. Certainly the most important application of this principle must be in the development of a new spiral bevel gear system based on CONICAL EPIHELICYCLOIDS, which are capable of being hobbed by a machine based upon the principle of the redesigned dividing head. The development work necessary in this area is large since it will require a whole new mathematical base for the system and in particular, the mating pairs geometry and manufacturing method.

The principles introduced by this section of the work also have an application in the manufacture of such mechanisms as the "Screw Extruders" and "Plasticisers" used in the Polymer industries.

# CHAPTER X

## CONCLUSION

The usually held viewpoint that interference is destructive has been shown to be eroneous by demonstrating that the mechanism can be used beneficially in a number of ways.

These areas have been highlighted and a complete theory given which will be of assistance in cutting tool design, as well as clarifying the nature of some current problems with standard tool manufacturing practice.

New ground has been broken in the field of variable lead helices, by not only developing an analytical method, but by showing new ways of producing such surfaces. This part of the work provides the basis for several new ideas in machine tool Kinematics.

# CHAPTER XI

## FUTURE WORK

The first obvious area of future work will be the production of a design data bank for cutting tools of both constant and variable lead. These must necessarily be of use to cutting tool designers and lead to more efficient metal removal as a consequence.

Probably the most important new work, however, will be that associated with the development of new manufacturing techniques for spiral bevel gears and non-linear screws which currently provide many design and manufacturing problems. It will also be necessary to establish the mathematical base and standardisation procedures for such proposed systems.

# APPENDIX 1

## COMPUTER PROGRAMMES

(A) Constant Lead

(B) Rake Angle Calculation

(C) Variable Lead

(A1) REFORMO - CONSTANT LEAD

(Rectangular Form Cutter - On Centre or Set Over)

FLOWCHART FOR REFORMO

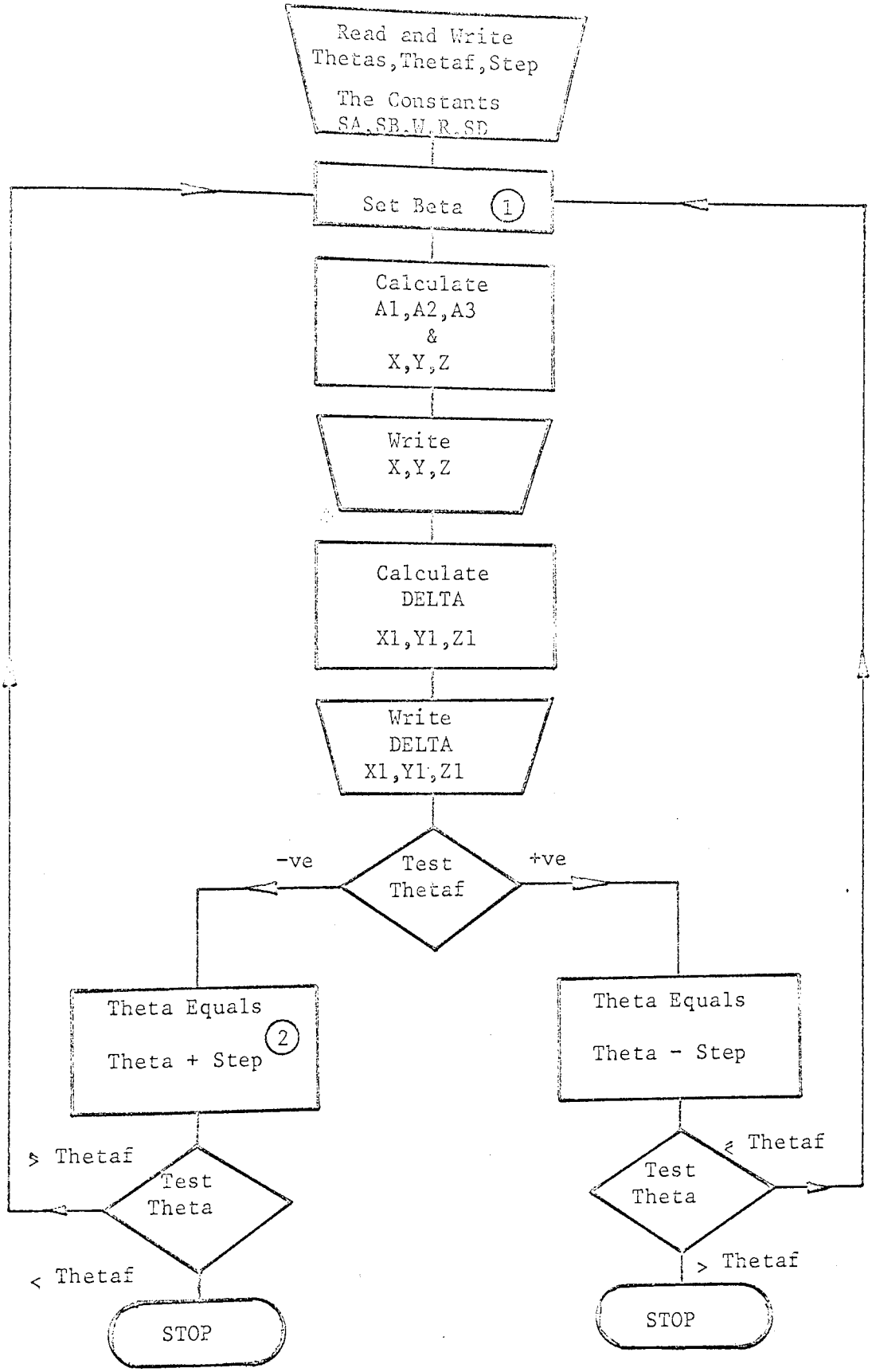

## FORTRAN PROGRAMME FOR PLANE INTERSECTION CURVE REFORMO

```
JOB :EPS2054,REFORMO,JD(JT 100,MZ 20K)
UAFORTRAN LINES 2000
C
      MASTER REFORMO
C
C  WRITE RESULTS HEADING
C
      WRITE(2,100)
C
      READ(1,101) THETAS,THETAF,STEP
      WRITE(2,102)THETAS,THETAF,STEP
C
C  READ CONSTANTS FOR RUN
C
      READ(1,101) SA,SB,W,R,SD
      WRITE(2,103)SA,SB,W,R,SD
C
      THETA = THETAS
C
    1 SC = SQRT(SA*SA + SB*SB)/(R-SD)
C
      B1 = SC*THETA
C
C  PUT BETA EQUAL TO 0.0 IF CUTTER ON CENTRE
C
      BETA = 0.1818
C
      YYY = SQRT(SA*SA + SB*SB)
C
      A1 = SA-SD+R*(1.0-COS(BETA)*COS(B1))+W*SIN(BETA)
      A2 = SB*W*COS(BETA)+R*(SA*SIN(B1)+SB*SIN(BETA)*COS(B1))
     *  /YYY
      A3 = W*SA*COS(BETA)+R*(SA*SIN(BETA)*COS(B1)-SB*SIN(B1))
     *  /YYY
C
C  CALCULATE VALUES OF X,Y,Z
C
      X = A1*COS(THETA) + A2*SIN(THETA)
      Y = A1*SIN(THETA) - A2*COS(THETA)
      Z = A3 + SB*THETA
C
      WRITE(2,104) X,Y,Z
C
      BETAP = -Z/SB
C
      SBETAP = SIN(BETAP)
```

```
C
      WRITE(2,1000) BETAP,SBETAP
C
      X1 = X*COS(BETAP) - Y*SIN(BETAP)
      Y1 = X*SIN(BETAP) + Y*COS(BETAP)
      Z1 = Z + SB*BETAP
C
      WRITE(2,106) X1,Y1,Z1
C
C   CHANGE THETA STATEMENT FOR LEADING OR TRAILING EDGE
C
      IF(THETAF .LT. 0.0) GO TO 2
C
      THETA = THETA + STEP
C
      IF(THETA .LT. THETAF) GO TO 1
C
    2 THETA = THETA - STEP
C
      IF(THETA .GT. THETAF) GO TO 1
C
      STOP
C
C   ******** FORMAT STATEMENTS ********
C
  100 FORMAT(1H1,///29H****** RESULTS ******///)
C
  101 FORMAT(5F0.0)
C
  102 FORMAT(///
     *9X,52HTHETAS                                          ,F16.8//
     *9X,52HTHETAF                                          ,F16.8//
     *9X,52HTHE STEP SIZE                                   ,F16.8//)
C
  103 FORMAT(///
     *9X,52HSA                                              ,F16.8//
     *9X,52HSB                                              ,F16.8//
     *9X,52HW                                               ,F16.8//
     *9X,52HR                                               ,F16.8//
     *9X,52HSD                                              ,F16.8//)
C
  104 FORMAT(1H ///,3(2X,F16.8)///)
C
  106 FORMAT(1H ,//3(2X,F16.8))
C
 1000 FORMAT(1H ,///4H***,2(2X,F16.8))
C
      END
      FINISH


C  INSERT DATA CARDS FOR THETAS,THETAF,STEP,CONSTANTS
****
```

(A2) VEEFORMO - CONSTANT LEAD

(Vee Form Cutter - On Centre or Set Over)

FLOWCHART FOR VEEFORMO

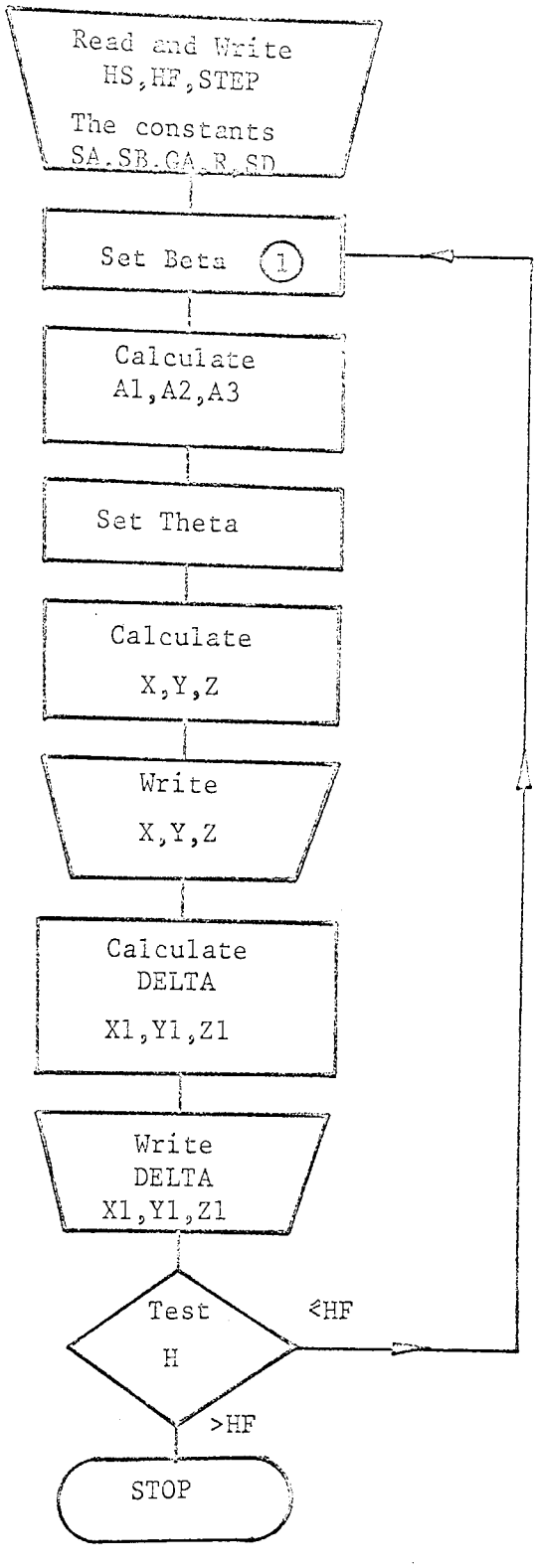

## FORTRAN PROGRAMME FOR PLANE INTERSECTION CURVE VEEFORMO

```
JOB :EPS2054,VEEFORMO,JD(JT 100,MZ 20K)
UAFORTRAN LINES 2000
C
      MASTER VEEFORMO
C
C  WRITE RESULTS HEADING
C
      WRITE(2,100)
C
      READ(1,101) HS,HF,STEP
      WRITE(2,102)HS,HF,STEP
C
C  READ CONSTANTS FOR RUN
C
      READ(1,101) SA,SB,GA,R,SD
      WRITE(2,103)SA,SB,GA,R,SD
C
      H = HS
C
C  PUT BETA EQUAL TO 0.0 IF CUTTER ON CENTRE
C
    1 BETA = 0.1818
C
      YYY = SQRT(SA*SA + SB*SB)
C
      Q1 = SIN(BETA)
      Q2 = COS(BETA)
C
      P1 = SB*COS(BETA)/YYY
      P2 = SB*SIN(BETA)/YYY
      P3 = SA/YYY
C
      S1 = SA*COS(BETA)/YYY
      S2 = SA*SIN(BETA)/YYY
      S3 = SB/YYY
C
      A1 = SA+R-SD-Q2*(R-H)-Q1*H*TAN(GA)
      A2 = P2*(R-H)+P1*H*TAN(GA)
      A3 = S2*(R-H)+S1*H*TAN(GA)
C
C  CALCULATE VALUES OF X,Y,Z
C
C  SET VALUE OF THETA
C
      THETA = 0.0
C
      X = A1*COS(THETA) + A2*SIN(THETA)
      Y = A1*SIN(THETA) - A2*COS(THETA)
      Z = A3 + SB*THETA
```

```
C
      WRITE(2,104) X,Y,Z
C
      BETAP = -Z/SB
C
      SBETAP = SIN(BETAP)
C
      WRITE(2,1000) BETAP,SBETAP
C
      X1 = X*COS(BETAP) - Y*SIN(BETAP)
      Y1 = X*SIN(BETAP) + Y*COS(BETAP)
      Z1 = Z + SB*BETAP
C
      WRITE(2,106) X1,Y1,Z1
C
      H = H + STEP
C
      IF(H .LT. HF) GO TO 1
C
      STOP
C
C  ******** FORMAT STATEMENTS ********
C
  100 FORMAT(1H1,///29H****** RESULTS ******///)
C
  101 FORMAT(5F0.0)
C
  102 FORMAT(///
     *9X,52HHS                                                ,F16.8/
     *9X,52HHF                                                ,F16.8/
     *9X,52HTHE STEP SIZE                                     ,F16.8//)
C
  103 FORMAT(///
     *9X,52HSA                                                ,F16.8/
     *9X,52HSB                                                ,F16.8/
     *9X,52HGA                                                ,F16.8/
     *9X,52HR                                                 ,F16.8/
     *9X,52HSD                                                ,F16.8//)
C
  104 FORMAT(1H ///,3(2X,F16.8)///)
C
  106 FORMAT(1H ,//3(2X,F16.8))
C
 1000 FORMAT(1H ,///4H***,2(2X,F16.8))
C
      END
      FINISH


C  INSERT DATA CARDS FOR HS,HF,STEP,CONSTANTS
****
```

(A3) CIRFORMO - CONSTANT LEAD

(Circular Form Cutter - On Centre or Set Over)

FLOWCHART FOR CIRFORMO

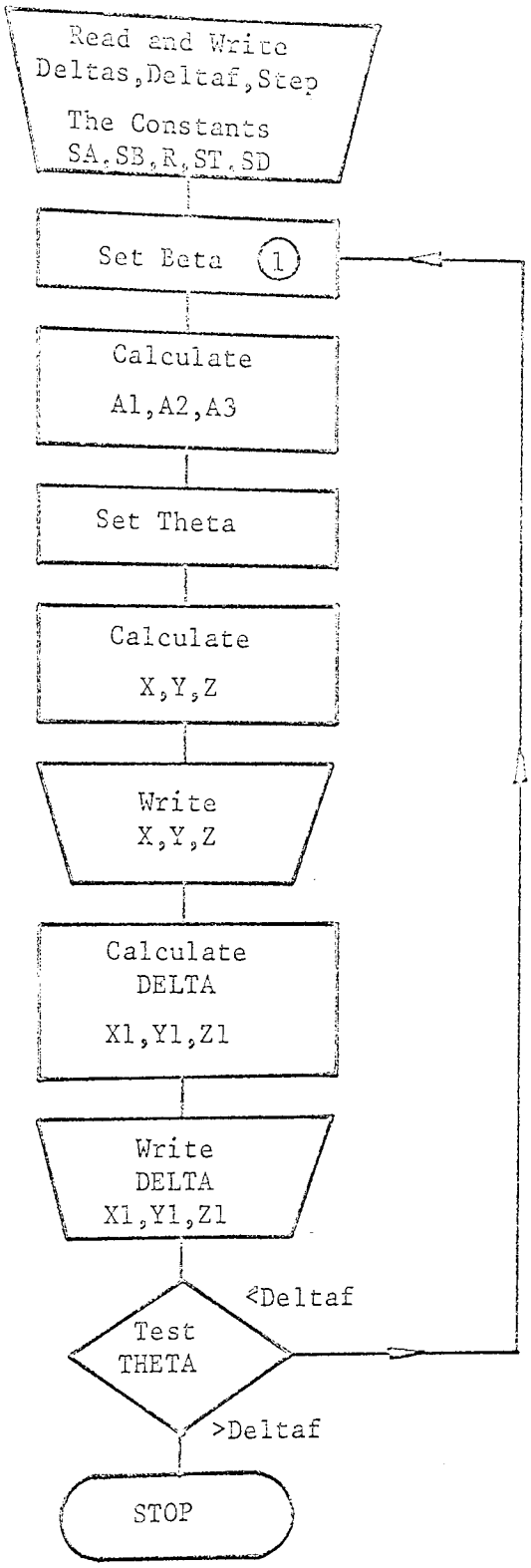

## FORTRAN PROGRAMME FOR PLANE INTERSECTION CURVE CIRFORMO

```
JOB :EPS2054,CIRFORMO,JD(JT 100,MZ 20K)
UAFORTRAN LINES 2000
C
      MASTER CIRFORMO
C
C  WRITE RESULTS HEADING
C
      WRITE(2,100)
C
      READ(1,101) DELTAS,DELTAF,STEP
      WRITE(2,102)DELTAS,DELTAF,STEP
C
C  READ CONSTANTS FOR RUN
C
      READ(1,101) SA,SB,ST,R,SD
      WRITE(2,103)SA,SB,ST,R,SD
C
      DELTA = DELTAS
C
C  PUT BETA EQUAL TO 0.0 IF CUTTER ON CENTRE
C
    1 BETA = 0.1818
C
      YYY = SQRT(SA*SA + SB*SB)
C
      Q1 = SIN(BETA)
      Q2 = COS(BETA)
C
      P1 = SB*COS(BETA)/YYY
      P2 = SB*SIN(BETA)/YYY
C
      S1 = SA*COS(BETA)/YYY
      S2 = SA*SIN(BETA)/YYY
C
      A1 = -Q12(R-ST*(1.0-COS(DELTA))) + Q2*ST*SIN(DELTA)
     *    +SA+R-SD
C
      A2 = P2*(R-ST*(1.0-COS(DELTA))) + P1*ST*SIN(DELTA)
C
      A3 = S2*(R-ST*(1.0-COS(DELTA))) + S1*ST*SIN(DELTA)
C
C  CALCULATE VALUES OF X,Y,Z
C
C  SET VALUE OF THETA
C
      THETA = 0.0
C
      X = A1*COS(THETA) + A2*SIN(THETA
      Y = A1*SIN(THETA) - A2*COS(THETA)
      Z = A3 + SB*THETA
```

```
C
      WRITE(2,104) X,Y,Z
C
      BETAP = -Z/SB
C
      SBETAP = SIN(BETAP)
C
      WRITE(2,1000) BETAP,SBETAP
C
      X1 = X*COS(BETAP) - Y*SIN(BETAP)
      Y1 = X*SIN(BETAP) + Y*COS(BETAP)
      Z1 = Z + SB*BETAP
C
      WRITE(2,106) X1,Y1,Z1
C
      DELTA = DELTA + STEP
C
      IF(DELTA .LT. THETAF) GO TO 1
C
      STOP
C
C  ******** FORMAT STATEMENTS ********
C
  100 FORMAT(1H1,///29H****** RESULTS ******///)
C
  101 FORMAT(5F0.0)
C
  102 FORMAT(///
     *9X,52HDELTAS                                          ,F16.8//
     *9X,52HDELTAF                                          ,F16.8//
     *9X,52HTHE STEP SIZE                                   ,F16.8//)
C
  103 FORMAT(///
     *9X,52HSA                                              ,F16.8//
     *9X,52HSB                                              ,F16.8//
     *9X,52HST                                              ,F16.8//
     *9X,52HR                                               ,F16,8//
     *9X,52HSD                                              ,F16,8//)
C
  104 FORMAT(1H ///,3(2X,F16.8)///)
C
  106 FORMAT(1H ///3(2X,F16.8))
C
 1000 FORMAT(1H ///,4H***,2(2X,F16.8))
C
      END
      FINISH


C  INSERT DATA CARDS FOR DELTAS,DELTAF,STEP,CONSTANTS
****
```

(B1) VESCO - CONSTANT LEAD

(Vee Form Cutter - Set Over)

TRUE NORMAL RAKE ANGLE FOR ENGLISH ELECTRIC FORM CUTTER: RE -- ETHERIDGE & SCOTT

FLOWCHART FOR VESCO

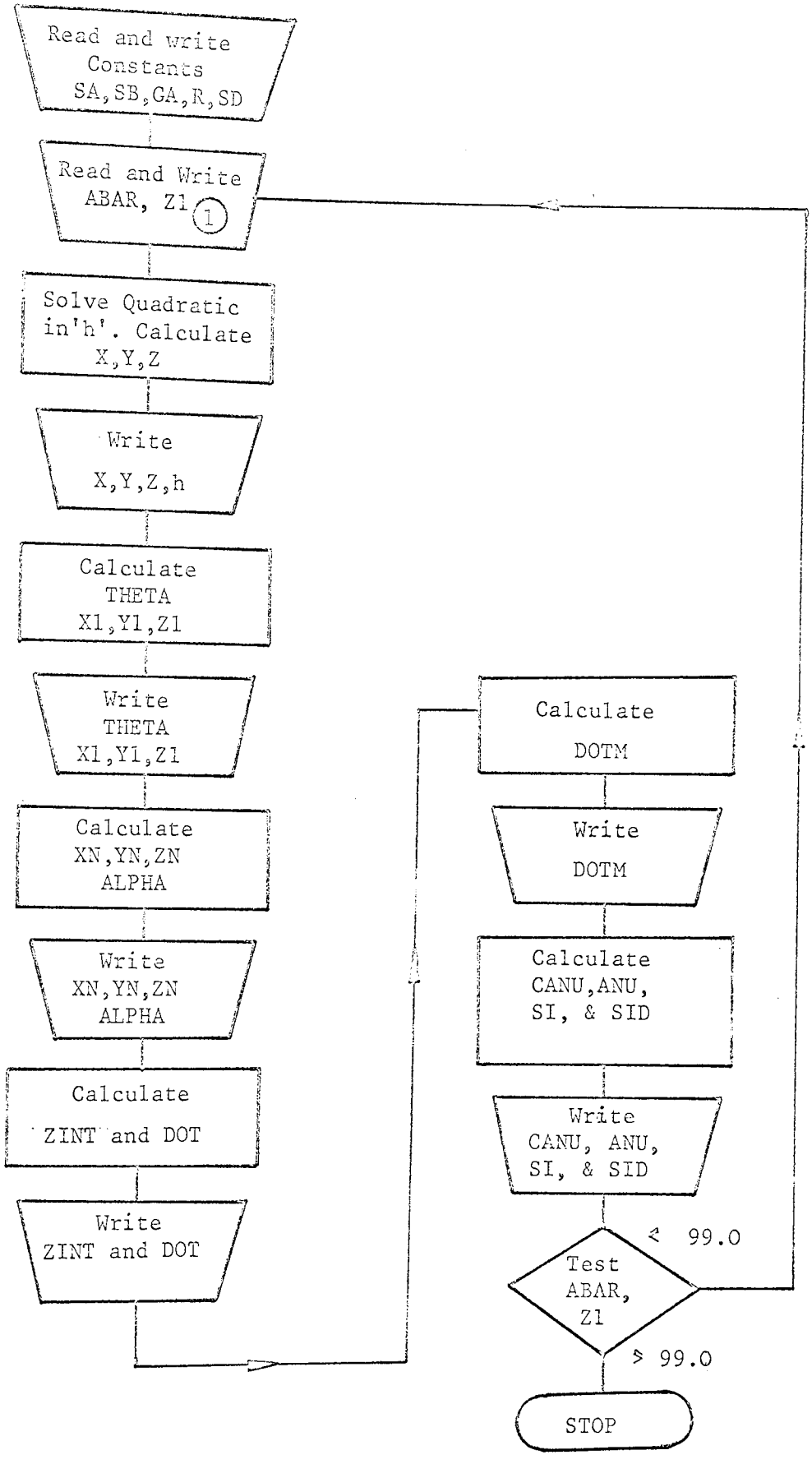

## FORTRAN PROGRAMME FOR TRUE NORMAL RAKE ANGLE

```
JOB :EPS2054,VESCO,JD(JT 120,MZ 20K)
UAFORTRAN LINES 2000
C
      MASTER VESCO
C
C  WRITE RESULTS HEADING
C
      WRITE(2,100)
C
      READ(1,101) SA,SB,GA,R,SD
      WRITE(2,103)SA,SB,GA,R,SD
C
C  READ VALUES OF ZED AND RADIUS FOR RAKE ANGLE DETERMINATION
C
      READ(1,101) ABAR,Z1
      WRITE(2,121)ABAR,Z1
C
      IF(ABAR .GE. 99.0) STOP
C
      YYY = SQRT(SA*SA + SB*SB)
C
      BETA = 0.1845
C
      Q1 = SIN(BETA)
      Q2 = COS(BETA)
C
      P1 = SB*COS(BETA)/YYY
      P2 = SB*SIN(BETA)/YYY
      P3 = SA/YYY
C
      S1 = SA*COS(BETA)/YYY
      S2 = SA*SIN(BETA)/YYY
      S3 = SB/YYY
C
C  CALCULATE VALUE FOR H
C
      A = SA - SD + R*(1.0 - Q2)
      B = Q2 - Q1*TAN(GA)
      D = P2*R
      E = P2 - P1*TAN(GA)
C
      BB1 = A*A + D*D
      BB2 = 2.0*A*B - 2.0*D*E
      BB3 = B*B + E*E
C
      P = BB2/BB3
      Q = (BB1 - ABAR*ABAR)/BB3
```

```
C
      H = -P/2.0 + (SQRT(P*P - 4.0*Q))/2.0
C
      WRITE(2,250) H
C
C  CALCULATE VALUES OF X,Y,Z FOR ZERO THETA
C
      THETA = 0.0
C
      A1 = SA - SD + R*(1.0 - Q2) + H*(Q2 - Q1*TAN(GA))
      A2 = H*(P1*TAN(GA) - P2) + P2*R
      A3 = H*(S1*TAN(GA) - S2) + S2*R
C
      X = A1*COS(THETA) + A2*SIN(THETA)
      Y = A1*SIN(THETA) - A2*COS(THETA)
      Z = A3 + SB*THETA
C
      WRITE(2,104) X,Y,Z
C
C  CALCULATE THETA IN ORDER TO FIND X1,Y1,Z1
C
      THETA = (Z1 - Z)/SB
C
      WRITE(2,1000) THETA
C
C  CALCULATE X1,Y1,Z1
C
      X1 = X*COS(THETA) - Y*SIN(THETA)
      Y1 = X*SIN(THETA) + Y*COS(THETA)
      Z1 = Z + SB*THETA
C
      WRITE(2,106) X1,Y1,Z1
C
C CALCULATE XN,YN,ZN,BX,BY,BZ
C
      B1 = COS(BETA) - SIN(BETA)*TAN(GA)
      B2 = SB*(COS(BETA)*TAN(GA) - SIN(BETA))/YYY
      B3 = SA*(COS(BETA)*TAN(GA) - SIN(BETA))/YYY
C
      R1 = SQRT(B1*B1 + B2*B2)
      R2 = SQRT(A1*A1 + A2*A2)
C
      DELTA = ATAN(A2/A1)
      ALPHA = ATAN(B2/B1)
C
      WRITE(2,130) DELTA
C
      C1 = A3*R2
      C2 = SB*R1
      C3 = R1*R2
C
      SIDA = SIN(DELTA - ALPHA)
      CODA = COS(DELTA - ALPHA)
```

```
C
      BBB = SQRT(C1*C1+C2*C2-2.0*C1*C2*SIDA+C3*C3*CODA*CODA)
C
      XN = (C1*COS(DELTA-THETA) + C2*SIN(ALPHA-THETA))/BBB
      YN = -(C1*SIN(DELTA-THETA) - C2*COS(ALPHA-THETA))/BBB
      ZN = -C3*CODA/BBB
C
      WRITE(2,108) ALPHA,XN,YN,ZN
C
      BX = R1*COS(ALPHA-THETA)
      BY = -R1*SIN(ALPHA-THETA)
      BZ = B3
C
C   CALCULATE INTERCEPT WITH Z AXIS
C
      SL1 = (YN*BZ - ZN*BY)/(XN*BY - YN*BX)
      SL2 = (XN*BZ - ZN*BX)/(XN*BY - YN*BX)
C
      ZINT = X1*SL1 - Y1*SL2 + Z1
C
      WRITE(2,109) ZINT
C
C   CALCULATE NBAR DOT PQ2 (CALL IT DOT)
C
      DOT = X1*XN + Y1*YN + (Z1-ZINT)*ZN
C
      WRITE(2,110) DOT
C
C   CALCULATE MAGNITUDE OF NBAR DOT PQ2 (CALL IT DOTM)
C
      DOTM = SQRT(X1*X1 + Y1*Y1 + (ZINT-Z1)*(ZINT-Z1))
C
      WRITE(2,115) DOTM
C
C   CALCULATE COS(NU)   (CALL IT CANU)
C
      CANU = DOT/DOTM
C
      ANU = ACOS(CANU)
C
      WRITE(2,117) ANU
C
      SI = 3.14159/2.0 - ANU
C
C  CONVERTFROM RADIANS TO DEGREES
C
      SID = 57.29578*SI
C
      WRITE(2,120) SI,SID
C
      GO TO 1
```

```
C
C   ******** FORMAT STATEMENTS ********
C
  100 FORMAT(1H1,///'****** RESULTS ******'///)
C
  101 FORMAT(9F0.0)
C
  103 FORMAT(1H ,2X,'SA =',F8.4,2X,'SB =',F8.4,2X,'GA =',
     * F8.4,2X,'R =',F8.4,2X,'SD =',F8.4//)
C
  104 FORMAT(1H ,2X,'X =',F8.4,2X,'Y =',F8.4,2X,'Z =',F8.4//)
C
 1000 FORMAT(1H ,9X,'****** THE VALUE OF THETA IS...',F8.4//)
C
  106 FORMAT(1H ,2X,'X1 =',F8.4,2X,'Y1 =',F8.4,2X,'Z1 =',F8.4/)
C
  108 FORMAT(1H ,//9X,'*****THE VALUE OF ALPHA IS...',F8.4//
     *   5X,'XN =',F8.4,5X,'YN =',F8.4,5X,'ZN =',F8.4//)
C
  109 FORMAT(1H ,//9X,'****** THE VALUE OF ZINT...',F8.4//)
C
  110 FORMAT(1H ,//9X.'******THE VALUE OF DOT IS...',F8.4//)
C
  115 FORMAT(1H ,//9X,'******THE VALUE OF DOTM ....',F8.4//)
C
  117 FORMAT(1H ,//9X,'******THE VALUE OF ANU IS...',F8.4//)
C
  120 FORMAT(1H ,//9X,'******THE VALUE OF SI IS....',F8.4///
     * 9X,'******** SID AS CALCULATED IS....',F8.4///)
C
  121 FORMAT(1H1,12X,'ABAR =',F8.4,12X,'Z1 =',F8.4//)
C
  130 FORMAT(1H ,9X,'******THE VALUE OF DELTA IS....',F8.4//)
C
  250 FORMAT(1H ,5X,'****** CALCULATED VALUE OF H IS...',F8.4/)
C
      END
      FINISH


C  INSERT DATA CARDS FOR CONSTANTS,ABAR AND Z1
****
```

(B2) VENSCO - CONSTANT LEAD

(Vee Form Cutter - Set Over)

NORMAL RAKE ANGLE IN BASE PLANE FOR ENGLISH ELECTRIC FORM CUTTER: RE - ETHERIDGE & SCOTT

FLOWCHART FOR VENSCO

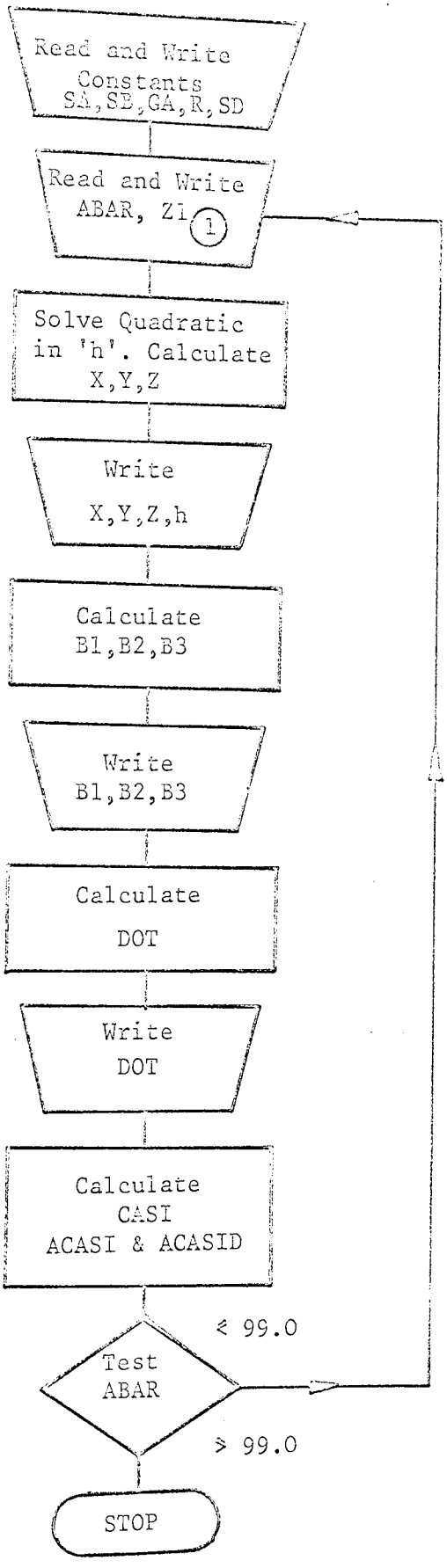

## FORTRAN PROGRAMME FOR RAKE ANGLE IN BASE PLANE

```
JOB :EPS2054,VENSCO,JD(JT 100,MZ 20K)
UAFORTRAN LINES 2000
C
      MASTER VENSCO
C
C  WRITE RESULTS HEADING
C
      WRITE(2,100)
C
C  READ CONSTANTS FOR RUN
C
      READ(1,101) SA,SB,GA,R,SD
      WRITE(2,103)SA,SB,GA,R,SD
C
C  READ VALUES OF ZED AND RADIUS FOR RAKE ANGLE DETERMINATION
C
    1 READ(1,101) ABAR,Z1
      WRITE(2,121)ABAR,Z1
C
      IF(ABAR .GE. 99.0) STOP
C
      YYY = SQRT(SA*SA + SB*SB)
C
      BETA = 0.1845
C
      Q1 = SIN(BETA)
      Q2 = COS(BETA)
C
      P1 = SB*COS(BETA)/YYY
      P2 = SB*SIN(BETA)/YYY
      P3 = SA/YYY
C
      S1 = SA*COS(BETA)/YYY
      S2 = SA*SIN(BETA)/YYY
      S3 = SB/YYY
C
C  CALCULATE VALUE OF H
C
      A = SA - SD + R*(1.0 - Q2)
      B = Q2 - Q1*TAN(GA)
      D = P2*R
      E = P2 - P1*TAN(GA)
C
      BB1 = A*A + D*D
      BB2 = 2.0*A*B - 2.0*D*E
      BB3 = B*B + E*E
C
      P = BB2/BB3
      Q = (BB1 - ABAR*ABAR)/BB3
```

```
C
      H = -P/2.0 + (SQRT(P*P - 4.0*Q))/2.0
C
      WRITE(2,250) H
C
C   CALCULATE VALUES OF X,Y,Z FOR ZERO THETA
C
      THETA = 0.0
C
      A1 = SA - SD + R*(1.0 - Q2) + H*(Q2 - Q1*TAN(GA))
      A2 = H*(P1*TAN(GA) - P2) + P2*R
      A3 = H*(S1*TAN(GA) - S2) + S2*R
C
C
      X = A1*COS(THETA) + A2*SIN(THETA)
      Y = A1*SIN(THETA) - A2*COS(THETA)
      Z = A3 + SB*THETA
C
      WRITE(2,255) X,Y,Z
C
      B1 = COS(BETA) - SIN(BETA)*TAN(GA)
      B2 = SB*(COS(BETA)*TAN(GA) - SIN(BETA))/YYY
      B3 = SA*(COS(BETA)*TAN(GA) - SIN(BETA))/YYY
C
      WRITE(2,2000) B1,B2,B3
C
      DOT = X*B1 + Z*B3 - Y*B2
C
      ROO1 = SQRT(B1*B1 + B2*B2 + B3*B3)
      ROO2 = SQRT(X*X + Y*Y + Z*Z)
C
      EEE = ROO1*ROO2
C
      CASI = DOT/EEE
C
      ACASI = ACOS(CASI)
C
      ACASID = 57.29578*ACASI
C
      WRITE(2,124) CASI,ACASI,ACASID
C
      GO TO 1
C
C   ******** FORMAT STATEMENTS ********
C
  100 FORMAT(1H1,///'****** RESULTS ******'///)
C
  101 FORMAT(9F0.0)
C
  103 FORMAT(1H ,2X,'SA =',F8.4,2X,'SB =',F8.4,2X,'GA =',
     *  F8.4,2X,'R =',F8.4,2X,'SD =',F8.4//)
C
  121 FORMAT(1H1,//12X,'ABAR =',F8.4,12X,'Z1 =',F8.4//)
C
  250 FORMAT(1H ,5X,'******* CALCULATED VALUE OF H IS ..'F8.4//)
```

```
C
  255 FORMAT(1H ,//9X,'X =',F8.4,9X,'Y =',F8.4,9X,'Z =',F8.4//)
C
 2000 FORMAT(1H ,9X,'B1 =',F8.4,9X,'B2 =',F8.4,9X,'B3 =',F8.4/)
C
  124 FORMAT(1H ,//9X,'*** THE VALUE OF CASI ...',F8.4//
     *   9X,'*** THE VALUE OF ACASI ...',F8.4/////
     *   9X,'*** THE VALUE OF ACASID IN DEGREES ...',F8.4//)
C
      END
      FINISH


C  INSERT DATA CARDS FOR CONSTANTS, ASAR AND Z1
****
```

(B3) VETSCO - CONSTANT LEAD

(Vee Form Cutter - Set Over)

RAKE ANGLE IN A TRANSVERSE PLANE FOR ENGLISH ELECTRIC FORM CUTTER: RE - ETHERIDGE & SCOTT

FLOWCHART FOR VETSCO

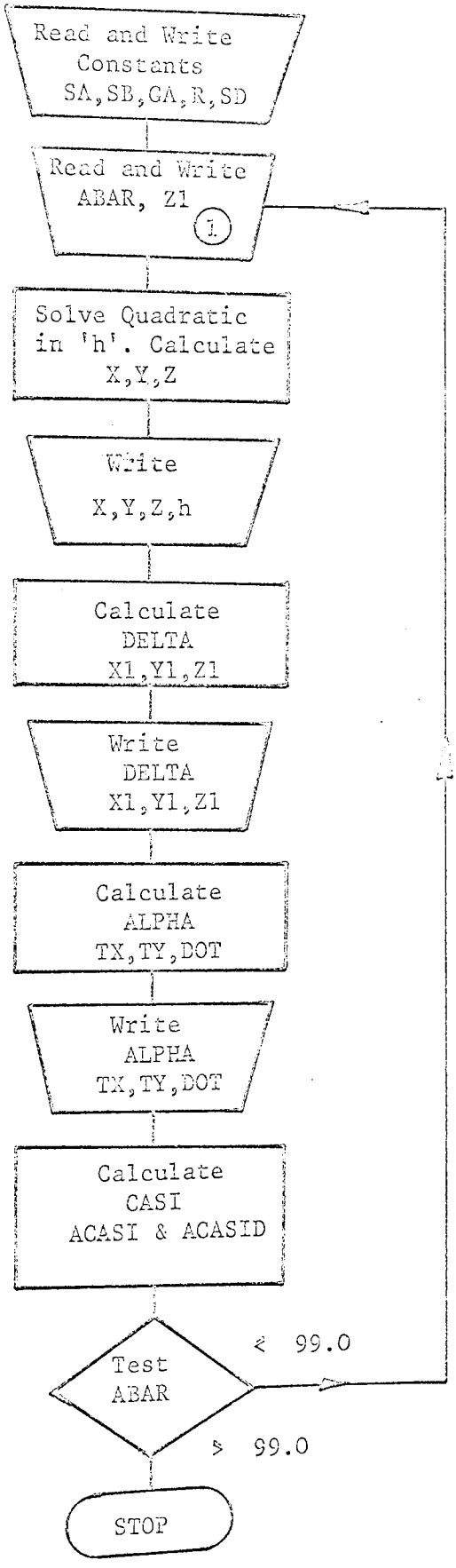

## FORTRAN PROGRAMME FOR RAKE ANGLE IN TRANSVERSE PLANE VETSCO

```
JOB :EPS2054,VETSCO,JD(JT 100,MZ 20K)
UAFORTRAN LINES 2000
C
      MASTER VETSCO
C
C   WRITE RESULTS HEADING
C
      WRITE(2,100)
C
C   READ CONSTANTS FOR RUN
C
      READ(1,101) SA,SB,GA,R,SD
      WRITE(2,103)SA,SB,GA,R,SD
C
C   READ VALUES OF ZED AND RADIUS FOR RAKE ANGLE DETERMINATION
C
      READ(1,101) ABAR,Z1
      WRITE(2,121)ABAR,Z1
C
      IF(ABAR .GE. 99.0) STOP
C
      YYY = SQRT(SA*SA + SB*SB)
C
      BETA = 0.1845
C
      Q1 = SIN(BETA)
      Q2 = COS(BETA)
C
      P1 = SB*COS(BETA)/YYY
      P2 = SB*SIN(BETA)/YYY
      P3 = SA/YYY
C
      S1 = SA*COS(BETA)/YYY
      S2 = SA*SIN(BETA)/YYY
      S3 = SB/YYY
C
C   CALCULATE VALUE OF H
C
      A = SA - SD + R*(1.0 - Q2)
      B = Q2 - Q1*TAN(GA)
      D = P2*R
      E = P2 - P1*TAN(GA)
C
      BB1 = A*A + D*D
      BB2 = 2.0*A*B - 2.0*D*E
      BB3 = B*B +E*E
```

```
C
      P = BB2/BB3
      Q = (BB1 - ABAR*ABAR)/BB3
C
      H = -P/2.0 + (SQRT(P*P - 4.0*Q))/2.0
C
      WRITE(2,250) H
C
C CALCULATE VALUES OF X,Y,Z FOR ZERO THETA
C
      THETA = 0.0
C
      A1 = SA - SD + R*(1.0 -Q2) + H*(Q2 - Q1*TAN(GA))
      A2 = H*(P1*TAN(GA) - P2) + P2*R
      A3 = H*(S1*TAN(GA) - S2) + S2*R
C
C
      X = A1*COS(THETA) + A2*SIN(THETA)
      Y = A1*SIN(THETA) - A2*COS(THETA)
      Z = A3 + SB*THETA
C
      WRITE(2,255) X,Y,Z
C
C
      DELTA = -Z/SB
C
      X1 = X*COS(DELTA) - Y*SIN(DELTA)
      Y1 = X*SIN(DELTA) + Y*COS(DELTA)
      Z1 = Z + SB*DELTA
C
      WRITE(2,105) DELTA,X1,Y1,Z1
C
      ALPHA = ATAN(Y/X)
C
      WRITE(2,106) ALPHA
C
      PPP = COS(DELTA - ALPHA)*COS(DELTA - ALPHA)
C
      TX = -1.0/PPP
      TY = 1.0
C
      WRITE(2,2000) TX,TY
C
      ROO1 = SQRT(X1*X1 + Y1*Y1)
      ROO2 = SQRT(TX*TX + 1.0)
C
      EEE = ROO1*ROO2
C
      DOT = TX*X1 + TY*Y1
C
      CASI = DOT/EEE
C
      ACASI = ACOS(CASI)
```

```
C
      ACASID = 57.29578*ACASI
C
      WRITE(2,124) CASI,ACASI,ACASID
C
      GO TO 1
C
C  ******** FORMAT STATEMENTS ********
C
  100 FORMAT(1H1,///'******** RESULTS ********'///)
C
  101 FORMAT(9F0.0)
C
  103 FORMAT(1H ,2X,'SA =',F8.4,2X,'SB =',F8.4,2X,'GA =',
     *  F8.4,2X,'R =',F8.4,2X,'SD =',F8.4,2X,'STEP =',F8.4//)
C
  106 FORMAT(1H ,9X,'****** THE VALUE OF ALPHA IS...',F8.4//)
C
  121 FORMAT(1H1,9X,'ABAR =',F8.4,9X,'Z1 =',F8.4//)
C
  105 FORMAT(1H ,9X,'**** THE VALUE OF DELTA IS...',F8.4//
     *  5X,'X1 =',F8.4,5X,'Y1 =',F8.4,5X,'Z1 =',F8.4///)
C
  255 FORMAT(1H ,//9X,'X =',F8.4,9X,'Y =',F8.4,9X,'Z =',F8.4//)
C
 2000 FORMAT(1H ,9X,'TX =',F8.4,9X,'TY =',F8.4///)
C
  124 FORMAT(1H ,//9X,'**** THE VALUE OF CASI IS ...',F16.8,
     *  9X,'**** THE VALUE OF ACASI IS ....',F16.8/////
     *  9X,'**** THE VALUE OF ACASID IN DEGREES IS ...',F16.8//)
C
       END
       FINISH


C  INSERT DATA CARDS FOR CONSTANTS, ABAR AND Z1
****
```

(C1) VALREFORMOE - VARIABLE LEAD

(Rectangular Form Cutter - End Mill)

FLOWCHART FOR VALREFORMOE

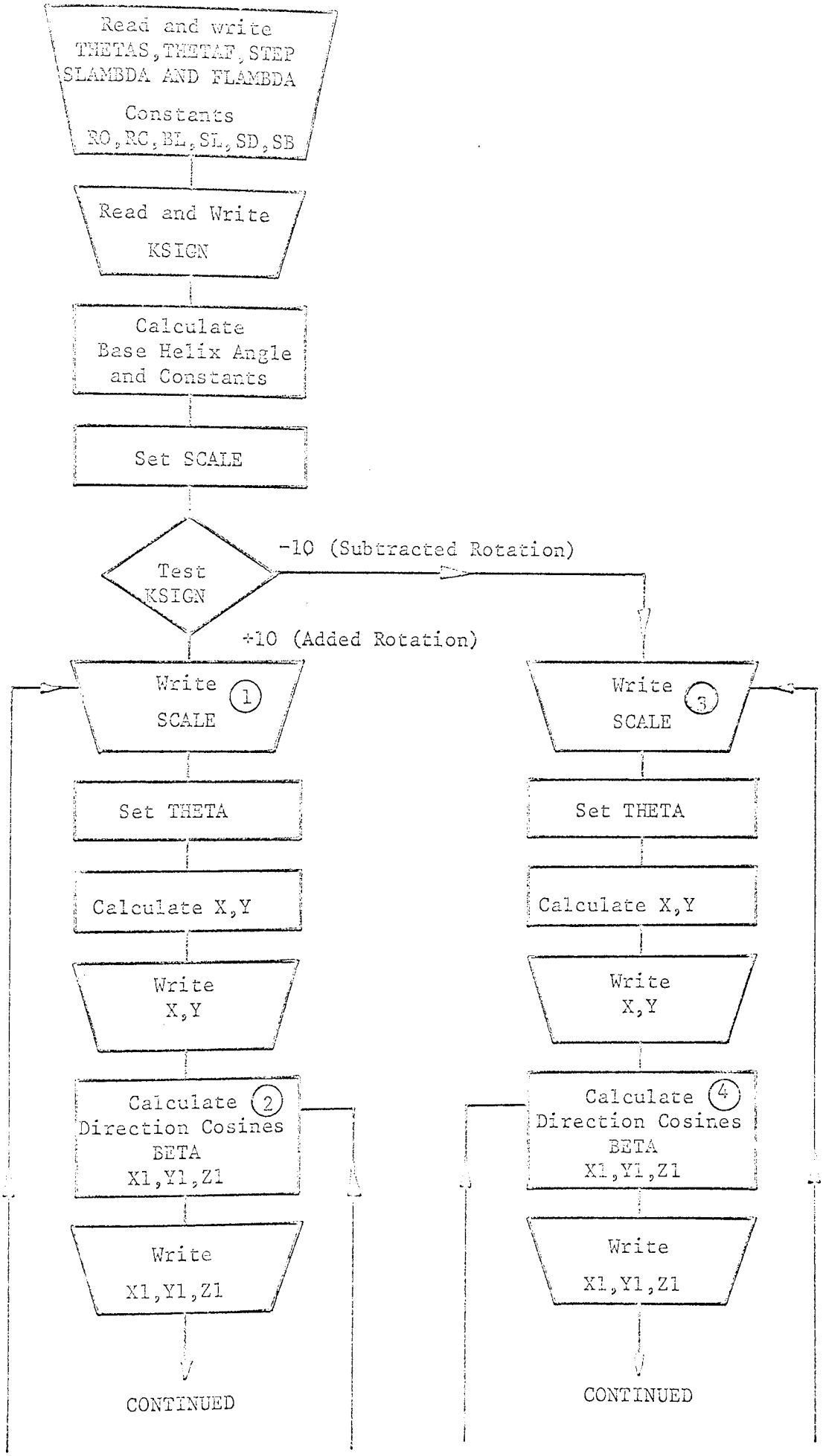

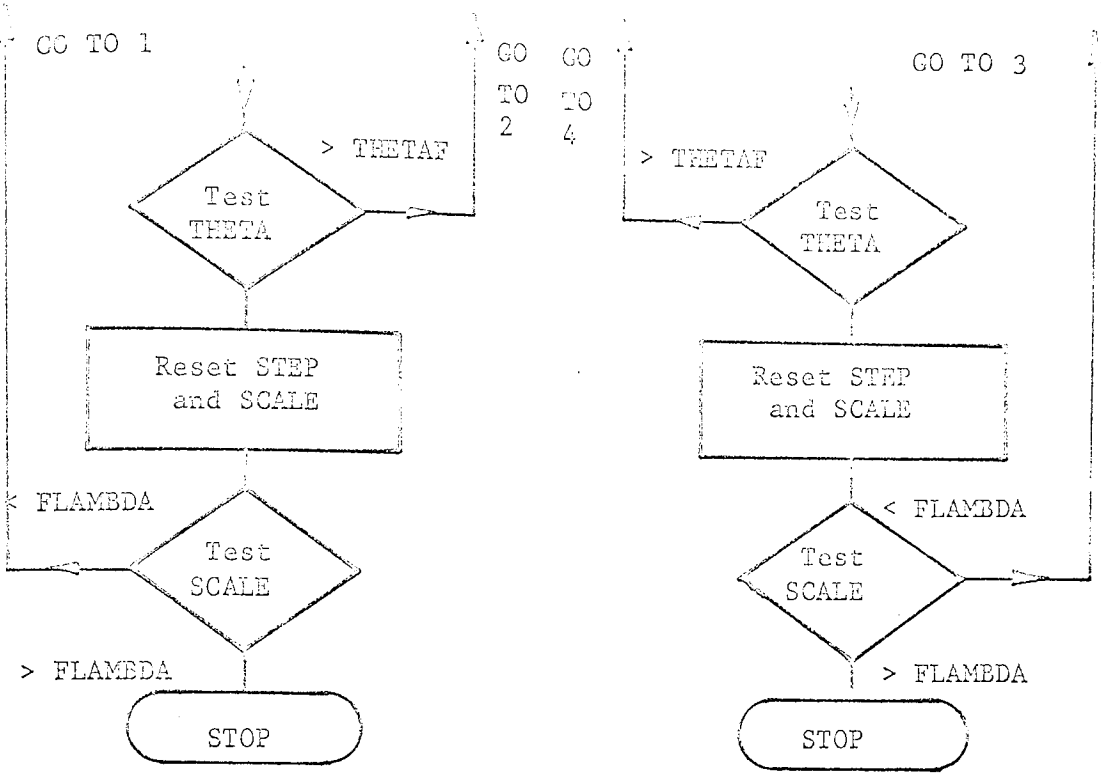
GO TO 1
GO TO 2
GO TO 3
GO TO 4
> THETAF
Test THETA
Reset STEP and SCALE
< FLAMBDA
Test SCALE
> FLAMBDA
STOP
> THETAF
Test THETA
Reset STEP and SCALE
< FLAMBDA
Test SCALE
> FLAMBDA
STOP

## FORTRAN PROGRAMME FOR HELICAL SURFACE VALREFORMOE

```
JOB :EPS2054,VALREFORMOE,JD(JT 100,MZ 20K)
UAFORTRAN LINES 2000
C
      MASTER VALREFORMOE
C
C   WRITE RESULTS HEADING
C
      WRITE(2,100)
C
C   READ RANGE AND INCREMENTS OF THETA
C
      READ(1,101) THETAS,THETAF,STEP
      WRITE(2,102)THETAS,THETAF,STEP
C
C   READ CONSTANTS FOR RUN
C
      READ(1,101) RO,RC,BL,SL,SD,SB
      WRITE(2,104)RO,RC,BL,SL,SD,SB
C
C   READ RANGE AND INCREMENTS OF LAMBDA
C
      READ(1,101) SLAMBDA,FLAMBDA
      WRITE(2,103)SLAMBDA,FLAMBDA
C
C   CHANGE TO NEGATIVE ROTATION
C
      READ(1,109) KSIGN
      WRITE(2,108)KSIGN
C
C
      CL = 3.1415927*2.0*RO/10.0
C
      SIGMA = ATAN(CL)
C
      PPR = SQRT(SL*SL + 1.0)
C
      CONK = SL*COT(SIGMA)/PPR
C
      A = RO*CONK/SL
C
      VMOD = SQRT(RO*RO + SB*SB)
C
      SCALE = SLAMBDA
C
      IF(KSIGN .EQ. -10) GO TO 3
```

```
C
    1 WRITE(2,107) SCALE
C
      THETA = THETAS
C
C
      X = SD - SCALE
      Y = RC
C
      WRITE(2,105) X,Y
C
C
    2 EP2 = EXP(2.0*CONK*THETA)
      EP1 = EXP(CONK*THETA)
C
      SSS = CONK*A*A*EP2
      SST = A*RO*RO*CONK*EP1
C
      AAA = SQRT(RO*RO + A*A*EP2)
      TTT = AAA*AAA
      BBB = SQRT(RO*RO + (CONK*CONK + 1.0)*A*A*EP2)
      CCC = AAA*BBB
C
      PPP = CCC*VMOD
      PPS = BBB*VMOD
      PSS = AAA*VMOD
C
      DOTNN = TTT/CCC
      DOTNB = -CONK*A*EP1/BBB
      DOTNT = 0.0
C
      DOTBN = (SB*SSS +SST)/PPP
      DOTBB = (SB*A*EP1 + RO*RO)/PPS
      DOTBT = (-SB*RO + RO*A*EP1)/PSS
C
      XMOD = X*DOTNN + Y*DOTBN
      YMOD = X*DOTNB + Y*DOTBB
      ZMOD = X*DOTNT + Y*DOTBT
C
C
      VNIDOT = (-TTT*COS(THETA) +SSS*SIN(THETA))/CCC
      VNJDOT = (-TTT*SIN(THETA) - SSS*COS(THETA))/CCC
      VNKDOT = RO*CONK*A*EP1/CCC
C
      BIDOT = (CONK*A*EP1*COS(THETA) + A*EP1*SIN(THETA))/BBB
      BJDOT = (CONK*A*EP1*SIN(THETA) - A*EP1*COS(THETA))/BBB
      BKDOT = RO/BBB
C
      TIDOT = -RO*SIN(THETA)/AAA
      TJDOT = RO*COS(THETA)/AAA
      TKDOT = A*EP1/AAA
```

```
C
C
      ZL = SB*THETA
C
      BETA = ALOG(1.0 + SL*ZL/RO)/CONK
C
C
      X1 = XMOD*VNIDOT + YMOD*BIDOT + ZMOD*TIDOT + RO*COS(BETA)
      Y1 = XMOD*VNJDOT + YMOD*BJDOT + ZMOD*TJDOT + RO*SIN(BETA)
      Z1 = XMOD*VNKDOT + YMOD*BKDOT + ZMOD*TKDOT + SB*THETA
C
      WRITE(2,106) X1,Y1,Z1
C
C
      THETA = THETA + STEP
      IF(THETA .LT. THETAF) GO TO 2
C
C
      STEP1 = 2.0*STEP
C
      SCALE = SCALE + STEP1
      IF(SCALE .LE. FLAMBDA) GO TO 1
C
      STOP
C
C
C
    3 WRITE(2,107) SCALE
C
      THETA = THETAS
C
C
      X = SD - SCALE
      Y = RC
C
      WRITE(2,105) X,Y
C
C
    4 EP2 = EXP(-2.0*CONK*THETA)
      EP1 = EXP(-CONK*THETA)
C
      SSS = CONK*A*A*EP2
      SST = A*RO*RO*CONK*EP1
C
      AAA = SQRT(RO*RO + A*A*EP2)
      TTT = AAA*AAA
      BBB = SQRT(RO*RO + (CONK*CONK + 1.0)*A*A*EP2)
      CCC = AAA*BBB
C
      PPP = CCC*VMOD
      PPS = BBB*VMOD
      PSS = AAA*VMOD
```

```
C
      DOTNN = TTT/CCC
      DOTNB = CONK*A*EP1/BBB
      DOTNT = 0.0
C
      DOTBN = -(SB*SSS +SST)/PPP
      DOTBB = (SB*A*EP1 +RO*RO)/PPS
      DOTBT = (-SB*RO + RO*A*EP1)/PSS
C
      XMOD = X*DOTNN + Y*DOTBN
      YMOD = X*DOTNB + Y*DOTBB
      ZMOD = X*DOTNT + Y*DOTBT
C
C
      VNIDOT = -(TTT*COS(THETA) + SSS*SIN(THETA))/CCC
      VNJDOT = (-TTT*SIN(THETA) + SSS*COS(THETA))/CCC
      VNKDOT = -RO*CONK*A*EP1/CCC
C
      BIDOT = (-CONK*A*EP1*COS(THETA) + A*EP1*SIN(THETA))/BBB
      BJDOT = -(CONK*A*EP1*SIN(THETA) + A*EP1*COS(THETA))/BBB
      BKDOT = RO/BBB
C
      TIDOT = -RO*SIN(THETA)/AAA
      TJDOT = RO*COS(THETA)/AAA
      TKDOT = A*EP1/AAA
C
C
      ZL = SB*THETA
C
      BETA = -ALOG(1.0 - SL*ZL/RO)/CONK
C
C
      X1 = XMOD*VNIDOT + YMOD*BIDOT + ZMOD*TIDOT + RO*COS(BETA)
      Y1 = XMOD*VNJDOT + YMOD*BJDOT + ZMOD*TJDOT + RO*SIN(BETA)
      Z1 = XMOD*VNKDOT + YMOD*BKDOT + ZMOD*TKDOT + SB*THETA
C
      WRITE(2,106) X1,Y1,Z1
C
C
      THETA = THETA + STEP
      IF(THETA .LT. THETAF) GO TO 4
C
C
      STEP1 = 2.0*STEP
C
      SCALE = SCALE + STEP1
      IF(SCALE .LE. FLAMBDA) GO TO 3
C
      STOP
C
C  ******** FORMAT STATEMENTS ********
C
  100 FORMAT(1H1,'******** RESULTS ********'///)
```

```
C
  101 FORMAT(7F0.0)
C
  102 FORMAT(1H ,5X,'THETAS =',F8.4,5X,'THETAF =',F8.4,
     *   5X,'STEP =',F8.4///)
C
  103 FORMAT(1H ,9X,'SLAMBDA =',F8.4,9X,'FLAMBDA =',F8.4///)
C
  104 FORMAT(1H ,2X,'RO =',F8.4,2X,'RC =',F8.4,2X,'BL =',
     *   F8.4,2X,'SL =',F8.4,2X,'SD =',F8.4,2X,'SB = ',F8.4//)
C
  105 FORMAT(1H ,//3(2X,F16.8)///)
C
  106 FORMAT(1H ,//3(2X,F16.8)///)
C
  107 FORMAT(1H1,//'**** THE VALUE OF SCALE IS ....',F8.4///)
C
  108 FORMAT(1H ,5X,'KSIGN =',I3///)
C
  109 FORMAT(I3)
C
C
      END
      FINISH


C   INSERT DATA CARDS FOR THETAS,THETAF,STEP,CONSTANTS,SLAMBDA,
    FLAMBDA,. AND KSIGN
****
```

## (C2) VALREFORMOD - VARIABLE LEAD

(Rectangular Form Cutter - Disc Cutter)

FLOWCHART FOR VALREFORMOD

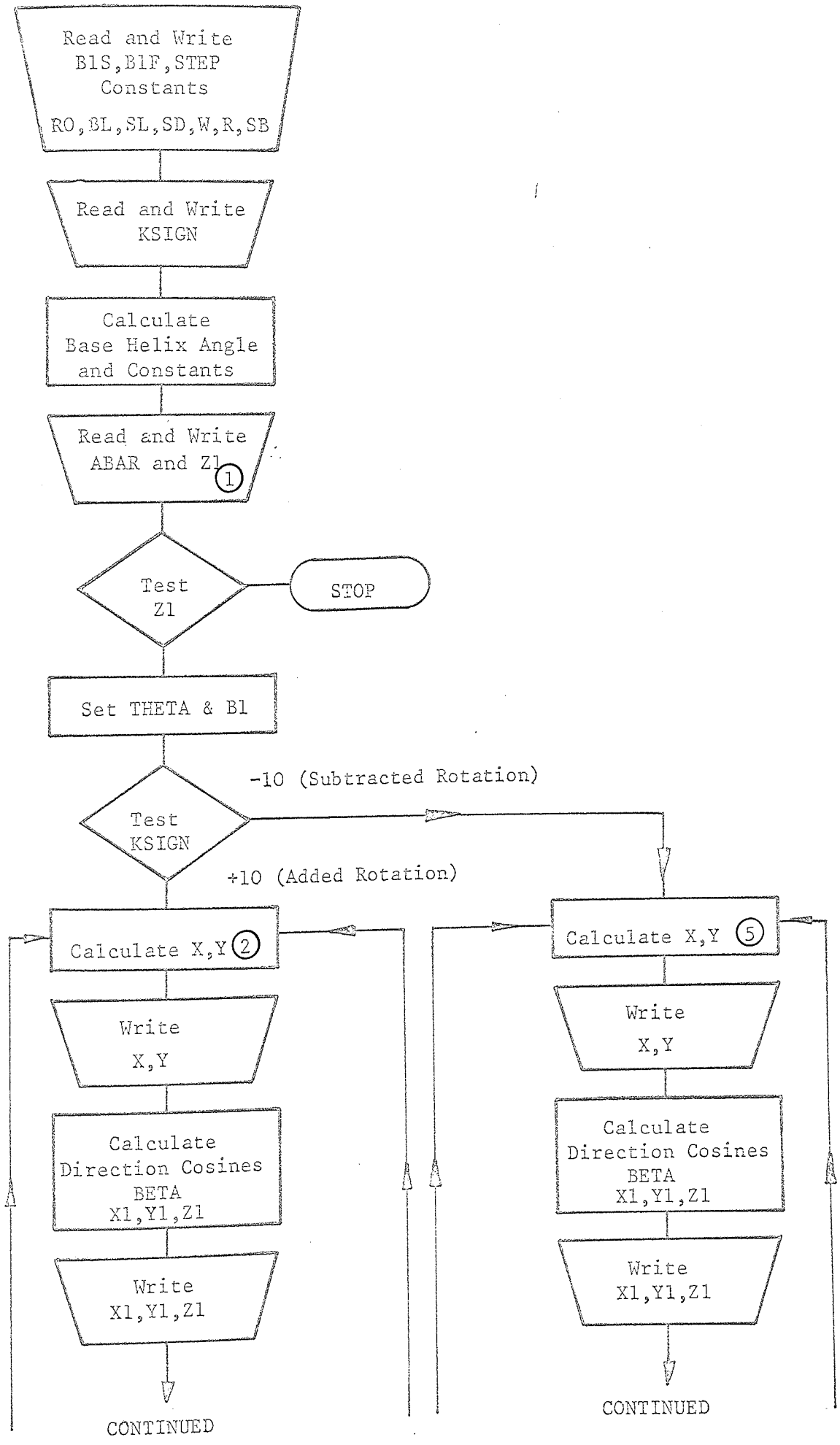

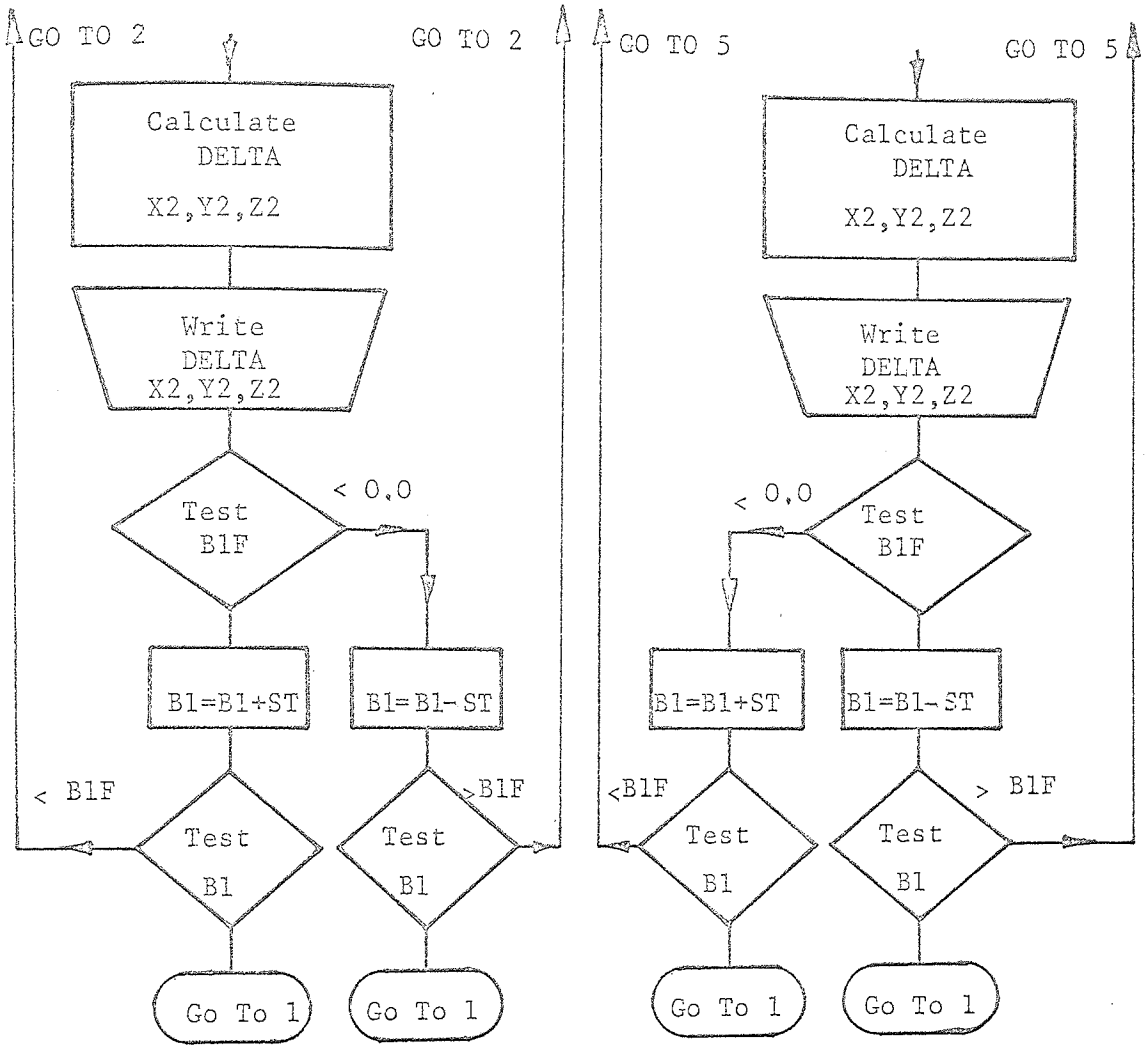
GO TO 2
GO TO 2
Calculate DELTA X2,Y2,Z2
Write DELTA X2,Y2,Z2
Test B1F
< 0.0
B1=B1+ST
B1=B1-ST
< B1F
>B1F
Test B1
Test B1
Go To 1
Go To 1
GO TO 5
GO TO 5
Calculate DELTA X2,Y2,Z2
Write DELTA X2,Y2,Z2
< 0.0
Test B1F
B1=B1+ST
B1=B1-ST
<B1F
> B1F
Test B1
Test B1
Go To 1
Go To 1

## FORTRAN PROGRAMME FOR PLANE INTERSECTION CURVE VALREFORMOD

```
JOB :EPS2054,VALREFORMOD,JD(JT 100,MZ 20K)
UAFORTRAN LINES 2000
C
      MASTER VALREFORMOD
C
C   WRITE RESULTS HEADING
C
      WRITE(2,100)
C
C   READ RANGE AND INCREMENTS OF B1
C
      READ(1,101) B1S,B1F,STEP
      WRITE(2,102)B1S,B1F,STEP
C
C   READ CONSTANTS FOR RUN
C
      READ(1,101) RO,BL,SL,SD,W,R,SB
      WRITE(2,103)RO,BL,SL,SD,W,R,SB
C
C   CHANGE TO NEGATIVE ROTATION
C
      READ(1,109) KSIGN
      WRITE(2,108)KSIGN
C
      CL = 6.2831854*RO/10.0
C
      SIGMA = ATAN(CL)
C
      PPR = SQRT(SL*SL + 1.0)
C
      CONK = SL*COT(SIGMA)/PPR
C
      A = RO*CONK/SL
C
      VMOD = SQRT(RO*RO + SB*SB)
C
C   READ VALUES OF PLANES
C
    1 READ(1,101) Z2
      WRITE(2,104)Z2
C
      IF(Z2 .GE. 99.0) STOP
C
      THETA = 0.0
```

```
C
      B1 = B1S
C
      IF(KSIGN .EQ. -10) GO TO 5
C
C
    2 EP2 = EXP(2.0*CONK*THETA)
      EP1 = EXP(CONK*THETA)
C
C
      X = SD - R*(1.0 - COS(B1))
      Y = W
      Z = -R*SIN(B1)
C
      WRITE(2,105) X,Y,Z
C
C
      SSS = CONK*A*A*EP2
      SST = A*RO*RO*CONK*EP1
C
C
      AAA = SQRT(RO*RO + A*A*EP2)
      BBB = SQRT(RO*RO + (CONK*CONK + 1.0)*A*A*EP2)
      CCC = AAA*BBB
      TTT = AAA*AAA
C
C
      PPP = CCC*VMOD
      PPS = BBB*VMOD
      PSS = AAA*VMOD
C
C
    3 ZL = SB*THETA
C
      BETA = ALOG(1.0 + SL*ZL/RO)/CONK
C
C
      DOTNN = TTT/CCC
      DOTNB = -CONK*A*EP1/BBB
      DOTNT = 0.0
C
C
      DOTBN = (SB*SSS + SST)/PPP
      DOTBB = (SB*A*EP1 + RO*RO)/PPS
      DOTBT = (-SB*RO + RO*A*EP1)/PSS
C
C
      DOTTN = (-RO*SSS + SB*RO*A*CONK*EP1)/PPP
      DOTTB = (-RO*A*EP1 + SB*RO)/PPS
      DOTTT = (RO*RO + SB*A*EP1)/PSS
C
C
      XMOD = X*DOTNN + Y*DOTBN + Z*DOTTN
      YMOD = X*DOTNB + Y*DOTBB + Z*DOTTB
      ZMOD = X*DOTNT + Y*DOTBT + Z*DOTTT
```

```
C
C
      VNIDOT = (-TTT*COS(THETA) + SSS*SIN(THETA))/CCC
      VNJDOT = (-TTT*SIN(THETA) - SSS*COS(THETA))/CCC
      VNKDOT = RO*CONK*A*EP1/CCC
C
C
      BIDOT = (CONK*A*EP1*COS(THETA) + A*EP1*SIN(THETA)/BBB
      BJDOT = (CONK*A*EP1*SIN(THETA) - A*EP1*COS(THETA)/BBB
      BKDOT = RO/BBB
C
C
      TIDOT = -RO*SIN(THETA)/AAA
      TJDOT = RO*COS(THETA)/AAA
      TKDOT = A*EP1/AAA
C
C
      X1 = XMOD*VNIDOT + YMOD*BIDOT + ZMOD*TIDOT + RO*COS(BETA)
      Y1 = XMOD*VNJDOT + YMOD*BJDOT + ZMOD*TJDOT + RO*SIN(BETA)
      Z1 = XMOD*VNKDOT + YMOD*BKDOT + ZMOD*TKDOT + SB*THETA
C
      WRITE(2,106) X1,Y1,Z1
C
C
      ZMAG = ((Z2 - Z1)*SL/RO + 1.0)
      ZBAR = ZMAG + ABS(ZMAG)
C
      IF(ZBAR .EQ. 0.0) GO TO 1
C
      DELTA = ALOG(ZMAG)/CONK
C
C
      X2 = X1*COS(DELTA) - Y1*SIN(DELTA)
      Y2 = X1*SIN(DELTA) + Y1*COS(DELTA)
      Z2 = Z1 + RO*(EXP(CONK*DELTA) - 1.0)/SL
C
      WRITE(2,107) DELTA,X1,Y1,Z1
C
      IF(B1F .LT. 0.0) GO TO 8
C
      B1 = B1 + STEP
      IF(B1 .LT.B1F) GO TO 2
C
      GO TO 1
C
C
C
    8 B1 = B1 - STEP
      IF(B1 .GT. B1F) GO TO 2
C
      GO TO 1
C
C
C
C
```

```
C
    5 EP2 = EXP(-2.0*CONK*THETA)
      EP1 = EXP(-CONK*THETA)
C
C
      X = SD - R*(1.0 - COS(B1))
      Y = W
      Z = -R*SIN(B1)
C
      WRITE(2,105) X,Y,Z
C
C
      SSS = CONK*A*A*EP2
      SST = A*RO*RO*CONK*EP1
C
C
      AAA = SQRT(RO*RO + A*A*EP2)
      BBB = SQRT(RO*RO + (CONK*CONK +1.0)*A*A*EP2)
      CCC = AAA*BBB
      TTT = AAA*AAA
C
C
      PPP = CCC*VMOD
      PPS = BBB*VMOD
      PSS = AAA*VMOD
C
C
    6 ZL = SB*THETA
C
      BETA = -ALOG(1.0 - SL*ZL/RO)/CONK
C
C
      DOTNN = TTT/CCC
      DOTNB = CONK*A*EP1/BBB
      DOTNT = 0.0
C
C
      DOTBN = -(SB*SSS + SST)/PPP
      DOTBB = (SB*A*EP1 + RO*RO)/PPS
      DOTBT = (-SB*RO + RO*A*EP1)/PSS
C
C
      DOTTN = (RO*SSS - SB*RO*CONK*A*EP1)/PPP
      DOTTB = (-RO*A*EP1 + RO*SB)/PPS
      DOTTT = (RO*RO + SB*A*EP1)/PSS
C
C
      XMOD = X*DOTNN + Y*DOTBN + Z*DOTTN
      YMOD = X*DOTNB + Y*DOTBB + Z*DOTTB
      ZMOD = X*DOTNT + Y*DOTBT + Z*DOTTT
C
C
      VNIDOT = -(TTT*COS(THETA) + SSS*SIN(THETA))/CCC
      VNJDOT = (-TTT*SIN(THETA) + SSS*COS(THETA))/CCC
      VNKDOT = -RO*CONK*A*EP1/CCC
```

```
C
C
      BIDOT = (-CONK*A*EP1*COS(THETA) + A*EP1*SIN(THETA))/BBB
      BJDOT = -(CONK*A*EP1*SIN(THETA) + A*EP1*COS(THETA))/BBB
      BKDOT = RO/BBB
C
C
      TIDOT = -RO*SIN(THETA)/AAA
      TJDOT = RO*COS(THETA)/AAA
      TKDOT = A*EP1/AAA
C
C
      X1 = XMOD*VNIDOT + YMOD*BIDOT + ZMOD*TIDOT + RO*COS(BETA)
      Y1 = XMOD*VNJDOT + YMOD*BJDOT + ZMOD*TJDOT + RO*SIN(BETA)
      Z1 = XMOD*VNKDOT + YMOD*BKDOT + ZMOD*TKDOT + SB*THETA
C
      WRITE(2,106) X1,Y1,Z1
C
C
      ZMAG = (1.0 - (Z2 - Z1)*SL/RO)
      ZBAR = ZMAG +ABS(ZMAG)
C
      IF(ZBAR .EQ. 0.0) GO TO 1
C
      DELTA = -ALOG(ZMAG)/CONK
C
C
      X2 = X1*COS(DELTA) - Y1*SIN(DELTA)
      Y2 = X1*SIN(DELTA) + Y1*COS(DELTA)
      Z2 = Z1 + RO*(1.0 - EXP(-CONK*DELTA))/SL
C
      WRITE(2,107) DELTA,X2,Y2,Z2
C
      IF(B1F .LT. 0.0) GO TO 9
C
      B1 = B1 + STEP
      IF(B1 .LT. B1F) GO TO 5
C
      GO TO 1
C
C
C
      B1 = B1 -STEP
      IF(B1 .GT. B1F) GO TO 5
C
      GO TO 1
C
C
C  ******** FORMAT STATEMENTS ********
C
  100 FORMAT(1H1,'****** RESULTS ******',///)
C
  101 FORMAT(7F0.0)
C
  102 FORMAT(1H ,5X,'B1S =',F8.4,5X,'B1F =',F8.4,5X,'STEP =',
     *  F8.4///)
```

```
C
  103 FORMAT(1H ,2X,'RO =',F8.4,2X,'BL =',F8.4,2X,'SL =',
     *   F8.4,2X,'SD =',F8.4,2X,'W =',F8.4,2X,'R =',F8.4,
     *   2X,'SB =',F8.4///)
C
  104 FORMAT(1H1,9X,'***** THE PLANE IS *****',F8.4/////)
C
  105 FORMAT(1H ,//3(2X,F16.8)///)
C
  106 FORMAT(1H ,//3(2X,F16.8)////)
C
  107 FORMAT(1H ,//4(2X,F16.8)////)
C
  108 FORMAT(1H ,5X,'KSIGN =',I3///)
C
  109 FORMAT(I3)
C
C
      END
      FINISH


C  INSERT DATA CARDS FOR B1S,B1F,STEP,CONSTANTS,KSIGN,PLANES
****
```

# APPENDIX 2

## PROTOTYPE DIVIDING HEAD

(A) Design Specification

(B) Kinematic Analysis

## (A) DESIGN SPECIFICATION FOR MODIFIED DIVIDING HEAD.

Centre height above work table: 6.5 in

Spindle Nose: No. 4 Morse Taper

Index Plates: Brown & Sharpe type

3 Plates:

No.1 - 15, 16, 17, 18, 19 & 20 holes

No.2 - 21, 23, 27, 29, 31 & 33 holes

No.3 - 37, 39, 41, 43, 47 & 49 holes

Direct indexing provided by plate and indent.

Superposed rotation provided by externally coupled differential of ratio "k" provided by standard hobbing differential gear set. Internal ratio provided by Sun and Planet differential mechanism.

External Gear Set (40 gears 1.25 mm module)

21, 22, 23, 24, 25, 27, 29, 30, 31, 34,
35, 36, 37, 38, 39, 40, 41, 43, 45, 47,
49, 50, 53, 58, 59, 60, 61, 62, 64, 66,
67, 69, 70, 71, 72, 74, 75, 76, 78, 80.

Differential Gear Mechanism

16 D.P. Spur Gear Set

| | | |
|---|---|---|
| Annulus - 60 tooth | D = 3.9063 in | $D_o$ = 3.7500 in |
| Sun - 30 tooth | D = 1.8750 in | $D_o$ = 2.0000 in |

Planets (3) - 15 tooth

D = 0.9375 in $D_o$ = 1.0625 in

Worm Ratio Gears

Direct Input Ratio 40/1

| Worm | Wheel |
|---|---|
| Single Start | 40 tooth |
| D = 1.250 in | D = 3.339 in |
| $D_o$ = 1.4166 in | $D_o$ = 3.5056 in |
| P = 12 | P = 12 |

Centre distance for pair = 2.2945 in

Indirect Input Ratio 30/1

| Worm | Wheel |
|---|---|
| Single Start | 30 tooth |
| D = 1.250 in | D = 2.5047 in |
| $D_o$ = 1.4166 in | $D_o$ = 2.6713 in |
| P = 12 | P = 12 |

Centre distance for pair = 1.886 in

## (B) KINEMATIC ANALYSIS OF SUPERPOSED ROTATION MECHANISM.

(i) Motion Analysis for The Differential

From the theory for a simple sun and planet epicyclic

Motion of Sun Due to Annulus Rotation with Arm Fixed

$$\phi_{SA} = - \frac{r_A}{r_S} \theta_A$$

where $\phi_{SA}$ = Angular displacement of sun due to annulus movement

$\theta_A$ = Angular displacement of annulus

$r_A$ = Pitch radius of annulus

$r_S$ = Pitch radius of sun

and for the differential used in this mechanism

$$\phi_{SA} = - \frac{60}{30} \cdot \theta_A = - 2\theta_A \qquad \text{.....(A1)}$$

Motion of Sun Due to Arm Rotation with Annulus Fixed

$$\phi_{sa} = \beta + \frac{r_a}{r_s} \beta$$

where $\phi_{sa}$ = Angular displacement of sun due to arms movement

$\beta$ = Angular displacement of arm

$r_a$ = Radius of arm

For the particular differential

$$\phi_{sa} = \beta \left[1 + \frac{60}{30}\right] = + 3\beta \qquad \text{.....(A2)}$$

(ii) Motion of the System

In a right handed system positive rotation is defined to be clockwise so for one positive rotation of the input worm the annulus rotates 1/40

turns negatively. If the gear ratio to be superposed is k, then the arm will rotate ± k for this same input.

Therefore

$$\phi_{SA} = -2\left[-1/40\right] = 1/20 \text{ revolutions}$$

and

$$\phi_{sa} = \pm 3k/30 = \pm k/10 \text{ revolutions}$$

The total movement of the sun for this input will be, therefore, the algebraic sum of these two motions.

i.e.

$$\phi_T = \phi_{SA} + \phi_{sa} = \frac{1}{20} \pm \frac{k}{10}$$

$$= \frac{1}{20}\left[1 \pm 2k\right] \qquad \text{.....(A3)}$$

If the lead set on the machine is L, then from equation (A1) the natural lead of the device will be L/2 because only 20 revolutions of the annulus are required to give one revolution of the work spindle; whereas in the conventional head 40 revolutions of the input worm would be required for one revolution of the work. Equation (A3) for this condition becomes

$$\phi_T = \frac{20}{20}\left[1 \pm 2k\right] = 1 \pm 2k \qquad \text{.....(A4)}$$

(iii) Application of Superposed Rotation

(a) Differential Indexing:

Example: 107 divisions required.

To obtain this ratio set the index plate for the approximate division of 105.

From the theory for this head the required indexing for this division will be

$$I = \frac{20}{105} = \frac{4}{21}$$

i.e. 4 holes on a 21 circle.

The required superposed rotation from equation (A4) is

$$2k = \left[\frac{4}{21} \cdot 107\right] - 20 = 0.31095238$$

therefore

$$2k = \frac{8}{21}$$

and

$$k = \frac{4}{21}$$

This amount must be subtracted, so the required gear train will be

$$\frac{\text{driver}}{\text{driven}} = \frac{4}{21} = \frac{1}{3} \cdot \frac{4}{7} = \frac{24}{72} \cdot \frac{40}{70}$$

N.B. An idler must be used if a rotation is to be additive.

(b) Variable Lead Helicoids:

Variable lead helicoids can be produced by either use of a cam and follower driving the cage of the differential or, alternatively, by a constant gear ratio driving the cage in conjunction with a fixed angular offset for the worktable.

If a cam is employed, then it will be necessary to use a stepping gear box mounted over the two worm shafts with the cam system externally mounted on this reduction box. The gear box system will alter the ratios between the cage and the cam follower to 1/1 and reduce the ratio between the cam and the primary input worm by 1/20.

i.e. Ratio between primary input worm and camshaft = 1/20

since the internal ratio of the system is $\frac{2}{1} \cdot \frac{1}{40} = \frac{1}{20}$

and Ratio between follower and secondary input worm = 10/1

since the internal ratio of the system is $3 \cdot \frac{1}{30} = \frac{1}{10}$

For a logarithmic lead the cam profile will be designed according to the polar equation

$$r = r_o e^{\pm k\theta}$$

where r and k have the meaning described in Chapter VI and

$$\theta = \pm \frac{1}{k} \log_e \left[ 1 \pm \frac{mz}{r_o} \right]$$

N.B. (k in this expression is not the gear ratio of the superposed system).

If this superposed rotation were added or subtracted by means of a simple gear train then the increments would be arithmetic and not logarithmic.

Example:

$r_o = 1.125$ $\sigma = 35.25^o$ $m = \tan 30^o = 0.57735$

Machine Lead = 20 in Natural Lead = 10 in

Table of Logarithmic Increments for Added Rotation

| z (in) | 1/k | $\theta$ (Superposed) Radians | Increment (rad) |
|---|---|---|---|
| 0.0 | 1.4138 | 0.0 | 0.99857 |
| 2.0 | " | 0.99857 | 0.57940 |
| 4.0 | " | 1.57797 | 0.40979 |
| 6.0 | " | 1.98776 | 0.31731 |
| 8.0 | " | 2.30507 | 0.25899 |
| 10.0 | " | 2.56406 | |

If this rotation was added arithmetically a gear train would be required as follows:

$$\frac{\text{driver}}{\text{driven}} = \frac{2.56406}{2\pi} = 0.408083$$

A practical ratio is obtained using continued fractions and intermediary ratios.

i.e.

$$\frac{\text{driver}}{\text{driven}} = \frac{56}{135} = \frac{40}{75} \cdot \frac{63}{81} = 0.414815$$

$$\text{error in ratio} = \frac{(0.414815 - 0.408083)}{0.40803} \times 100\ ^{o}/o$$

$$= 1.65\ ^{o}/o$$

The uniform rotation added for a 2 in increment in lead would be 0.512812 radians and comparison with the above table highlights the differences over one revolution of the work.

(c) Short Leads:

If a short lead is required then the superposed ratio will be obtained as follows

$$L_s = b'\theta = \frac{b\theta}{(1 + 2k)} \qquad \text{.....(A5)}$$

The lead of the work for one revolution will be given by substituting $\theta = 2\pi$ in equation (A5)

therefore

$$L_s = \frac{2\pi b}{(1 + 2k)}$$

therefore

$$k = \frac{1}{2}\left[\frac{2\pi b}{L_s} - 1\right] \qquad \text{.....(A6)}$$

where b = the lead per radian for the machine

$b'$ = the lead per radian for the system

$L_s$ = the short lead required

k = the superposed ratio

Example:

Machine lead = 8 in b = 1.27324 in/radian

Short lead required = 0.75 in

therefore

$$k = \frac{1}{2}\left[\frac{8}{0.75} - 1\right] = 4.8333/1$$

Here once again a continued fraction is required and an approximate ratio for k will be

$$\frac{\text{driver}}{\text{driven}} = \frac{78}{34} \cdot \frac{80}{38} = 4.82972/1$$

$$\text{Error in the ratio} = \frac{(4.83333 - 4.82972)}{4.83333} \times 100\ ^{o}/o$$

$$= 0.0747\ ^{o}/o$$

REFERENCES


| | | |
|---|---|---|
| (1) | WOODBURY R.S. | "Studies in the History of Machine Tools". M.I.T. Press, Cambridge, Mass, U.S.A., 1972 |
| (2) | ROLT L.T.C. | "Tools for the Job". Batsford, London, 1965. |
| (3) | BUCKINGHAM E. | "Analytical Mechanics of Gears". McGraw-Hill, New York, U.S.A., 1949. |
| (4) | TUPLIN W.A. | "Involute Gear Geometry". Chatto & Windus, London, 1962. |
| (5) | MERRITT H.E. | "Gears". Pitman, London, 1962. |
| (6) | PARKINSON A.C. & DAWNEY W.H. | "Gears, Gear Production and Measurement". Pitman, London, 1948. |
| (7) | HOUGHTON P.S. | "Gears - Spur, Helical, Bevel, Internal, Epicyclic, Worm". Technical Press, London, 1970. |
| (8) | BEVAN T. | "The Theory of Machines". Longmans, Green & Co., London, 1958. |
| (9) | DENT R. | "Production Engineering" Vol. 2. E.U.P., London, 1964. |
| (10) | DUDLEY D.W. & PORITSKY W. | "On Cutting & Hobbing Gears and Worms". A.S.M.E. Journal of Applied Mechanics, 1943, 10, No.4A139. |
| (11) | YOUNG A.G. | "The Computation of Gear, Gear Cutting and Cam Profiles". M.T.I.R.A. Report 1974. |
| (12) | CHAPMAN W.A.J. | "Workshop Technology" Vol. 3. Arnold, London, 1951. |
| (13) | HUGO S.W. | "The Exact Width of a Helical Slot Milled by a Disc Cutter". Mech. World, Vol. 142, 1962. |
| (14) | ETHERIDGE R.A. | "An Analysis of the Interference Produced in a Helical Slot Produced with Disc Type Cutters". Int. Journal of M/C Tool Design & Res., Vol. 10, 1970. |

| | | |
|---|---|---|
| (15) | KUDINOV A.V. | "Errors of Helical Surfaces Cut with Disc Type Tools". Machines and Tooling, Vol. 44, No.10, 1973. |
| (16) | FRIEDMAN M.Y., BOLESLAVSKI M. & MEISTER I. | "The Profile of a Helical Slot Machined by a Disc-type Cutter with an Infinitesimal Width Cutter". Proc. of 13th M.T.D.R. Conf., MacMillan, London, 1973. |
| (17) | WAYNHAM J. | "The Correction of Helically Fluted Conical Cutters". Undergraduate Project Report, U.A.B., 1970. |
| (18) | THORNLEY R.H. | "Production of Varying Lead Helical Slab Mills". Private Communication, 1974. |
| (19) | MABBON J.P. & SABBERWAL A.J.P. | "How to Make Variable Lead Slab Mills". Metalworking Production, Vol. 106, No. 9, 1962. |
| (20) | SABBERWAL A.J.P. & KAVINA Y.B. | "An Investigation into The Cutting Forces and Wear Characteristics of Helical Milling Cutters". Proc. of 3rd M.T.D.R. Conf., Pergamon Publishing Co., London, 1963. |
| (21) | ETHERIDGE R.A. & SCOTT A.J.A. | "An Investigation into The Uneven Flank Wear On A Helically Fluted Form Cutter for Machining The Steam Face of Turbine Blades". Proc. of 15th M.T.D.R. Conf., MacMillan, London, 1975. |
| (22) | SCOTT A.J.A. | "An Investigation of Uneven Tool Wear In A Large Helically Fluted Milling Cutter". M.Sc. Dissertation, U.A.B., 1968. |
| (23) | SPIEGEL M.R. | "Vector Analysis". Shaum Publishing Co., New York, U.S.A., 1959. |
| (24) | REKTORY K. | "Survey of Applicable Mathematics". Illiffe, London, 1969. |
| (25) | AYRES F. | "Matrices". Shaum Publishing Co., New York, U.S.A., 1959. |

PRESSURE ANGLE - 14.5°

DIAMETRAL PITCH - 1.0

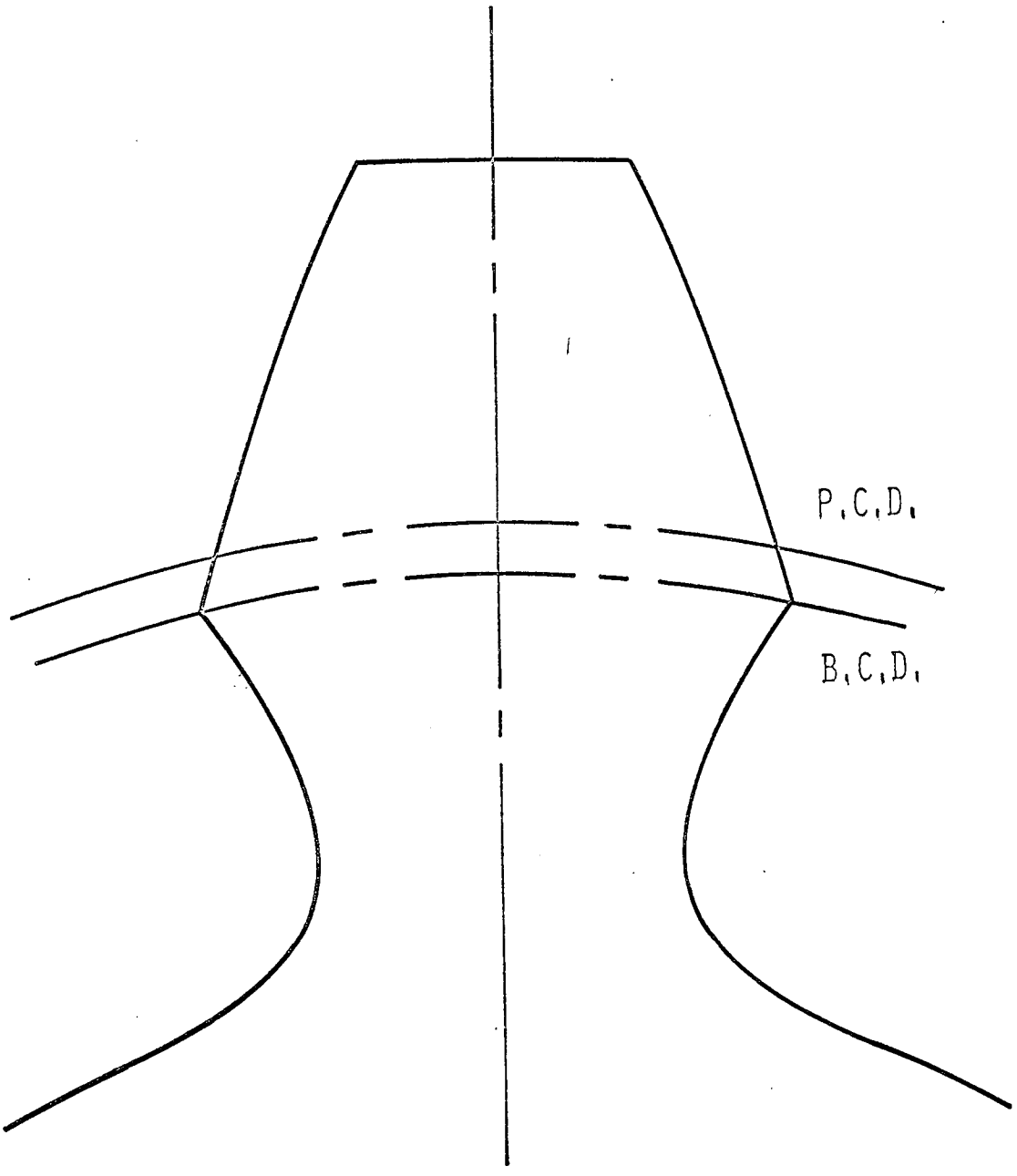


FIGURE 1

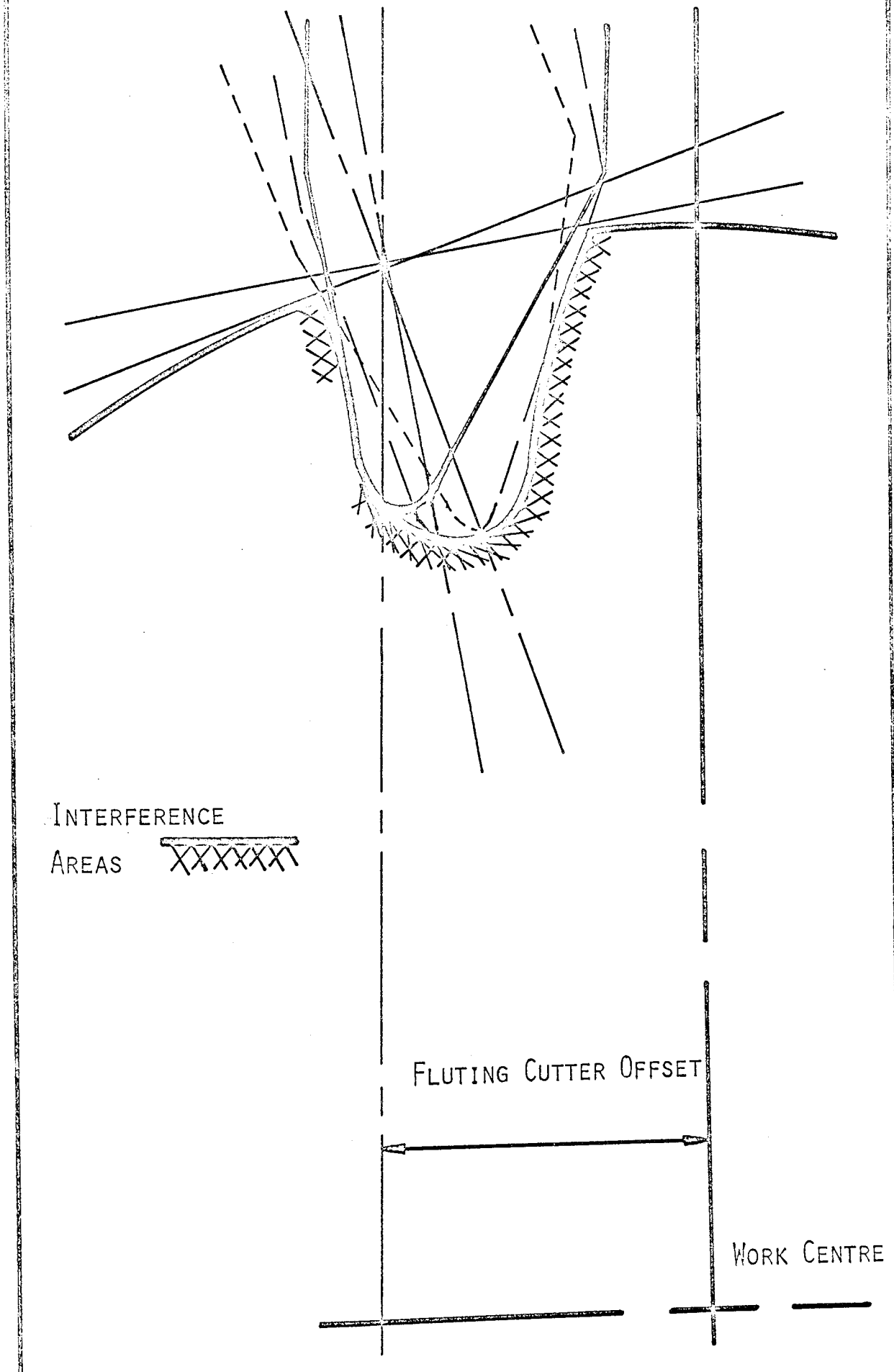


FIGURE 2

Plate i

SURFACES OF REVOLUTION

RULED SURFACES

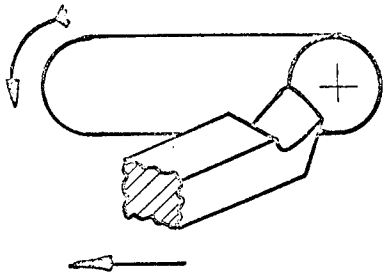

TURNING

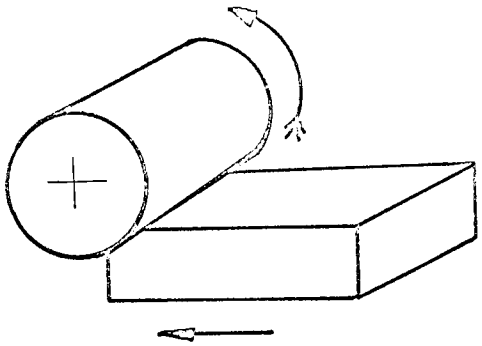

MILLING

CYLINDRICAL GRINDING

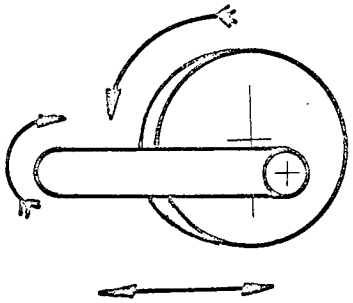

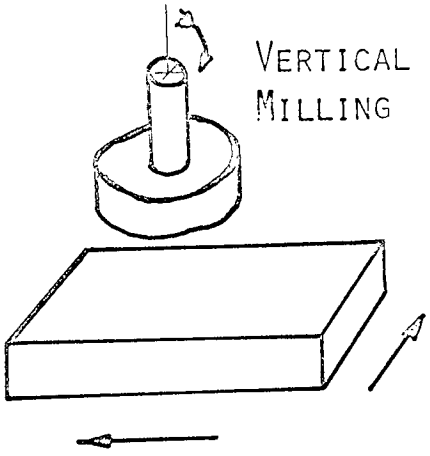

VERTICAL MILLING

CENTRELESS GRINDING

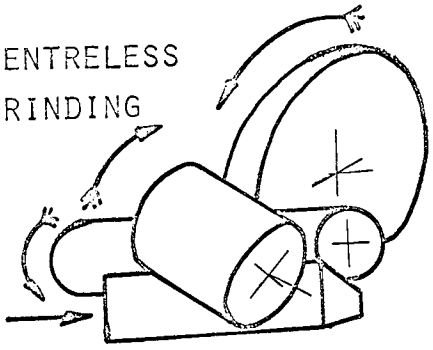

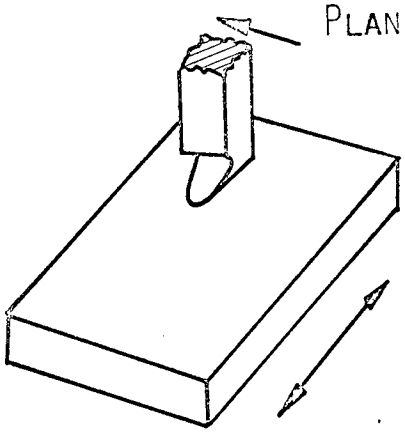

PLANING

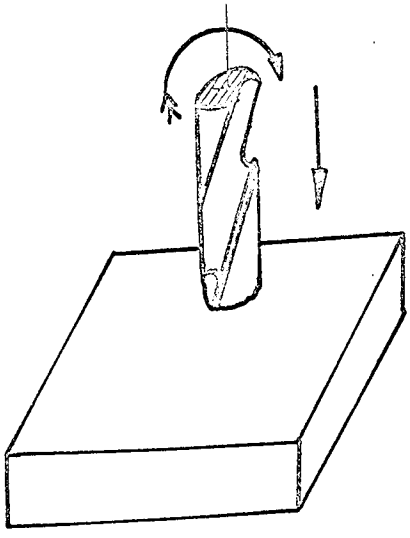

DRILLING

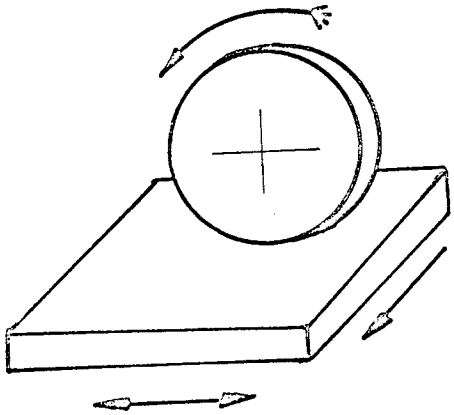

SURFACE GRINDING

FIGURE 3

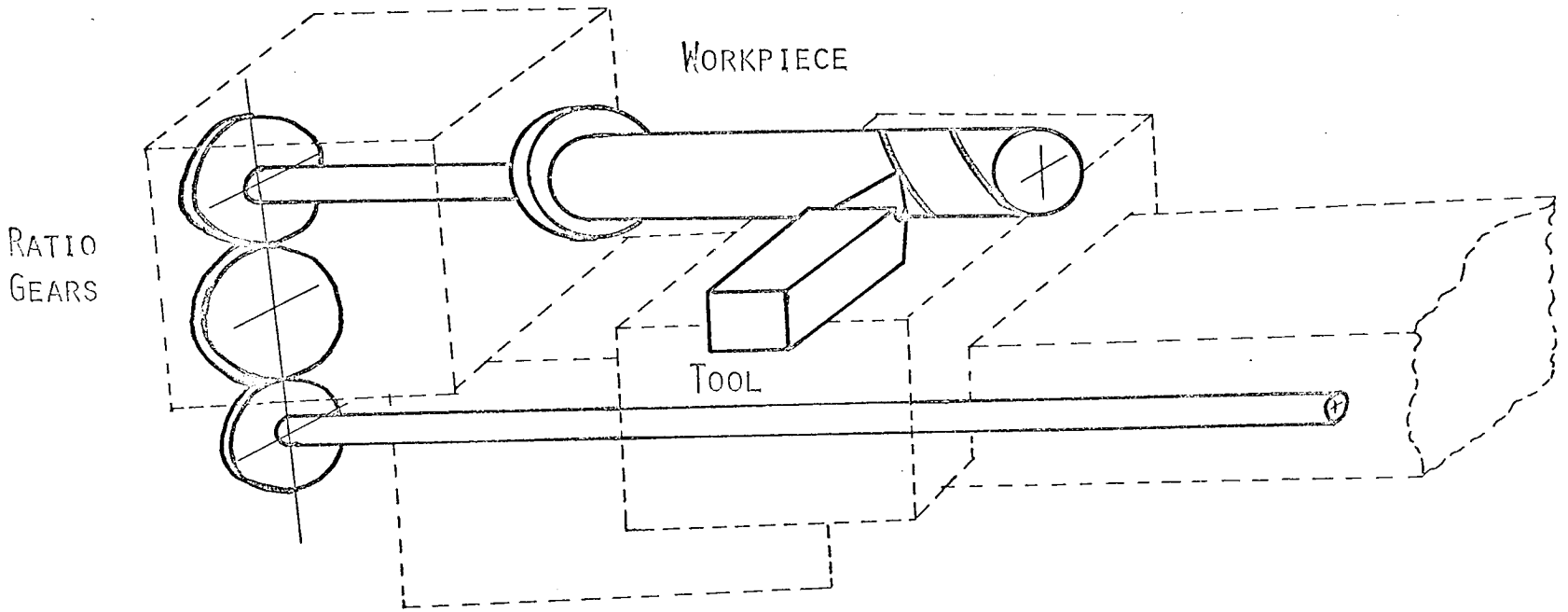


FIGURE 4

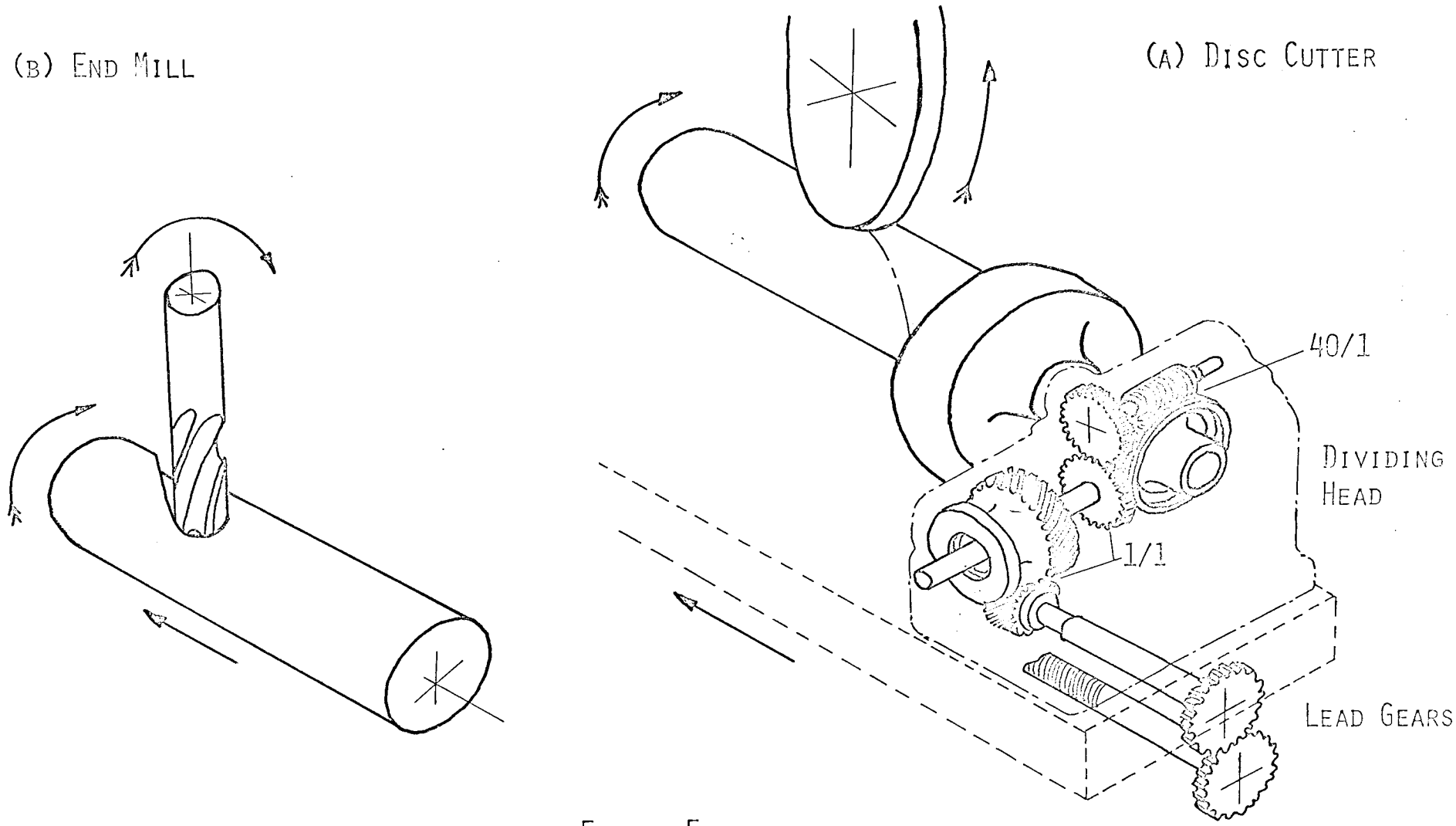


Figure 5

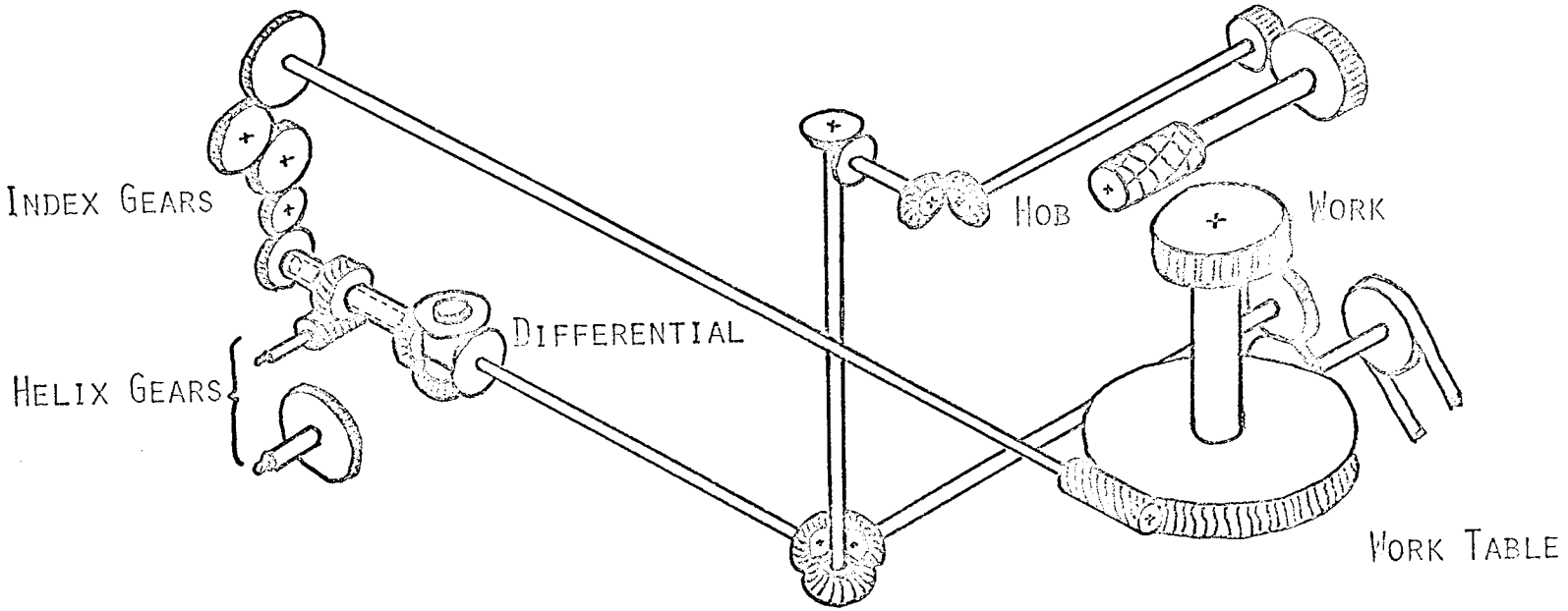


FIGURE 6

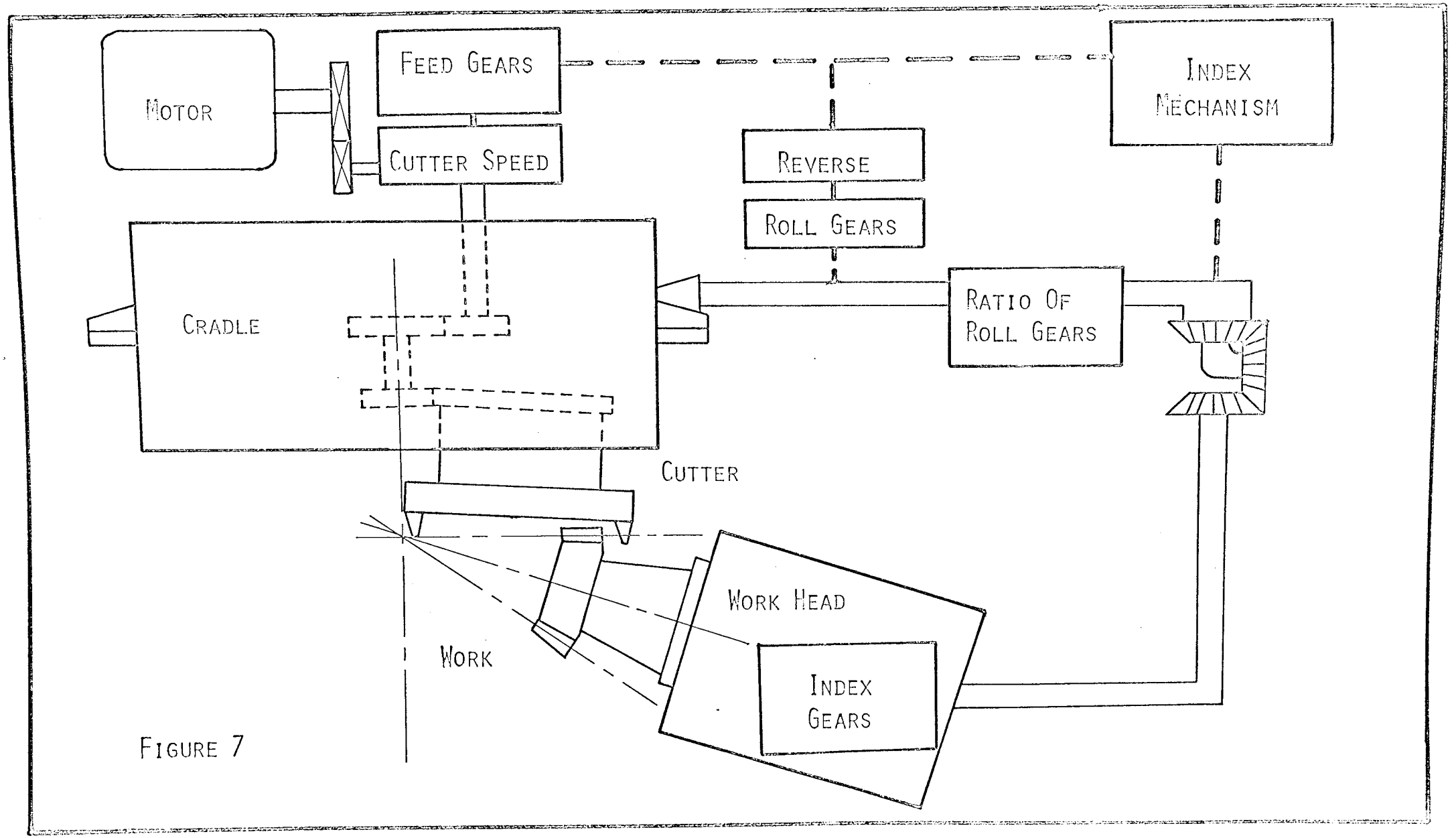
MOTOR
FEED GEARS
CUTTER SPEED
INDEX MECHANISM
REVERSE
ROLL GEARS
CRADLE
RATIO OF ROLL GEARS
CUTTER
WORK HEAD
WORK
INDEX GEARS

FIGURE 7

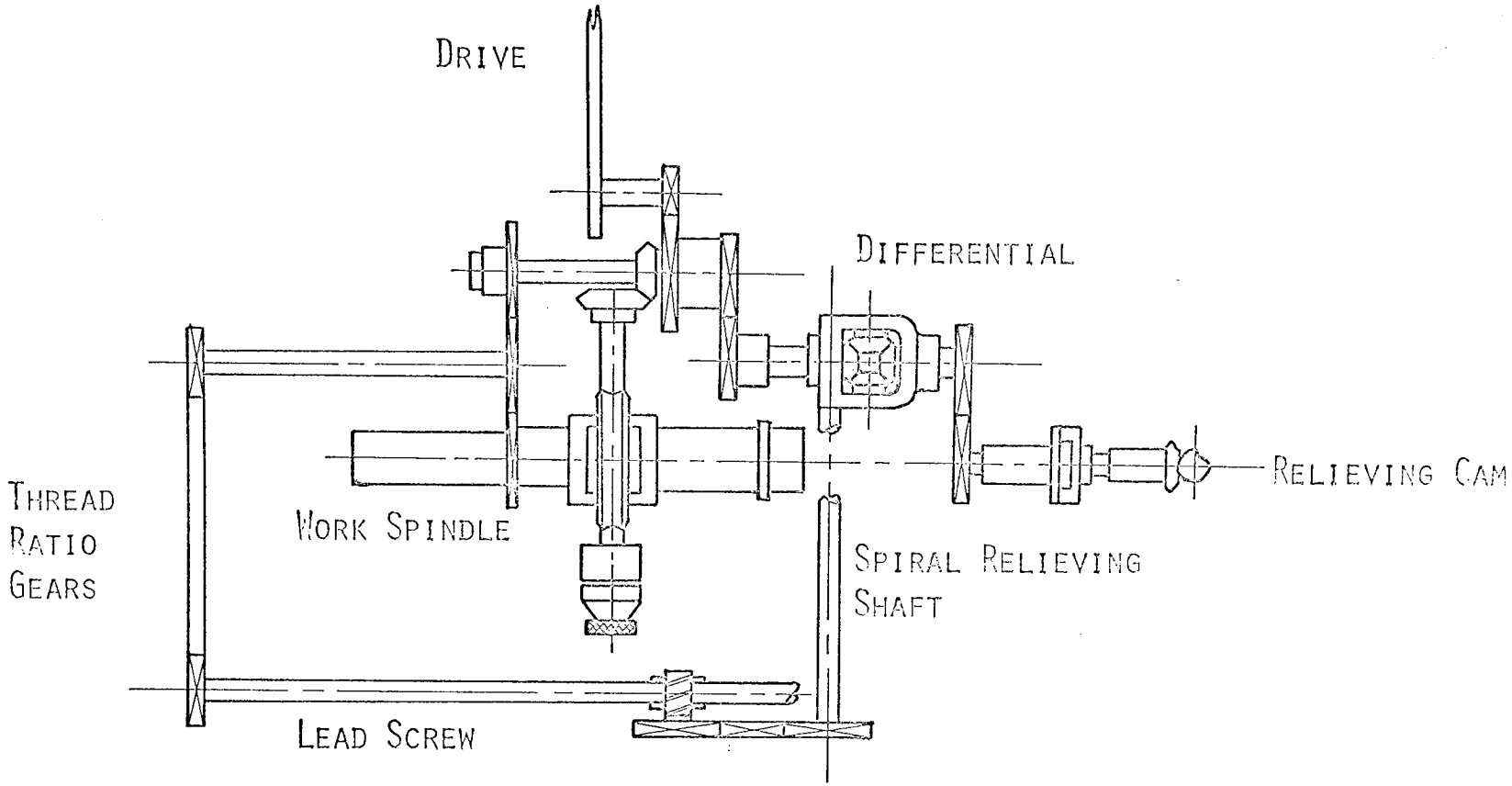
DRIVE
DIFFERENTIAL
THREAD
RATIO
GEARS
WORK SPINDLE
RELIEVING CAM
SPIRAL RELIEVING
SHAFT
LEAD SCREW

FIGURE 8

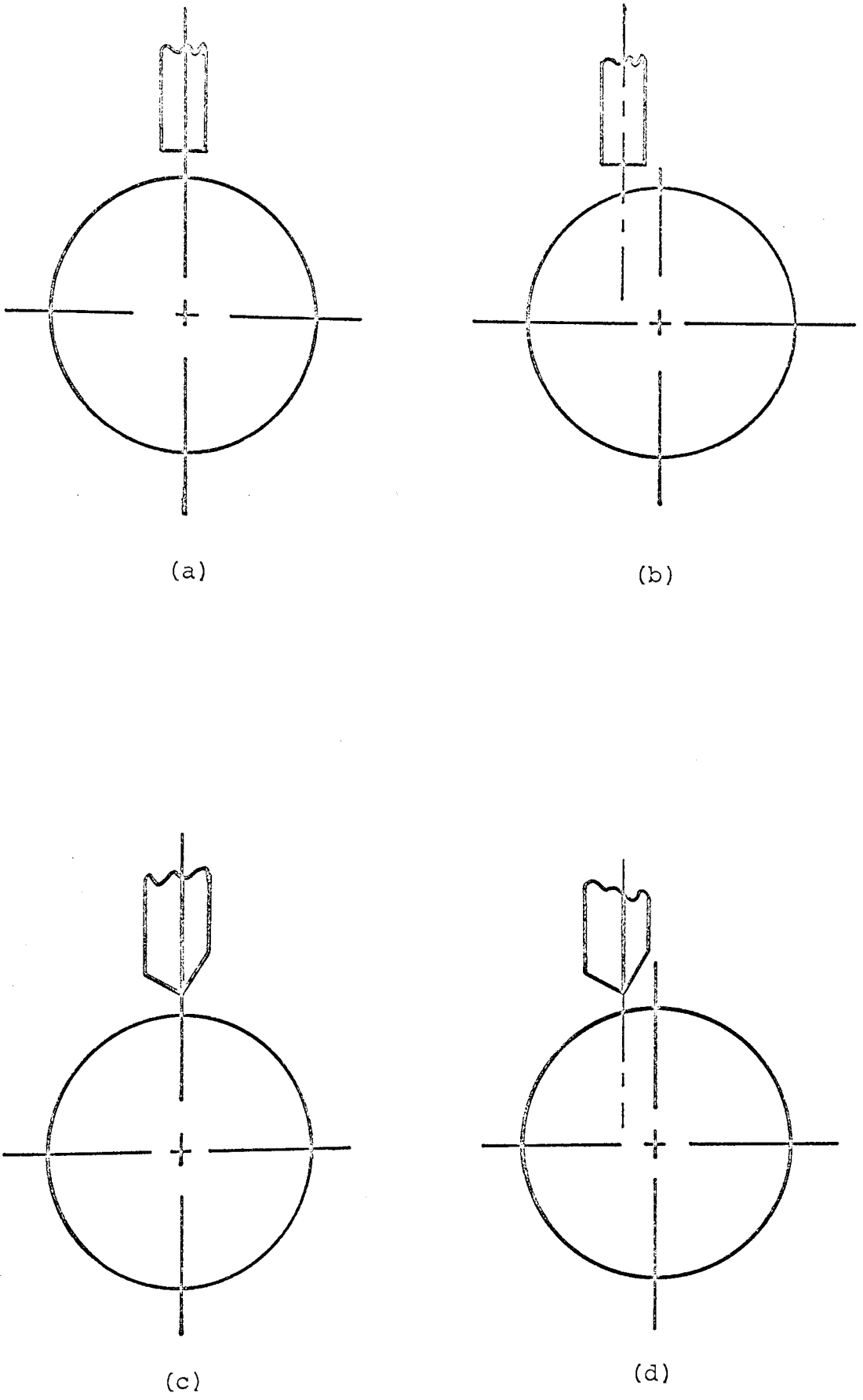


FIGURE 9

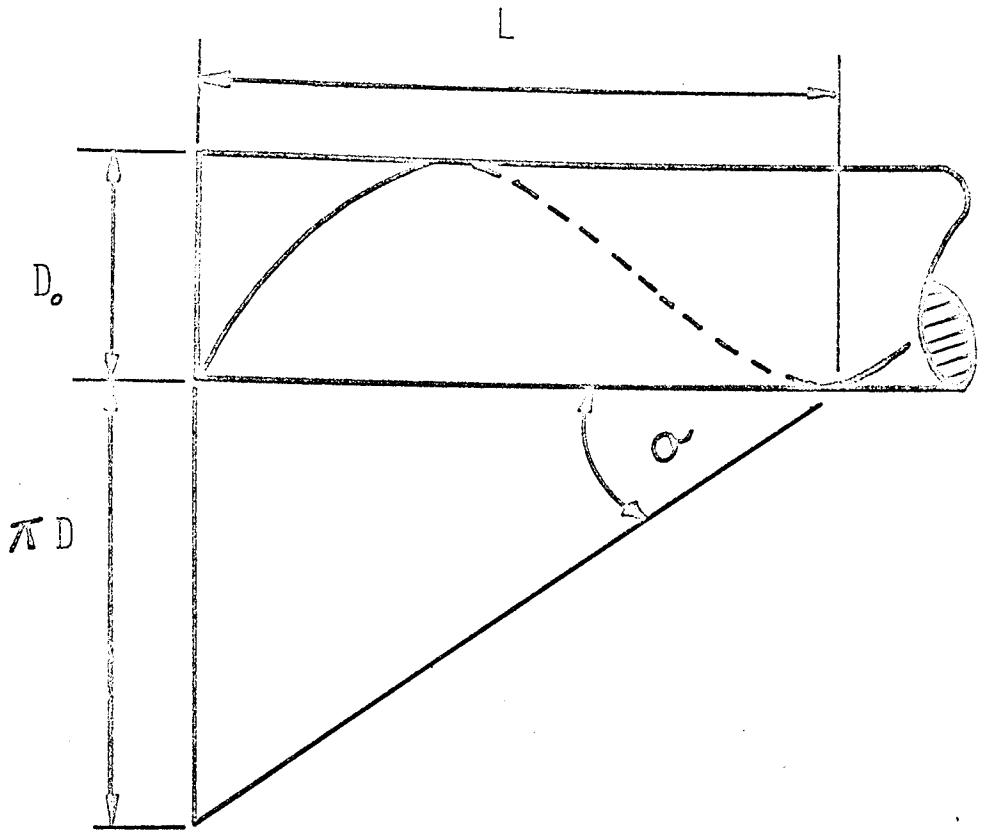


FIGURE 10

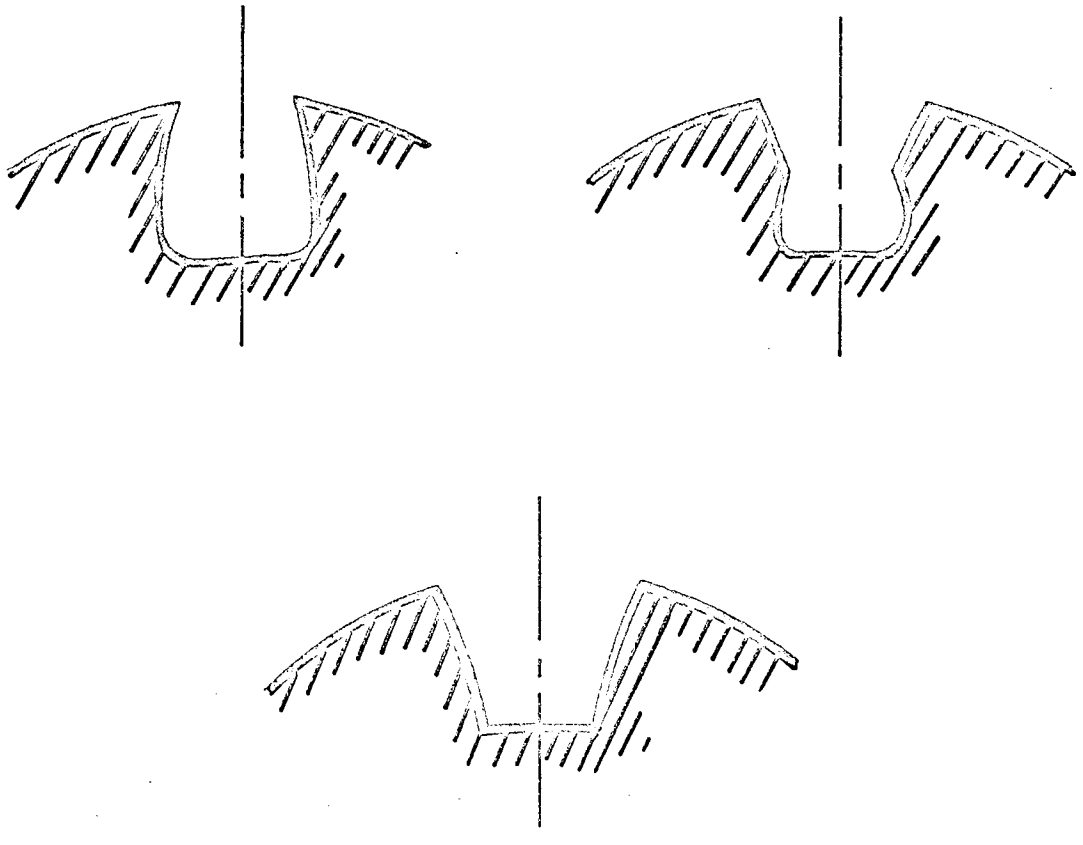

FIGURE 11

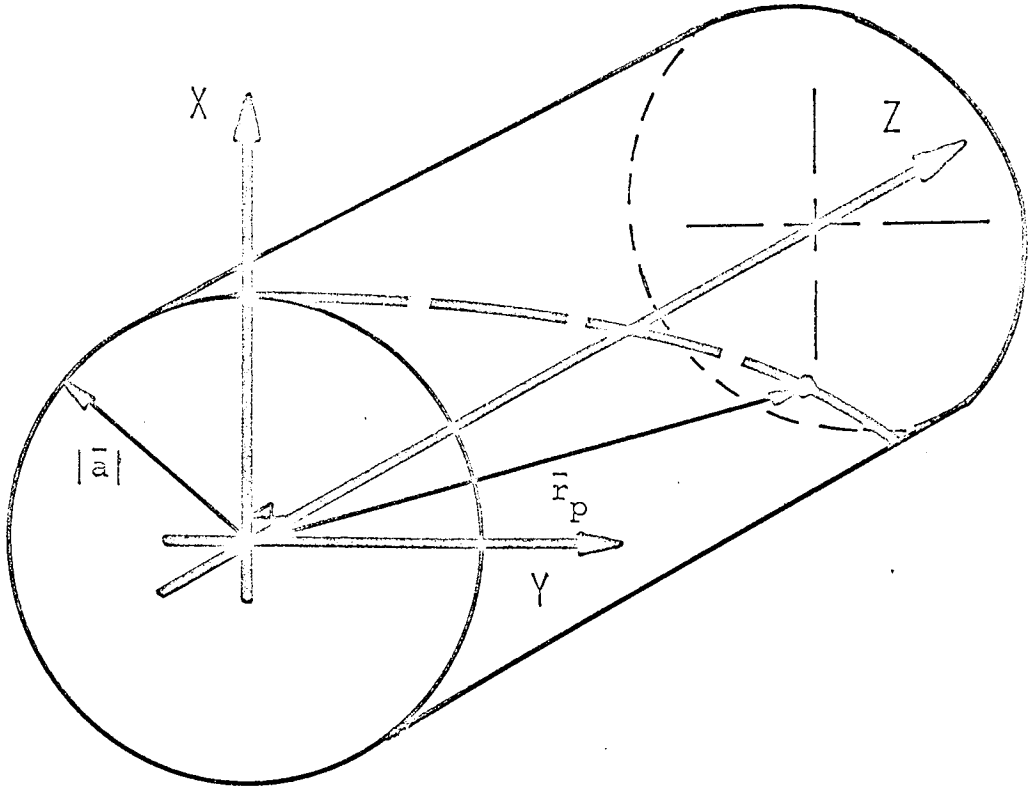


FIGURE 12

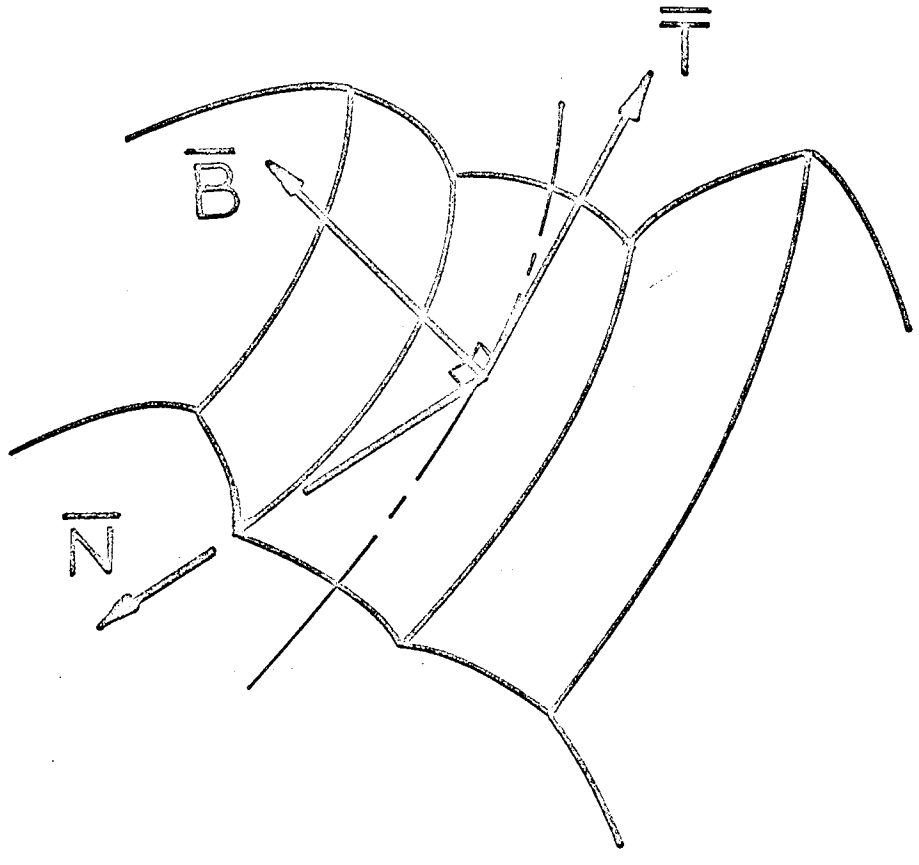


FIGURE 13

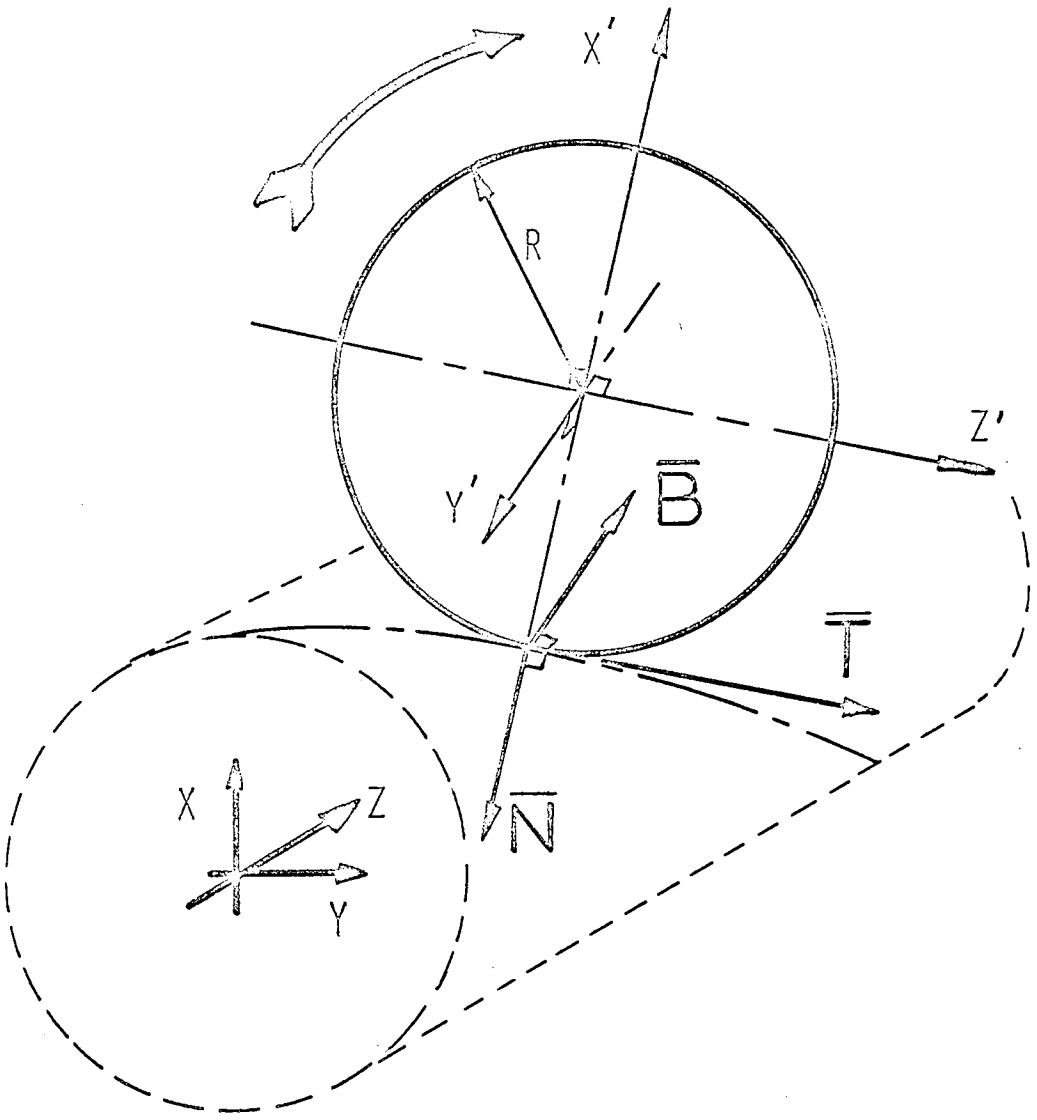


FIGURE 14

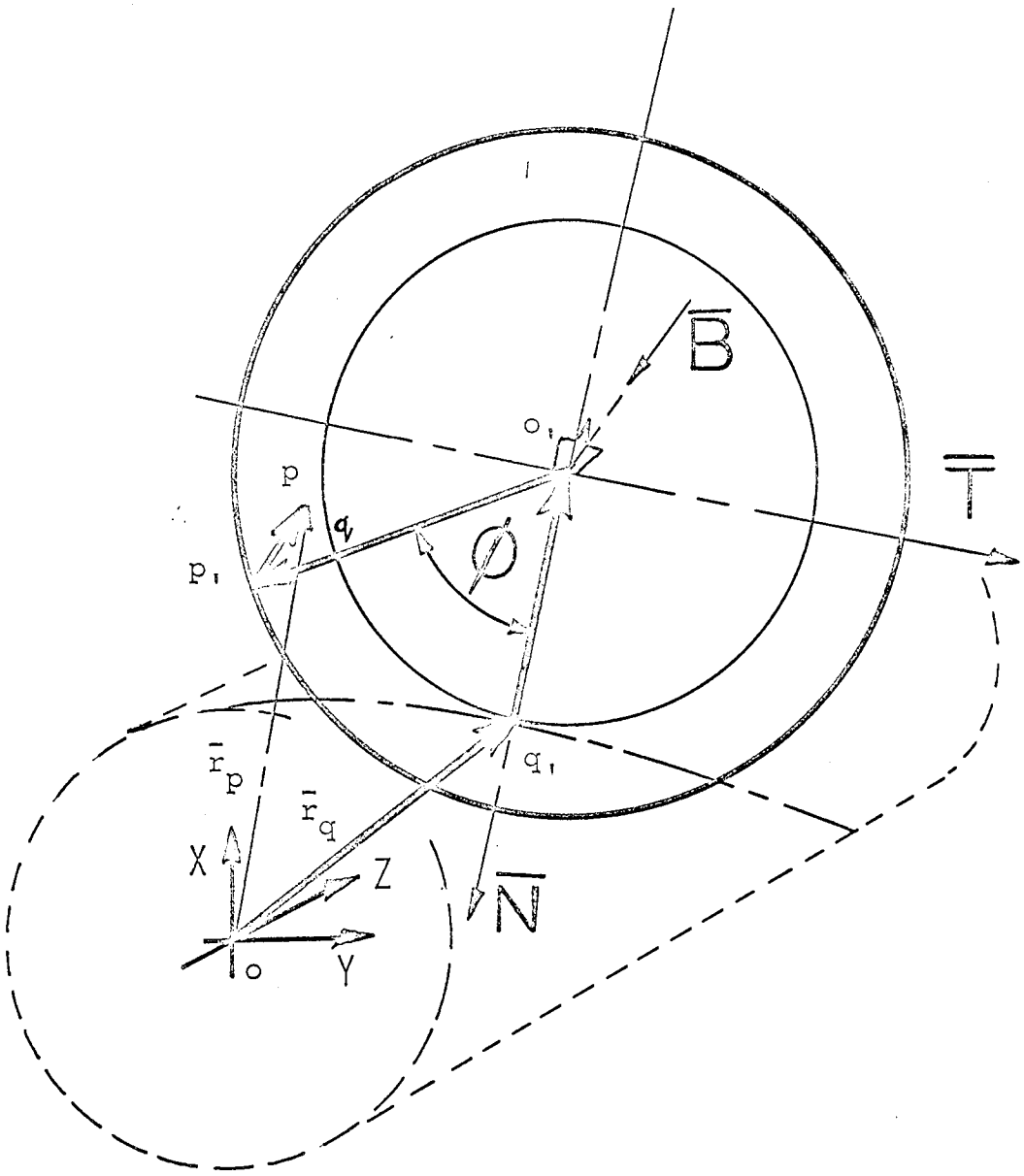


FIGURE 15

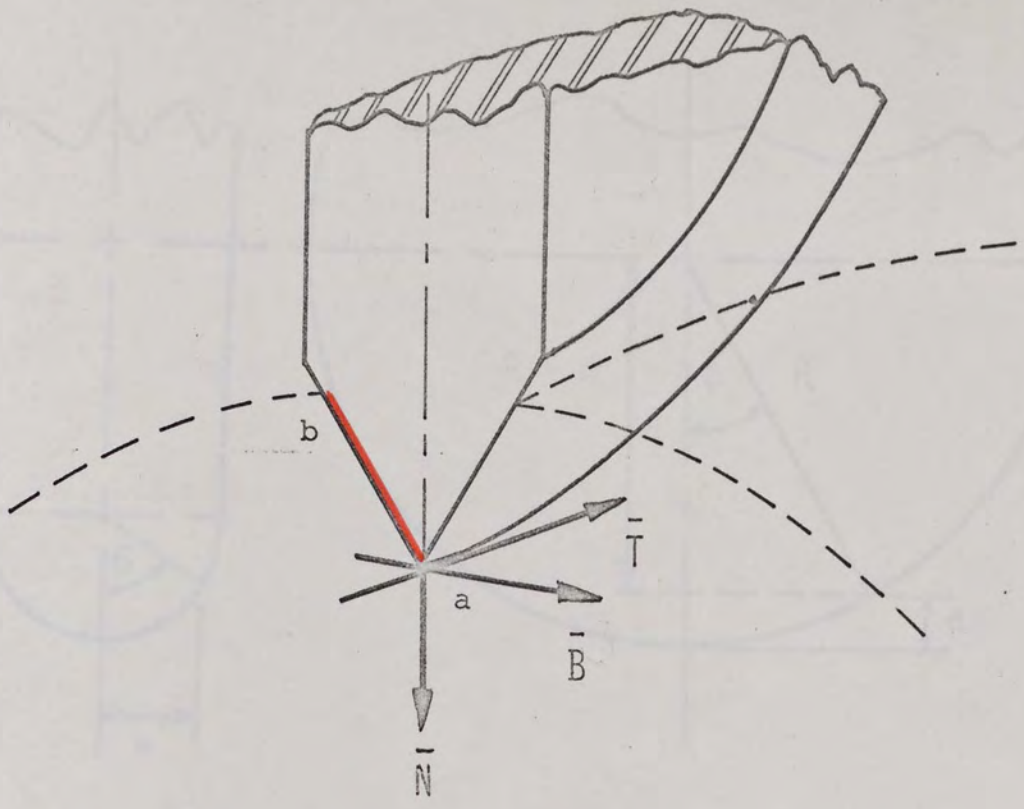


FIGURE 16

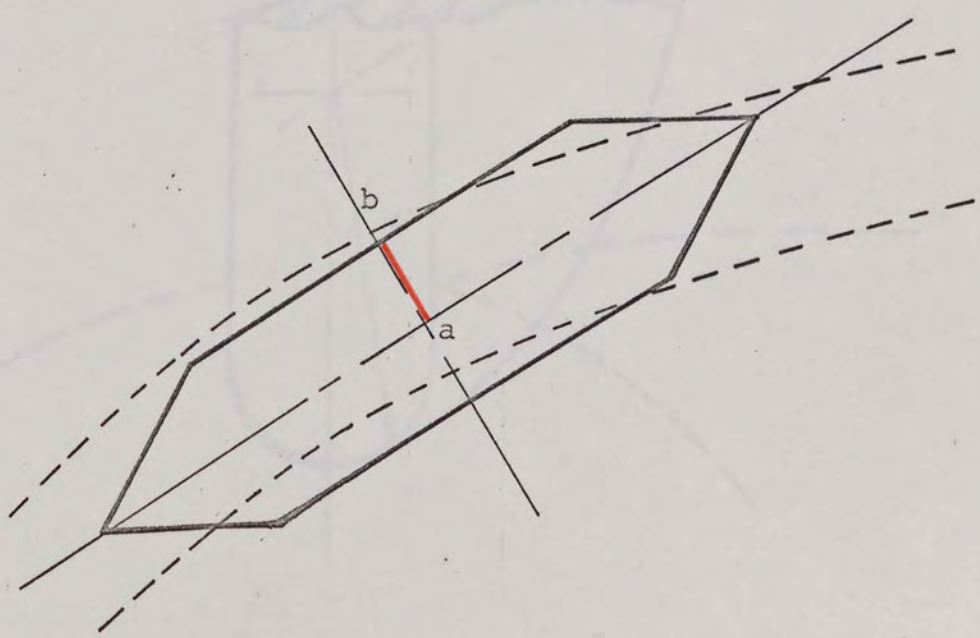


FIGURE 17

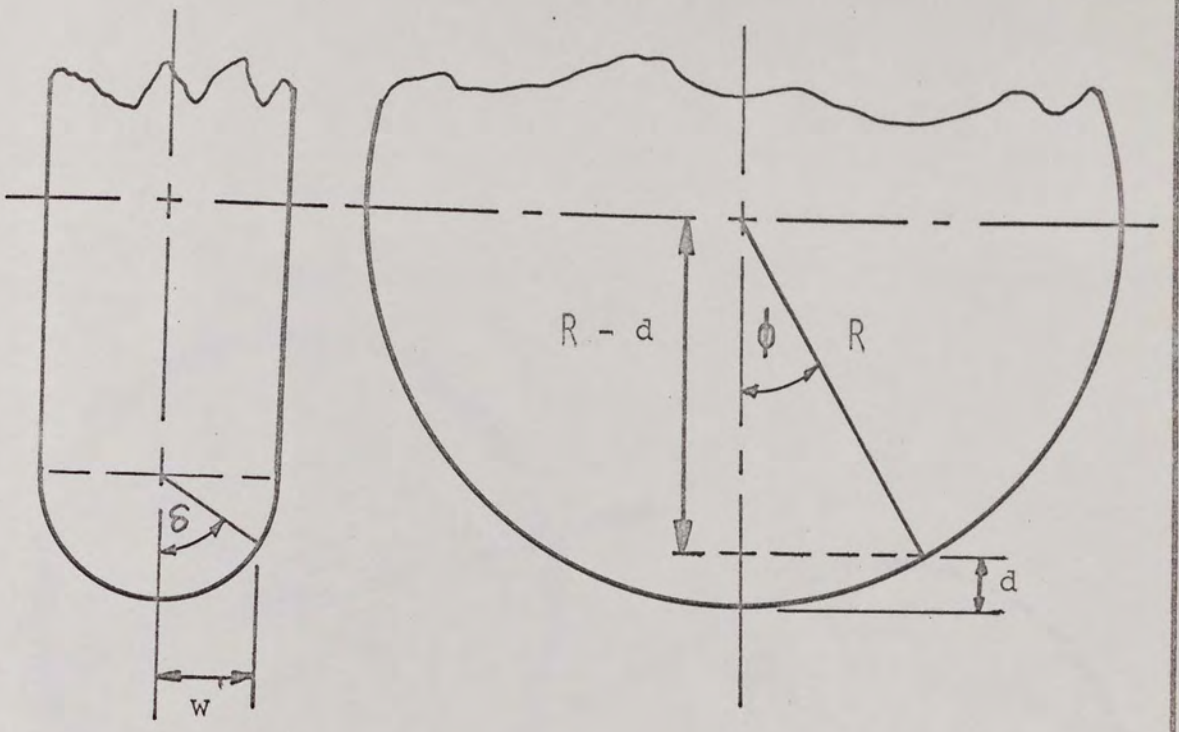


FIGURE 18

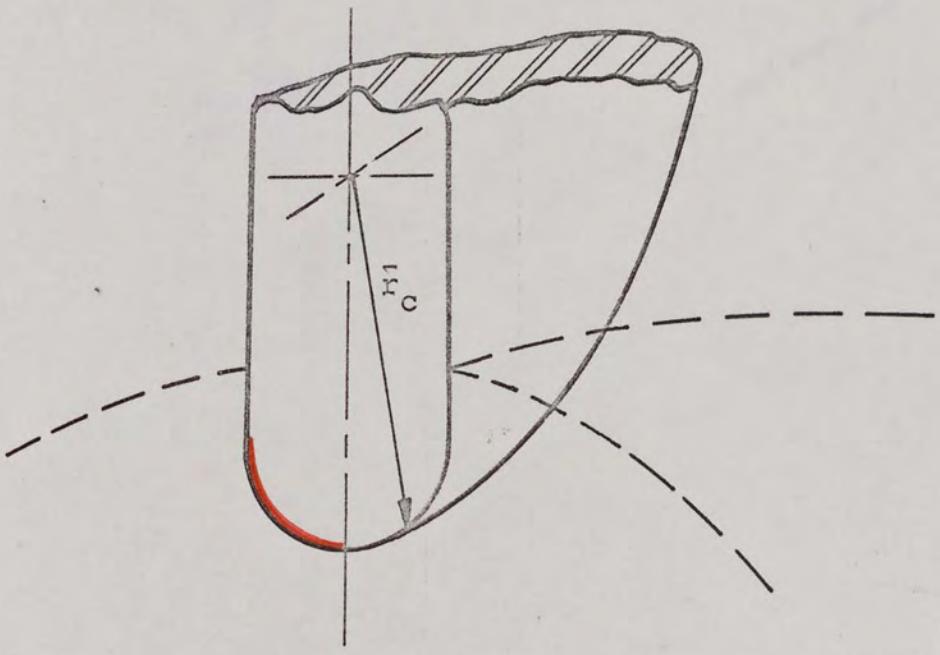


FIGURE 19

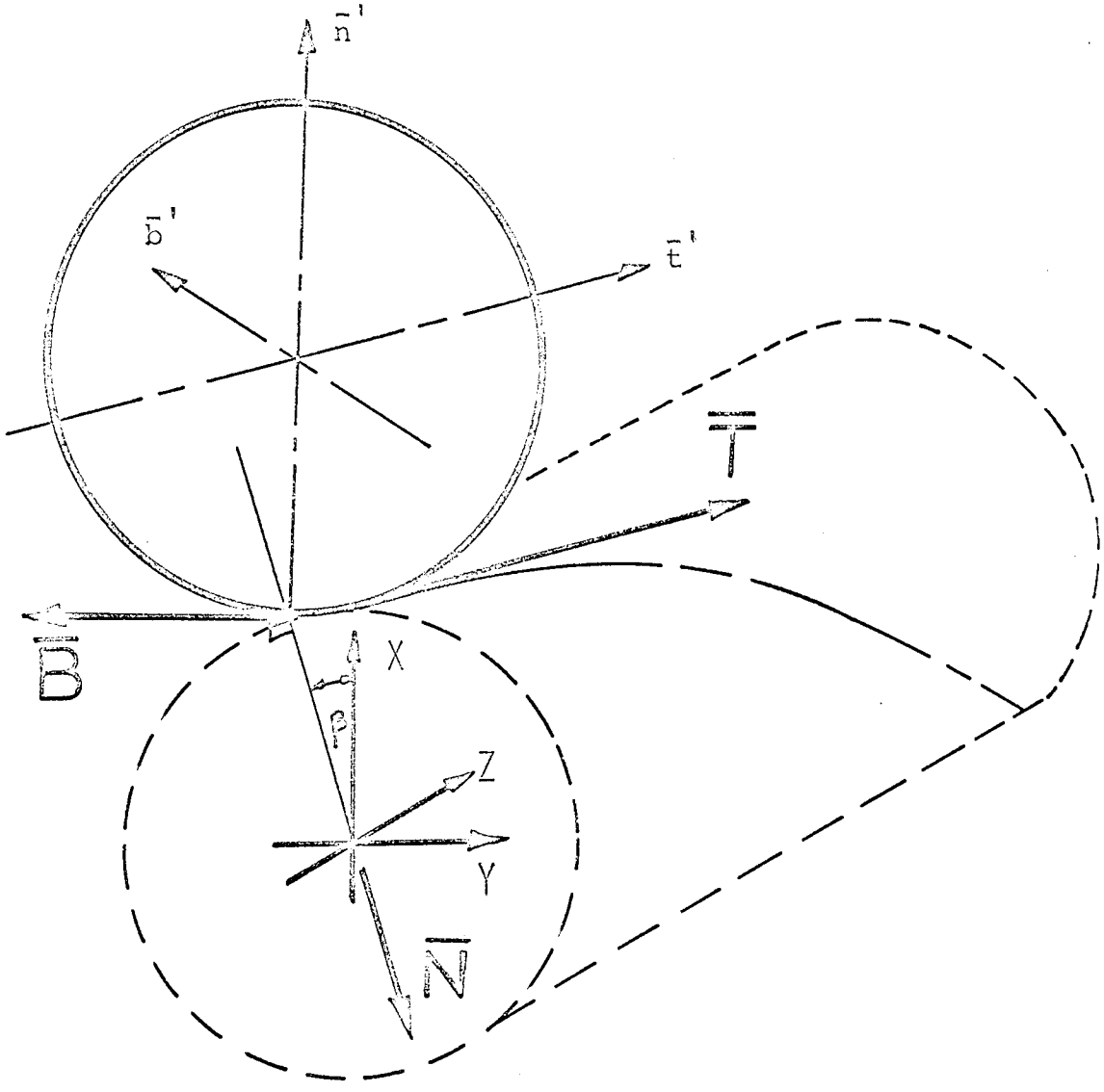


FIGURE 20

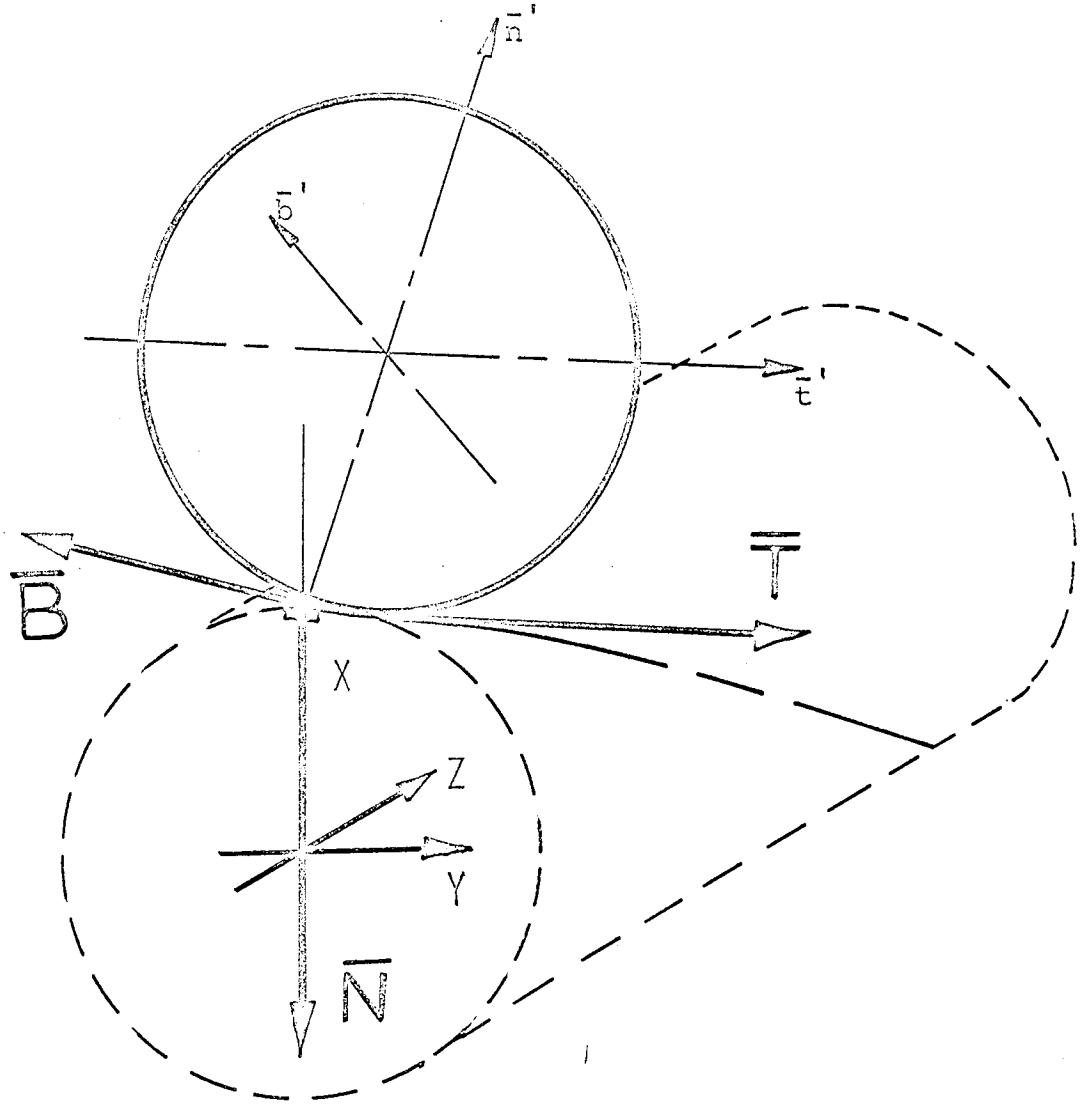


FIGURE 21.

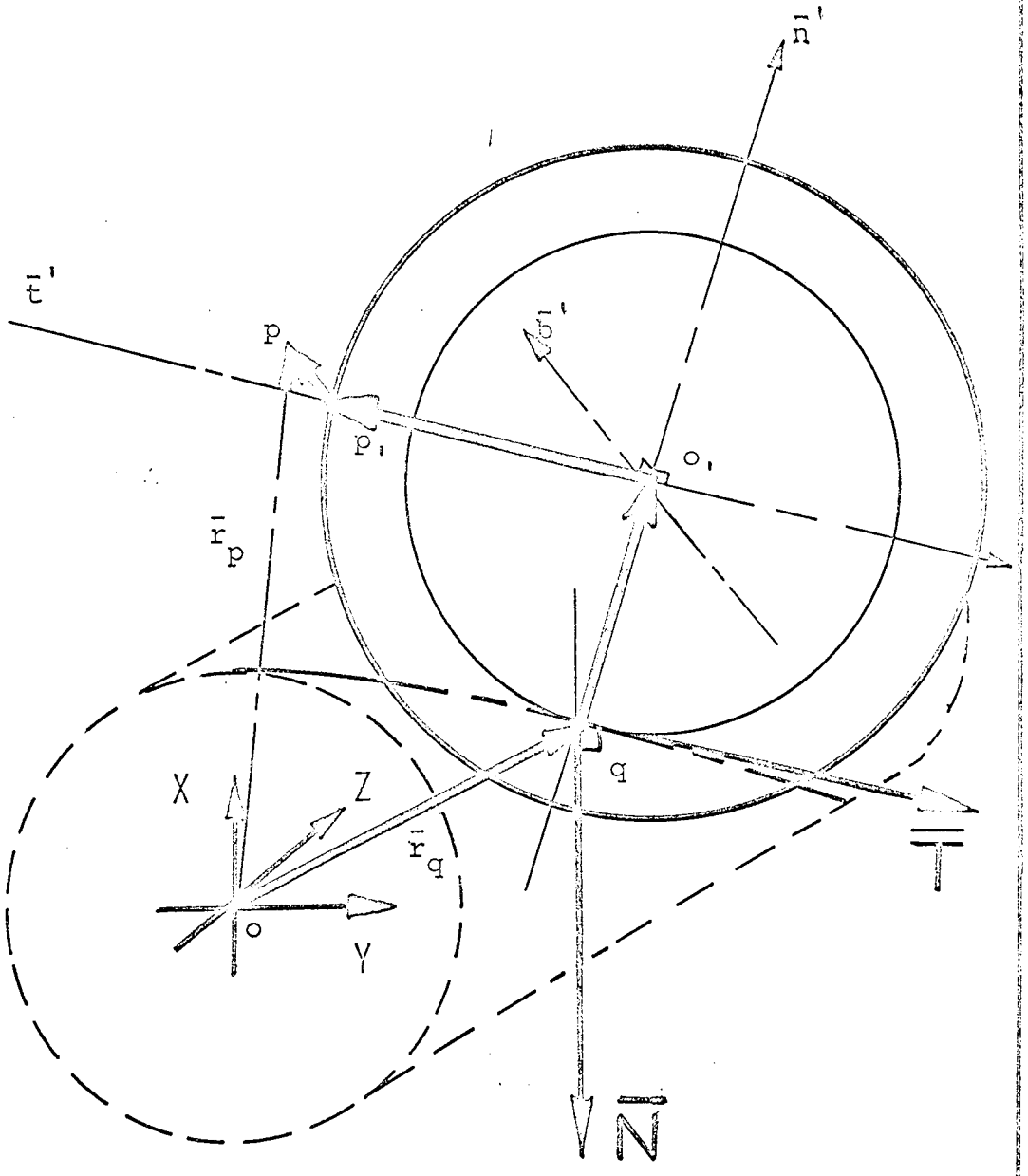


FIGURE 22

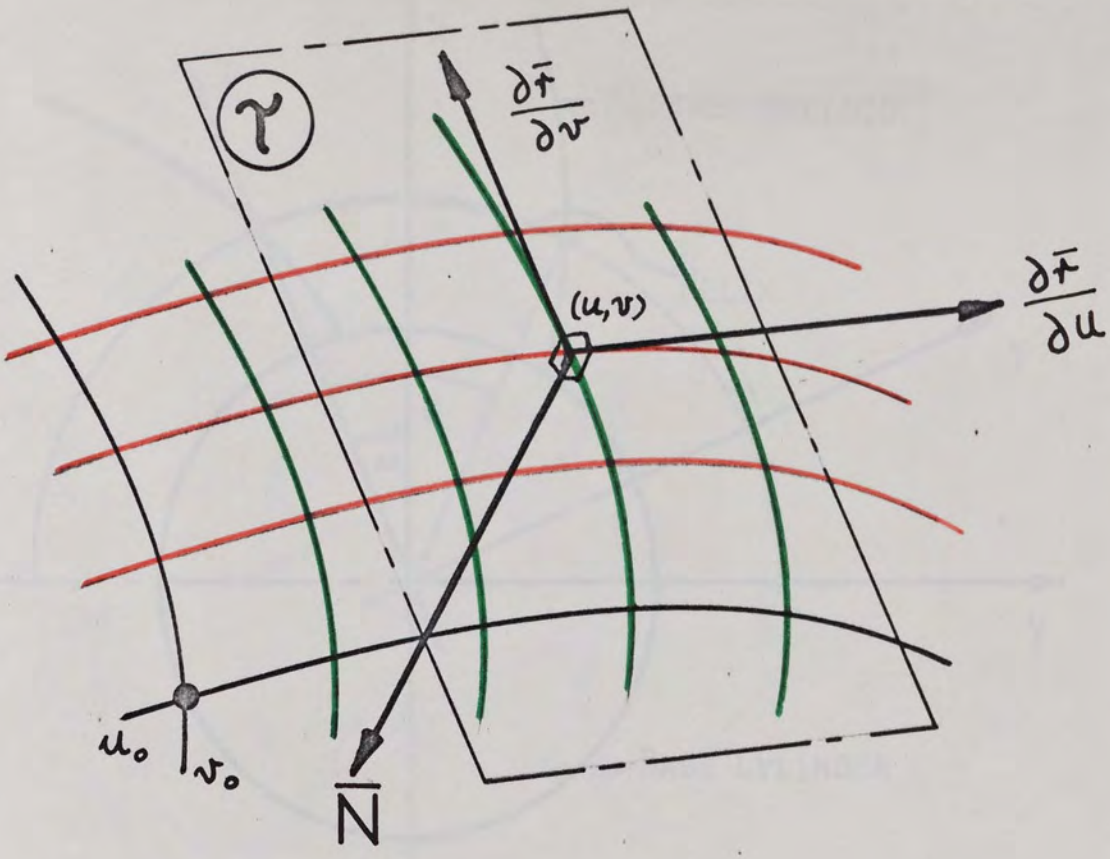


FIGURE 23

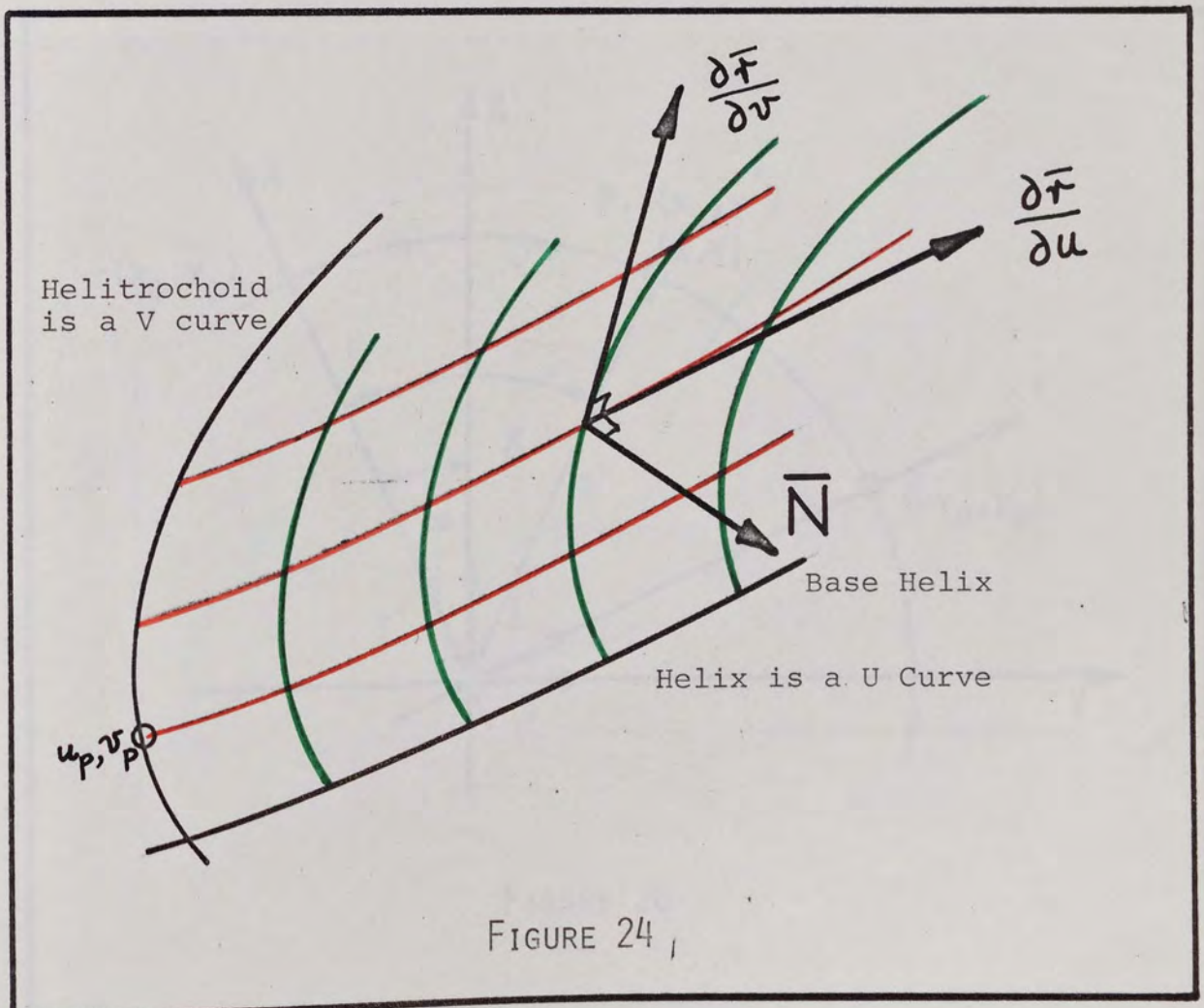


FIGURE 24

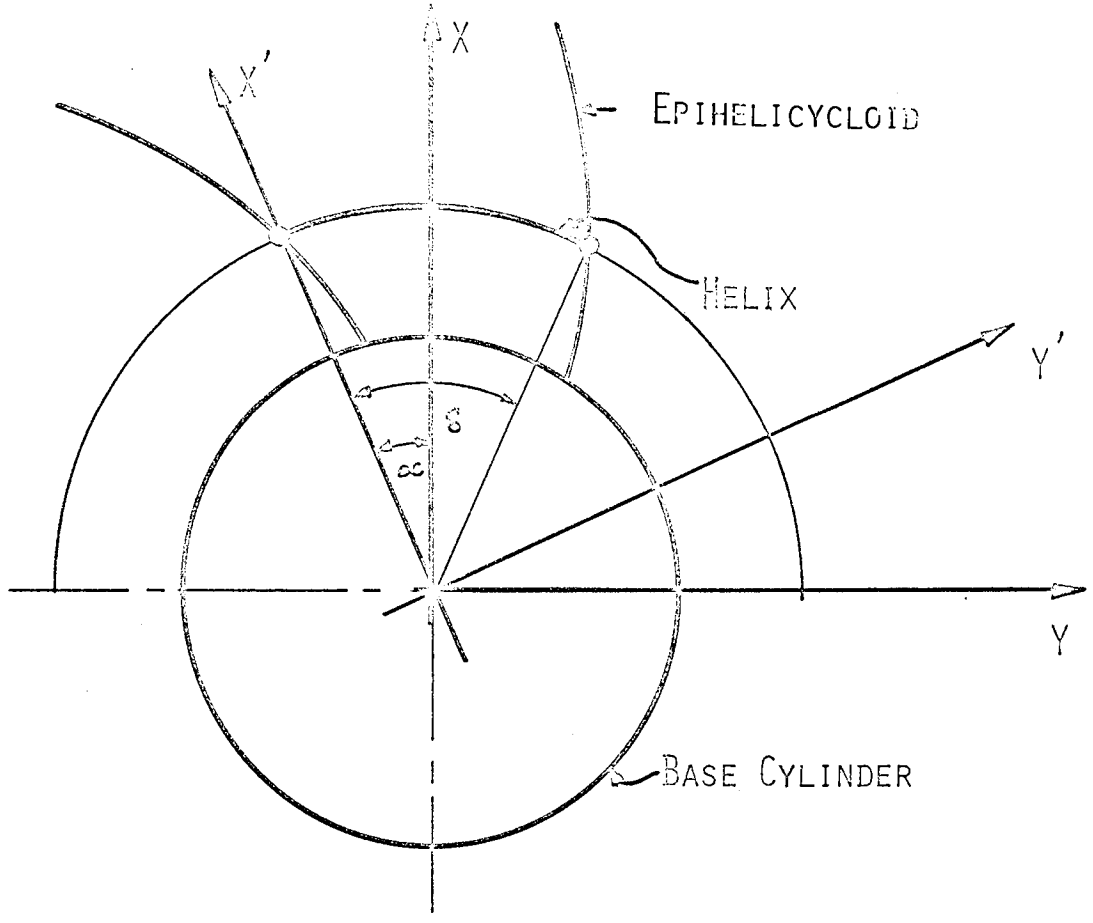


FIGURE 25

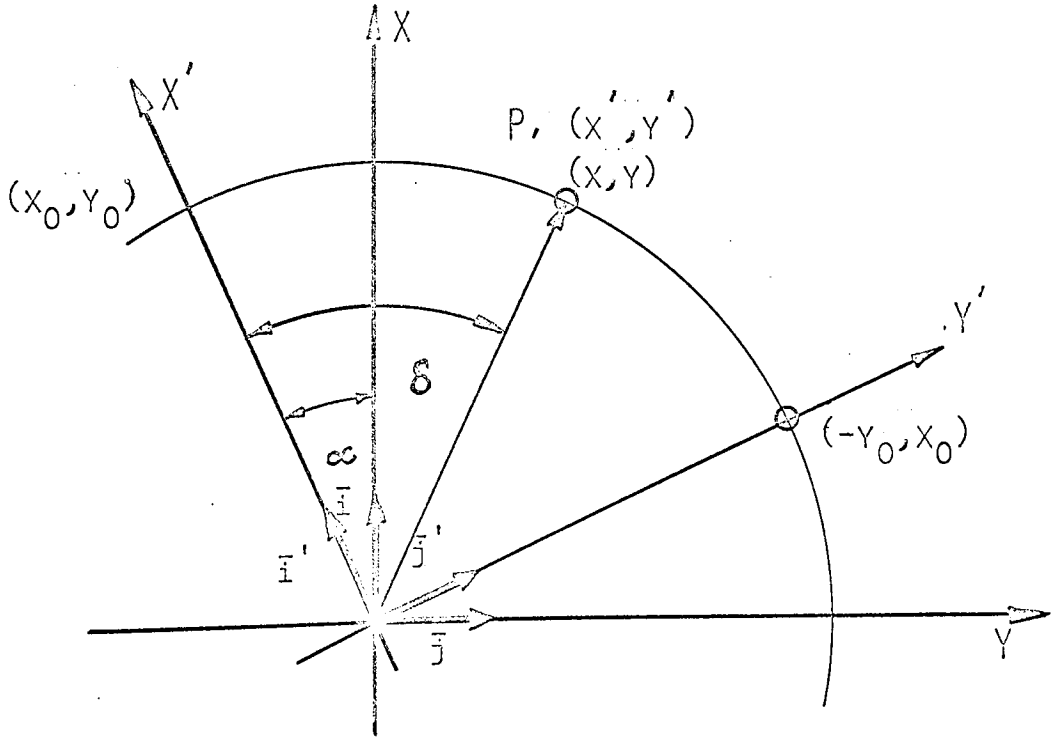


FIGURE 26

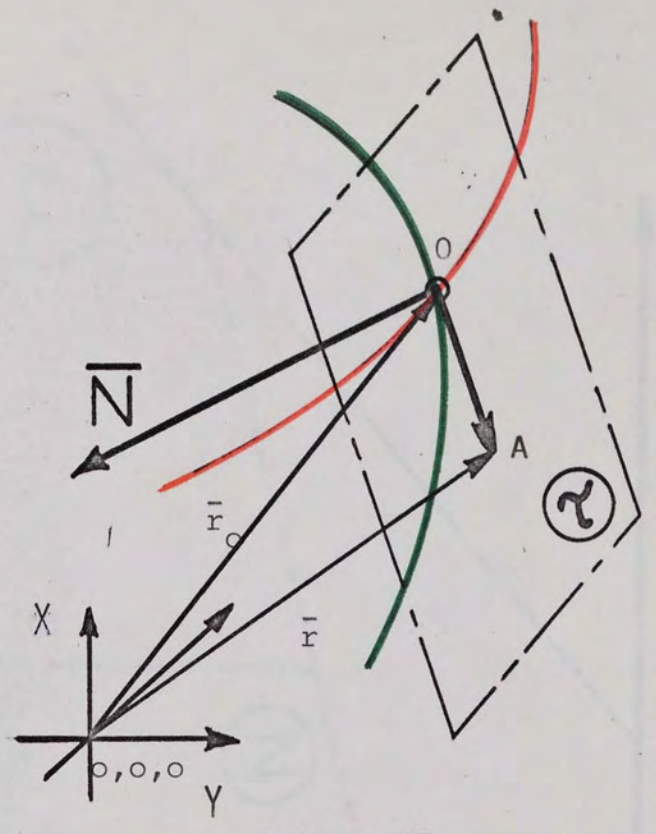


FIGURE 27

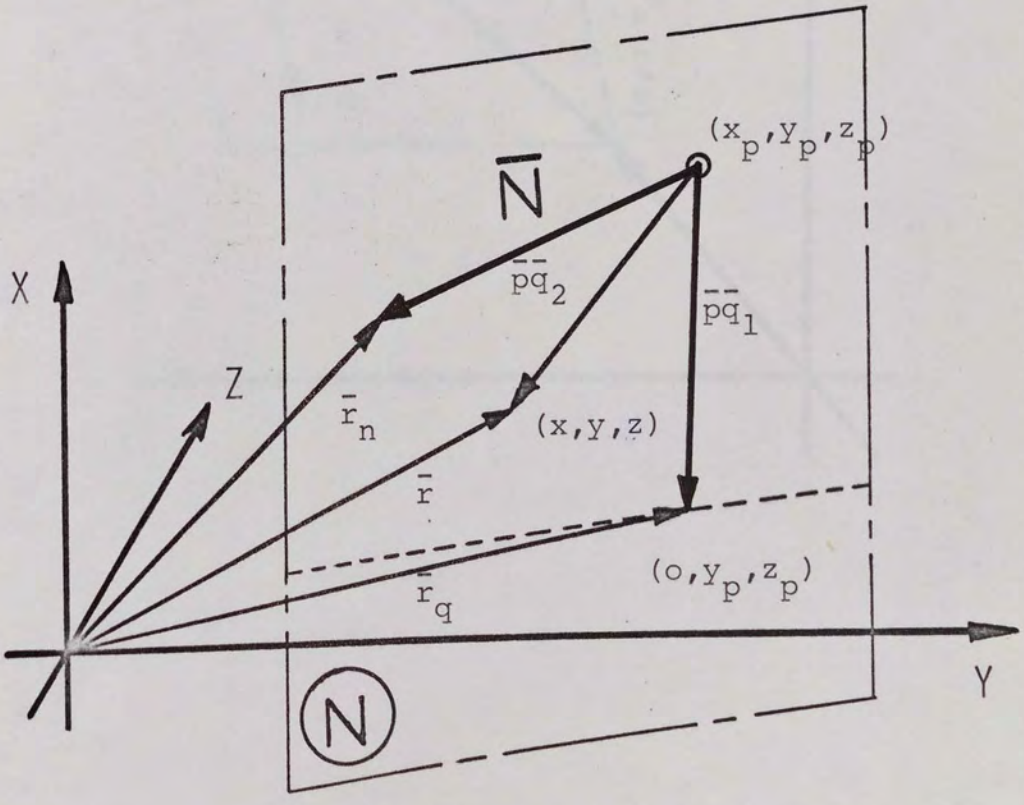


FIGURE 28

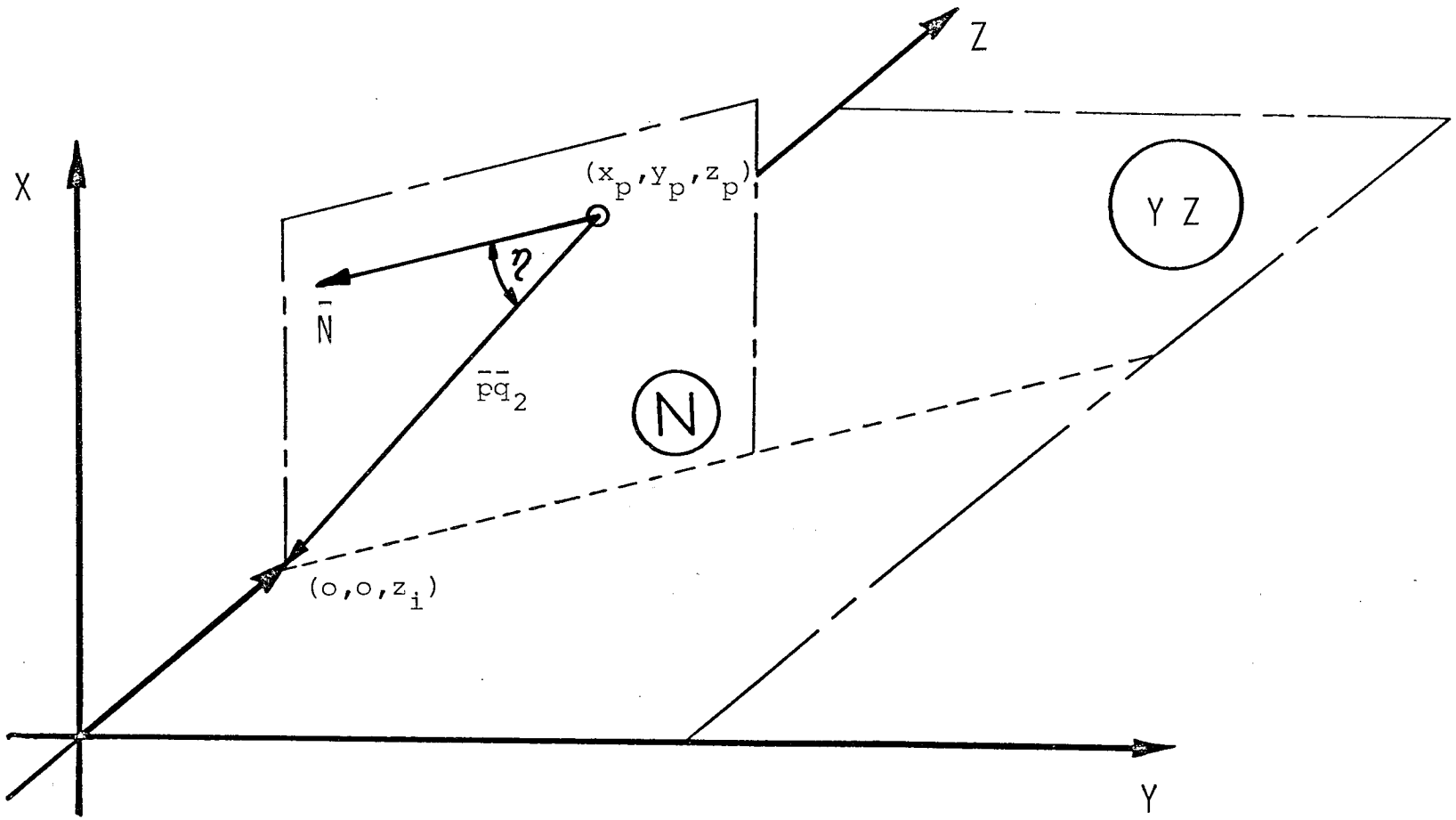


FIGURE 29

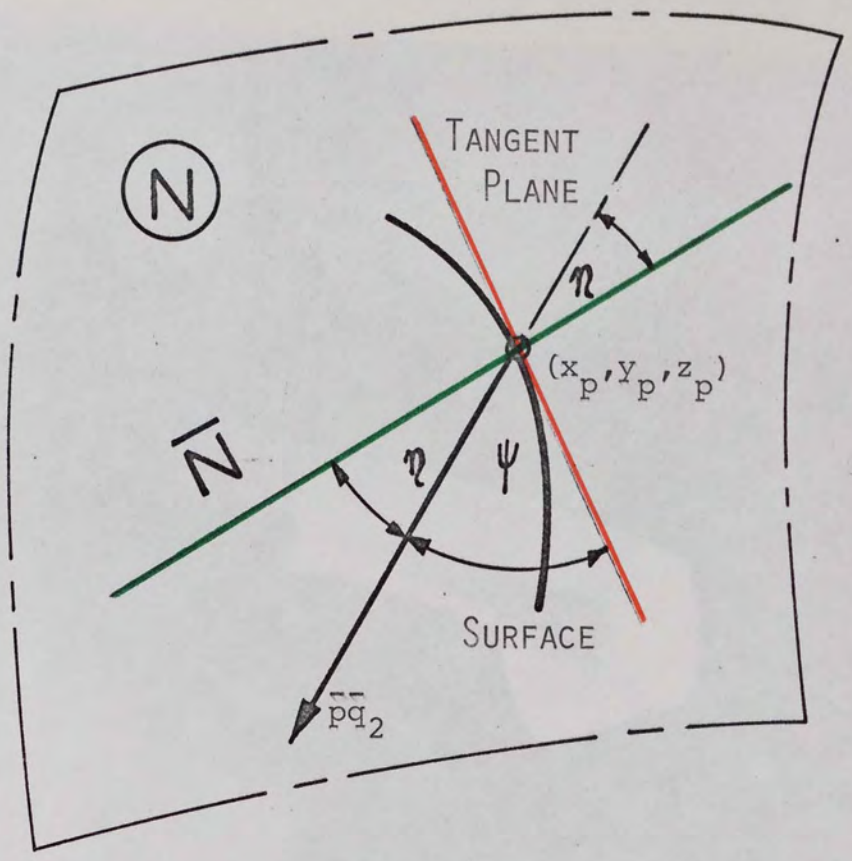


FIGURE 30

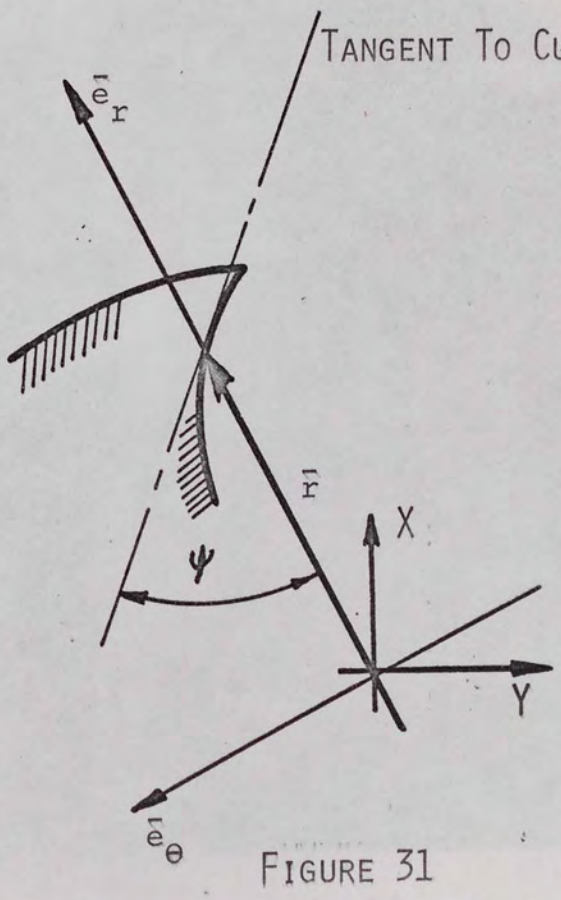


FIGURE 31

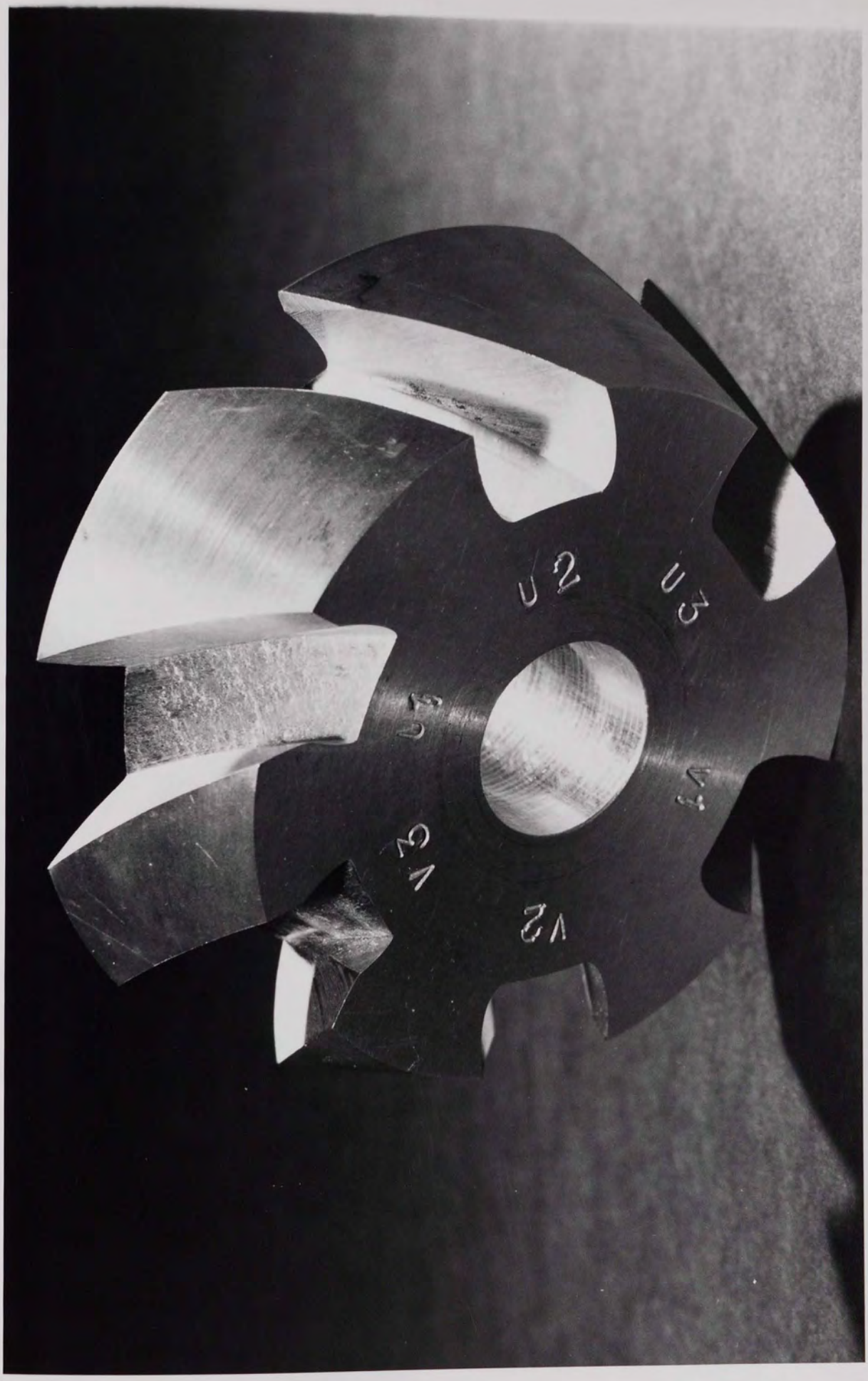


Plate ii

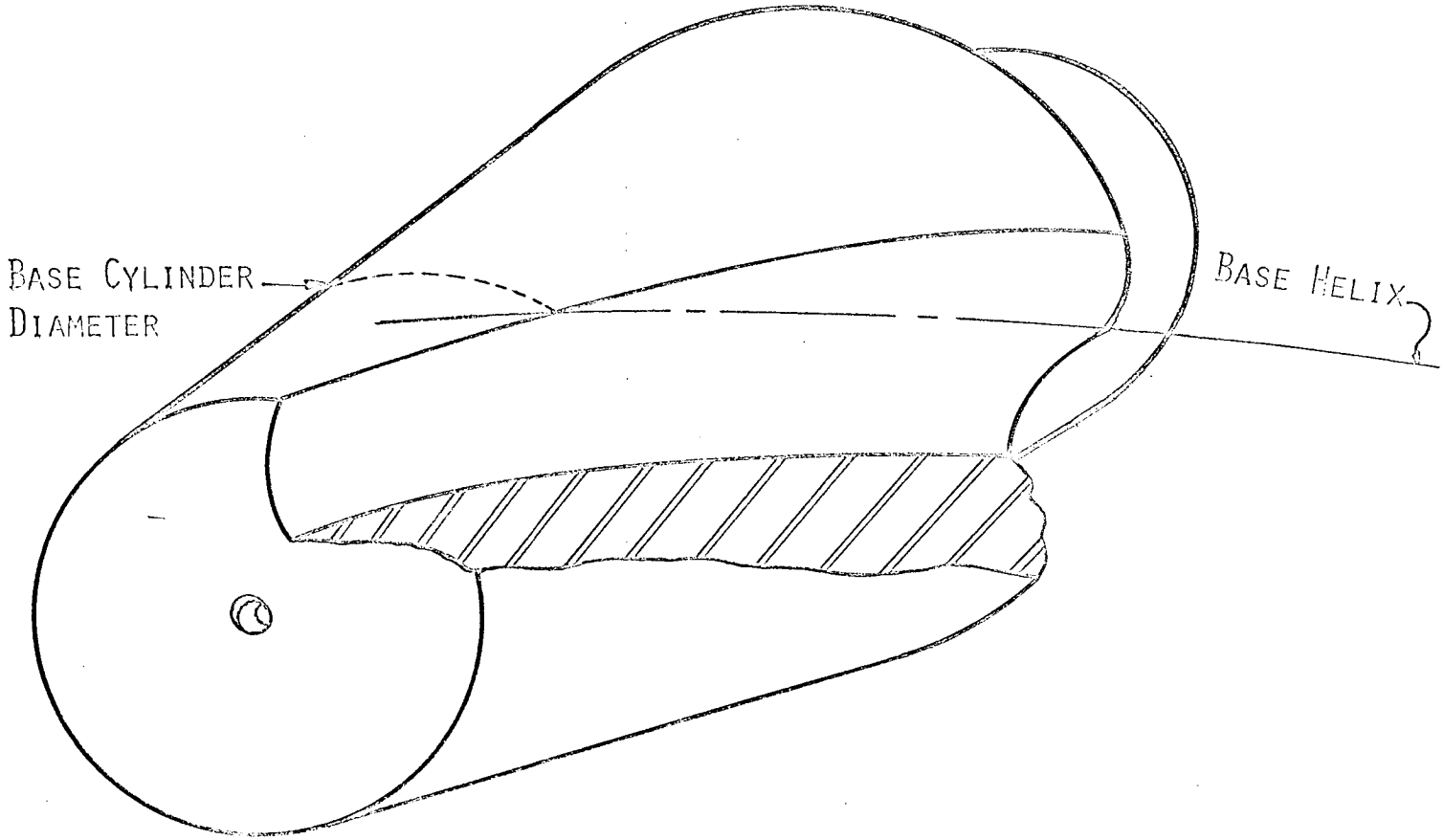


FIGURE 32

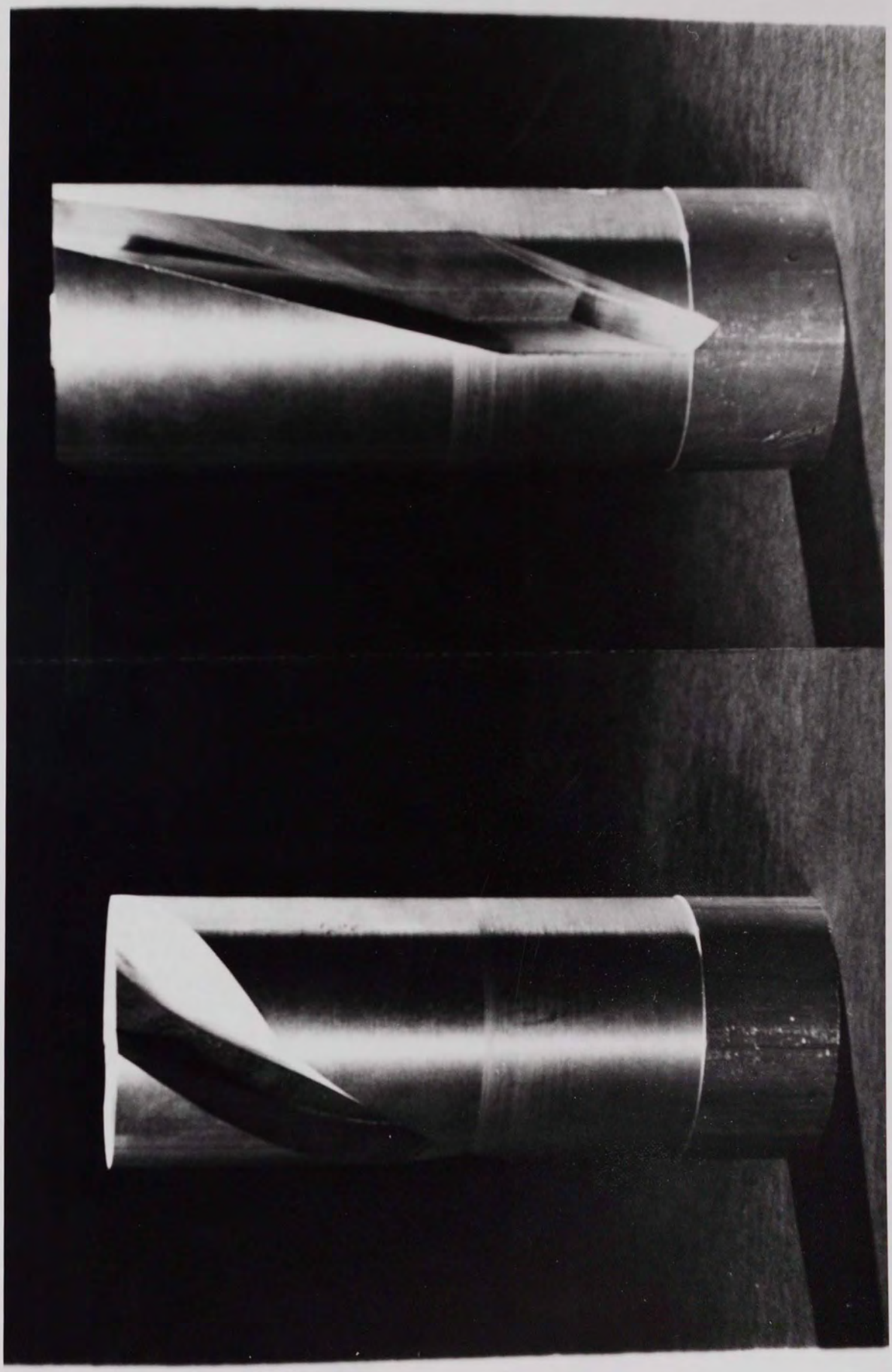

Plate iii

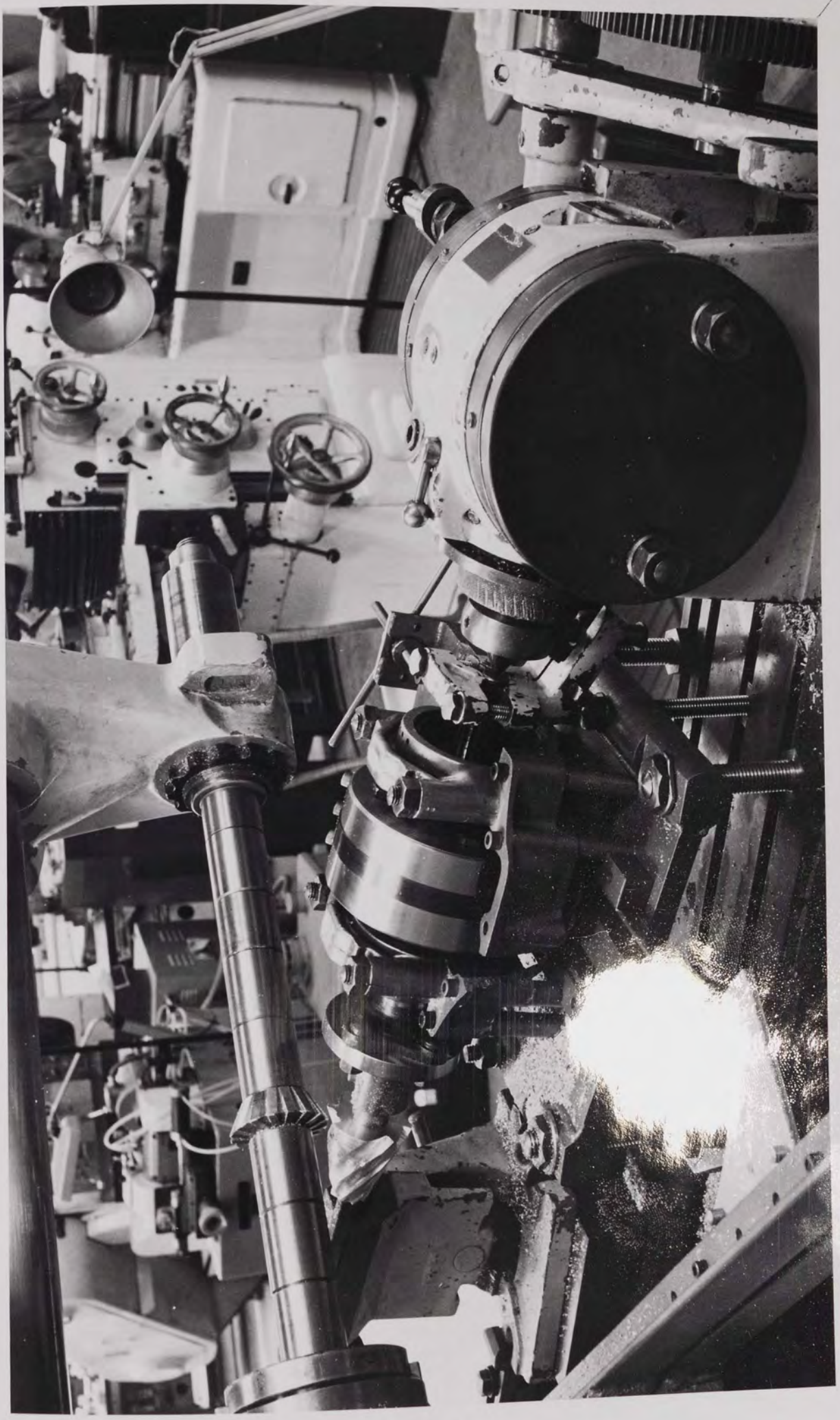

plate iv

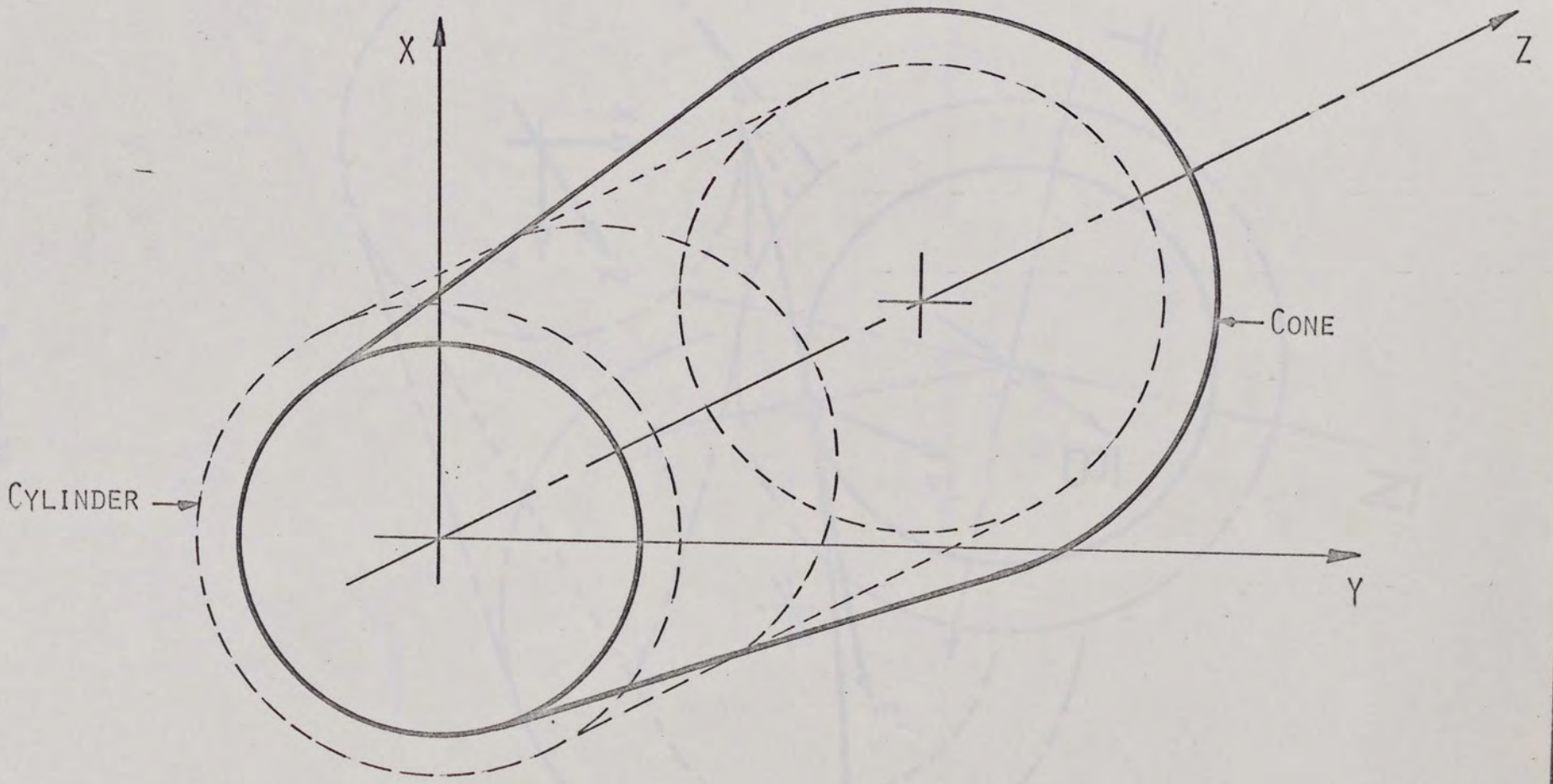


FIGURE 33

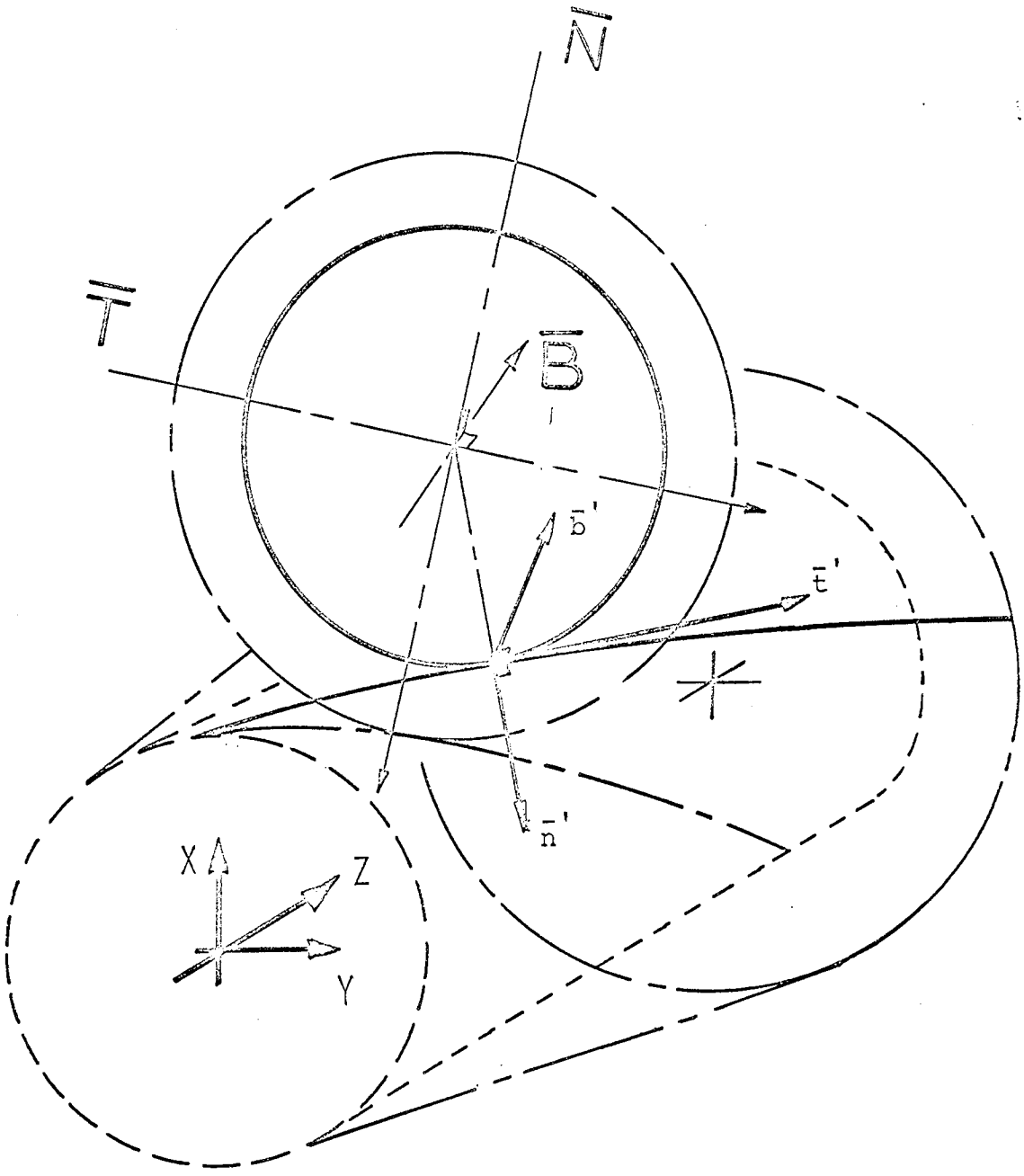


FIGURE 34

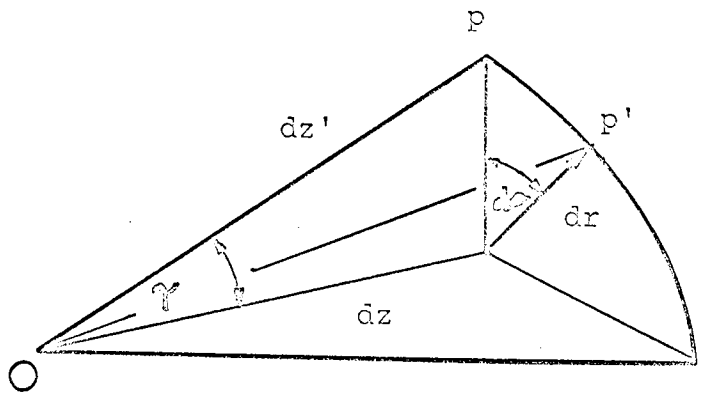


FIGURE 35

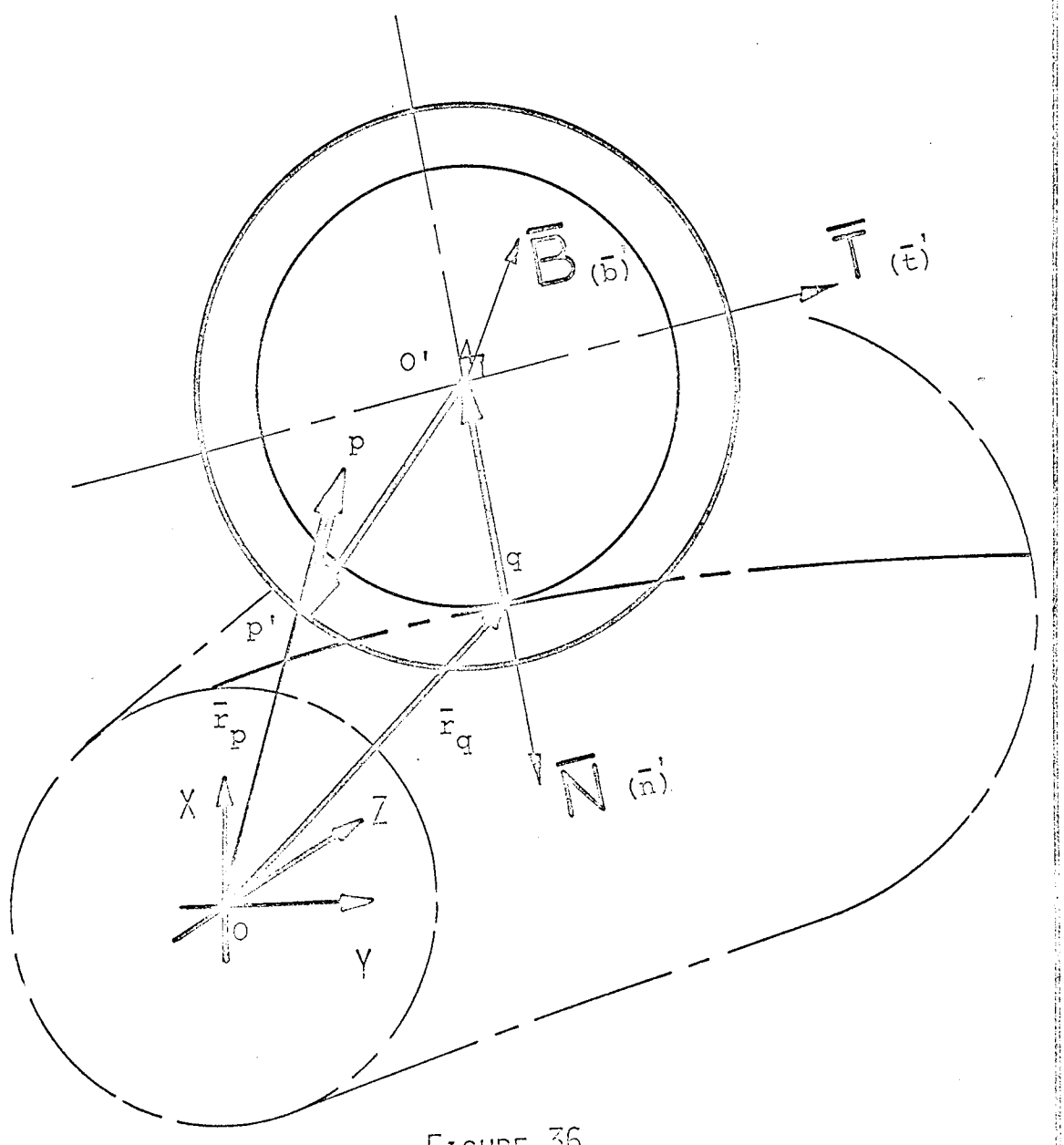


FIGURE 36

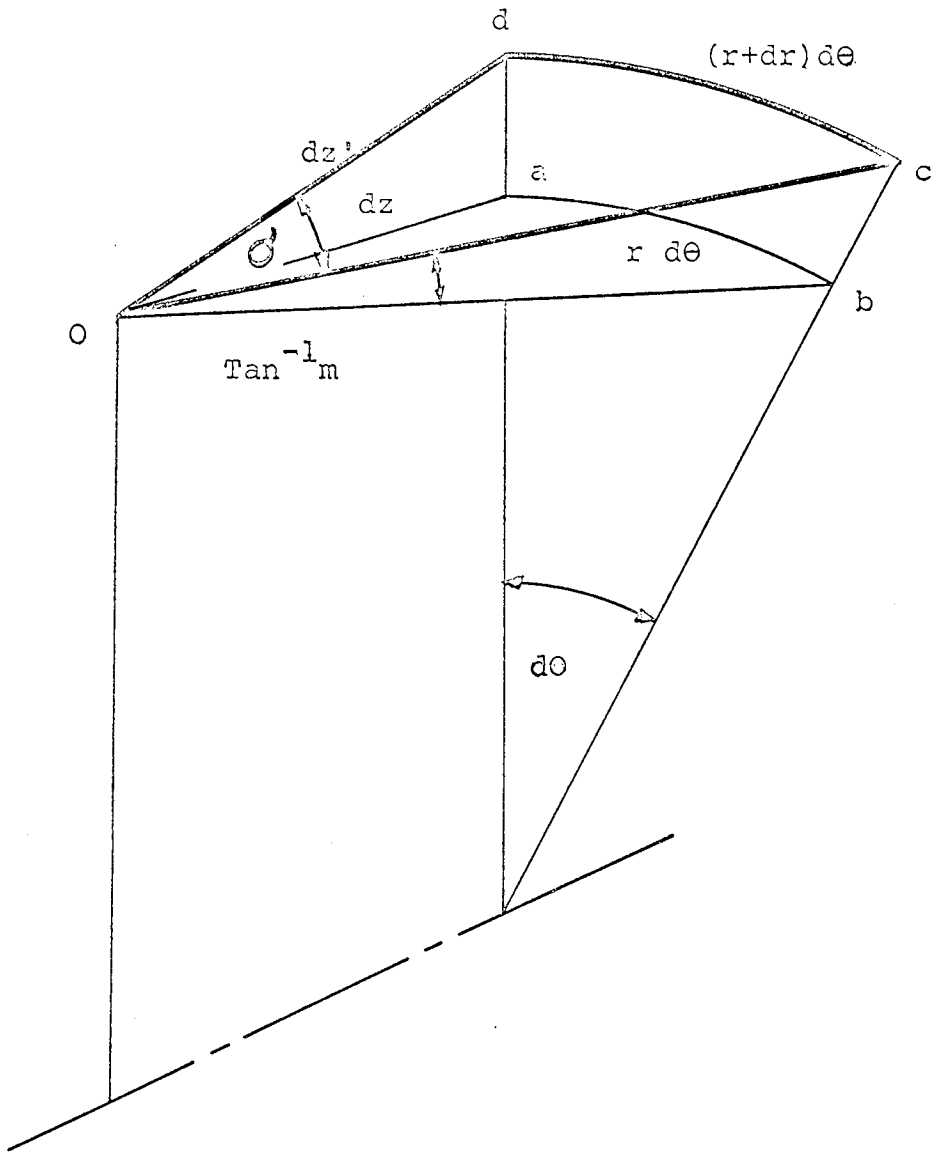


FIGURE 37

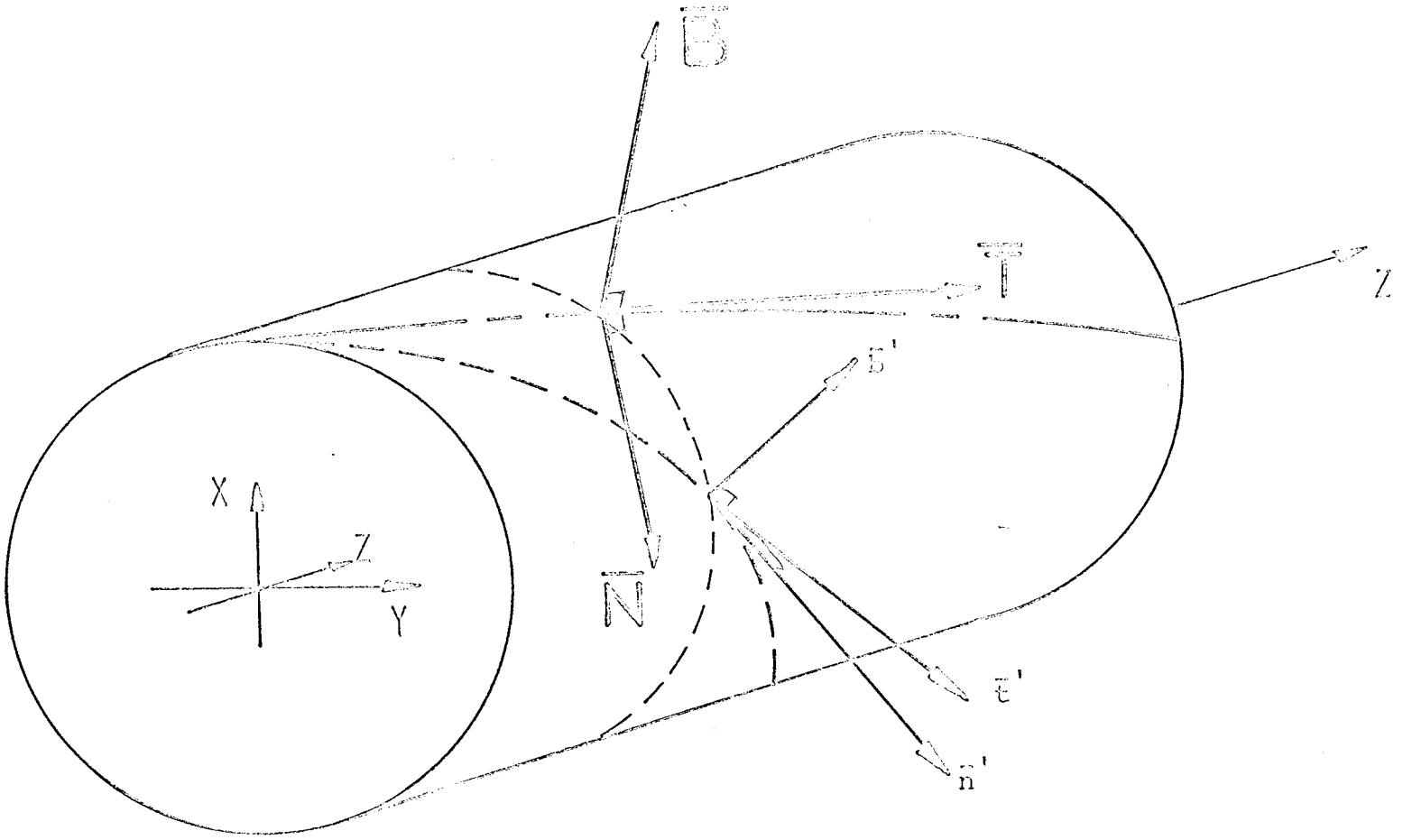


FIGURE 38

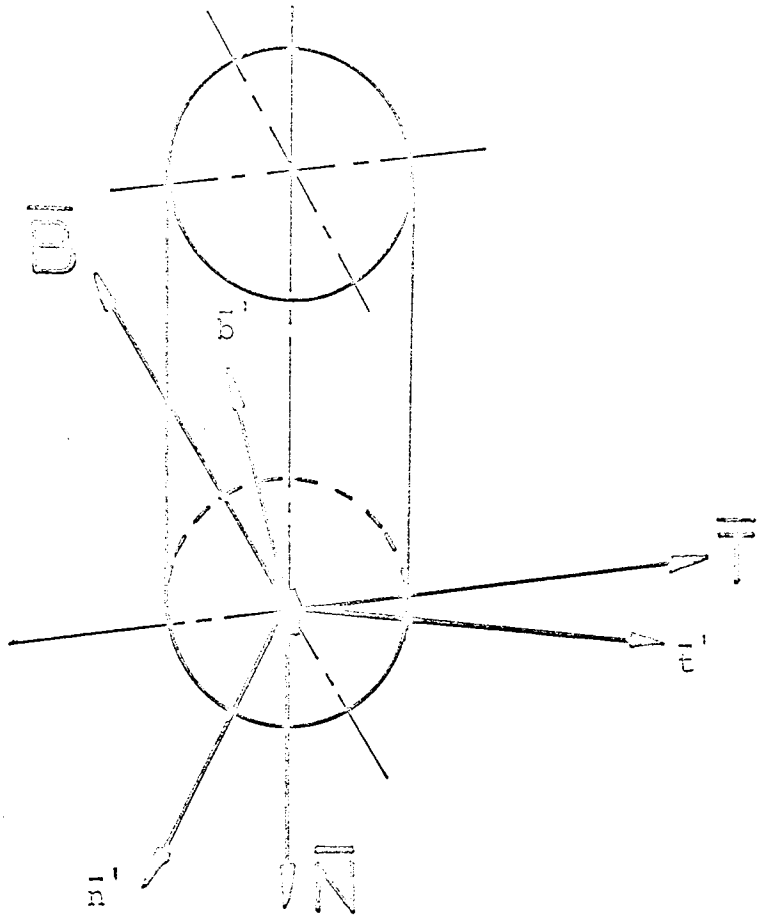


FIGURE 39

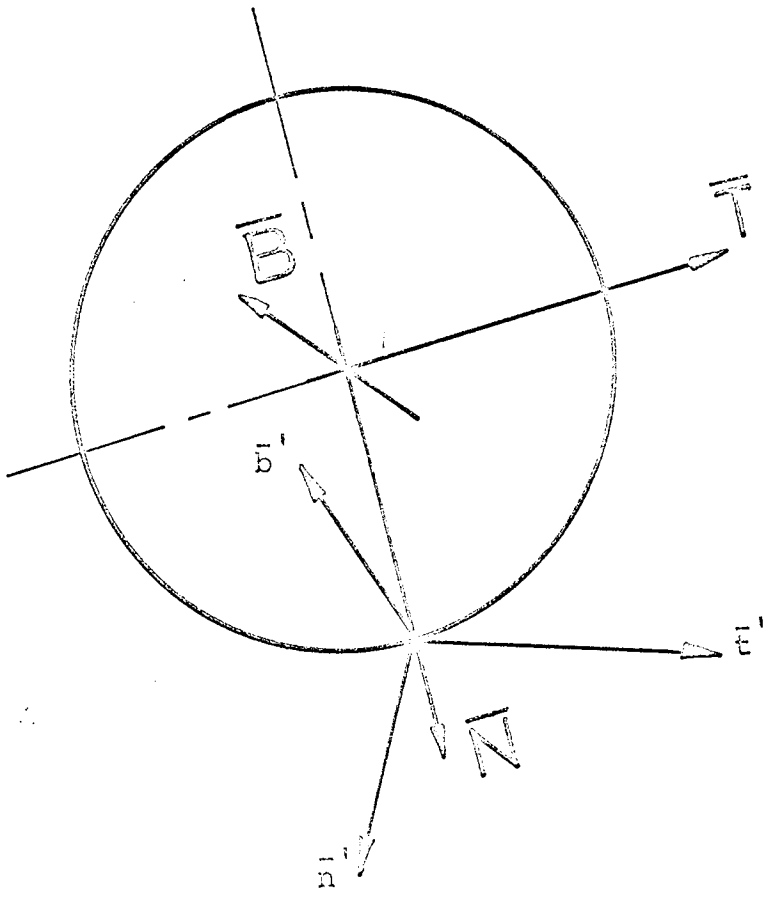


FIGURE 40

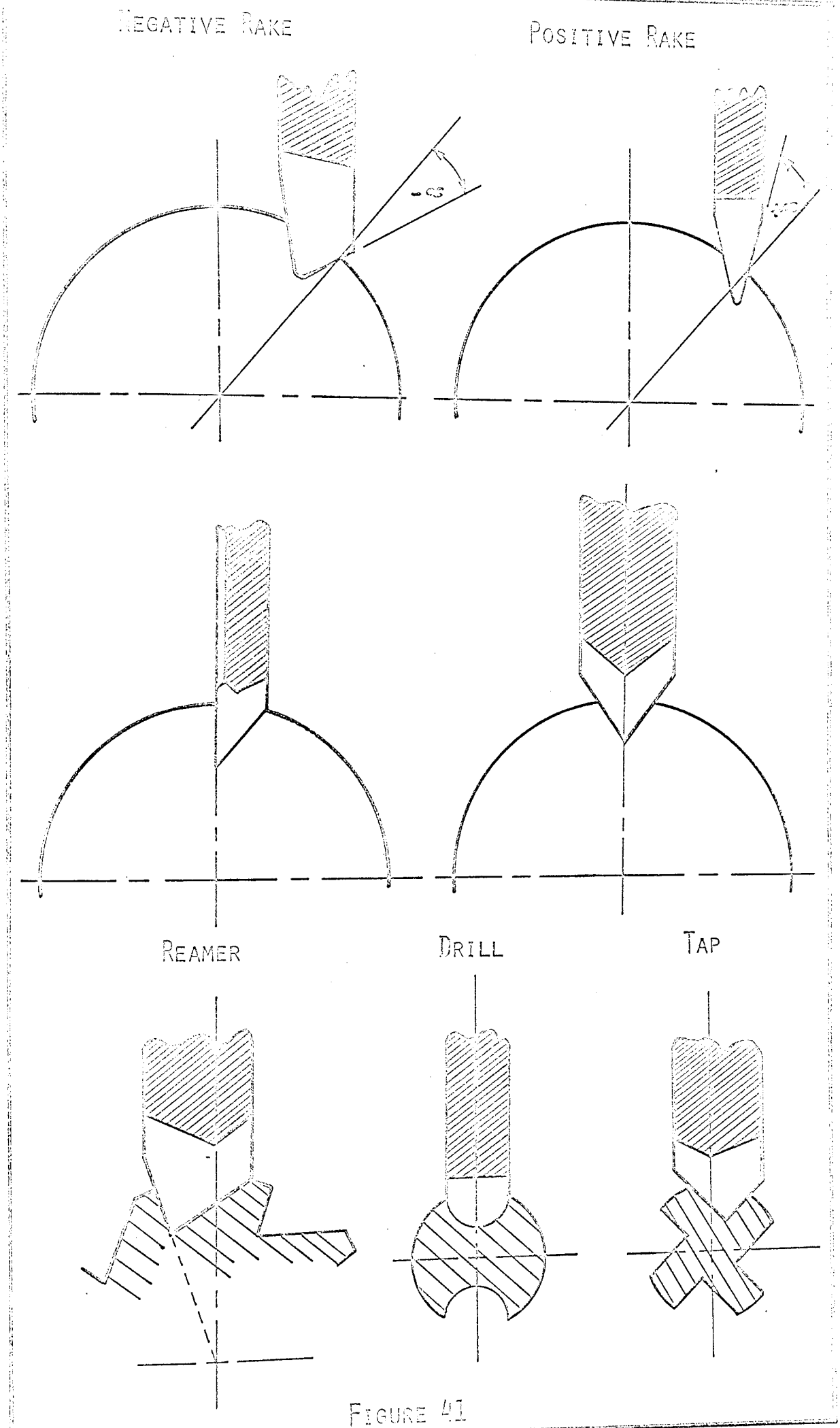


FIGURE 41

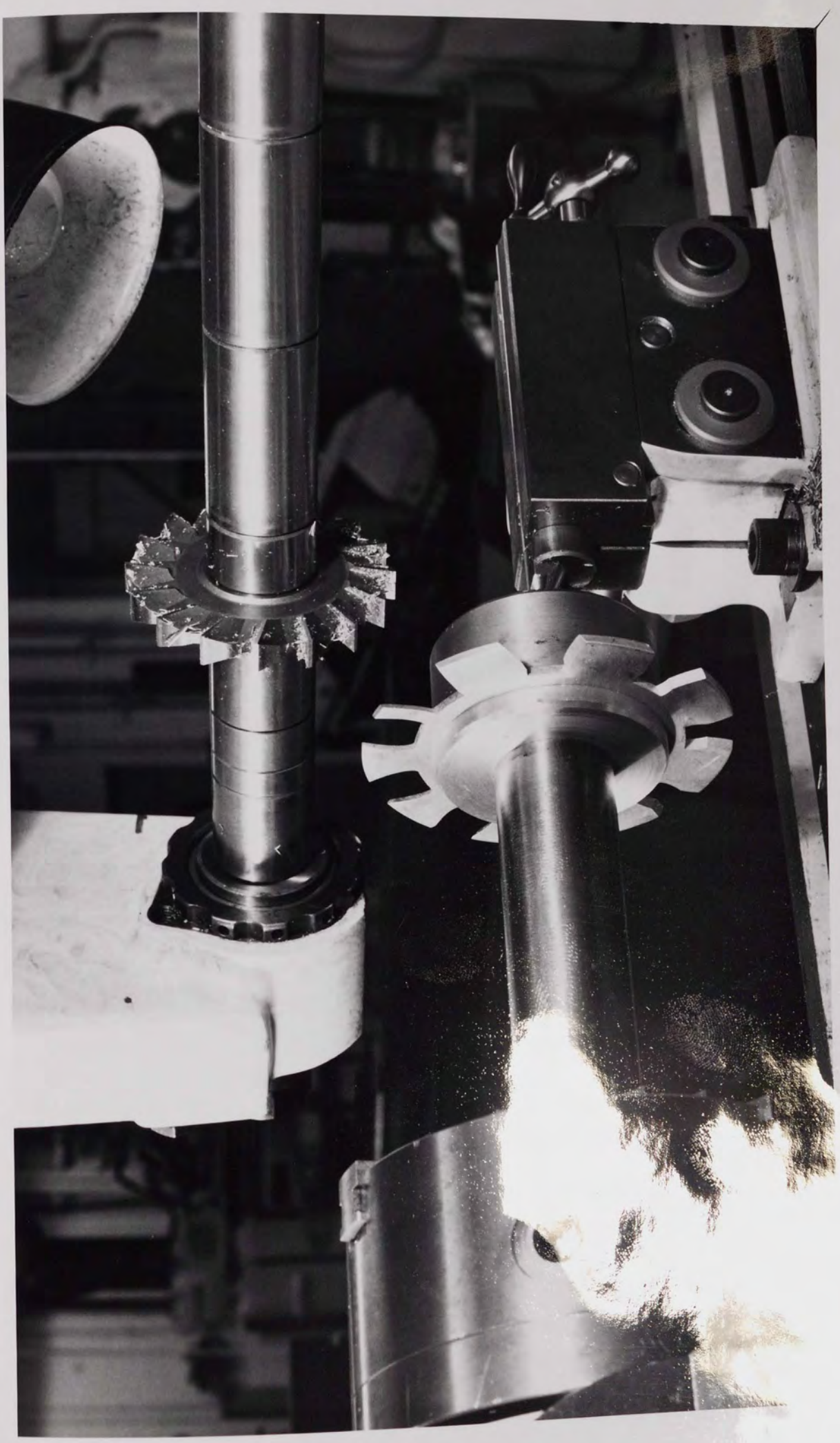

plate v

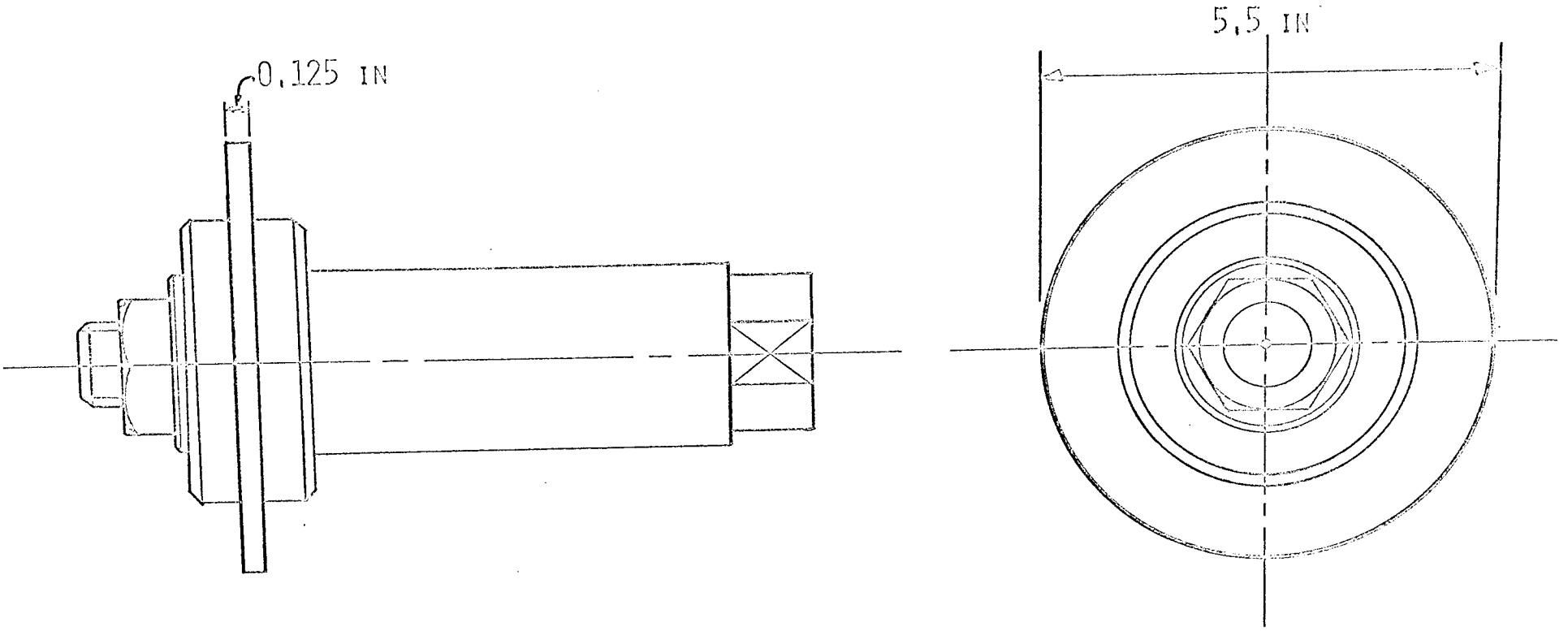


FIGURE 42

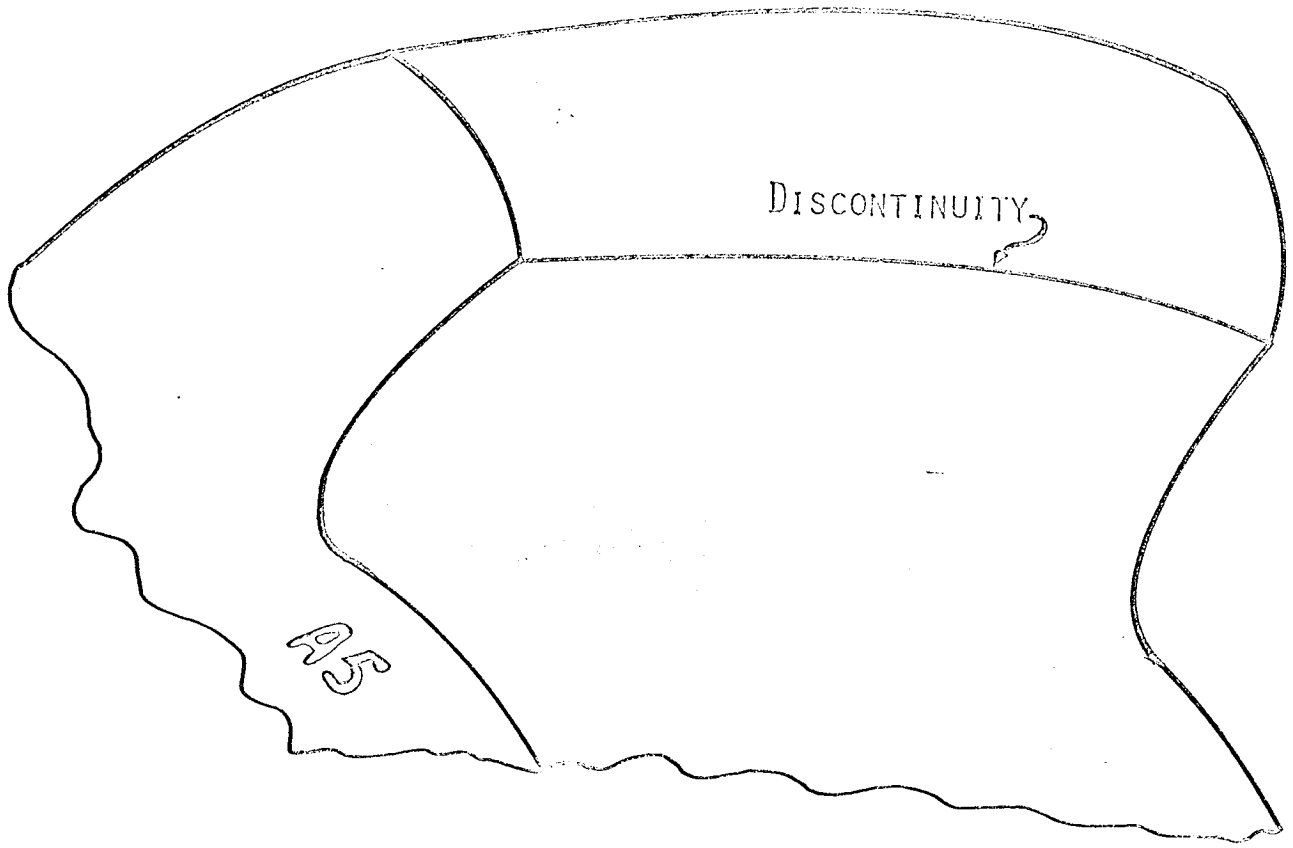


FIGURE 43

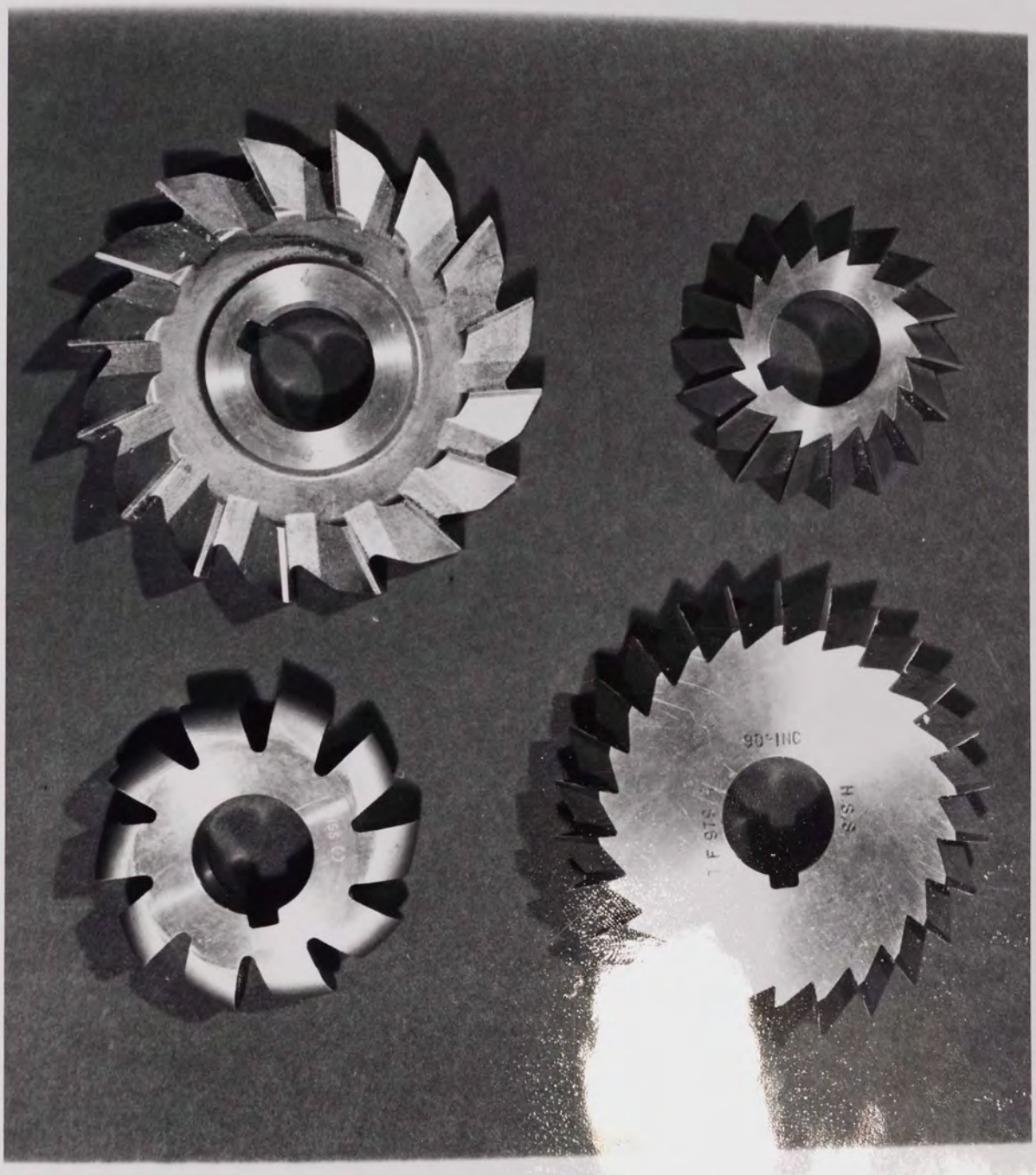


Plate vi

TEST A1
SCALE - 10X

EXPERIMENTAL

THEORETICAL

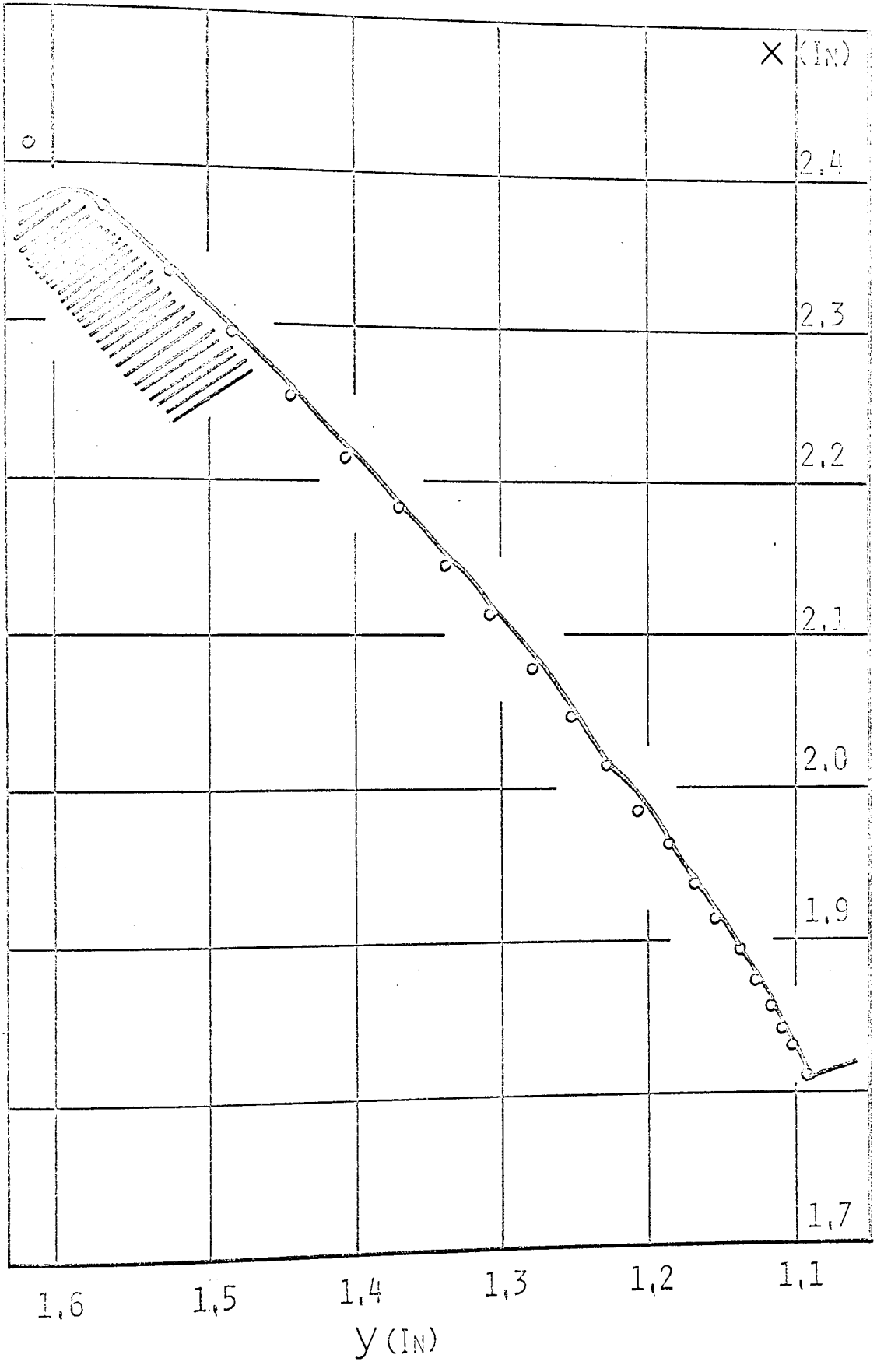


FIGURE 44

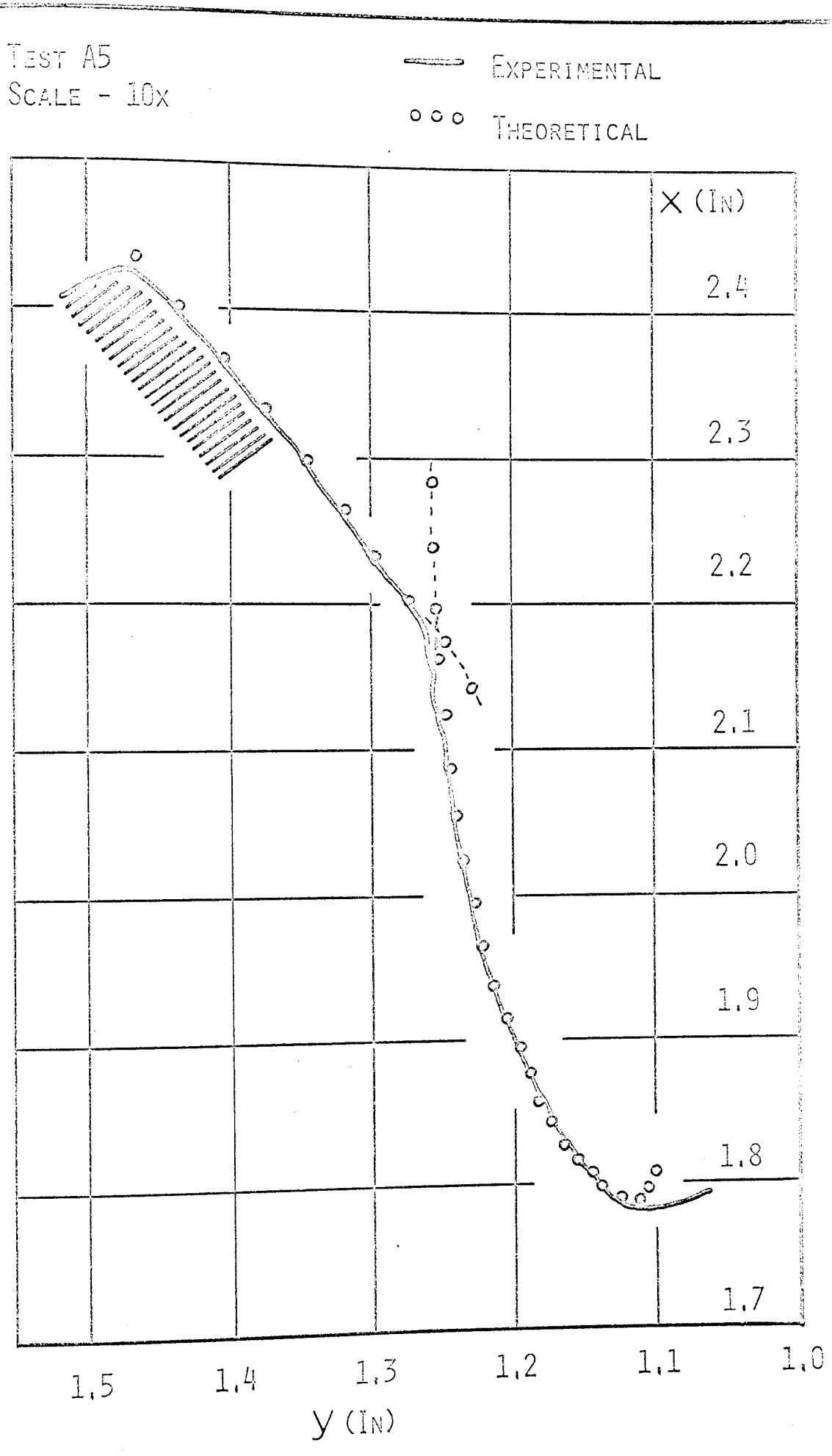
TEST A5
SCALE - 10X
EXPERIMENTAL
THEORETICAL
X (IN)
2.4
2.3
2.2
2.1
2.0
1.9
1.8
1.7
1.5
1.4
1.3
1.2
1.1
1.0
y (IN)

FIGURE 45

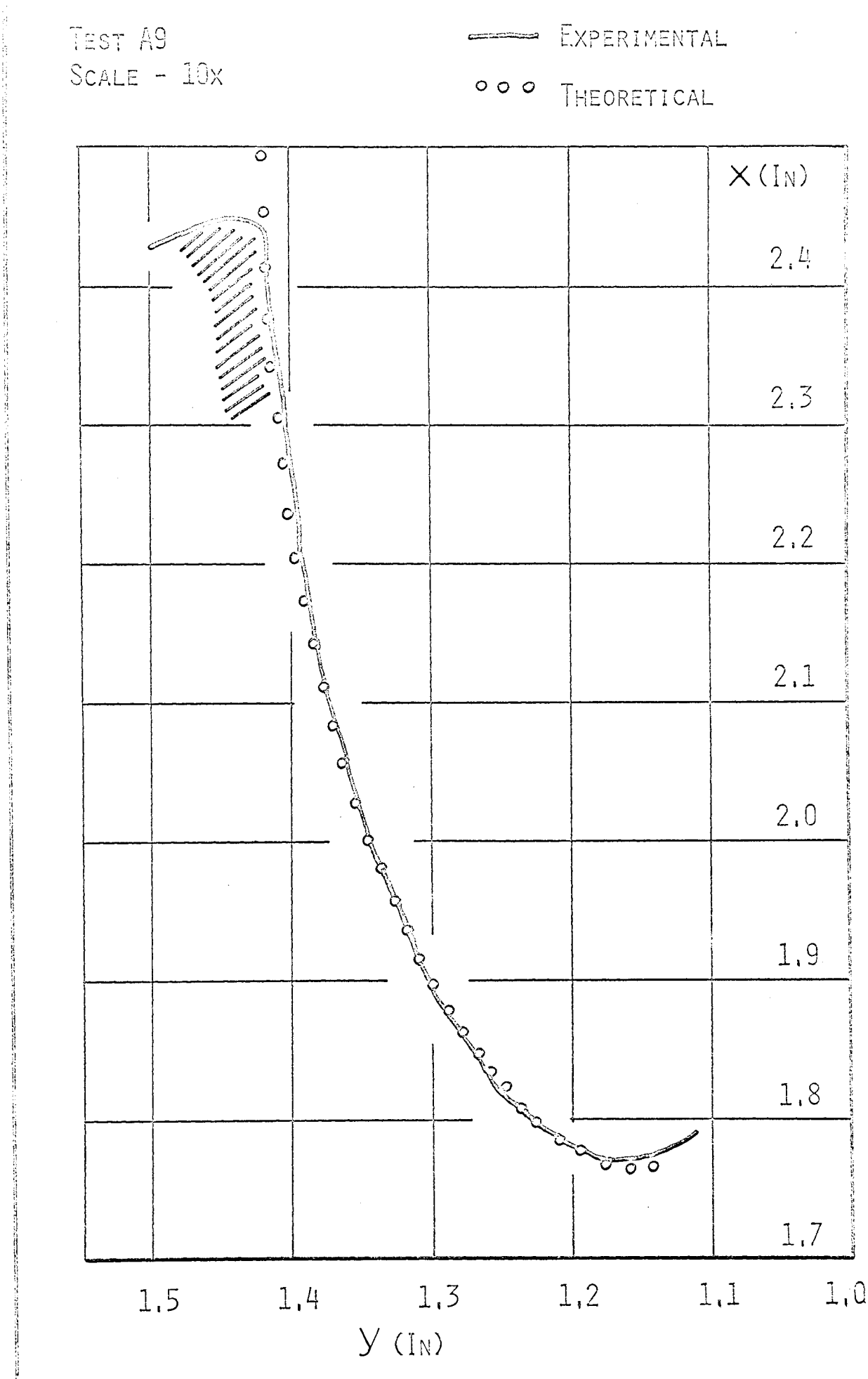
TEST A9
SCALE - 10X
EXPERIMENTAL
THEORETICAL
X (IN)
2.4
2.3
2.2
2.1
2.0
1.9
1.8
1.7
1.5
1.4
1.3
1.2
1.1
1.0
Y (IN)

FIGURE 46

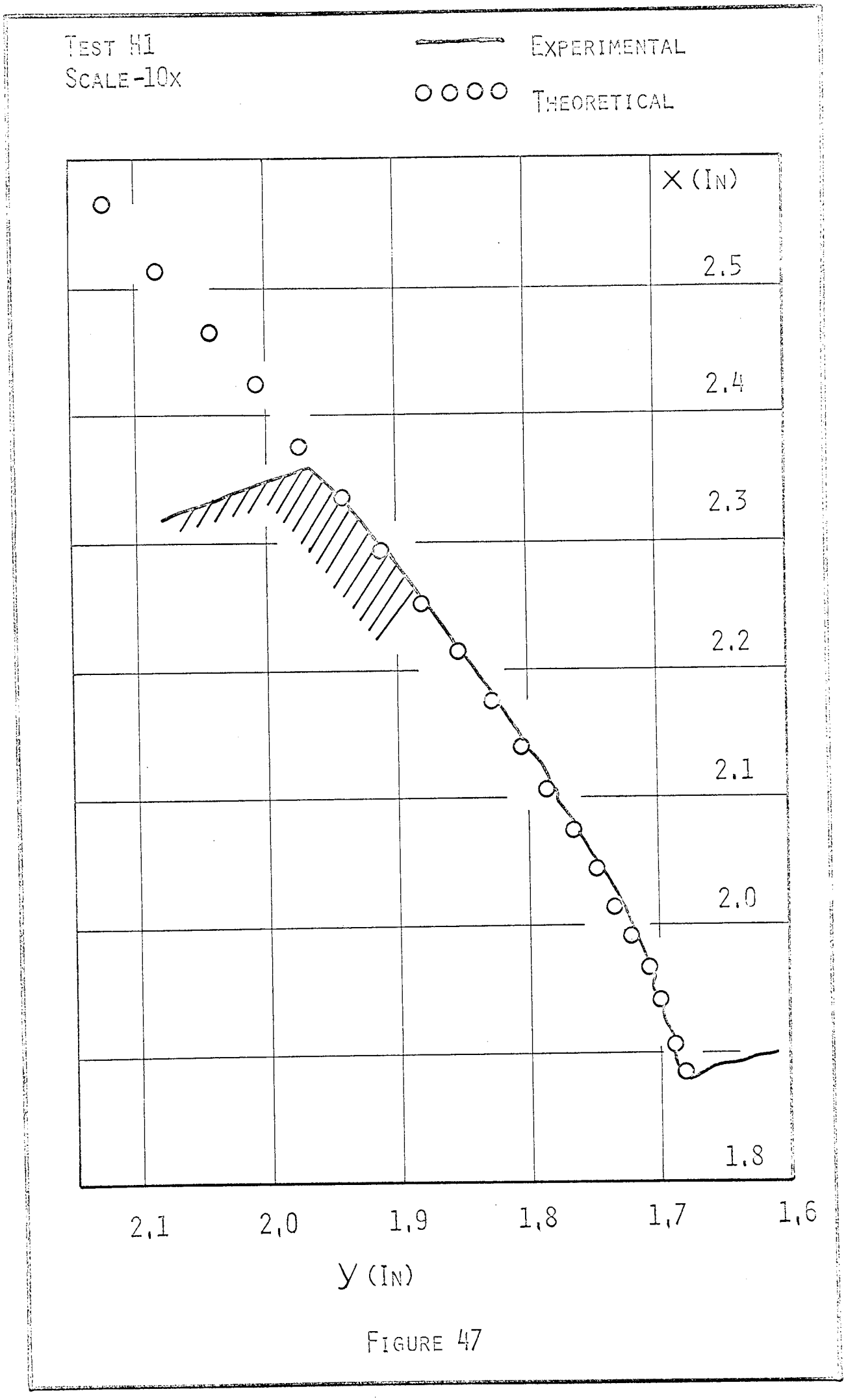
TEST H1
SCALE-10X
EXPERIMENTAL
THEORETICAL
X (IN)
2.5
2.4
2.3
2.2
2.1
2.0
1.8
2.1
2.0
1.9
1.8
1.7
1.6
Y (IN)

FIGURE 47

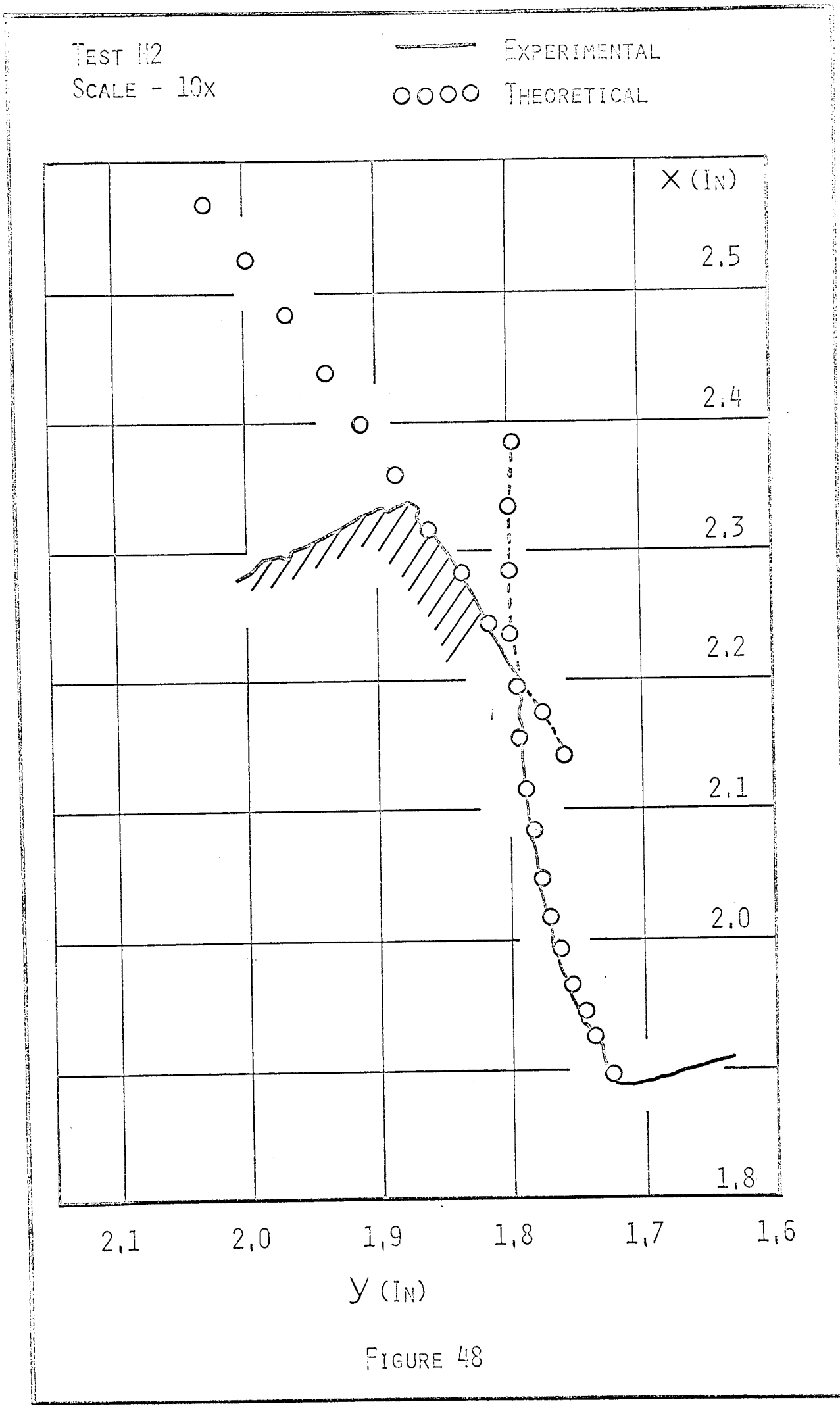
TEST H2
SCALE - 10X
EXPERIMENTAL
THEORETICAL
X (IN)
2.5
2.4
2.3
2.2
2.1
2.0
1.8
2.1
2.0
1.9
1.8
1.7
1.6
Y (IN)

FIGURE 48

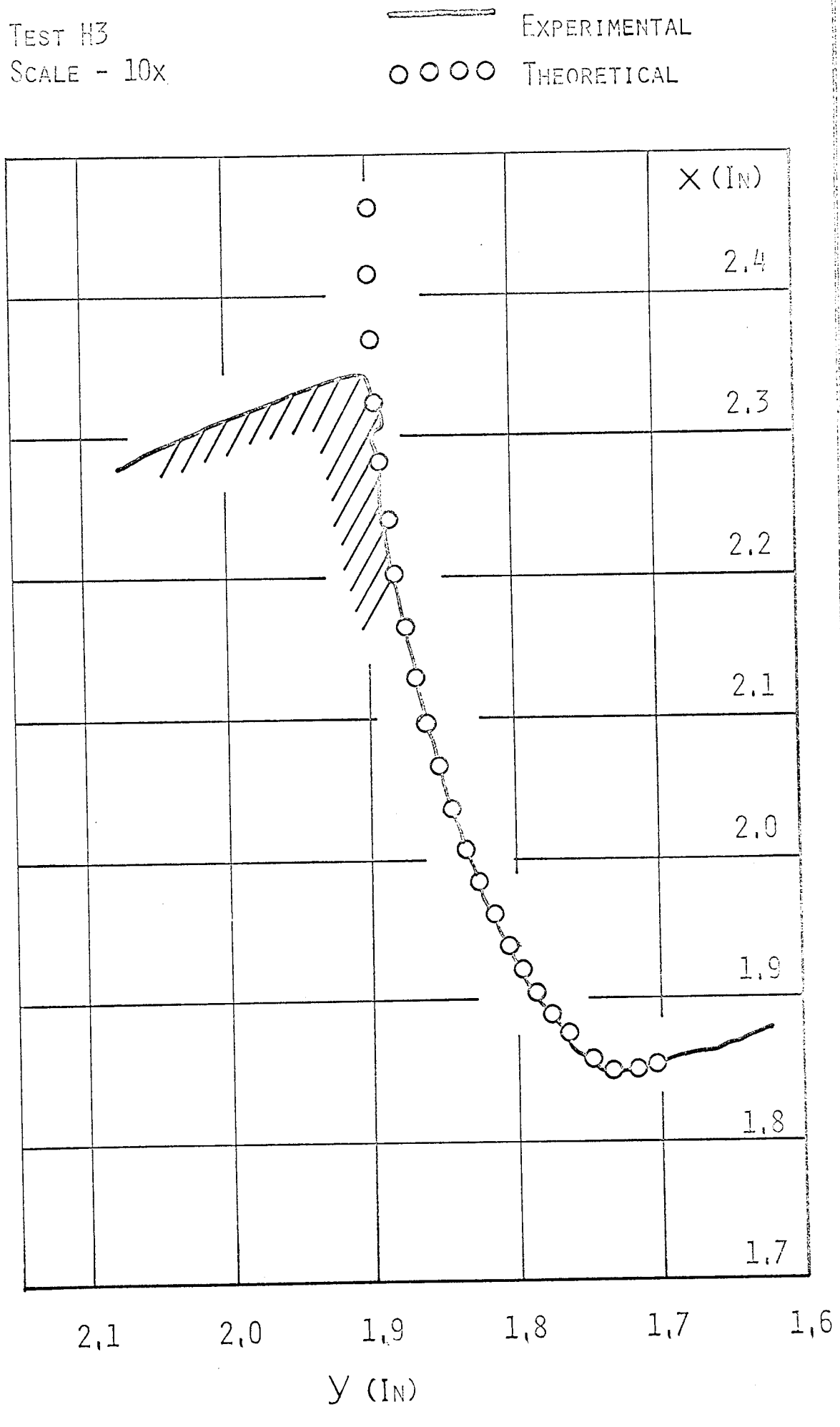
TEST H3
SCALE - 10X
EXPERIMENTAL
THEORETICAL
X (IN)
2.4
2.3
2.2
2.1
2.0
1.9
1.8
1.7
2.1
2.0
1.9
1.8
1.7
1.6
Y (IN)

FIGURE 49

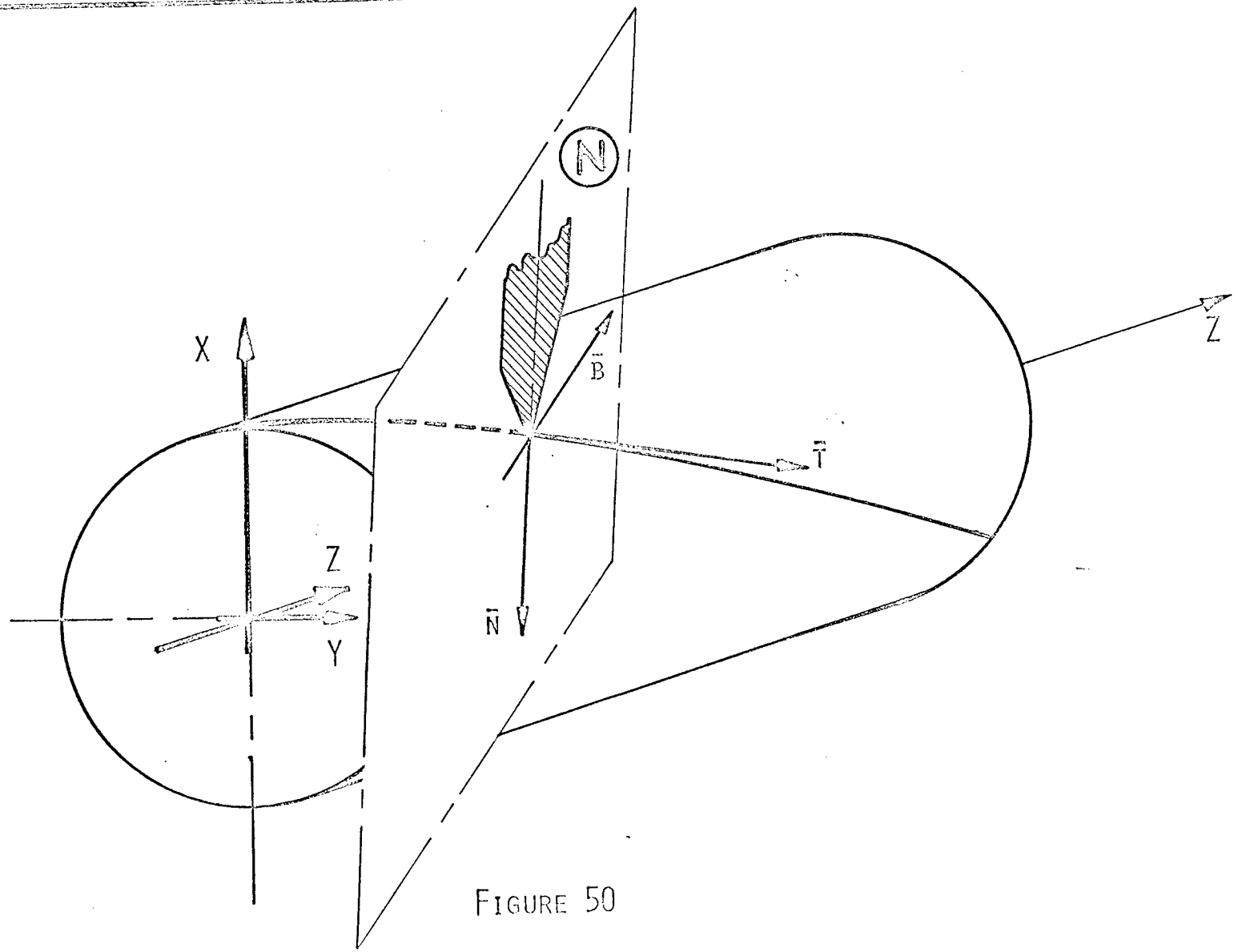


FIGURE 50

TEST B1
SCALE - 10X

EXPERIMENTAL
THEORETICAL

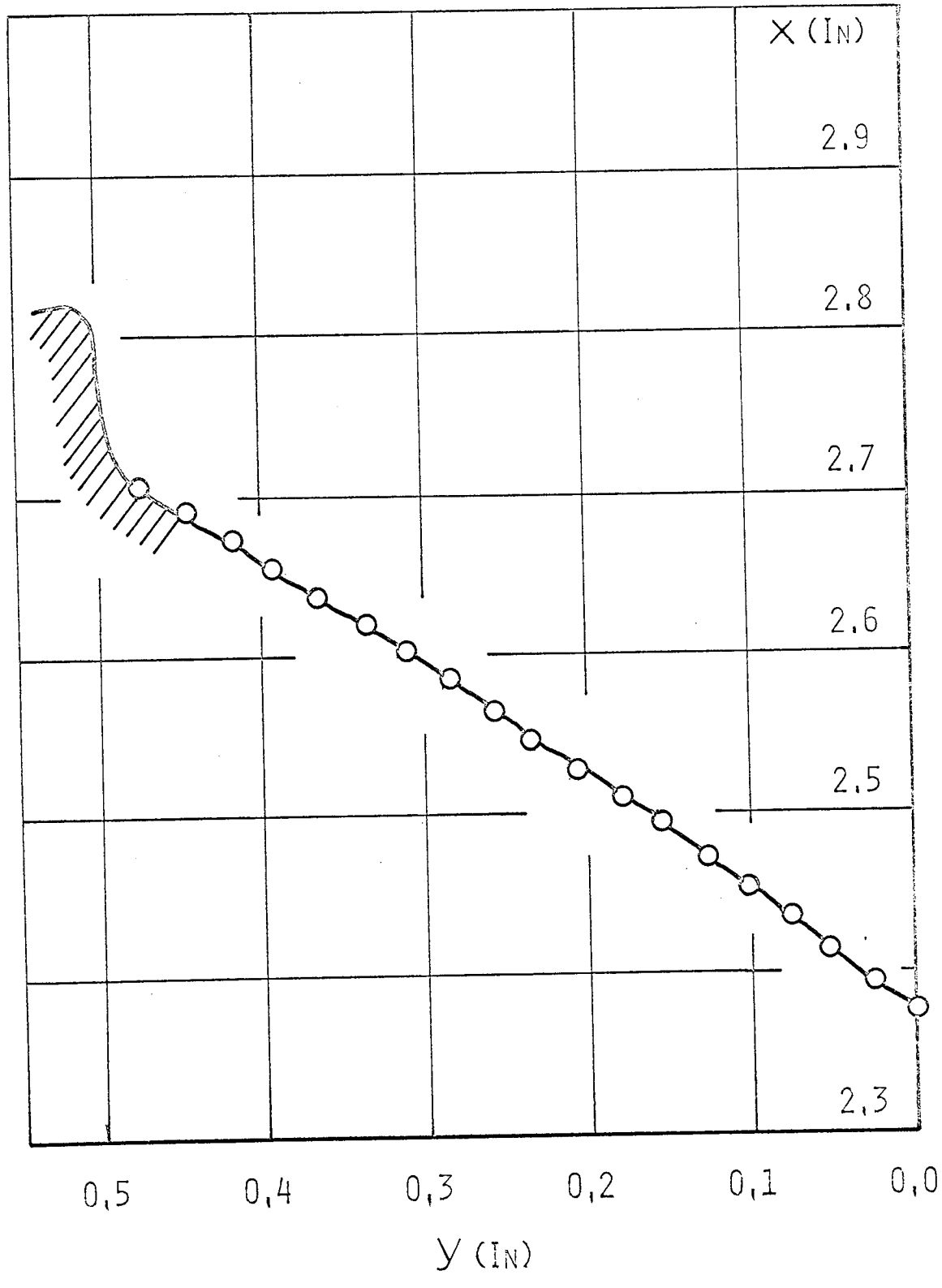


FIGURE 51

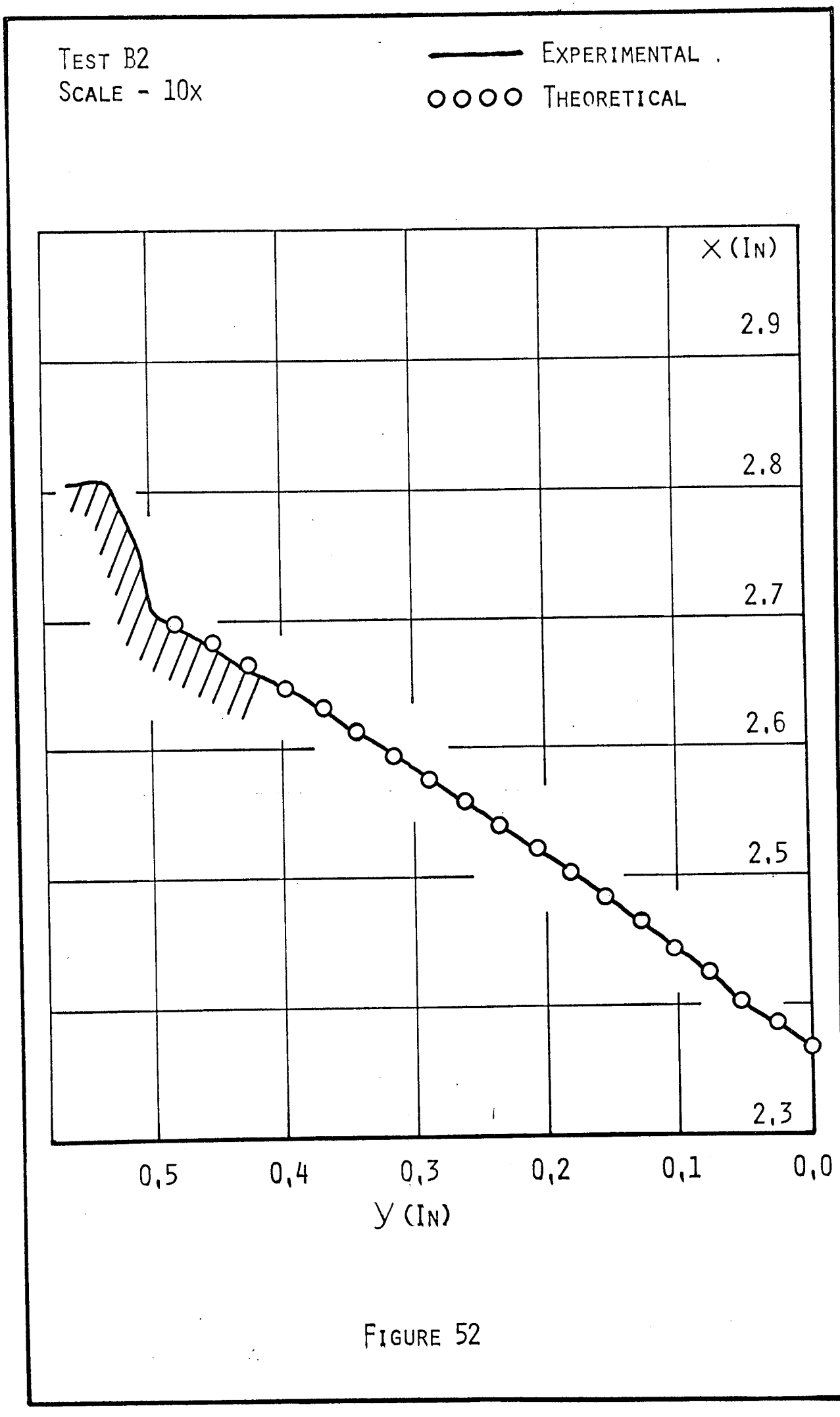
TEST B2
SCALE - 10X
EXPERIMENTAL
THEORETICAL
X (IN)
2.9
2.8
2.7
2.6
2.5
2.3
0,5
0,4
0,3
0,2
0,1
0,0
Y (IN)

FIGURE 52

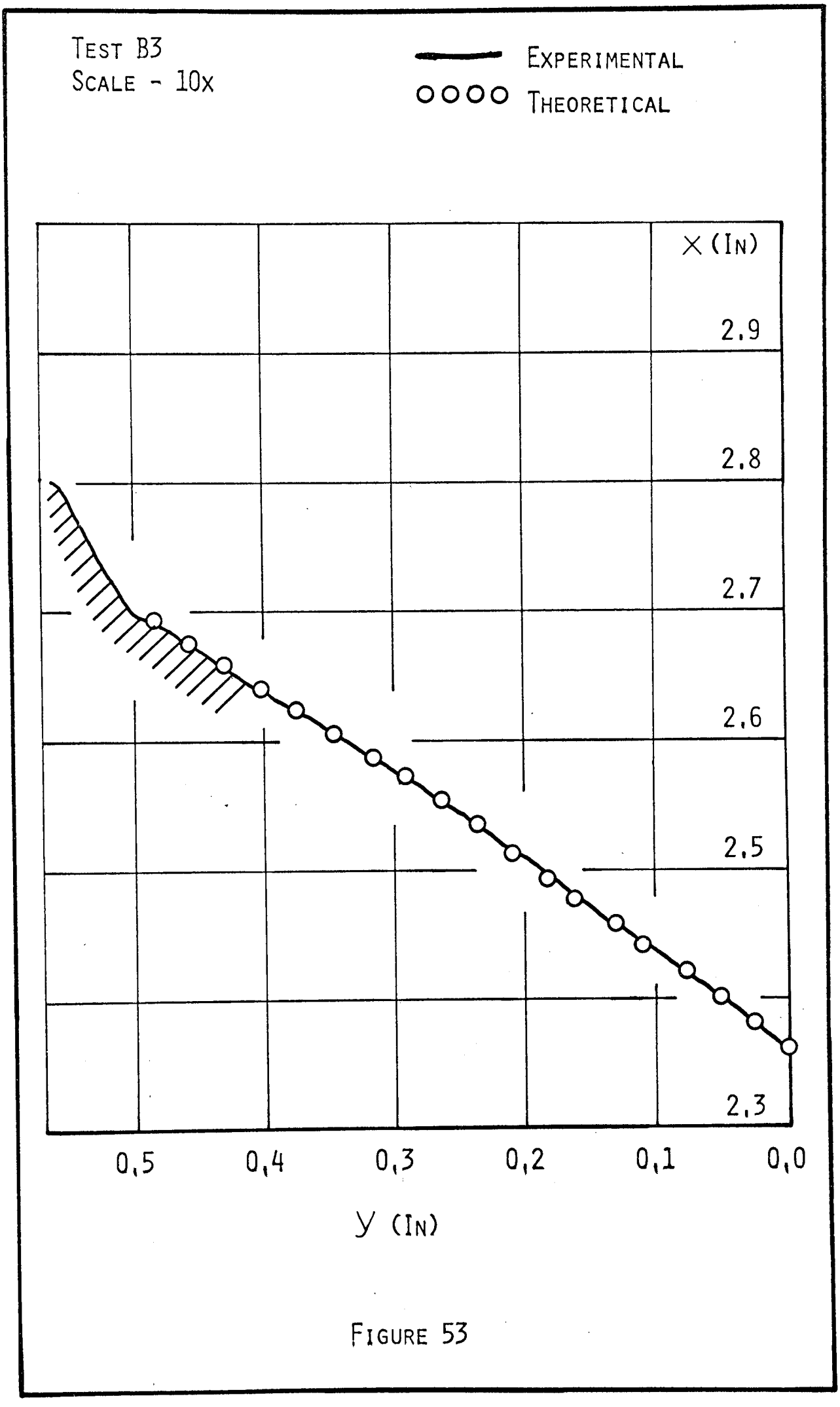
TEST B3
SCALE - 10X
EXPERIMENTAL
THEORETICAL
X (IN)
2.9
2.8
2.7
2.6
2.5
2.3
0.5
0.4
0.3
0.2
0.1
0.0
Y (IN)

FIGURE 53

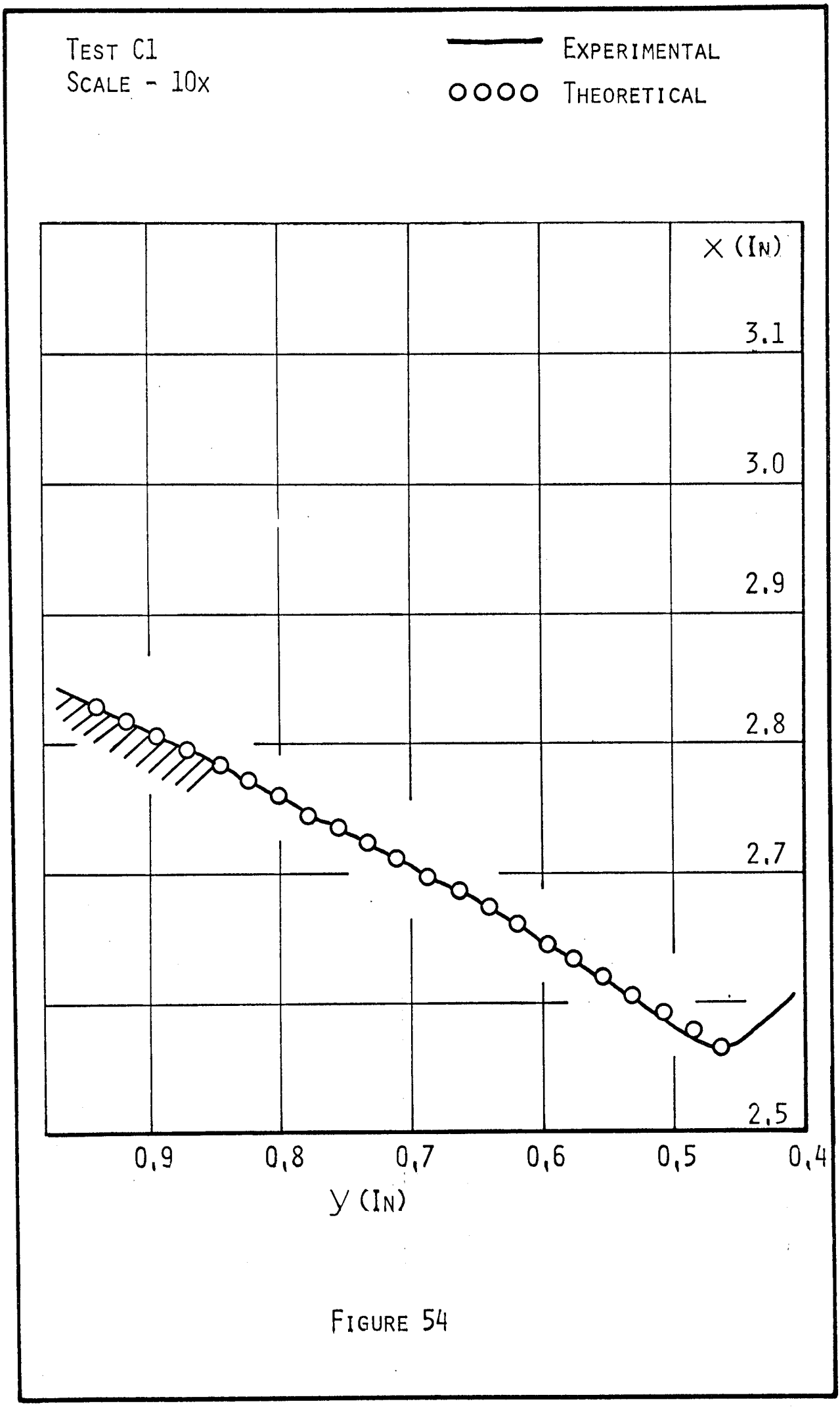
TEST C1
SCALE - 10X
EXPERIMENTAL
THEORETICAL
X (IN)
3.1
3.0
2.9
2.8
2.7
2.5
0,9
0,8
0,7
0,6
0,5
0,4
Y (IN)

FIGURE 54

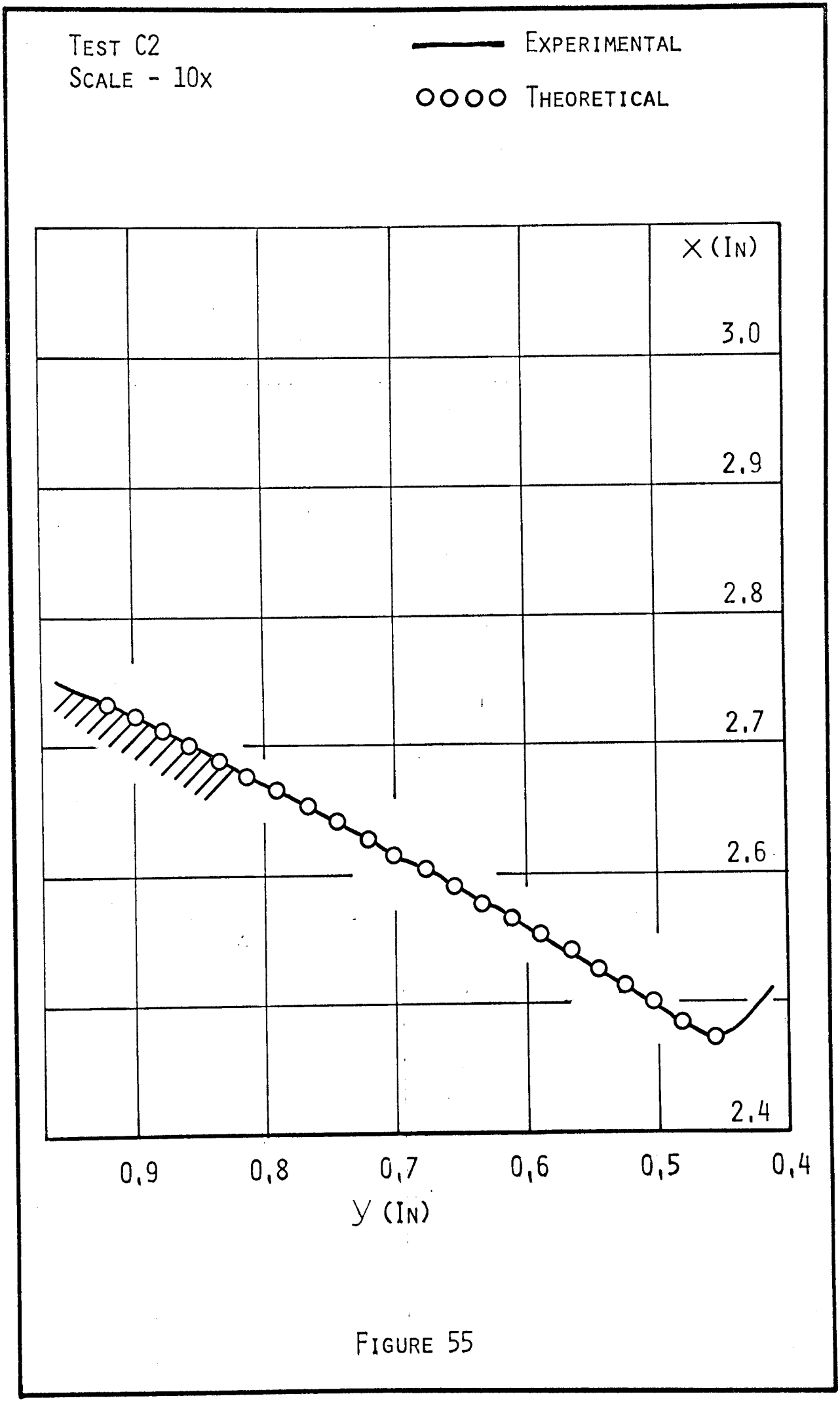
TEST C2
SCALE - 10X
EXPERIMENTAL
THEORETICAL
X (IN)
3.0
2.9
2.8
2.7
2.6
2.4
0,9
0,8
0,7
0,6
0,5
0,4
Y (IN)

FIGURE 55

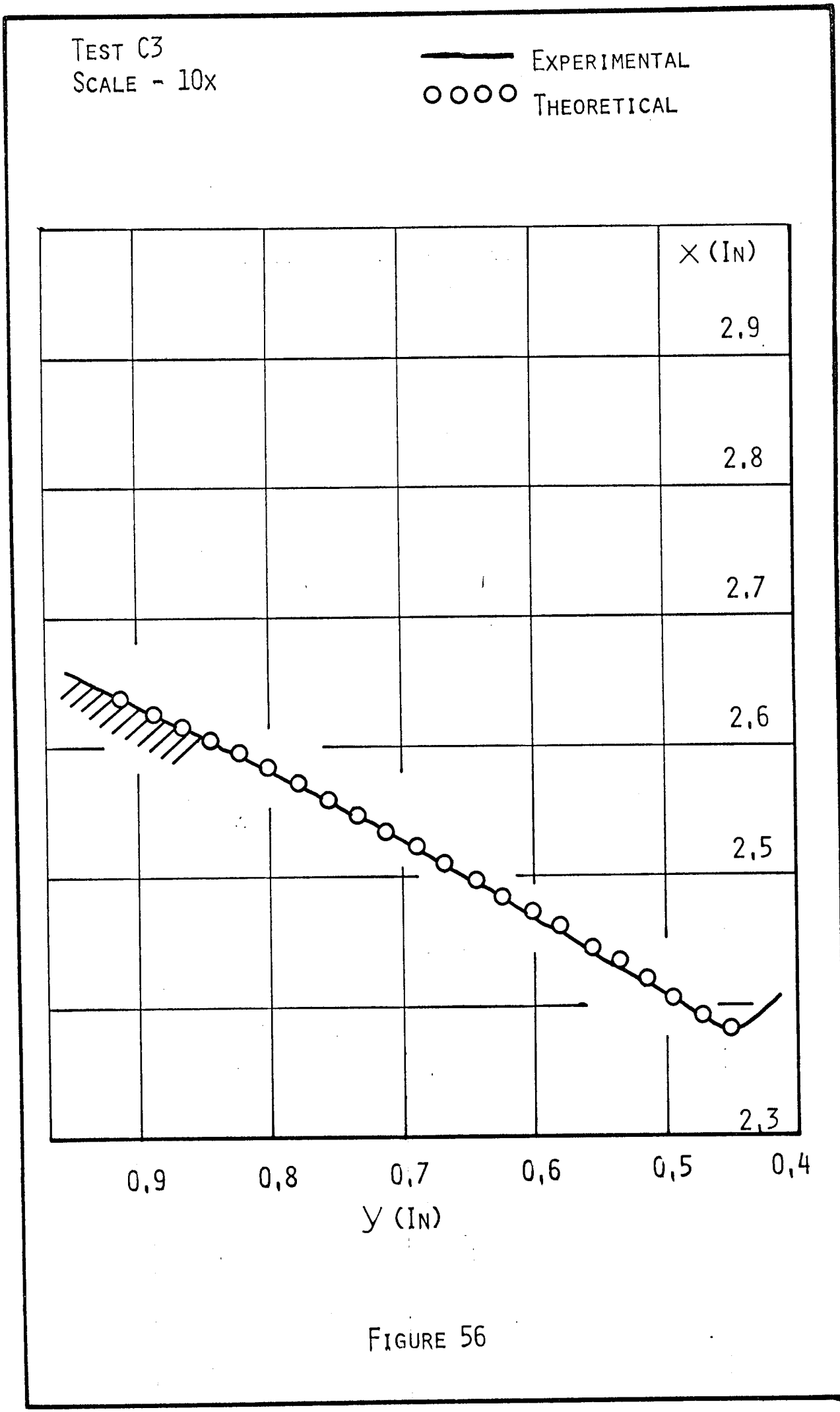
TEST C3
SCALE - 10X
EXPERIMENTAL
THEORETICAL
X (IN)
2.9
2.8
2.7
2.6
2.5
2.3
0.9
0.8
0.7
0.6
0.5
0.4
Y (IN)

FIGURE 56

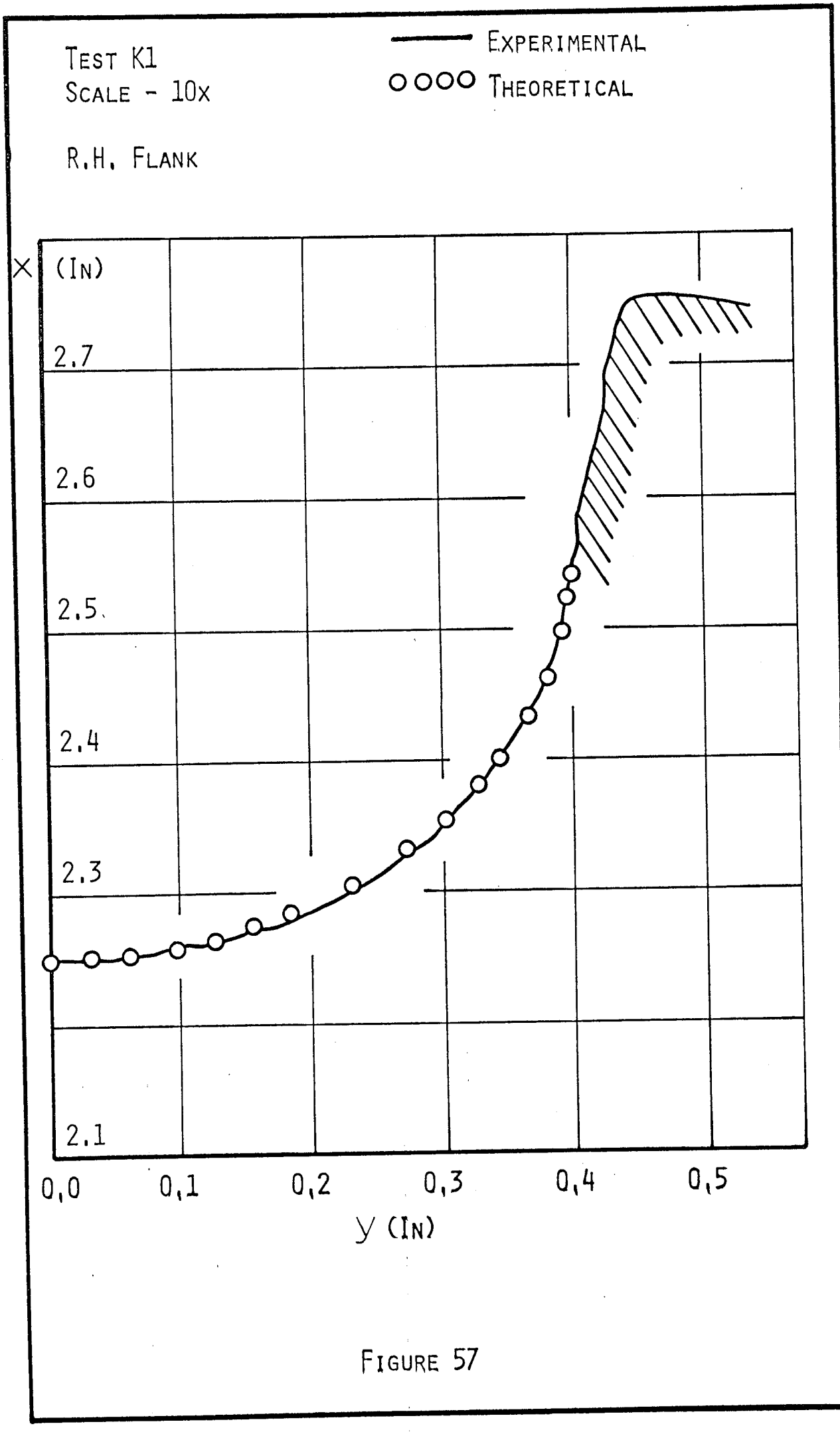
TEST K1
SCALE - 10X
R.H. FLANK
EXPERIMENTAL
THEORETICAL
X (IN)
2.7
2.6
2.5
2.4
2.3
2.1
0,0
0,1
0,2
0,3
0,4
0,5
Y (IN)

FIGURE 57

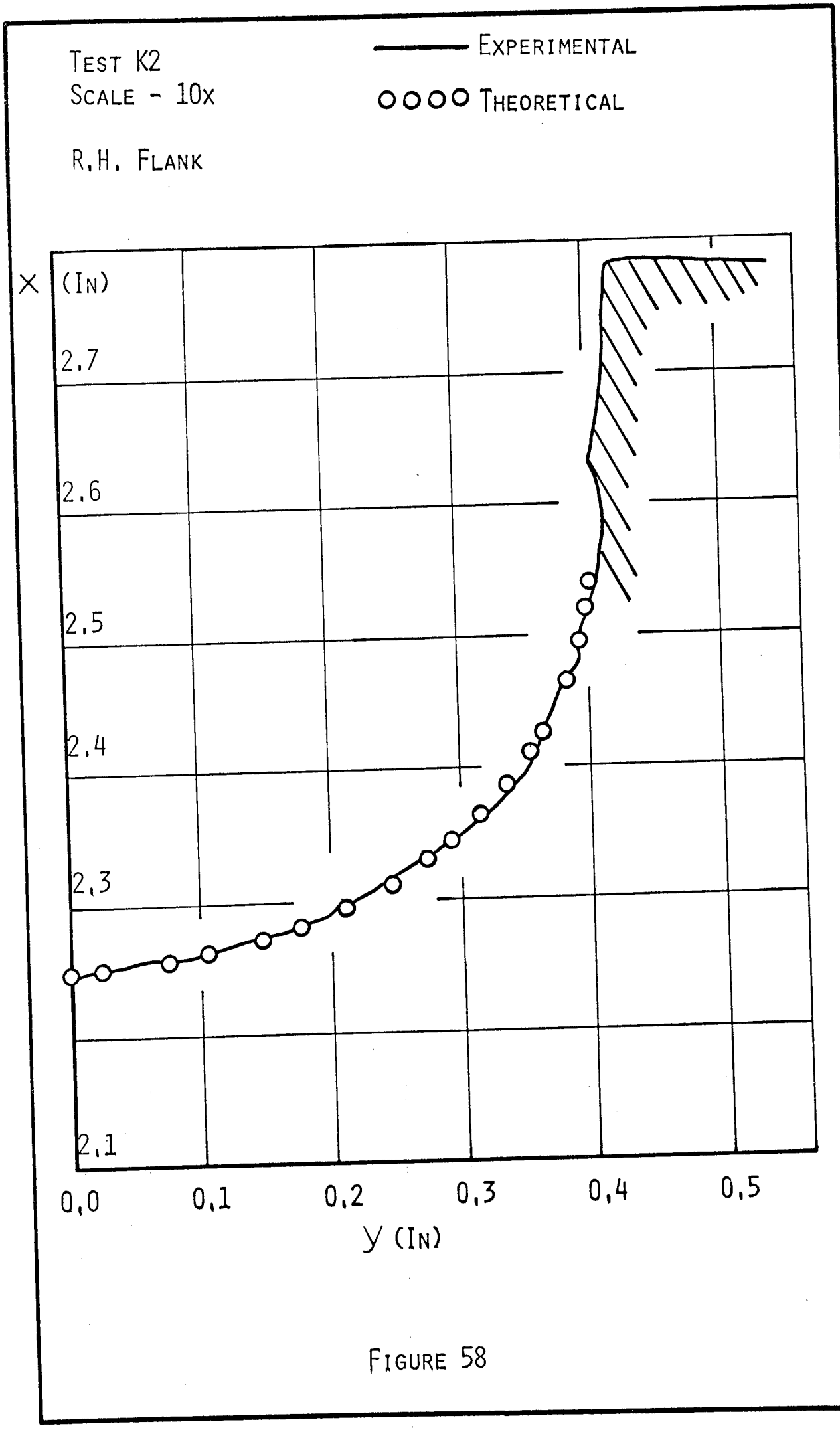
TEST K2
SCALE - 10X
R.H. FLANK
EXPERIMENTAL
THEORETICAL
X (IN)
2.7
2.6
2.5
2.4
2.3
2.1
0.0
0.1
0.2
0.3
0.4
0.5
Y (IN)

FIGURE 58

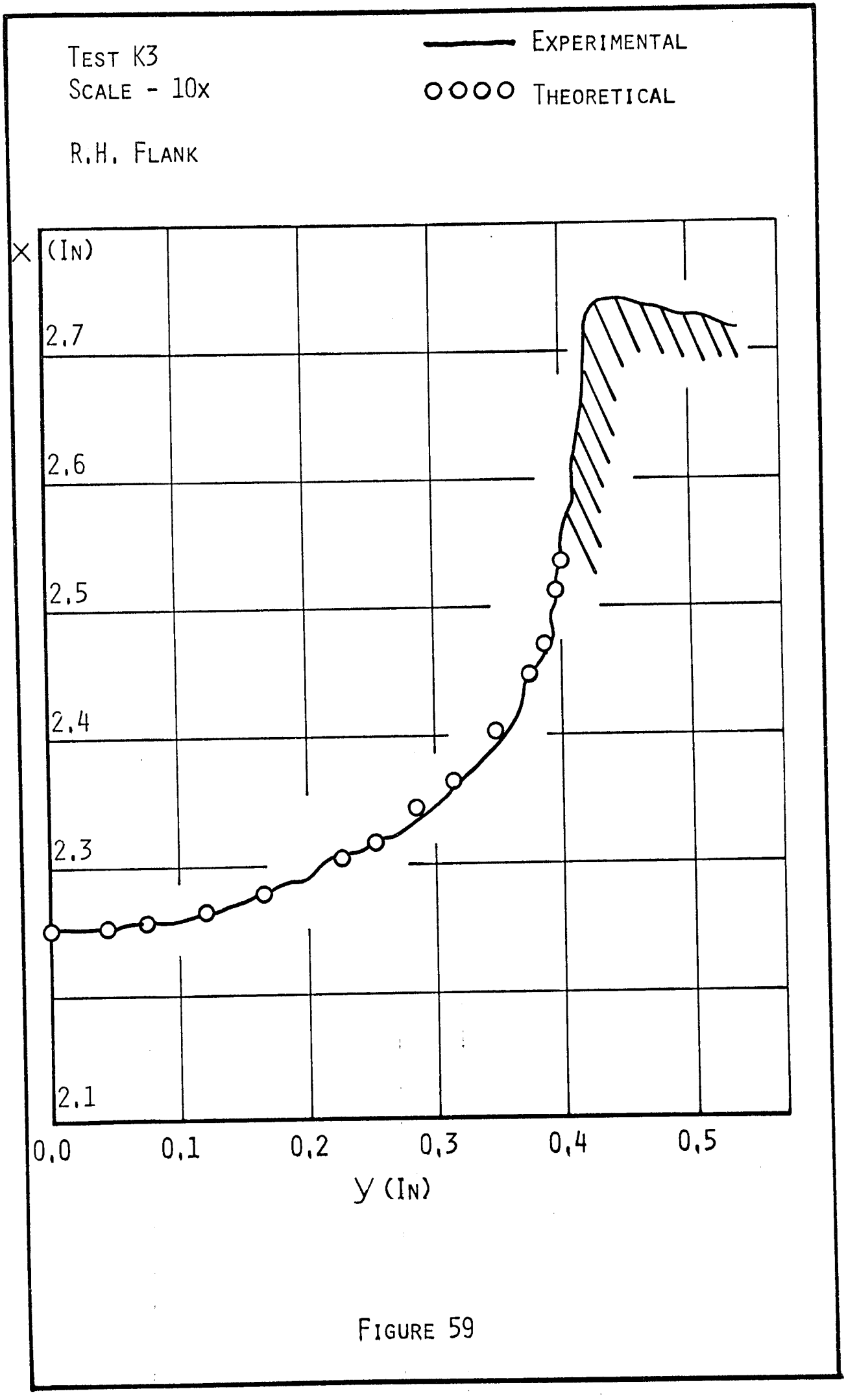
TEST K3
SCALE - 10X
R.H. FLANK
EXPERIMENTAL
THEORETICAL
X (IN)
2.7
2.6
2.5
2.4
2.3
2.1
0.0
0.1
0.2
0.3
0.4
0.5
Y (IN)

FIGURE 59

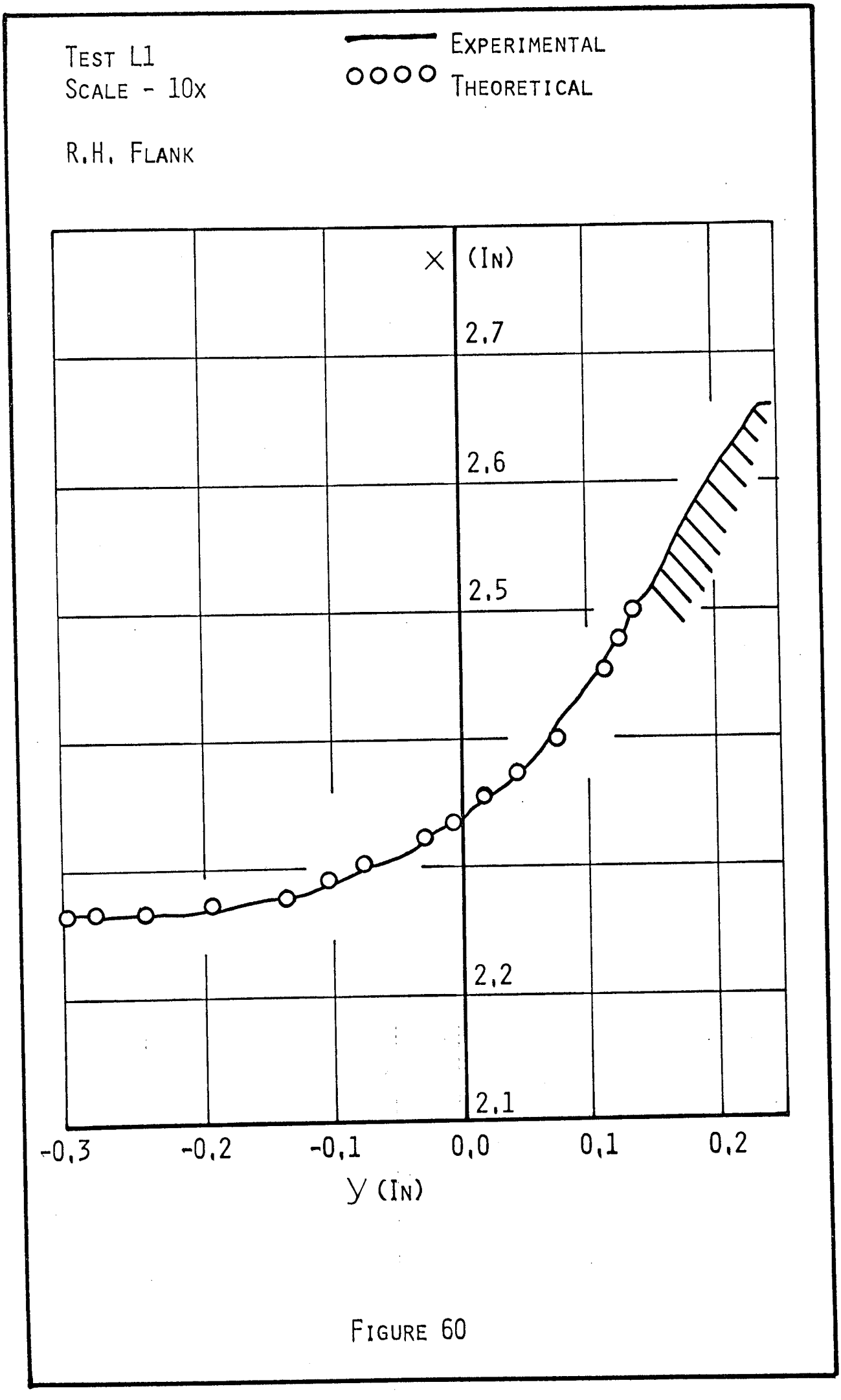
TEST L1
SCALE - 10X
R.H. FLANK
EXPERIMENTAL
THEORETICAL
X (IN)
2.7
2.6
2.5
2.2
2.1
-0.3
-0.2
-0.1
0.0
0.1
0.2
Y (IN)

FIGURE 60

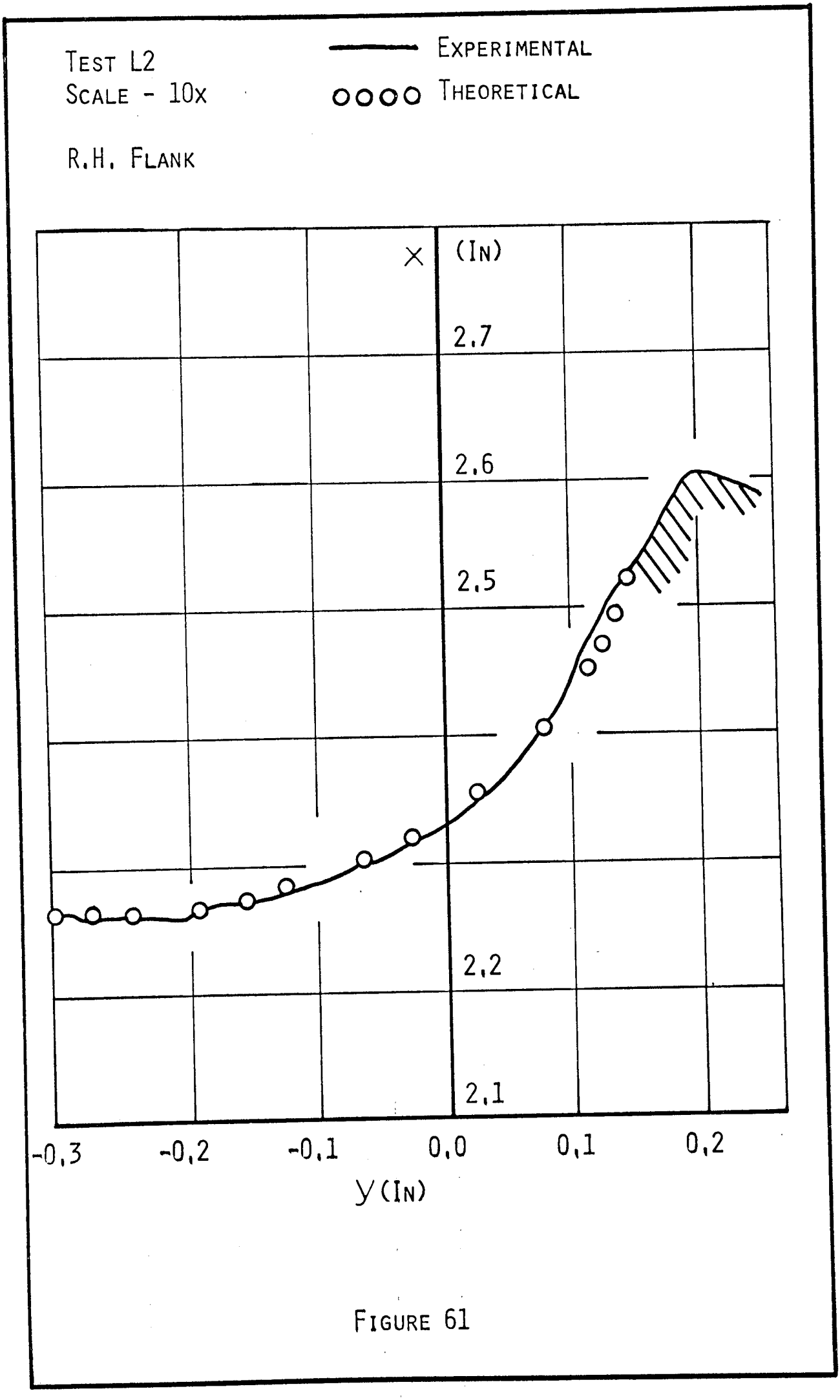
TEST L2
SCALE - 10X
EXPERIMENTAL
THEORETICAL
R.H. FLANK
X (IN)
2.7
2.6
2.5
2.2
2.1
-0.3
-0.2
-0.1
0.0
0.1
0.2
Y (IN)

FIGURE 61

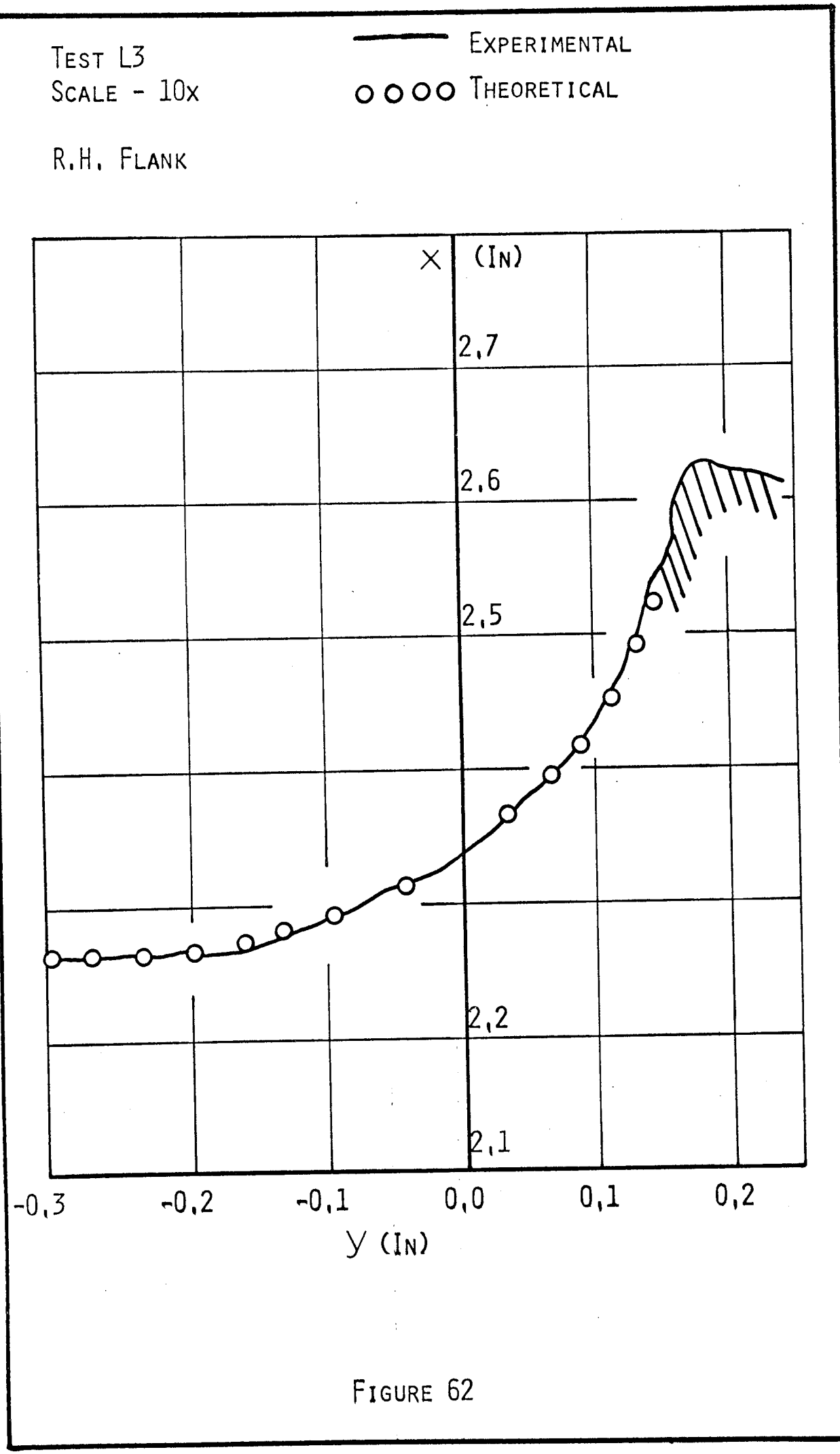
TEST L3
SCALE - 10X
R.H. FLANK
EXPERIMENTAL
THEORETICAL
X (IN)
2,7
2,6
2,5
2,2
2,1
-0,3
-0,2
-0,1
0,0
0,1
0,2
Y (IN)

FIGURE 62

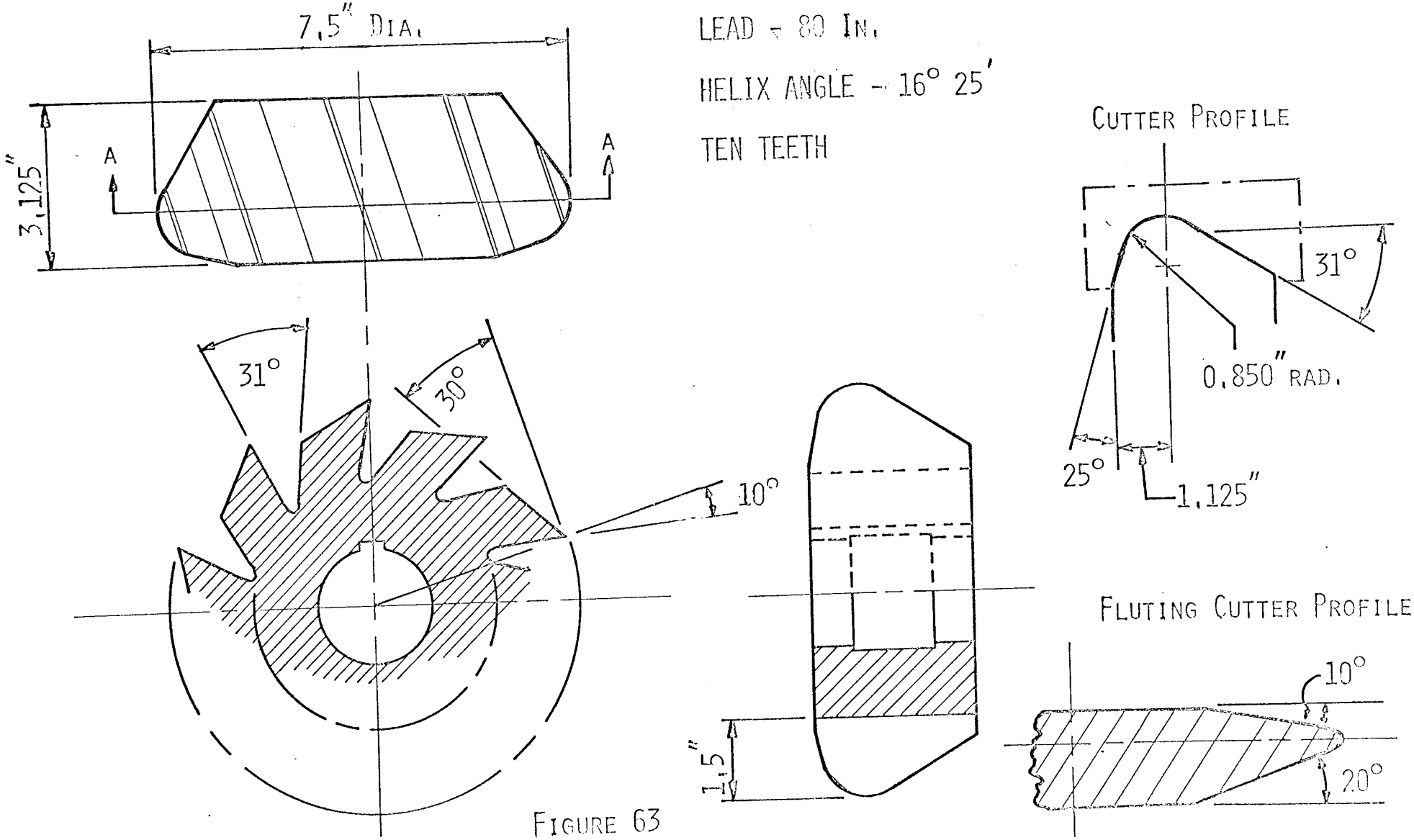
7.5" DIA.
LEAD = 80 IN.
HELIX ANGLE = 16° 25'
TEN TEETH
3.125"
A
A
CUTTER PROFILE
31°
0.850" RAD.
25°
1.125"
31°
30°
10°
1.5"
FLUTING CUTTER PROFILE
10°
20°

FIGURE 63

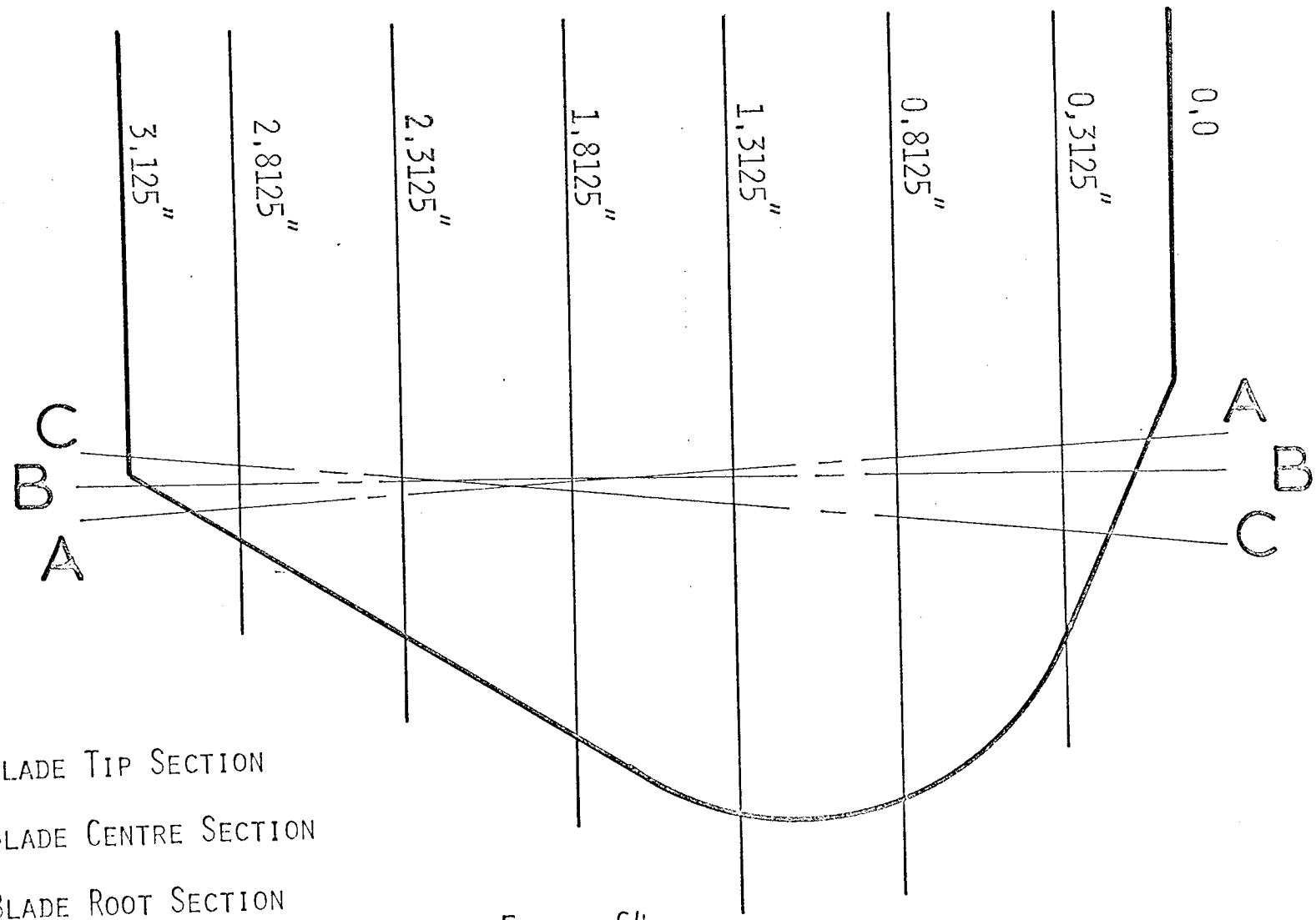


AA - Blade Tip Section

BB - Blade Centre Section

CC - Blade Root Section

Figure 64

(After Scott)

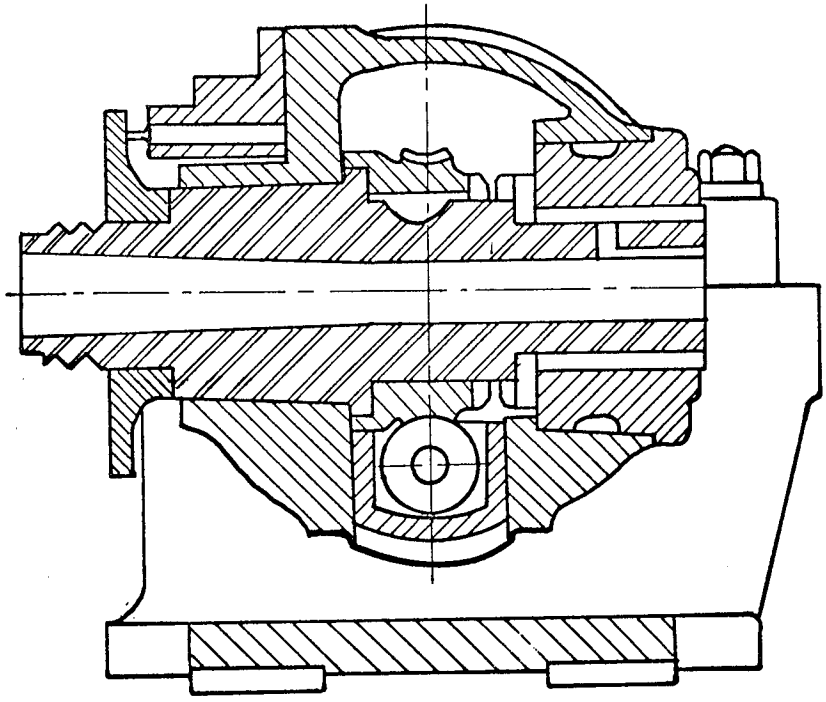

SECTIONAL VIEW

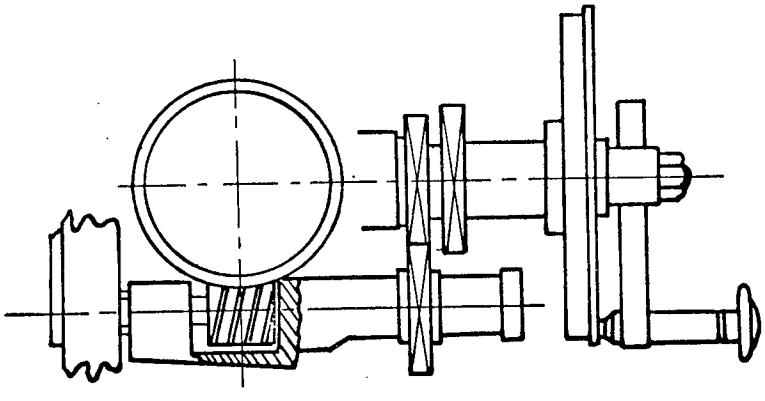

INDEX MECHANISM

FIGURE 65

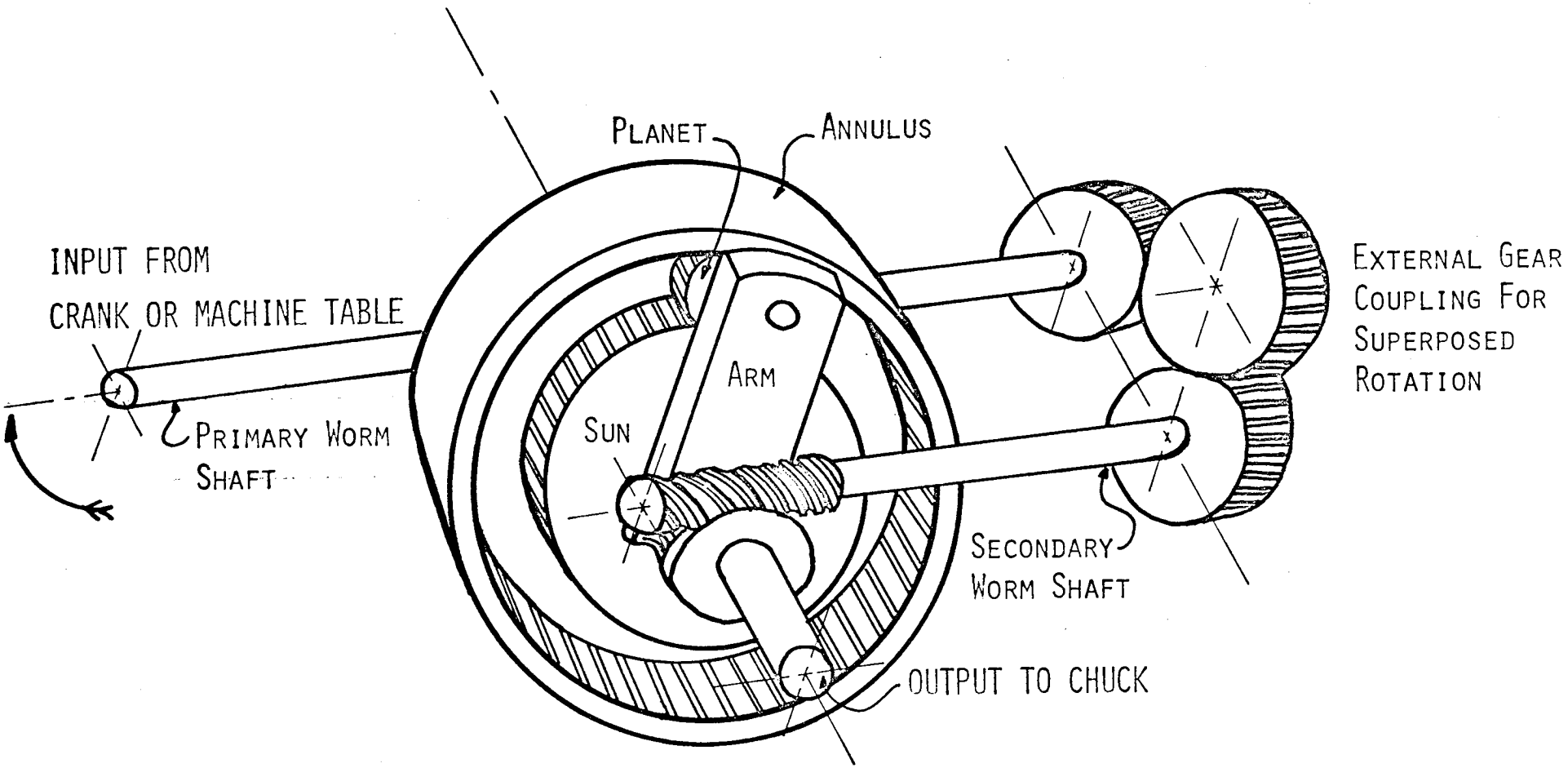
PLANET
ANNULUS
INPUT FROM
CRANK OR MACHINE TABLE
ARM
SUN
PRIMARY WORM
SHAFT
EXTERNAL GEAR
COUPLING FOR
SUPERPOSED
ROTATION
SECONDARY
WORM SHAFT
OUTPUT TO CHUCK

FIGURE 66

PROTOTYPE DIVIDING HEAD - SECTIONAL VIEW.

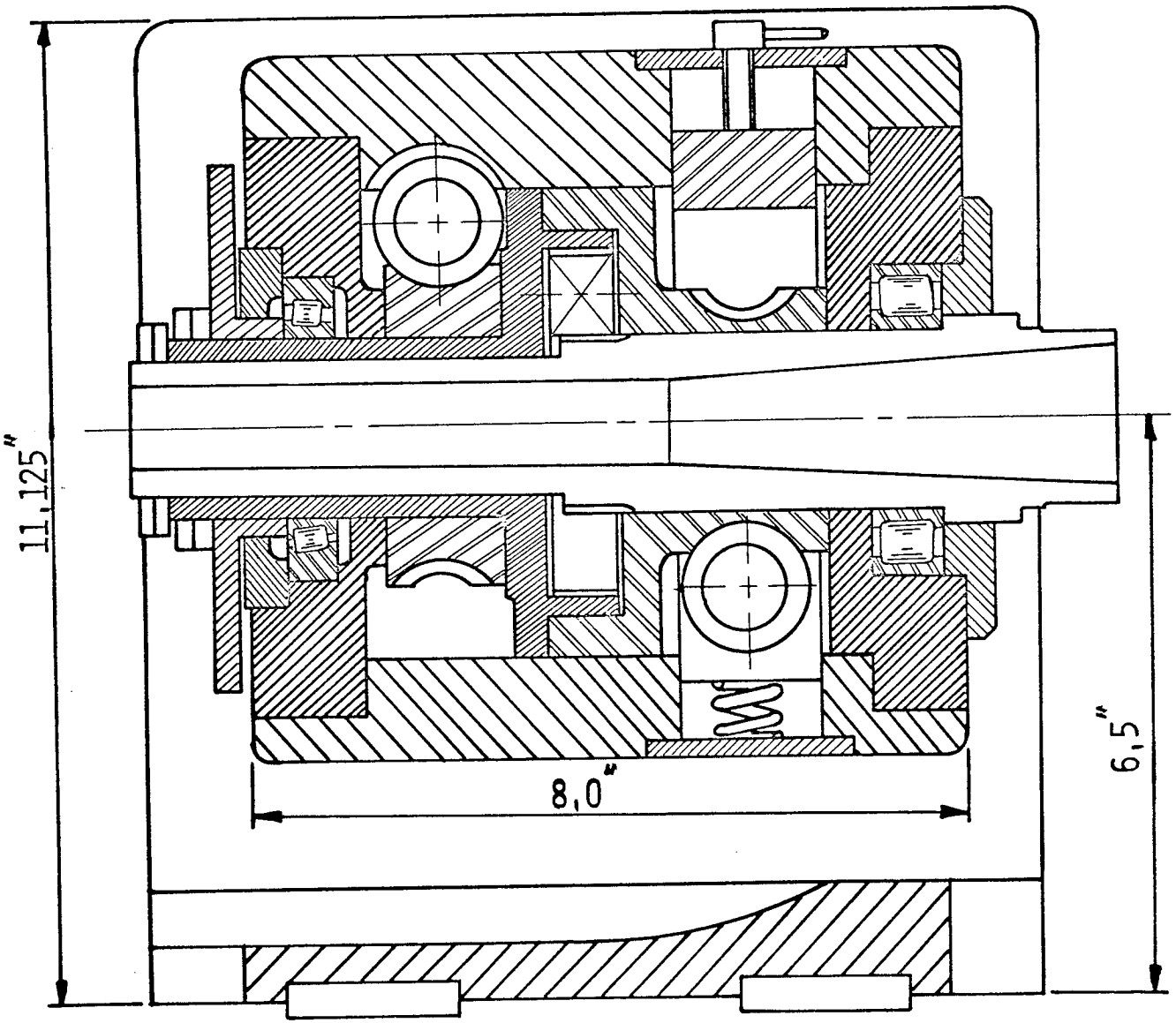


FIGURE 67

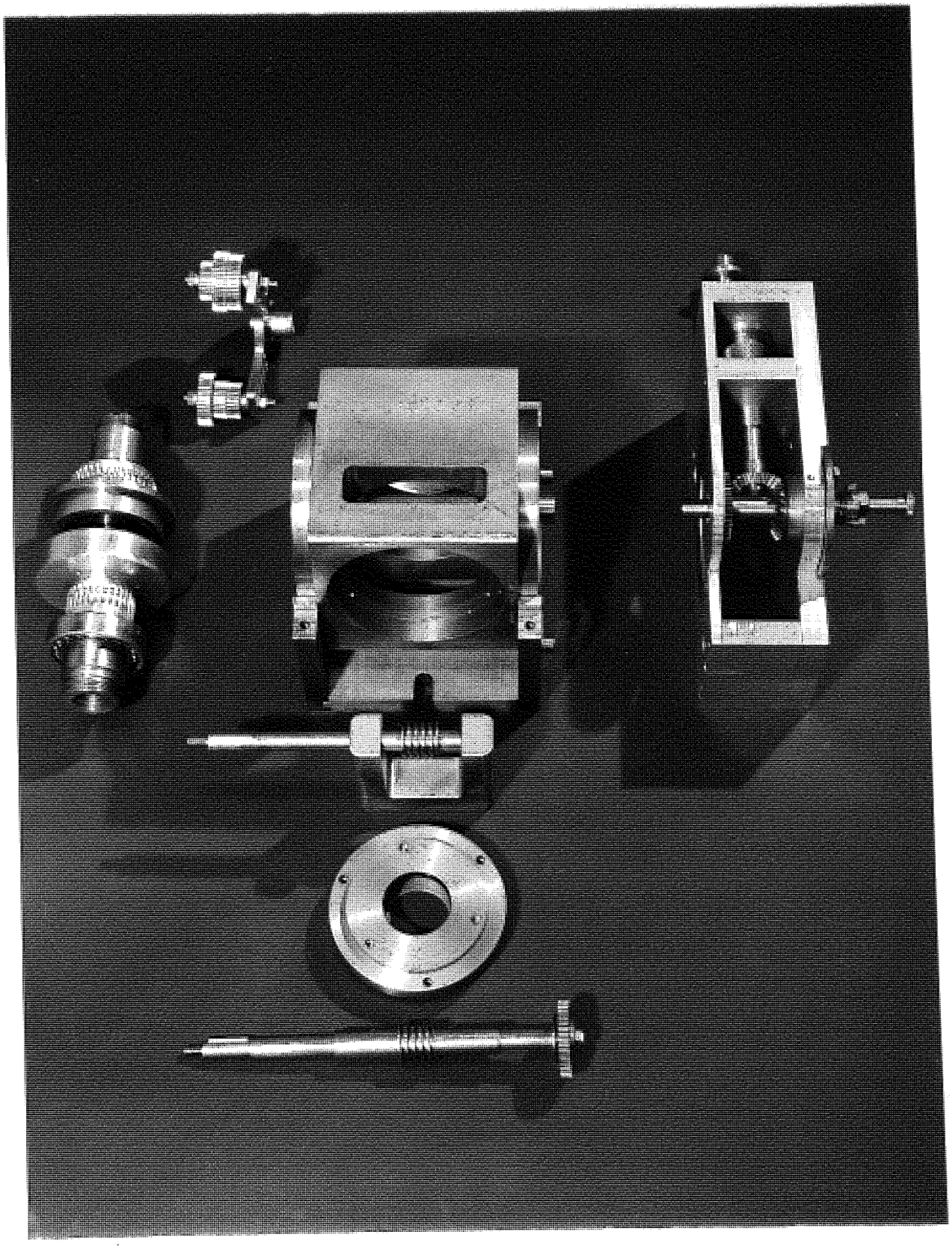

Plate vii

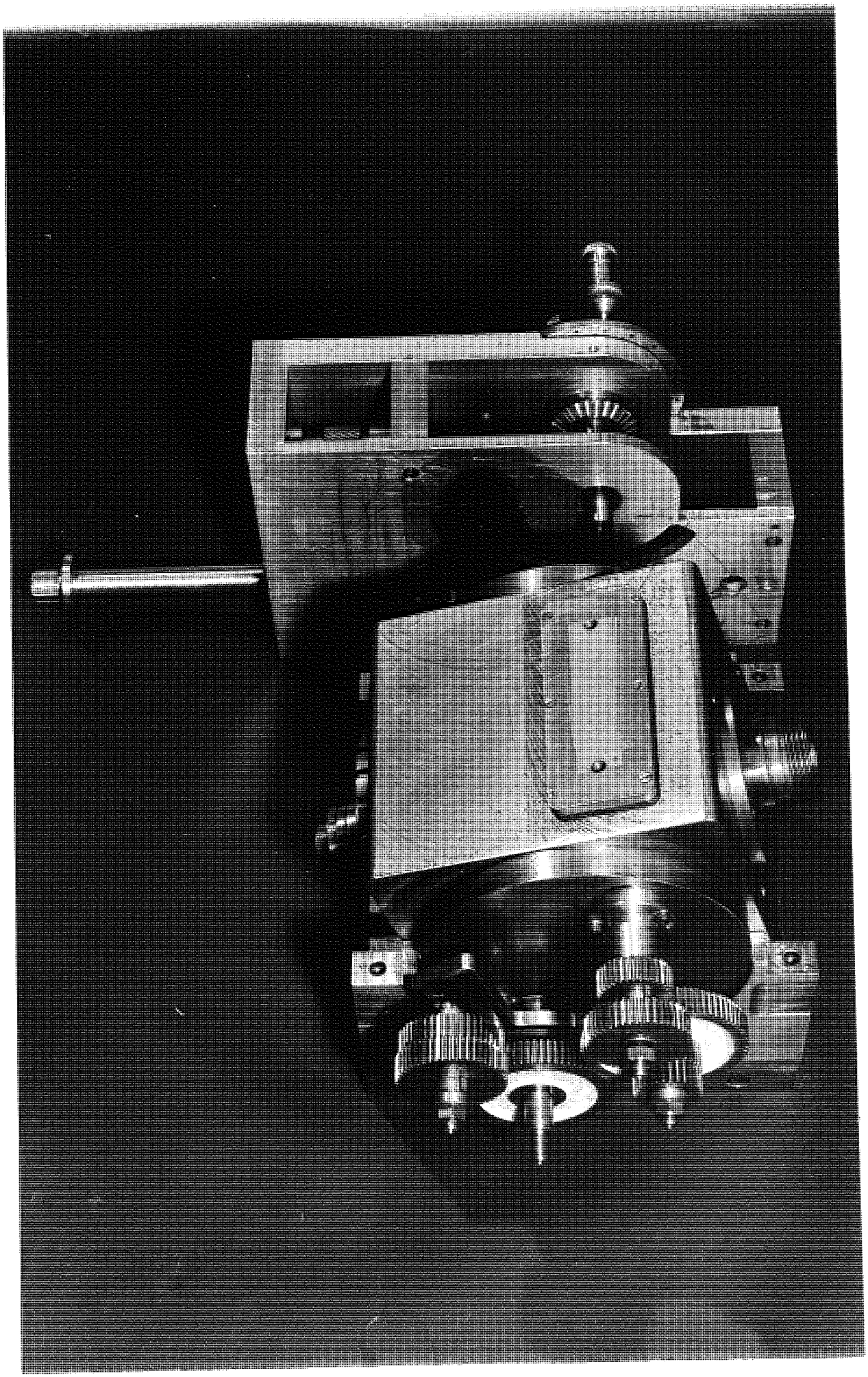

Plate viii

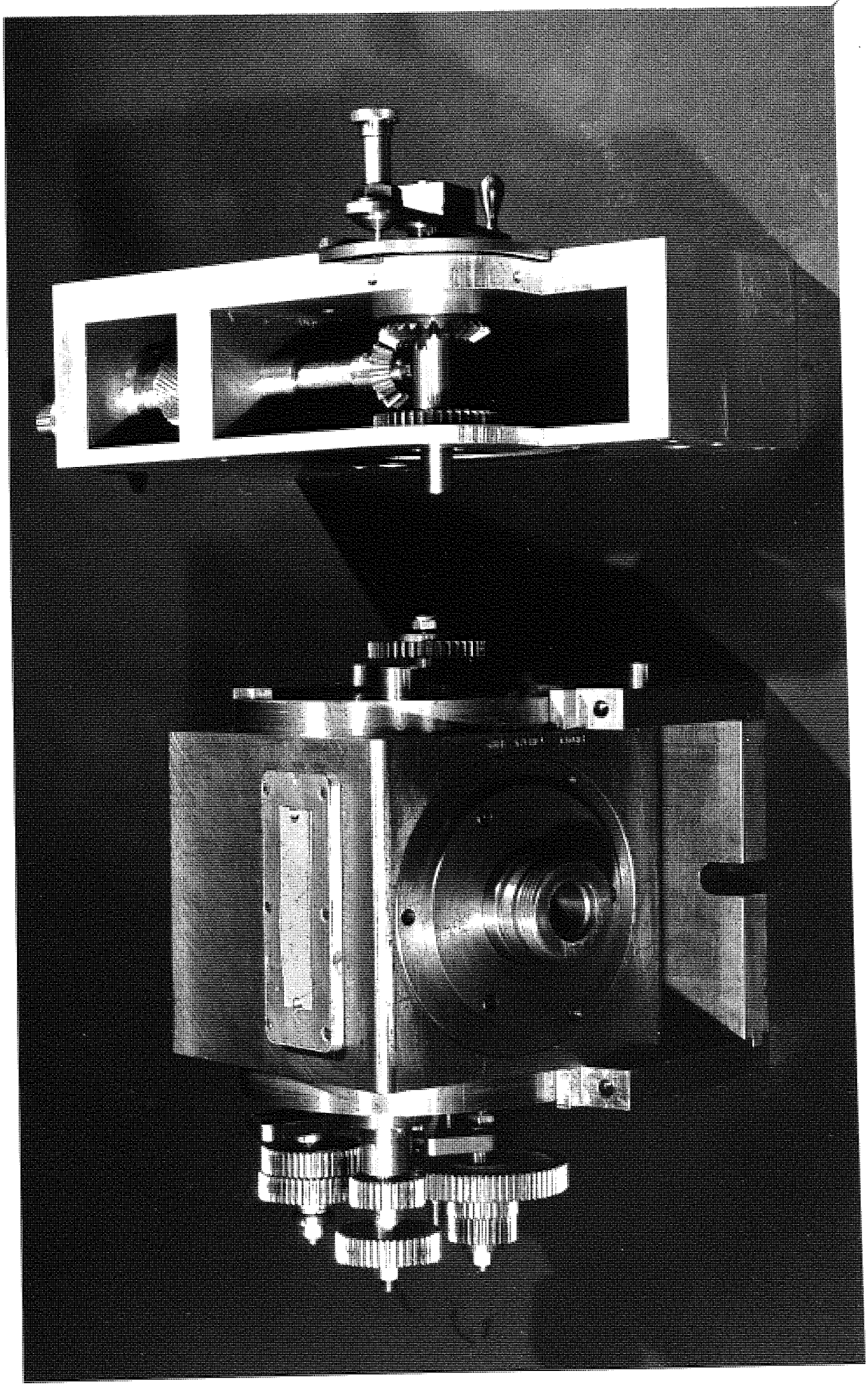

plate ix

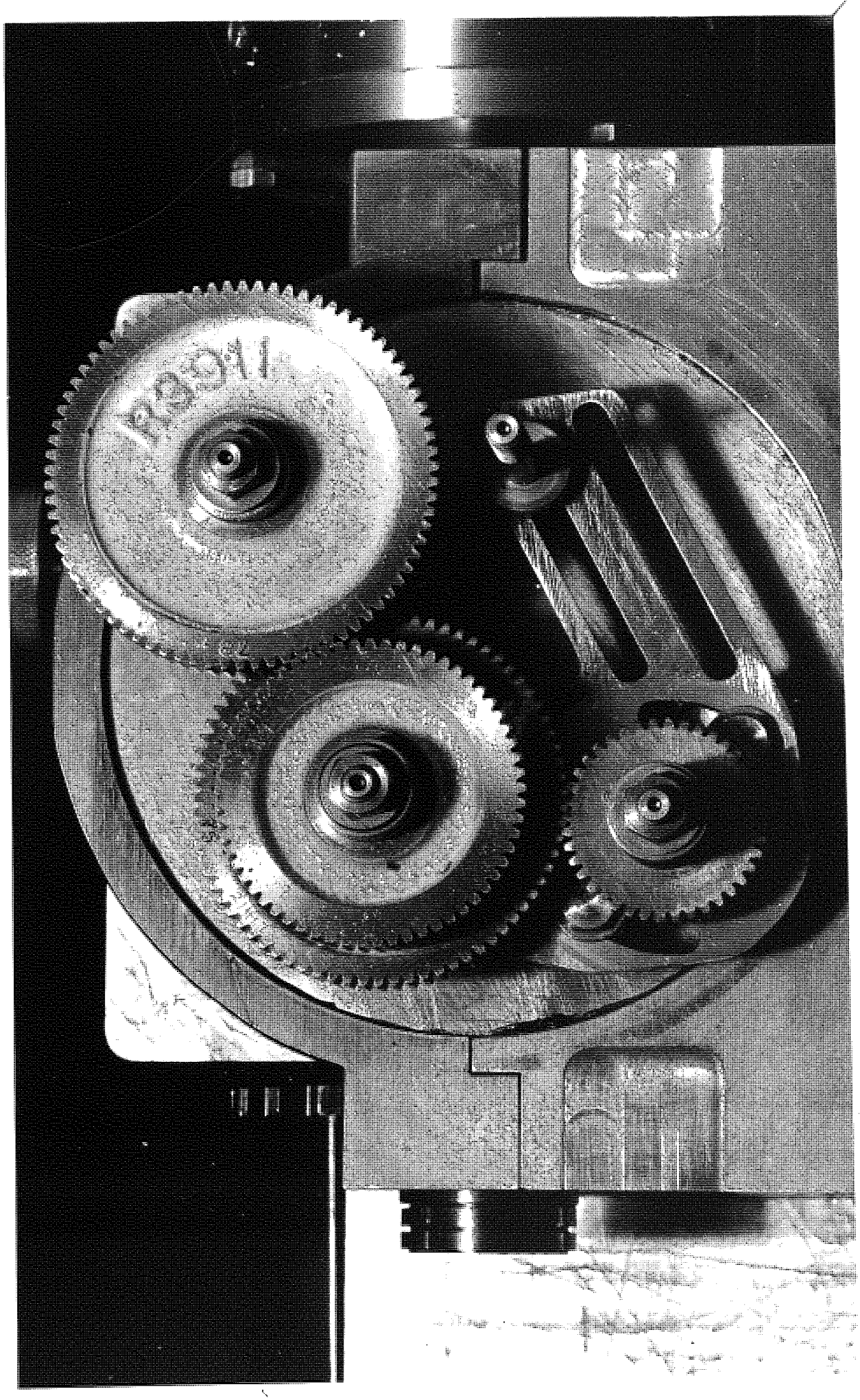

Plate x

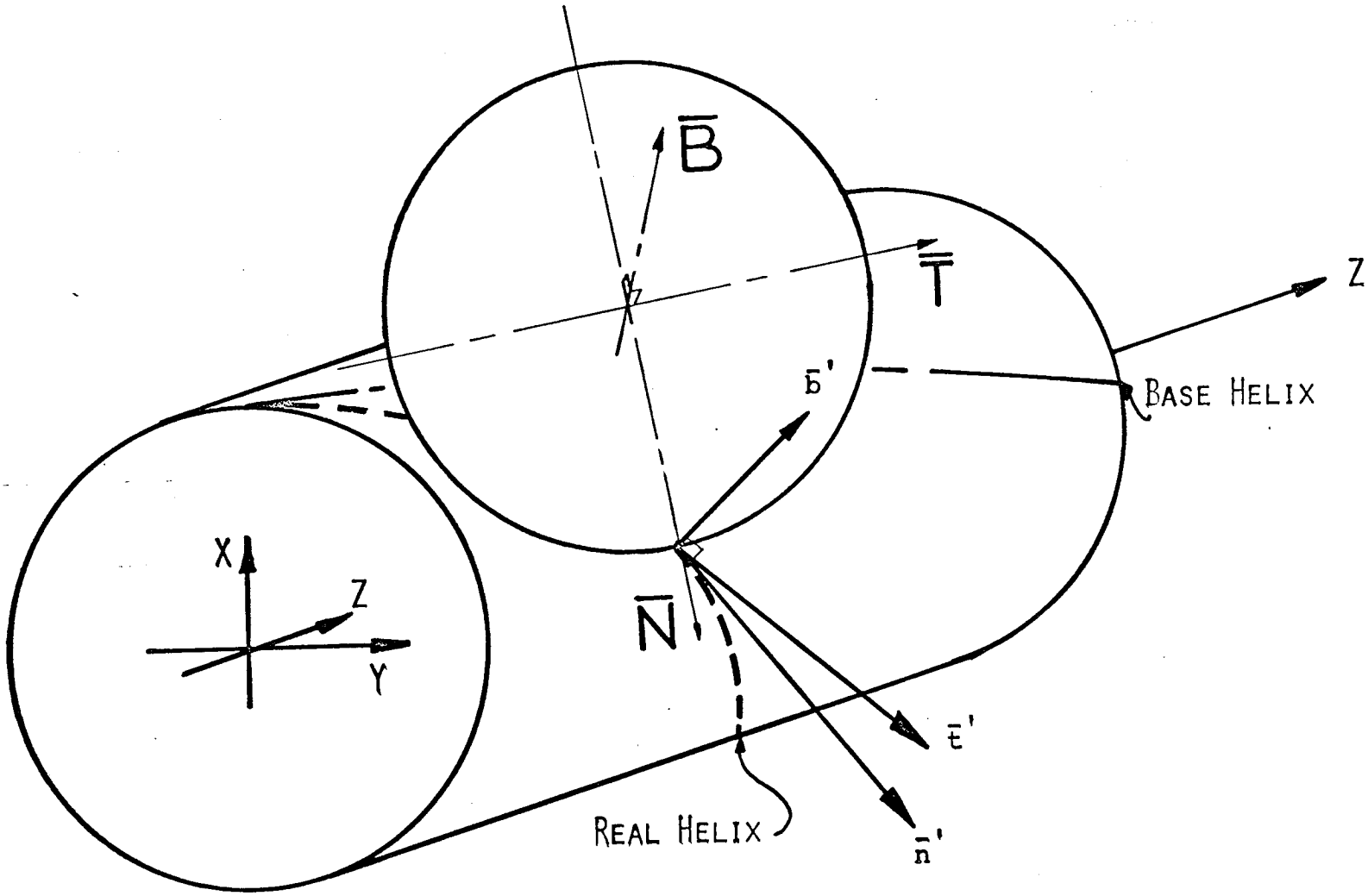


FIGURE 68

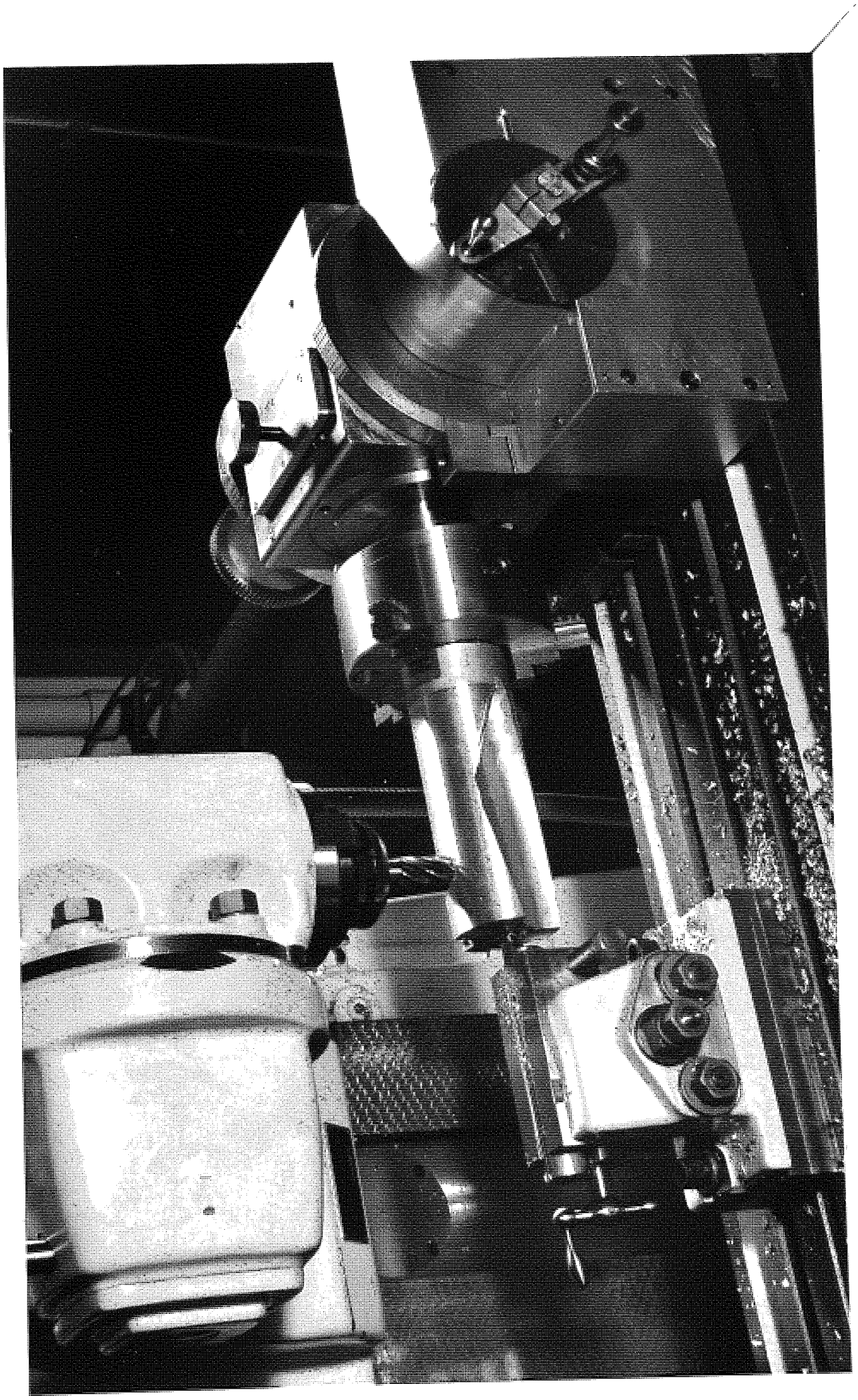

plate xi

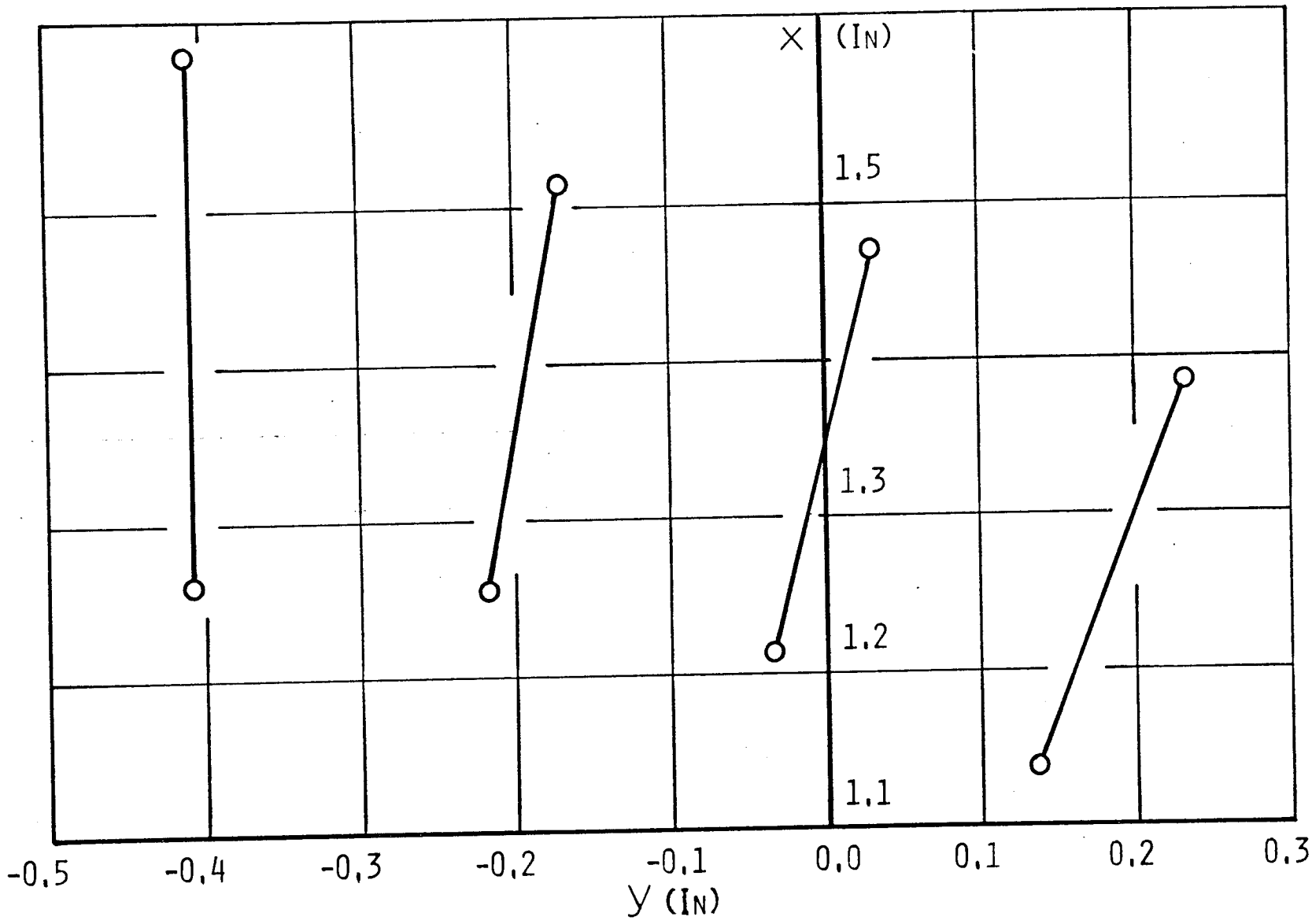


TEST VL1E
SCALE - 10X

SHORTENING LEAD

FIGURE 69

TEST VL2E
SCALE - 10X

LENGTHENING LEAD

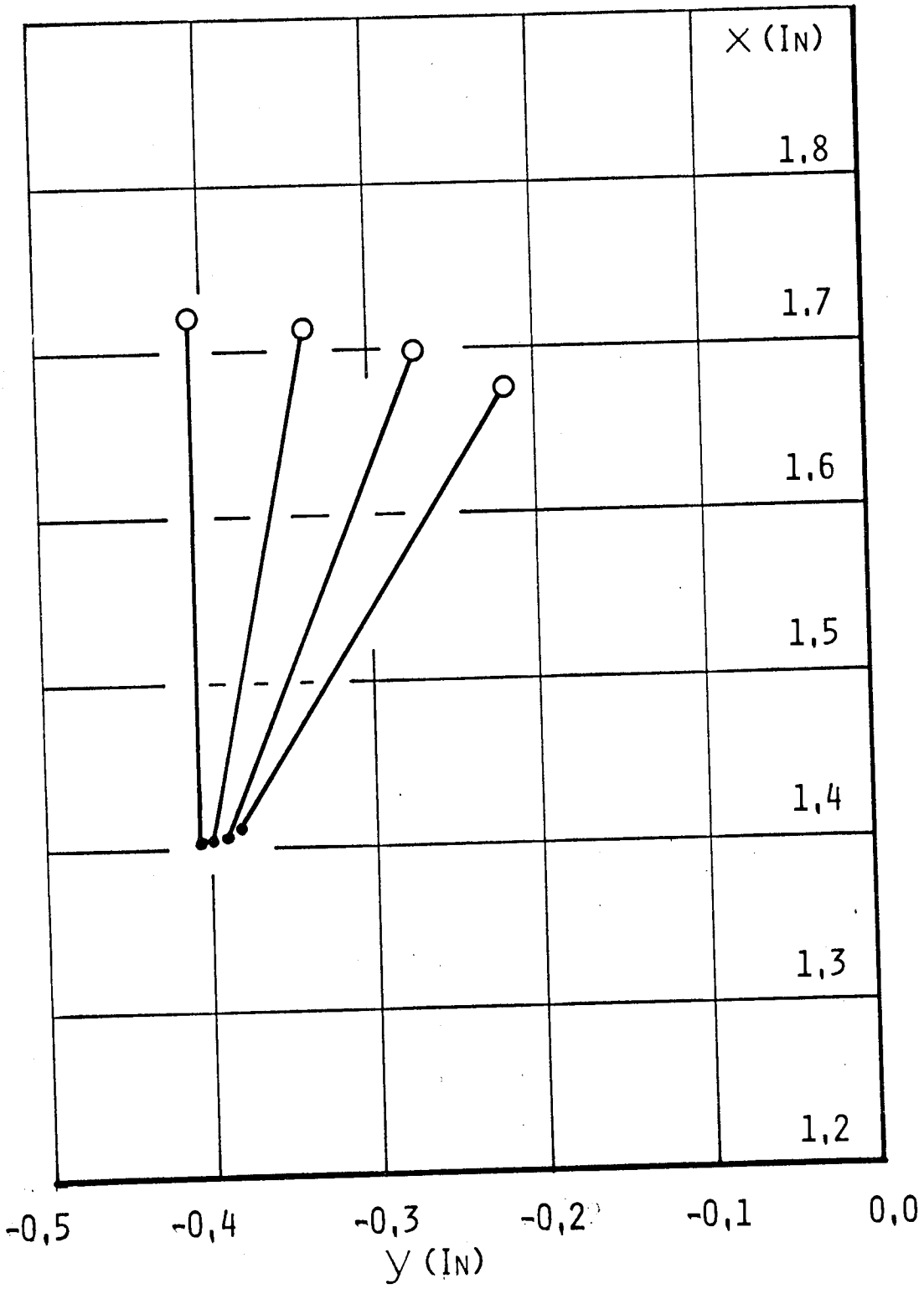


FIGURE 70

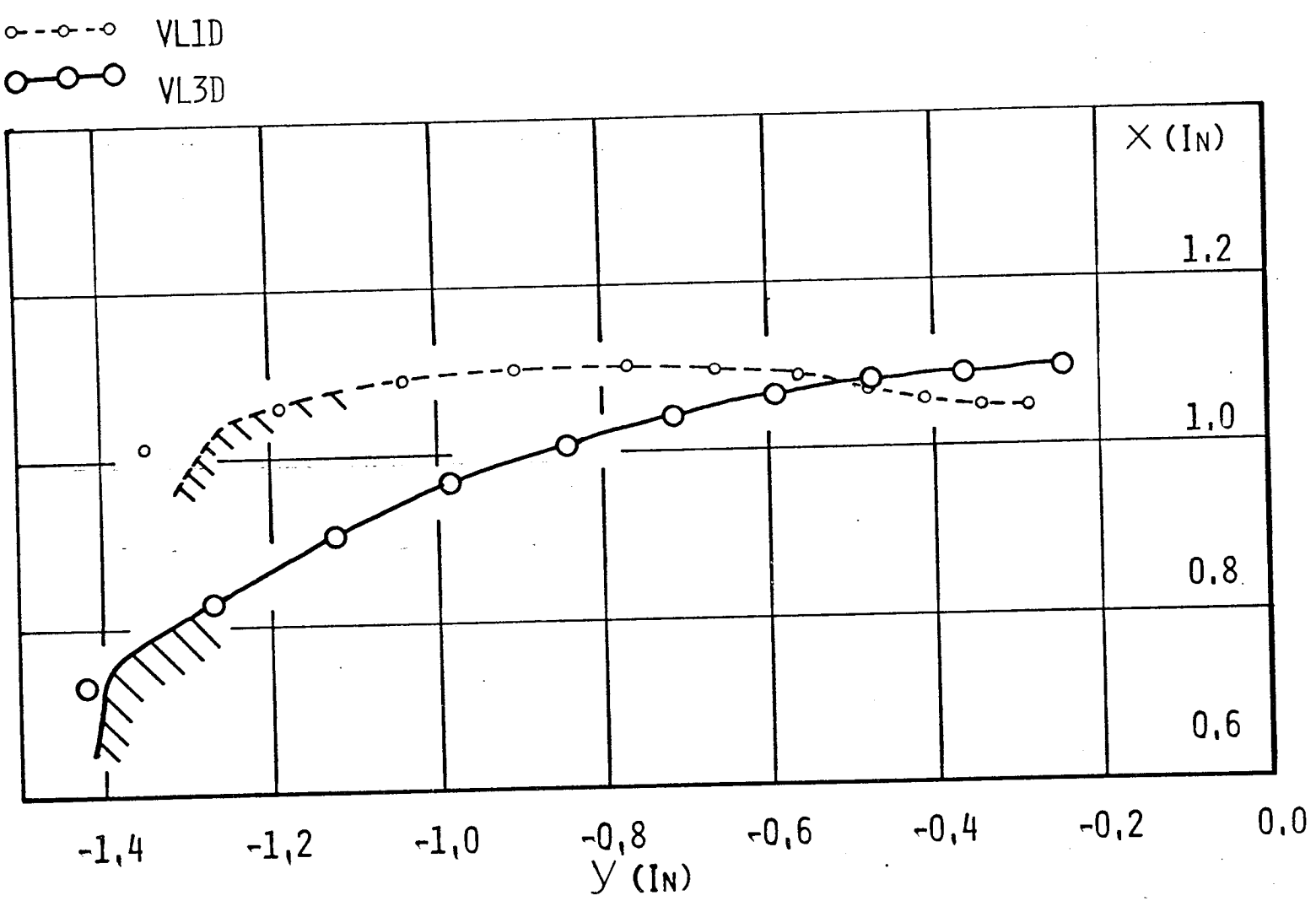


TESTS VL1D & VL3D
SCALE - 5X

SHORTENING LEAD

0.0 PLANE

FIGURE 71

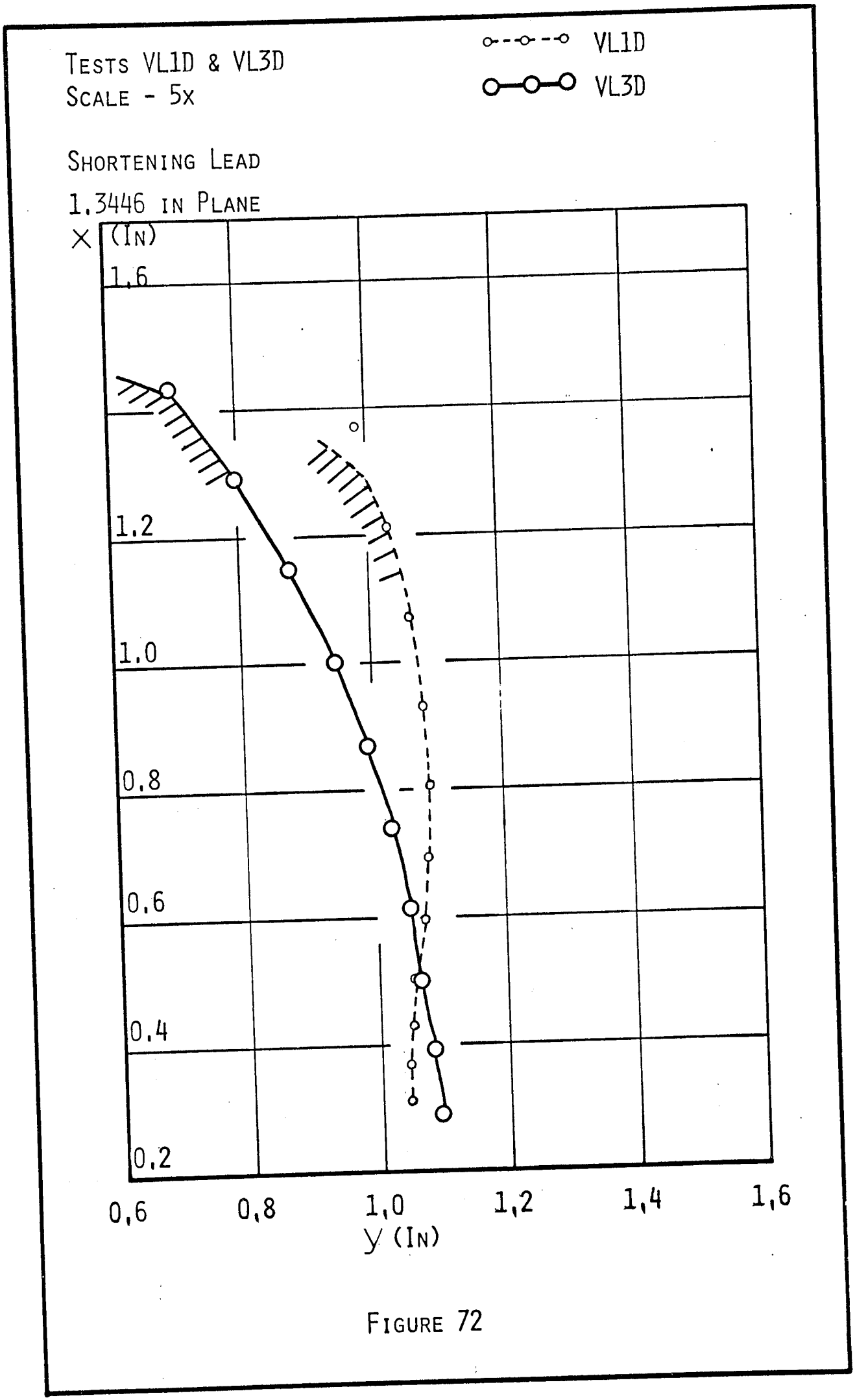
TESTS VL1D & VL3D
SCALE - 5X
VL1D
VL3D
SHORTENING LEAD
1.3446 IN PLANE
X (IN)
1.6
1.2
1.0
0.8
0.6
0.4
0.2
0.6
0.8
1.0
1.2
1.4
1.6
Y (IN)

FIGURE 72

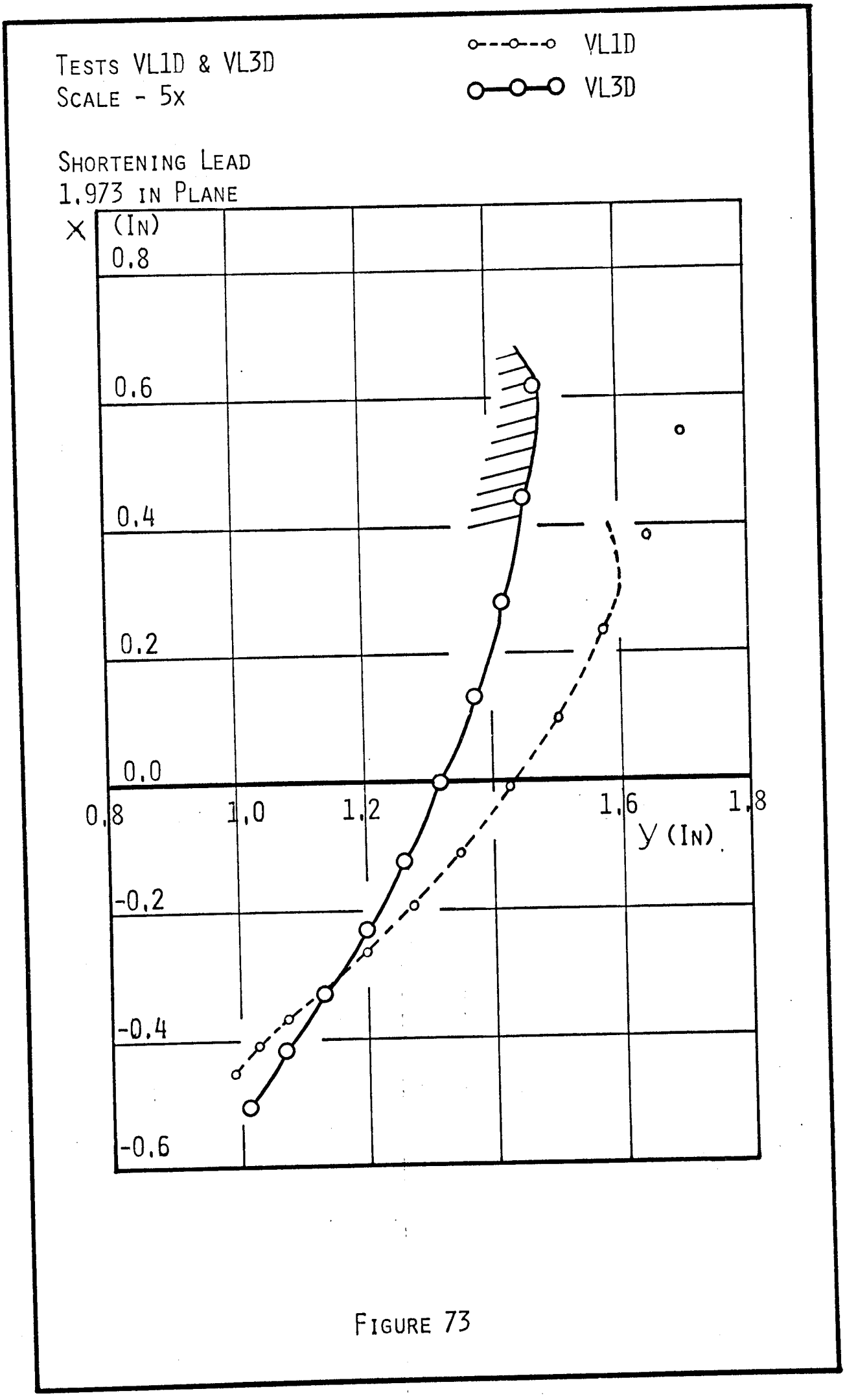
TESTS VL1D & VL3D
SCALE - 5X
VL1D
VL3D
SHORTENING LEAD
1.973 IN PLANE
X (IN)
0.8
0.6
0.4
0.2
0.0
-0.2
-0.4
-0.6
0.8
1.0
1.2
1.6
1.8
Y (IN)

FIGURE 73

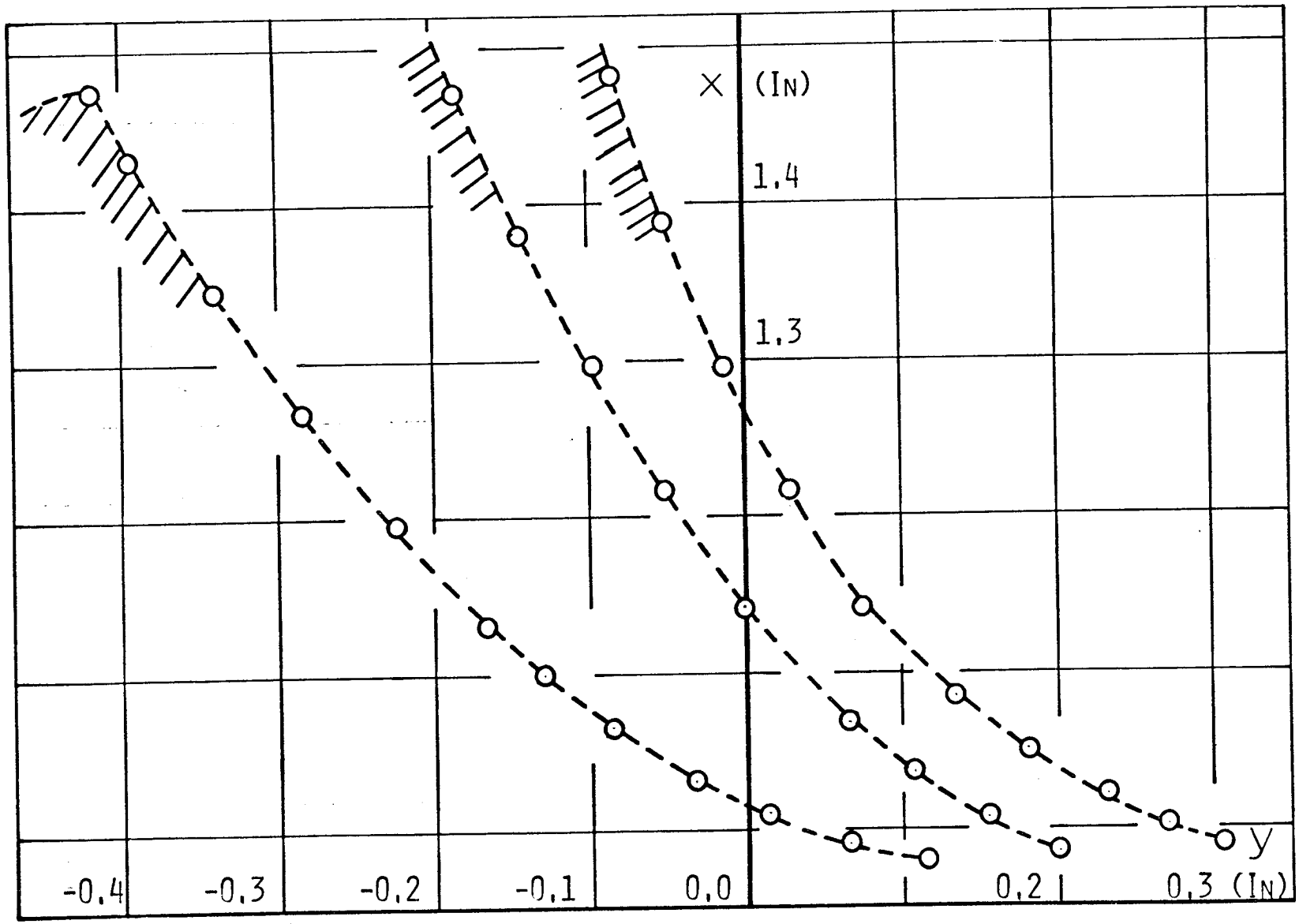


TEST VL2D
SCALE - 10X

LENGTHENING LEAD

0.0
1.3446 IN
1.973 IN
PLANES

FIGURE 74

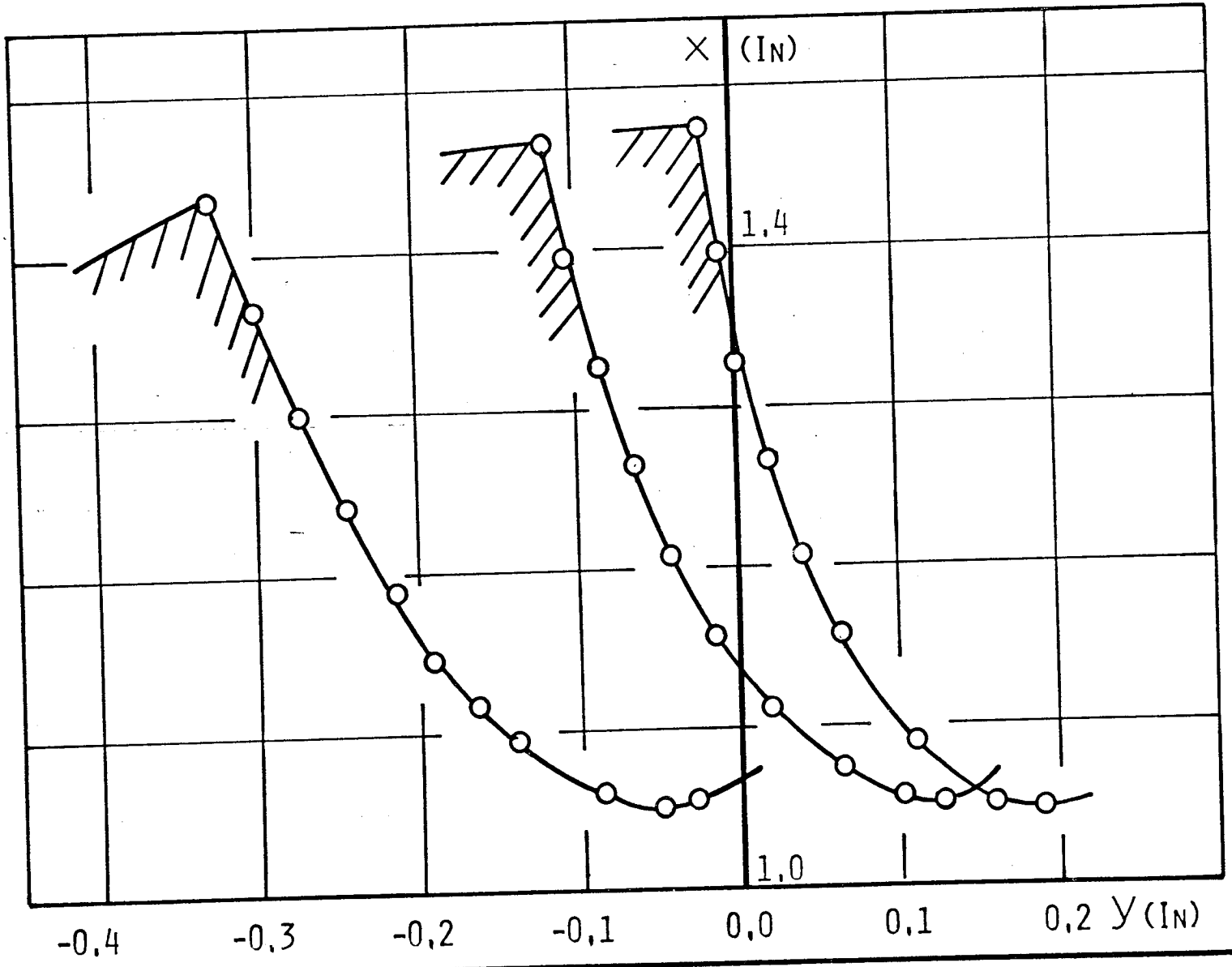


TEST VL4D
SCALE - 10X

LENGTHENING LEAD

0.0
1.3446 IN
1.973 IN
PLANES

FIGURE 75

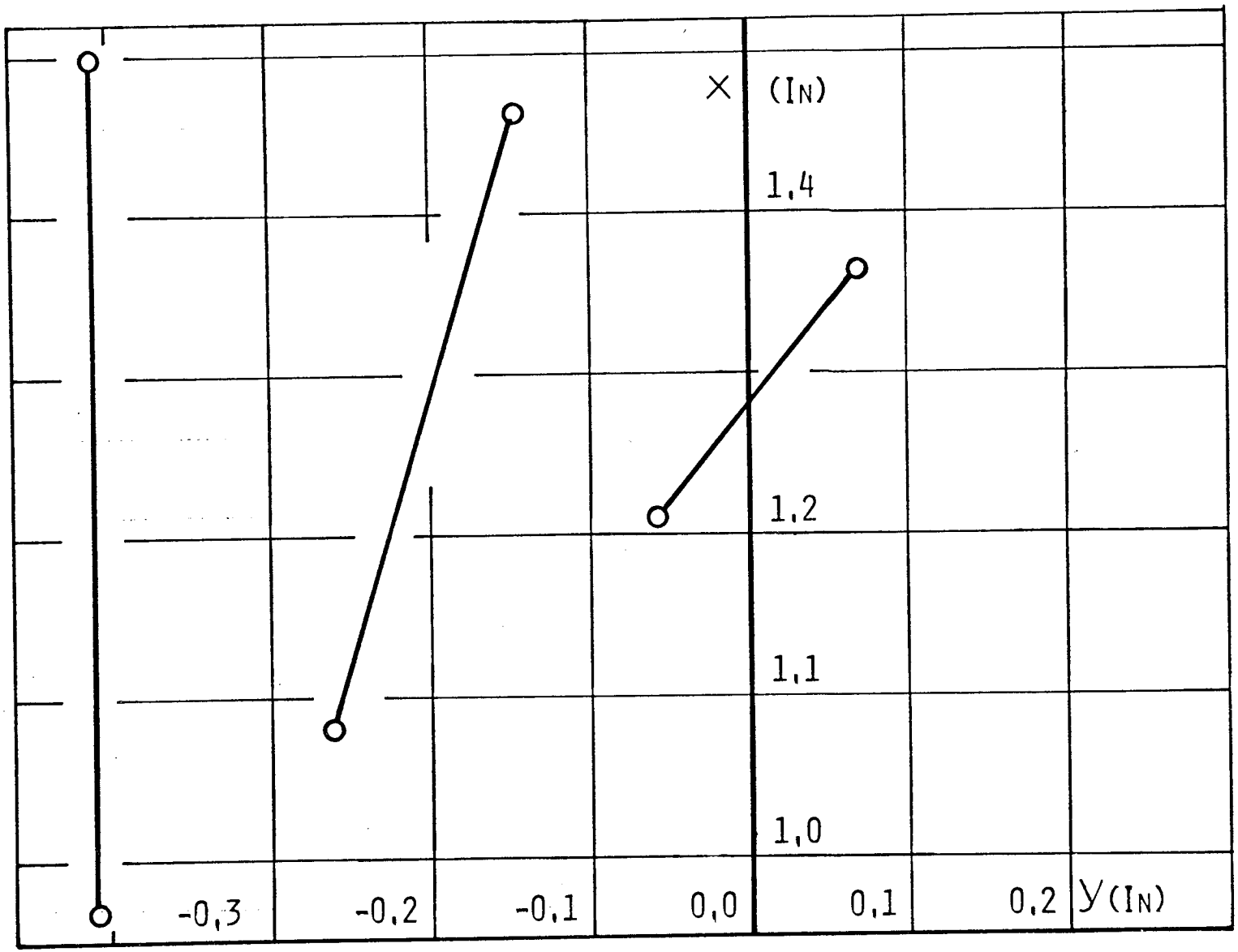


TEST VL1E
THEORETICAL
SCALE - 10X

SHORTENING
LOGARITHMIC LEAD

FIGURE 76

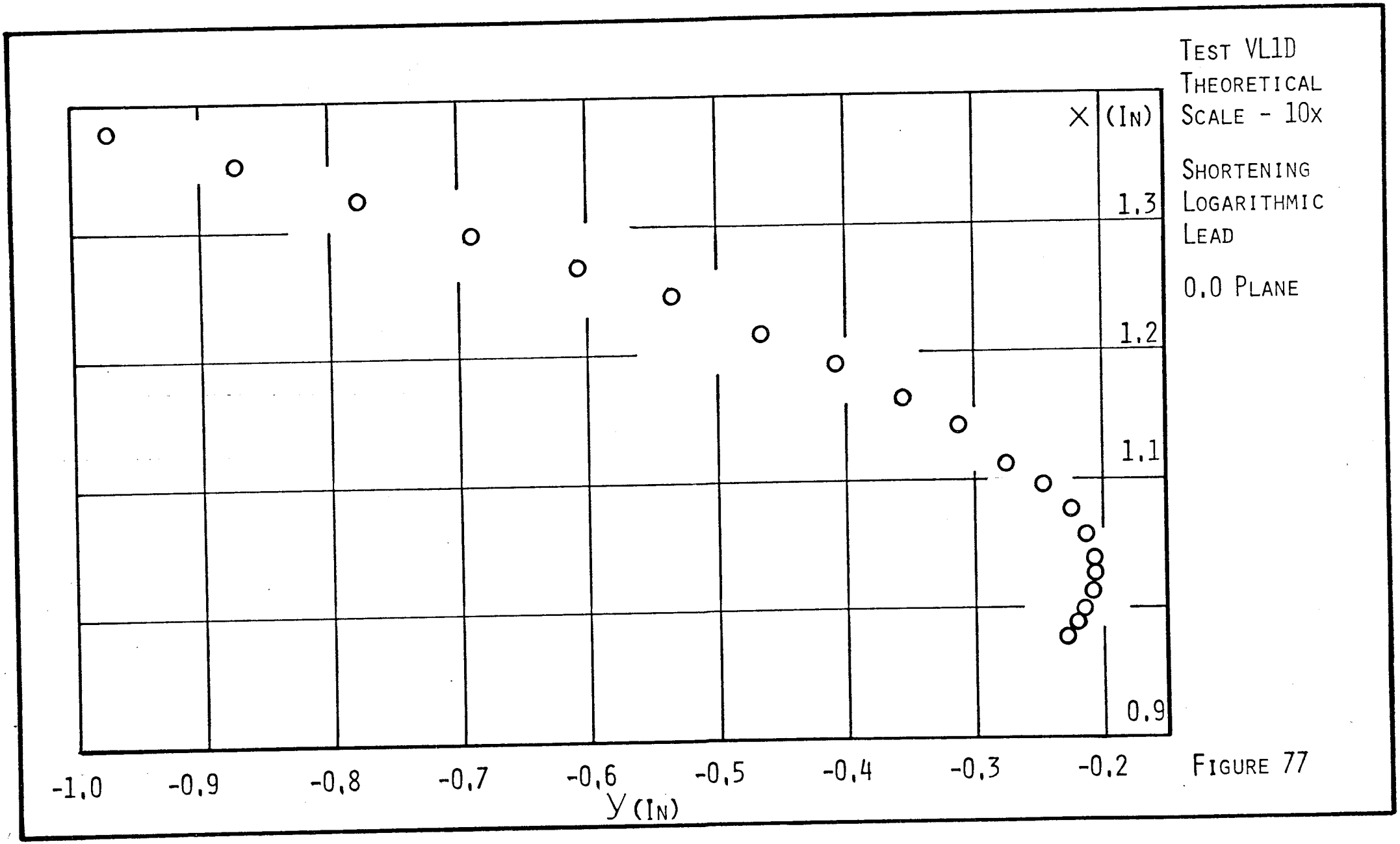
TEST VL1D
THEORETICAL
SCALE - 10X
SHORTENING
LOGARITHMIC
LEAD
0.0 PLANE
X (IN)
1.3
1.2
1.1
0.9
-1.0
-0.9
-0.8
-0.7
-0.6
-0.5
-0.4
-0.3
-0.2
Y (IN)

FIGURE 77

TEST VL1D - THEORETICAL
SCALE - 10X

SHORTENING LOGARITHMIC LEAD

1.3446 IN PLANE

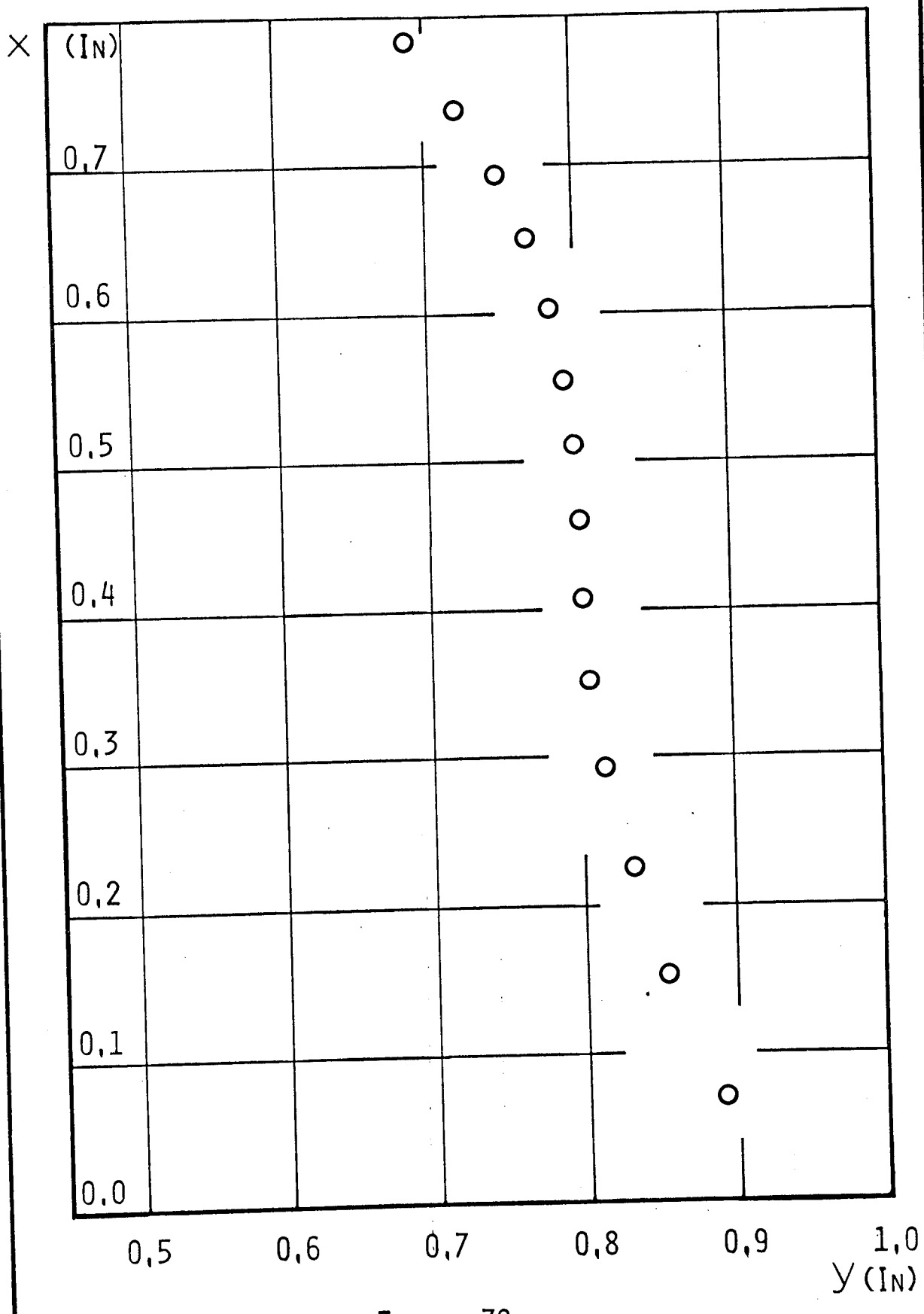


FIGURE 78

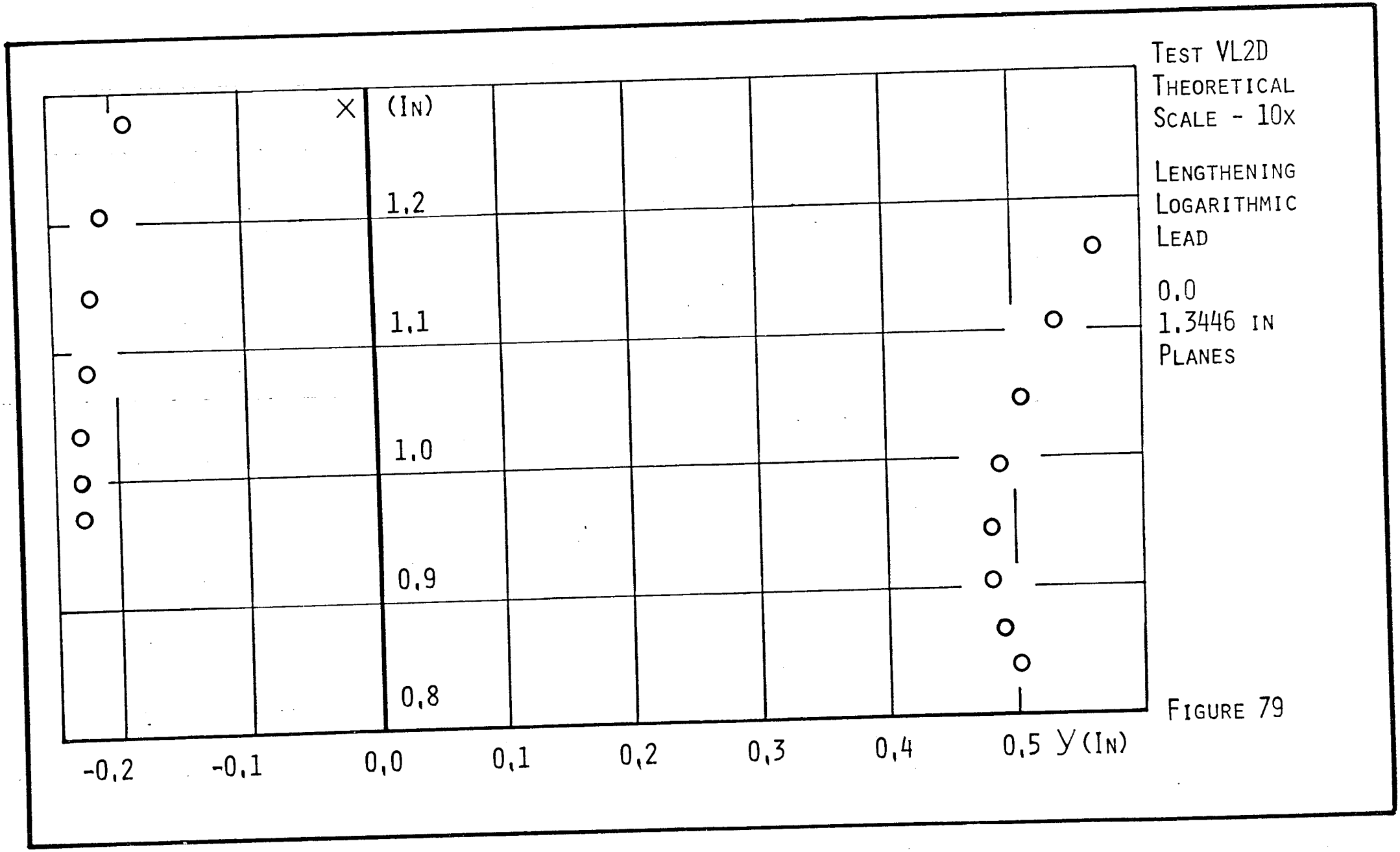


TEST VL2D
THEORETICAL
SCALE - 10X

LENGTHENING
LOGARITHMIC
LEAD

0.0
1.3446 IN
PLANES

FIGURE 79